Report No.
SSRP–06/13

DEVELOPMENT OF RESISTANCE FACTORS FOR LRFD DESIGN FOR FRP STRENGTHENING OF REINFORCED CONCRETE BRIDGES

by

REBECCA ATADERO

VISTASP M. KARBHARI

Department of Structural Engineering
University of California, San Diego
La Jolla, California 92093-0085

May 2006

University of California, San Diego

Department of Structural Engineering

Structural Systems Research Project

Report No. SSRP–06/15

DRAFT

Development of Resistance Factors for LRFD Design for FRP Strengthening of Reinforced Concrete Bridges

by

Rebecca Atadero

Graduate Student Researcher

Vistasp M. Karbhari

Professor of Structural Engineering

Department of Structural Engineering

University of California, San Diego

La Jolla, California 92093-0085

May 2006

1. Report No. FHWA/CA/ES-2006/11	2. Government Accession No.	3. Recipient's Catalog No.
4. Title and Subtitle Development of Load and Resistance Factor Design for FRP Strengthening of Reinforced Concrete Structures		5. Report Date 5/26/2006
		6. Performing Organization Code
7. Author(s) Rebecca A. Atadero and Vistasp M. Karbhari		8. Performing Organization Report No. UCSD / SSRP-06/13
9. Performing Organization Name and Address Department of Structural Engineering School of Engineering University of California, San Diego La Jolla, California 92093-0085		10. Work Unit No. (TRAIS)
		11. Contract or Grant No. 59A0401
12. Sponsoring Agency Name and Address California Department of Transportation Engineering Service Center 1801 30th St., West Building MS-9 Sacramento, California 95807		13. Type of Report and Period Covered Final Report – 5/26/2006
		14. Sponsoring Agency Code

15. Supplementary Notes
Prepared in cooperation with the State of California Department of Transportation. This report is the first of multiple reports.

16. Abstract

Externally-bonded fiber reinforced polymer (FRP) composites are an increasingly adopted technology for the renewal of existing concrete structures. In order to encourage the further use of these materials, a design code is needed that considers the inherent material variability of the composite, as well as the variations introduced during field manufacture and environmental exposure while in service. Load and Resistance Factor Design (LRFD) is a reliability-based design methodology that provides an ideal framework for these considerations and is compatible with existing trends in civil engineering design codes. This investigation studies the application of LRFD to FRP strengthening schemes, with an emphasis on wet layup, carbon-fiber composites applied to reinforced concrete T-beam bridge girders.

Models to describe variation in the existing structural materials and the structural loading are drawn from the literature. Techniques for reliability analysis are discussed and existing work on externally bonded FRP reliability is surveyed.

Stochastic variation in the FRP is characterized based on tensile testing of several sets of field manufactured wet layup composites. A general design procedure applicable to many different situations is proposed using a composite specific resistance factor to consider material variability, a set of Application Factors to account for deviations introduced through field manufacture, and an environment and service-life specific factor for FRP degradation.

Preliminary resistance factors for design of FRP strengthening are calibrated over a range of design scenarios. FRP degradation is considered based on existing durability models, and continued degradation of the structure due to general corrosion of the reinforcing steel is included. The girders used for calibration are selected as representative examples from a sample of California bridge plans. The reliability has been evaluated using simulation and first-order reliability methods. An example of the proposed design procedure, using the calibrated resistance factors, is provided.

The results of this work bring to light the many variables affecting the reliability of strengthened members, and the need for continuing research to better describe these variables. Two variables of particular significance, requiring extensive further study, are the state of the existing structure when strengthening is applied and the loads acting on the structure.

17. Key Words FRP, LRFD, Design of Strengthening	18. Distribution Statement No restrictions. This document is available to the public through the National Technical Information Service, Springfield, Virginia 22161.		
19. Security Classification (of this report) Unclassified	20. Security Classification (of this page) Unclassified	21. No. of Pages ~420	22. Price

Form DOT F 1700.7 (8-72) Reproduction of completed page authorized

DISCLAIMER

The opinions expressed in this report are those of the authors and do not represent positions of the California Department of Transportation.

TABLE OF CONTENTS

LIST OF FIGURES

xviii

LIST OF TABLES

ABSTRACT

Externally bonded fiber reinforced polymer (FRP) composites are an increasingly adopted technology for the renewal of existing concrete structures. In order to encourage the further use of these materials, a design code is needed that considers the inherent material variability of the composite, as well as the variations introduced during field manufacture and environmental exposure while in service. Load and Resistance Factor Design (LRFD) is a reliability-based design methodology that provides an ideal framework for these considerations and is compatible with existing trends in civil engineering design codes. This investigation studies the application of LRFD to FRP strengthening schemes with an emphasis on wet layup, carbon fiber composites applied to reinforced concrete T-beam bridge girders.

Models to describe variation in the existing structural materials and the structural loading are drawn from the literature. Techniques for reliability analysis are discussed, and existing work on externally bonded FRP reliability is surveyed.

Stochastic variation in the FRP is characterized based on tensile testing of several sets of field-manufactured, wet layup composites. A general design procedure applicable to many different situations is proposed using a composite specific resistance factor to consider material variability, a set of Application Factors to account for deviations introduced through field manufacture, and an environment and service-life specific factor for FRP degradation.

Preliminary resistance factors for design of FRP strengthening are calibrated over a range of design scenarios. FRP degradation is considered based on existing durability models, and continued degradation of the structure due to general corrosion of the reinforcing steel is included. The girders used for calibration are selected as representative examples from a sample of California bridge plans. The reliability has been evaluated using simulation and

first-order reliability methods. An example of the proposed design procedure, using the calibrated resistance factors, is provided.

The results of this work bring to light the many variables affecting the reliability of strengthened members and the need for continuing research to better describe these variables. Two variables of particular significance, requiring extensive further study, are the state of the existing structure when strengthening is applied and the loads acting on the structure.

Chapter 1. Introduction

1.1   Overview

Externally bonded fiber reinforced polymer composites (FRPs) are increasingly considered as a viable means of strengthening, retrofitting, and repairing existing reinforced concrete structures. In appropriate situations, these materials can offer significant advantages over more traditional techniques of adding new or replacing lost load carrying capacity. There is a pressing need for this type of technology as our country's infrastructure ages. A prime example can be found in the U.S. bridge inventory; in 2004 the Federal Highway Administration deemed over a quarter of the nation's bridges deficient based on data from 2002. Nearly fourteen percent of bridges were found to be structurally deficient, with an additional fourteen percent functionally obsolete (FHWA, 2004).   At the present time FRP strengthening is a technique seeing growing usage. In order to facilitate the continued growth of this technology and to provide for the long-term safety of designs using FRPs, it is vital that a design code is developed for their use in strengthening.   However, there are many challenges to be overcome in design code development such as the unique characteristics of FRPs, the incomplete database of material properties, and the somewhat limited understanding of the interaction between the FRP and the existing structure.

1.2   FRPs for Strengthening of Civil Structures

1.2.1   Fiber Reinforced Polymer Composites

A composite is a material that is composed of two or more distinct phases. The constituent materials work together to produce properties that are more desirable than those of the individual materials. FRPs are composed of a fibrous reinforcing phase embedded in a polymeric matrix. Typical fiber types include carbon, glass, and aramid. Many different

1

polymers may be used for the matrix phase. In strengthening applications the resin system is typically a thermosetting polymer such an epoxy or vinylester.

This combination of materials provides FRPs with a number of unique, and often advantageous, properties. FRPs are perhaps best known for their high specific strength and stiffness (defined as the property divided by the material density). Unidirectional composites may have specific strengths nearly an order of magnitude greater than those of common metals, such as steel or aluminum (Kaw, 1997). Other advantageous properties of composites include their enhanced fatigue resistance at the material level, resistance to corrosion, and tailorability.

There are many different methods used to fabricate composite materials. Several, such as autoclave forming and resin transfer molding, are impractical for use in civil applications. The most common forms of FRP used for strengthening are wet layup systems, manufactured directly on the structure through a manual process, and prefabricated strips, which are often manufactured through pultrusion and then bonded to the structure with adhesives. Other special systems may be used to provide automated wrapping of columns or apply post-tensioning (International, 2001).

1.2.2 Strengthening and Repair of Civil Structures

Structures designed by civil engineers are intended to have a long lifespan, and during that time there are many reasons why the structure may require strengthening or repair[1]. (Täljsten, 2002; Ellingwood, 1996). The most significant of these reasons include:

---

[1] It should be noted that strengthening generally implies adding capacity to a structure, while repair signifies returning a structure to its original capacity. This report treats these two applications of FRP to externally reinforce concrete structures interchangeably; however, the term strengthening is generally used.

1. *Environmental Exposure* - Civil structures are exposed to changing environmental conditions throughout their lifetimes. These factors can cause material degradation over time or impart significant damage during one extreme event. The impacts of environmental degradation will be especially felt in cases where regular maintenance is not performed.

2. *Changing Usage* - It is not uncommon for civil structures to outlive the purpose for which they were originally designed. Changes in tenancy or use may place different or larger load demands on the structure.

3. *Changing Design Standards* - Even if the use of the structure is not significantly changed, the standards the structure must meet may change over time.

4. *Errors in Design or Construction* - Civil structures may even require strengthening before they are ever used due to errors in the initial design or construction.

Strengthening is not new to civil applications; however, in the past it generally meant placing more concrete, bonding steel plates, or applying some sort of post-tensioning to the structure (The Concrete Society, 2000). Now many types of strengthening can be accomplished with FRPs (Täljsten, 2002; The Concrete Society, 2000). FRP strengthening can be applied to mitigate several failure modes. For flexural strengthening of beams, slabs, or girders, FRP plates can be applied to the tensile face of the concrete. Shear and torsional strengthening can be accomplished by placing FRP on the sides of beams. Columns are typically strengthened by wrapping the FRP around the column in the hoop direction, thus

increasing the confinement of the concrete core. This can be accomplished with wet lay-up or prefabricated cylindrical jackets.

1.2.3   Advantages of FRPs for Strengthening

The unique properties of FRPs result in many advantages from the perspective of strengthening designers (The Concrete Society, 2000; Täljsten, 2002; International, 2001; ACI, 2002; Maruyama, 2001).   FRPs do not suffer from corrosion as do steel plates, allowing the possibility of extended service lives or perhaps limiting required maintenance. Their high strength and stiffness to weight ratios mean that a smaller weight of FRP needs to be applied as compared to steel plate bonding. This low weight reduces transportation costs, significantly eases installation, even in tight spaces, and can eliminate the need for scaffolding, reducing traffic impact.   The low weight also means that FRPs add only a small amount to the structure's dead load. This allows more of the strengthening to be useful to the structure and also makes FRPs a repair option when significant additional weight could cause failure. Additionally, FRPs are typically applied in thin strips, resulting in very little change in the structural profile, an important feature on bridges or other structures that require clearances for vehicles or machinery.

The way that FRPs are manufactured also provides useful properties. By designing the placement of the reinforcing fibers, properties such as strength and modulus can be controlled in different directions. This allows the strengthening to act only in the needed direction, preventing it from changing the structural behavior in unintended ways. Because they are made from long thin fibers, FRPs are very easy to handle.   They can be made to wrap around curves and to accept the irregularities present in concrete surfaces. Furthermore, they can be manufactured in long lengths, eliminating the need for splices, and can be cut to length on site, eliminating sizing errors in the manufacturing stage.

1.2.4 Disadvantages of FRPs for Strengthening

Despite their numerous advantages FRPs are not without drawbacks (The Concrete Society, 2000; Täljsten, 2002; International, 2001). Unidirectional FRP materials are characterized by linear elastic behavior up to failure; this lack of yielding can result in less ductile structures unless this behavior is specifically considered at the design stage. These materials are very susceptible to damage from impact, fire, or vandalism, and as such need to be protected. Though FRPs do not exhibit corrosion, they are not immune to environmental impacts and do suffer degradation due to moisture, temperature, and UV rays. This disadvantage is of particular importance because there is currently little long-term information on the durability of composites in exposed environments. The initially high material cost of FRPs is also a drawback to many engineers, however, due to the cost advantages in transportation and installation offered by composites, the cost of a whole strengthening project can be comparable or even less than the same project strengthened with steel plates.

1.3 Design Code for FRP Strengthening

1.3.1 Need for a Design Code

Other limits to the use of composites in strengthening are related to the unique aspects of civil design (Ellingwood, 2003). Composite materials were initially developed and used in the mechanical and aerospace fields, fields that are significantly different from civil engineering. The typical mechanical or aerospace part will be mass-produced at the end of engineering design, making it economically feasible to conduct testing throughout the design stage and to specifically tailor materials for a particular project. Furthermore, the design requirements, such as load demands, are clearly defined and the manufacturing processes used in these fields allow for very tight control of finished properties. In contrast, each civil design is a unique project that is usually designed and built just once. Due to cost, size, and time

constraints, routine civil designs are rarely tested before construction, and when testing does occur it is usually performed on a scale model or only a critical portion of the design. In place of testing civil design is based on knowledge of material properties, analysis, and prior experience, which are often actualized in codes of practice. For example, the International Building Code is a model code that is based on recognized standards and specifications developed by individual organizations with expertise in different aspects of construction, such as the American Institute of Steel Construction (AISC) or the American Concrete Institute (ACI). Bridge design is usually based on the specifications of the American Association of State Highway and Transportation Officials (AASHTO). However, civil design is usually characterized by substantial uncertainty in load demands, especially those due to natural phenomena, and material properties that cannot be as tightly controlled. These uncertainties result in conservative specification of loads and material strengths in design codes.

When governments adopt design codes they become part of local, state, and federal law, exposing civil engineers to liability concerns for designs that do not meet the standard. In addition to their legal implications, design codes also serve as a set of minimum technical requirements for acceptable design and provide a pathway for research findings to make their way into practice (Ellingwood, 2000b). Thus, most design in civil engineering is based on codes of practice, and, without a comprehensive specification for FRP, it is unlikely that this promising new material will gain widespread acceptance and utilization. This is especially true because design with composite materials is not a typical component of the undergraduate civil engineering education. The lack of design code and designer experience are the most significant obstacles limiting the present use of composites in civil infrastructure.

1.3.2   Uncertainty in Structural Design

The goal of the structural engineer is to achieve structural safety in the face of numerous uncertainties. Nearly every variable considered in design is uncertain to varying degrees. Loads can be highly variable, especially when natural effects such as wind and earthquakes are considered. Materials have inherent variability and may suffer degradation when they are put in service. The models describing structural behavior are just that, models, and the uncertainty in their results is usually unknown. Even the service-life of the design is an uncertain quantity. The result of uncertainty is risk, which is often defined as the product of the probability of failure and the costs associated with failure (Ellingwood, 1994). Since the design variables are uncertain, there is a risk that the structure will fail due to overloading, when the loads exceed those for which the structure was designed, or that the structure will be understrength due weak materials or incorrect dimensions. Though it is impossible to completely eliminate risk, good engineering design can hold the risk to acceptable levels by accounting for the uncertainty inherent in design.

1.3.3   Design Philosophies as the Basis for Design Codes

Currently there are two main philosophies behind civil design: Working or Allowable Stress Design and probabilistic-based limit states design. Other approaches, such as Ultimate Strength Design or Load Factor Design, fall somewhere between these two approaches. In the United States probabilistic limit states design is typically implemented in the Load and Resistance Factor Design (LRFD) format. Other parts of the world, such as Europe and Canada, also have design codes with a probabilistic basis; however, the implementation differs from the LRFD format (Ellingwood, 1996).

1.3.3.1 Working Stress Design

Working Stress Design has served as the basis for structural calculations since the late 19th century when calculations first started to be used for design (Ellingwood, 2000a). In Working Stress Design the stresses in members due to service loads are elastically computed and compared to a specified allowable stress divided by a factor of safety. The basic checking equation used for Working Stress Design is shown in Eq. 1-1 wherein f is the elastically computed stress in the structure, F is the allowable stress, and FS is the factor of safety.

$$f \leq \frac{F}{FS}$$
Eq. 1-1

The factors of safety used in Working Stress Design are based on past experience and engineering judgment, not specific consideration of the uncertainties involved in design. As experience has been gained over time, factors of safety have generally been decreased (Ellingwood, 1994). In this design format there is only one factor to account for all the uncertainties that may be encountered in loads and resistance. This neglects the fact that different types of load may have different degrees of variation, resulting in a range of structural reliabilities. This variation in structural reliability is one of the key drawbacks to Working Stress Design.

1.3.3.2 Load and Resistance Factor Design

Load and Resistance Factor Design is a relatively new development in civil design. The theoretical basis for LRFD, structural reliability theory, was developed during the period from the late 1940s to the mid-1960s, at which point interest grew in incorporating the reliability research into standards for design (Ellingwood, 1994). The first LRFD specification was adopted in 1986 by AISC with the first LRFD edition of the *AISC Manual of Steel Construction* (Salmon and Johnson, 1996).

The LRFD approach to design is distinct from Working or Allowable Stress Design in two ways. First, it is based on a philosophy of defining pertinent limit states. A structure is said to reach a limit state when it fails to reach a level of performance for which it was designed. Limit states are typically divided into two categories: strength and serviceability. Strength limit states relate to the structure's ability to carry load and include limits such as the plastic capacity of a ductile member, fracture of brittle materials, and instability or buckling. Service limit states are primarily related to the comfort of occupants and include excessive deflection, vibration, and/or cracking (Salmon and Johnson, 1996). Including strength and serviceability, AASHTO defines four different kinds of limit states in the *AAHSTO LRFD Bridge Design Specifications* (AASHTO, 2004). Fatigue and fracture provisions are considered separately from the strength provisions and are intended to prevent failure through cyclic loading. The extreme event limit state specifically considers rare events such as earthquakes, floods, or collisions, which can be considered as statistically insignificant loads. In WSD structures are evaluated at typical service conditions; in LRFD structures are evaluated in the ways they are likely to fail by considering the applicable limit states.

LRFD is also different from Working Stress Design in that it is based on probabilistic analysis of the uncertainties present in design. The factors in LRFD based specifications are specifically calibrated such that the probability of reaching a particular limit state is acceptably small. This probability is most often measured in terms of the reliability index, β. In the development of a LRFD code, a target value of β is set, and design factors for load and resistance are selected such that a wide range of designs will be close to this target, usually with a bit of conservatism. The reliability index and the methods of structural reliability theory used to calibrate design factors are discussed further in Chapter 2 of this report.

The basic design equation in LRFD is shown in Eq. 1-2 where ϕ is the resistance factor, usually specific to material and failure mode and sometimes to a particular limit state, R_n is the nominal resistance, γ_i is the load factor specific to load i, and Q_i is the load effect due to load i.

$$\phi R_n \geq \sum_i \gamma_i Q_i$$ **Eq. 1-2**

In the LRFD format different types of loads such as dead, live, wind, snow, earthquake, etc. each have their own load factor. Different types of loads are given different load factors depending on their coefficient of variation. These factors were calibrated for buildings in the late seventies and are intended to be applicable for all design materials (Ellingwood, 1994; Galambos et al., 1982; Ellingwood et al., 1982). Load factors for bridge design were calibrated in the nineties for use in the *AASHTO LRFD Bridge Design Specifications* (Nowak, 1999). The variations in capacity caused by material variability, geometric uncertainty, and modeling error are accounted for by the resistance factor ϕ. Resistance factors generally depend on the material being used and the limit state being checked.

1.3.3.3   Advantages of LRFD

From the viewpoint of the designer LRFD is still a deterministic format with no explicit reliability calculations required. However, the probabilistic basis of LRFD is much more complex than the empirical basis of Working Stress Design. There are many advantages to the LRFD format (Ellingwood, 2000a; Salmon and Johnson, 1996).

1. Designs created with LRFD have much more uniform reliabilities than those created with Working Stress Design.

2. The random nature of materials and loads is handled in a rational and analytical manner; the factors are derived based on statistics not just experience. Since

the factors have an statistical basis it is much clearer when factors should be changed based on new research or technology.

3. Since LRFD is a limit states approach, structures are evaluated in the ways they are likely to fail. This can provide for better evaluation of serviceability limit states. It also makes the relationship between behavior and design easier to comprehend.

4. Since separate factors are used for load and resistance, research on one or the other can be conducted independently, and changes can be made to either side as new information is gained.

5. With load factors common to all materials LRFD simplifies the design process.

6. For unusual load cases or new materials LRFD provides a framework with which to approach design code development.

These advantages, plus the fact that LRFD is the design philosophy that most civil design is moving towards, make LRFD the design philosophy of choice for development of a code for FRP strengthening.

1.3.4 Current Design Guidelines for FRP Strengthening

There are several current guidelines for the use of FRP to strengthen reinforced concrete structures:

1. *Guide for the Design and Construction of Externally Bonded FRP Systems for Strengthening Concrete Structures*, published by the American Concrete Institute, 2002

2. *Externally Bonded FRP Reinforcement for RC Structures* published by the International Federation for Structural Concrete (fib), 2001

3. *Design Guidance for Strengthening Concrete Structures Using Fibre Composite Materials* from The Concrete Society, 2000

4. *Strengthening Reinforced Concrete Structures with Externally-Bonded Fibre Reinforced Polymers* from ISIS Canada, 2001 (Neale, 2001)

5. *FRP Strengthening of Existing Concrete Structures, Design Guidelines* by Björn Täljsten, 2002

6. *Recommendations for Upgrading of Concrete Structures with Use of Continuous Fiber Sheets,* from the Japanese Society of Civil Engineers, 2001 (Maruyama, 2001)

All of these guidelines draw together a large body of research into a document that is easily understood by designers, and as such they are a valuable advance in the use of FRPs to renew existing concrete structures. However, these documents also share many limitations. The guidelines are all quite similar in their design approach, and at first glance all appear very similar to LRFD. All use a limit states approach to defining design-checking equations. Design procedures and equations are given for basic strength limit states such as flexure or shear; however, the accuracy of these approaches is questionable in some cases, particularly shear. Debonding is discussed in all; however, the level of detail varies significantly. The approach to serviceability limit states also varies from guide to guide. All of the guidelines rely on the load factors already developed in relevant specifications for new design, and many use familiar resistance factors or partial material factors from probabilistic design codes for other materials. However, these design guidelines are not true probabilistic codes. No

calibration procedure was used to specifically derive the resistance factors in order to achieve a target reliability; in fact, no such target was even set. Thus, while these guidelines are a significant advance in the use of FRPs for the strengthening of concrete structures, there is still work to be done to develop a code in the preferred LRFD format.

1.4 Problem Statement and Research Objectives

1.4.1 Problem Description

Externally bonded fiber reinforced polymer composites have shown promising performance as a means of strengthening existing reinforced concrete structures. As the infrastructure of our country continues to become deficient due to ageing, environmental attack, and growing usage, the development and implementation of repair strategies, such as the external bonding of FRPs, can serve a vital role in economically promoting the safety of engineered structures. However, due in large part to a lack of design code and designer experience, this technology is currently under utilized.

Design guidelines are already available for the use of bonded FRPs as a strengthening measure. However, these guidelines are based on a deterministic format for design. Given the high level of material variability that can be exhibited by FRP systems, deterministic design is likely to produce an unacceptably large range of project reliabilities. The framework provided by LRFD is an ideal method for considering the inherent material uncertainty, as well as the time dependent material behavior, to produce designs with an acceptable level of structural reliability. Therefore, a design code in the LRFD format must be developed to promote the usage of FRP for strengthening.

Development of a LRFD based design procedure requires extensive data:

1. Statistical data characterizing the load and resistance variables

13

2. Methods for defining nominal or design values of load and resistance

3. Definition of applicable limit states and models for structural behavior at these limits

4. A range of application defining the cases for which the code is valid

5. A target reliability index

6. A method by which reliabilities can be calculated during the calibration process

With regard to FRP strengthening, some of this information is already available. For example, the statistical variation of traditional materials, such as steel and concrete, has been examined by previous researchers. Stochastic load models have been developed and used for both building and bridge structures. Researchers have developed many different expressions for modeling the behavior of structures strengthened with FRP. Structural reliability theory has reached the stage where there are a number of mature techniques for evaluation of structural reliability.

Despite this foundation of available information, there are still significant gaps in knowledge as well as significant challenges to the development of a probabilistic code for the design of FRP strengthening. For example, there is not an adequate existing database of FRP properties as used in civil infrastructure projects. Given the variation that is introduced during field manufacture and application of FRPs this is a significant shortcoming. The multitude of possible fiber/matrix combinations creates an additional level of complexity. Time dependent material properties have not been considered in the development of codes for other materials; however, this is an important concern for FRPs exposed to severe environments. Furthermore, as the existing load descriptions are intended for new designs, they contain many conservative assumptions and may be too demanding for renewal of existing structures. Many of the

14

existing equations for modeling the effect of FRPs on structural behavior are too involved for routine design use. Selection of an appropriate reliability target is also a challenge in that there is no direct basis for comparison.

1.4.2 Research Objectives

The intent of this research is to answer many of the questions regarding probabilistic design of FRP strengthening -- at least in a preliminary fashion -- and to use these answers to develop a LRFD approach to strengthening design. LRFD can be thought of as a general philosophy for approaching design; in order to tailor this philosophy to composite materials and to strengthening rather than new design, several sub-objectives have been identified and will be addressed in this report:

- Given the variety of composites available for strengthening, the proposed procedure must have the flexibility to accommodate this variety.

- The initial as well as time dependent properties of FRPs must be explicitly considered in order to ensure acceptable reliability over the proposed life of the strengthening.

- This procedure must recognize that the addition of extra capacity during strengthening can be much more costly than at the design stage. This requires special consideration of the assessment of initial accuracy of the target reliability level and the statistical models used for loading.

- Many structures will require strengthening due to deterioration, and the application of strengthening does not necessarily halt the deterioration process. Therefore, continued degradation of the structure and its effect on the time dependent reliability should be considered.

- The design methodology must be compatible with existing codes for new design.

- Given the current state of knowledge regarding FRPs and their use for strengthening, it is certain that advances will occur in the future. Therefore, as much as possible, the procedure should lend itself to incorporating new research results into the specifications without requiring full reliability based recalibration of the design code.

- However, because the design factors developed in this research must be considered as preliminary and likely to require recalibration in the future, the underlying data and procedures should be documented as clearly as possible to aid future work.

- To guide further development of LRFD for FRP strengthening critical gaps in the existing research should be identified and suggestions made as to how to fill the gaps in the most advantageous manner.

1.4.3 Research Approach

As discussed in Section 1.4.2 LRFD is simply a way of approaching structural design. In order to develop an effective LRFD procedure this general approach must be tailored to the circumstances in question. With regard to FRP strengthening of existing structures there are three main components to be considered: the FRP material, the structure to be strengthened, and the requirements of reliability based design. These three components are considered schematically in Figure 1-1.

16
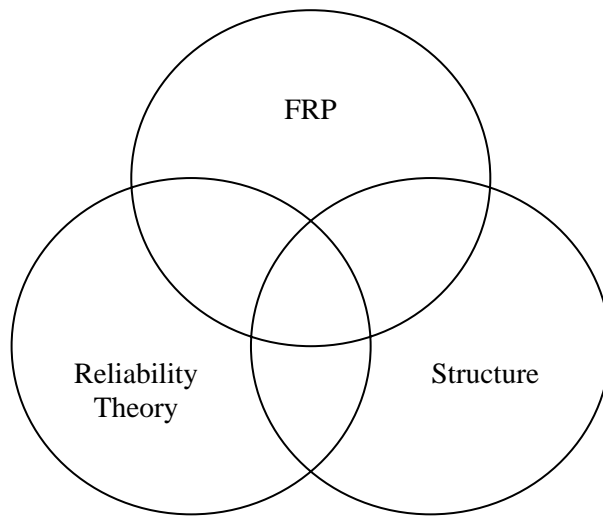
Figure 1-1 Components of Reliability Based Design for FRP Strengthening

The three components identified in Figure 1-1 are shown with significant amounts of overlap. This represents the need to consider the problem as a whole, rather than as three independent components. Each region on this diagram can be used to identify an aspect of developing LRFD for FRP strengthening. The significant questions associated with each portion of the diagram are given in Table 1-1.

Table 1-1 Questions to be Answered in LRFD Study

Region	Questions to be Answered
Structural Reliability	What is the reliability basis of a LRFD code? What reliability methods are available for use?
FRP / Structural Reliability	How is the FRP characterized statistically? How is this statistical characterization related to the design value?
FRP	What types of FRP is the code applicable to?
FRP / Structure	How is the FRP applied to the structure? (What limit states?) How is the effect of strengthening modeled?
Structure	What kind of structures is the code applicable to?
Structure / Structural Reliability	How can the existing structure be described statistically? How are loads on the structure described?
FRP / Structure / Structural Reliability	How should the design equation be formatted? (Where should the factors go?) What is an appropriate reliability target? What reliability method can accommodate the materials and limit states? What is the range of applicability of the design code?

The questions given in Table 1-1 have driven this research project, and their answers form the basis of this report. For purposes of the present work, several of these questions can be answered immediately, including the type of FRP, the type of structure, and the limit states considered. Though the design procedure, in particular the definition of material values for design, has been developed with an eye toward accommodating the full range of FRP materials, the specific examples given herein are for carbon fiber reinforced, wet layup composites. This focus was driven by the frequent use of carbon composites for strengthening and by the availability of data and material for assessing the variability of wet layup composites. Again, while the general format of design presented in this report is applicable to all types of structures, the specific example considered in this report is the class of T-beam bridge superstructures. This choice was largely motivated by the sponsor of this research, the

California Department of Transportation. Furthermore, the limit state considered in this example is the flexural capacity of the girders. This choice was made based on the availability of load and resistance models and will be discussed further later in the report. Answers to the remaining questions shown in Table 1-1 are developed throughout the remainder of this report.

It should be noted that, as research progressed on this project, it became abundantly clear that there are many topics where the existing state of knowledge is simply insufficient to provide for LRFD development without the use of extensive assumptions. The areas of uncertainty are diverse and most merit significant amounts of further study. The topic of strengthening of box girders is a pertinent one but is outside the scope of this investigation as defined by the funding agency.

1.4.4 Outline of the Report

This report follows the progressive development of a LRFD based design procedure for FRP strengthening. Chapter 2 is devoted to developing the background for the project including structural reliability methods, existing statistical data, and the model chosen for continuing structural degradation. Chapter 3 develops the statistical description and defines the design values for the FRP material. In Chapter 4 a full sample calibration is conducted and preliminary factors for design are given. The complete design procedure is summarized and a design example is provided in Chapter 5. Finally, Chapter 6 concludes this report with a summary of the main accomplishments of this work and a detailed discussion of the areas remaining for further study. Numerous appendices supplement the text by providing more detail on issues raised, descriptions of some of the procedures used herein, and additional tabulated data.

The background information for this research is presented in Chapter 2. This chapter starts with a discussion of structural reliability methods, including basic topics such as the safety margin and reliability index. Computational methods for determining the reliability index are briefly reviewed as well as special topics, such as system reliability. The chapter then gives an overview of the prior implementation of LRFD for design using other materials, such as steel, wood, and concrete. Previous work on applying reliability based design to FRP strengthening of concrete structures is discussed. The chapter also summarizes the available statistical data and degradation models used throughout the remainder of the report. The chapter concludes by discussing the selection of the target reliability index used to calibrate resistance factors.

In Chapter 3, the results of several sets of material test data are analyzed to determine appropriate statistical descriptors for FRP, including the distribution type, correlation between variables, and ranges for the mean and coefficient of variation of material properties. A value for use in design is specified as well as modification factors intended to account for the differences between laboratory tested properties and field manufactured properties. The effect of environmental degradation on FRP properties is also considered.

A large example calibration is the topic of Chapter 4. This chapter thoroughly describes the assumptions and calculation methods used to derive design factors. Specific data for the example, such as the range of material properties and geometric quantities and the models used for design, are also described. Preliminary factors for the design of flexural strengthening of T-beam bridge girders, considering the possibility of continued degradation, are presented.

Chapter 5 summarizes the results of this project. It describes the proposed design procedure in detail and provides a full design example using the FRP material design values

and preliminary design factors derived in this project. It is shown that the design procedure and calibrated factors are able to create designs meeting the target reliability; however, a thorough verification of the design factors is still required in the future.

The final chapter in this report, Chapter 6, is devoted to an inventory of further work needed to fully develop a LRFD specification for FRP strengthening. This work primarily involves improving and expanding available data for load models, resistance modeling and FRP properties, as well as research to improve the understanding of the state of the existing structure before the FRP is applied.

Chapter 2. Background for Structural Reliability, LRFD and Design Uncertainty

2.1 Introduction

The goal of this chapter is to develop a firm foundation for the development of reliability-based design for FRP strengthening. Topics covered herein include structural reliability methods, previous implementation of LRFD for other materials, prior work on the reliability of FRPs in civil applications, statistical descriptors for resistance and load variables, procedures for modeling the continued deterioration of structures through corrosion of the reinforcement, and selection of a target reliability index. For each specific topic, this chapter is organized to first provide some general background and to then discuss specific data, models, procedures, and assumptions that are utilized throughout the remainder of this report.

2.2 Structural Reliability Methods

2.2.1 Uncertainty and Risk

Uncertainty exists in nearly everything humans do, and the design of structures is no exception. There are several different types of uncertainty that contribute to the uncertain performance of structural systems. Uncertainty is traditionally divided into two categories, aleatory, referring to inherent or "natural" variability, and epistemic, describing errors that are related to a lack of complete knowledge and may be reduced with more information (Melchers, 1999). Haldar and Mahadevan (2000) recognize two broader categories of uncertainty, cognitive or qualitative uncertainty, which is related to vagueness caused by trying to represent reality in abstract form, and noncognitive or quantitative uncertainty.

Melchers (1999) gives a thorough breakdown of the different types of uncertainty that affect the design and performance of structures:

Phenomenological uncertainty is encountered whenever the structure is of a form that causes uncertainty in its eventual behavior or performance. This type of uncertainty usually affects novel structures, where designers do not have the benefit of previous experience to aid in the design process. This type of uncertainty is cognitive and cannot be included in a reliability analysis in a quantitative way.

Decision uncertainty is caused by the difficulty in determining whether or not an event has occurred. In terms of structures this type of uncertainty refers to whether or not a limit state has been violated. Decision uncertainty may be of particular importance with regard to serviceability limit states where it is difficult to draw a clear line distinguishing acceptable and unacceptable performance; however, it would be very difficult to model for analysis purposes.

Modeling uncertainty arises from the need to model natural phenomena with mathematical equations. This is an epistemic error that can typically be reduced through further research. If a relation between model predictions and actual test results can be found, modeling error can be accounted for in reliability analysis.

Prediction uncertainty arises from the need of designers to anticipate future conditions, such as the material properties achieved during construction and the loading the structure will be subject to during its lifetime. This type of uncertainty affects how variables are modeled and how the reliability calculations are carried out, but is not explicitly accounted for in the calculations themselves.

Physical uncertainty is the inherent randomness that exists in material properties and in the loads applied to a structure. This type of uncertainty may, perhaps, be reduced for materials through the use of better quality control, but it cannot be eliminated. This type of uncertainty makes up the bulk of the uncertainty considered in modern reliability analysis.

Statistical uncertainty arises from the need to estimate statistical descriptors such as the mean, variance, and probability distribution from limited sets of data. This type of uncertainty may be considered in analysis by allowing statistics such as mean and variance to be random variables or by performing multiple analyses with different values of the parameters.

Human error is the final category of uncertainty. Human errors may be divided into routine variations in performance and gross errors. Gross human errors are likely the most common cause of structural failures; however, they are generally not included in reliability calculations because they are very hard to model in a quantitative fashion. This is an important reason why calculated reliabilities do not directly correspond to actual observed failure rates, which are generally much higher (Melchers, 2001). Correctly modeling boundary conditions such as in scour in order to predict performance is also crucial. The presence of uncertainty creates risk. Risk is defined in some contexts as simply the probability that failure may occur. In other contexts risk is associated with the severity of the failure, and is calculated as the probability of failure times the cost of failure (Ellingwood, 1994).

2.2.2   Evaluation of Structural Reliability

2.2.2.1   Effect of Uncertainty

A primary goal of structural design is to create a structure such that the resistance capacity of the structure is greater than the load demands placed on it. This task is complicated by uncertainties because, in their presence, resistance and load cannot be described by deterministic quantities. Instead, uncertainties result in a range of possible resistance and load values and introduce the possibility that the applied load will exceed the capacity of the structure. The most basic situation, where only one resistance variable acts against just one load variable, is shown in Figure 2-1. In this figure the uncertainty in the resistance, *R*, and the load effect, *S*, is represented by probability density functions $f_R(r)$ and

$f_S(s)$. Following customary notation, random variables will be represented herein by capital letters, and individual realizations of a random variable will be represented with lower case letters. The following discussion on structural reliability is drawn from a number of sources (Melchers, 1999; Madsen et al., 1986; Haldar and Mahadevan, 2000; Conte, 2004).
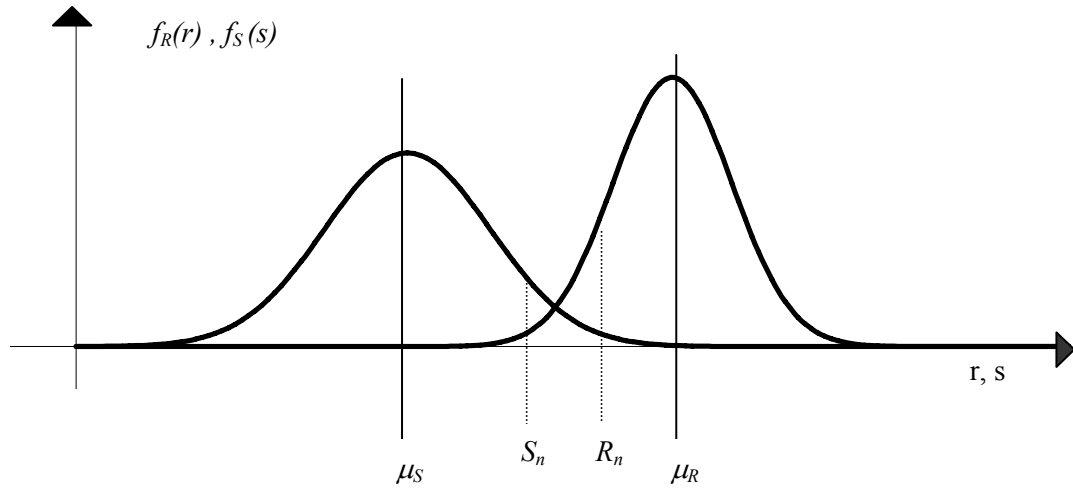
Figure 2-1 Basic Structural Reliability Problem

2.2.2.2 Deterministic Safety Factors

In Figure 2-1, μ_S and μ_R are the mean of the load and resistance, respectively, and S_n and R_n are the nominal load and capacity used for design. The nominal value is determined according to the design procedure in use. It may be a specified as a percentile of test results, calculated through the use of empirical or analytical equations, or prescribed in the code governing the design. In traditional deterministic design a safety factor would be calculated as the ratio of the nominal resistance to the nominal load, or a central safety factor could be calculated as the ratio of the mean of resistance to the mean of load. However, since they do not take into account the full distributions of load and resistance, safety factors calculated in this manner are unable to give an accurate assessment of the design safety.

The structural element whose load and resistance curves are shown in Figure 2-1 will fail if the load effect exceeds the resistance of the member. This can be seen to occur in the region of overlap between these two curves. The area of this region is not the probability of failure, as it is commonly mistaken to be. However, the size of this region can be considered to qualitatively indicate the probability of failure. By considering Figure 2-1 it can be seen that the probability of failure will change as the relative position of the two distributions changes (i.e. the mean values are changed causing a shift along the axis of one or both of the curves), as the amount of spread in one or both of the distributions changes (increased spread will increase the area of overlap), and as the shape of the distributions changes (for example from a Normal distribution to a Lognormal distribution). The traditional approach to design seeks to provide acceptable designs by shifting the position of the distributions through the use of safety factors. These design approaches do not, however, consider the shape or spread of the distribution. A more rational approach to design is to consider all three issues in selection of design criteria.

2.2.2.3 Basic Reliability Problem

The basic problem of structural reliability is to use statistical knowledge of uncertainties to compute the probability of structural failure. In actuality, computing the reliability of an entire structure is a very difficult task that will be briefly discussed in Section 2.2.2.7. The present discussion is pertinent to computing the reliability of a particular member with respect to a particular limit state.

Given a random resistance, R, and a random load demand, S, the probability of structural failure can be expressed in many ways, as shown by Melchers (1999):

$$p_f = P(R \leq S)$$

Eq. 2-1a

$$p_f = P(R - S \le 0)$$

<div align="right">**Eq. 2-1b**</div>

$$p_f = \left(\frac{R}{S} \le 1 \right)$$

<div align="right">**Eq. 2-1c**</div>

$$p_f = P(\ln R - \ln S \le 0)$$

<div align="right">**Eq. 2-1d**</div>

$$p_f = P[G(R,S) \le 0]$$

<div align="right">**Eq. 2-1e**</div>

Eq. 2-1e shows the most general form. In this statement $G(\ )$ is referred to as the limit state function. This function is used to denote the boundary between safe (or acceptable) structural behavior and unsafe (or unacceptable) behavior. When the value of $G(\ )$ is less than zero, the limit state is said to have been violated and the structure is in the unsafe zone. Thus, the probability of failure can be expressed as the probability that the limit state has been violated. Failure in this sense means that the structure fails to meet some criteria of performance, not necessarily that the member has indeed failed; for example, serviceability limit states may be evaluated where "failure" is defined as excessive deflection, even though the member can still support load. Furthermore, the limit state may be expressed in terms of many structural variables, not just the load and the resistance. For example, for the case of a bar element in pure tension, rather than expressing the limit state in terms of only R and S, the resistance could be expressed as a product of the area, A, and yield stress, σ_y, of the member as shown in Eq. 2-2. In the following discussion of structural reliability methods, just two variables, R and S, will be considered for simplicity and clarity.

$$G(A, \sigma_y, S) = A\sigma_y - S$$

<div align="right">**Eq. 2-2**</div>

In the most general case, load and resistance may be correlated random variables, and in order to evaluate the probability of limit state violation the joint probability density function (PDF), $f_{RS}(r,s)$, is required. Figure 2-2 shows contour lines of a general joint PDF. The volume contained in an area of dimensions Δr, Δs underneath the joint PDF represents the probability that the random variable R takes a value between r and Δr while at the same time the random variable S takes a value between s and Δs. The limit state function is shown by the dotted line.
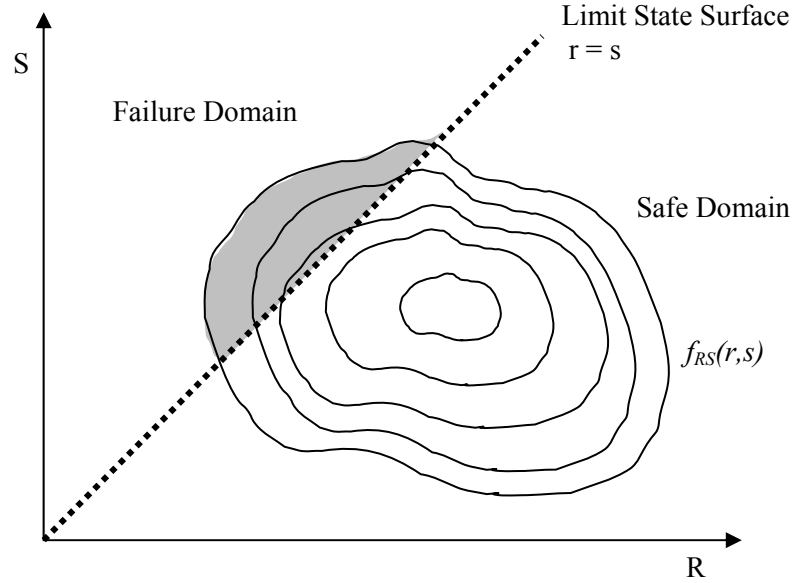
Figure 2-2 Graphical Representation of Probability of Failure

The area of the joint PDF shaded in grey represents the values for R and S where the limit state function is violated. In order to calculate the probability of failure, integration must be used to compute the total volume of probability under the joint PDF. This integral is expressed in Eq. 2-3. In the case where R and S are independent random variables, this equation can be expressed in terms of the marginal distributions of R and S as shown in Eq. 2-4 and Eq. 2-5. In these equations $F_R(\ )$ and $F_S(\ )$ are the cumulative density functions (CDF)

of *R* and *S*, respectively. The lower bound of integration on these equations is zero since resistance cannot be negative.

$$p_f = \iint_{G()\leq 0} f_{RS}(r,s)drds \qquad\qquad \textbf{Eq. 2-3}$$

$$p_f = \int_0^\infty F_R(s)f_S(s)ds \qquad\qquad \textbf{Eq. 2-4}$$

$$p_f = \int_0^\infty [1 - F_S(r)]f_R(r)dr \qquad\qquad \textbf{Eq. 2-5}$$

Eq. 2-3 may be generalized to account for as many random variables as are present in the problem by using the joint PDF for all variables. In general, obtaining a joint PDF for all variables is very difficult, and, even if one is available, analytical solution of these integrals is often impossible. Therefore other techniques must be used to estimate the reliability. However, there are some special cases that allow for direct solution.

2.2.2.4   The Reliability Index

The reliability index is denoted with the symbol β. It is often used as a substitute for the probability of failure. This substitution is typically used because the difference between the probability of failure calculated using reliability methods and that actually witnessed in the field makes it desirable to avoid stating an explicit probability of failure. The causes of this difference are discussed in Section 2.2.2.9. β may be used to compare different structures and can be used as the target in reliability-based design without mentioning a specific probability of failure.

The meaning of β can be best interpreted through consideration of one of the few cases where the probability integrals of Section 2.2.2.3 can be computed analytically. If *R* and *S* are

29

independent, Normally distributed variables, the linear safety margin, *Z=R-S,* is also a Normally distributed variable. Given the means, μ_R and μ_S, and variances, σ_R^2 and σ_S^2, of resistance and load, respectively, the mean and variance of *Z* can be expressed as shown in Eq. 2-6 and Eq. 2-7, respectively, following basic formulas for linear combinations of Normally distributed variables.

$$\mu_Z = \mu_R - \mu_S \qquad\qquad \textbf{Eq. 2-6}$$

$$\sigma_Z^2 = \sigma_R^2 + \sigma_S^2 \qquad\qquad \textbf{Eq. 2-7}$$

By computing the standard Normal variate of *Z,* Eq. 2-1b can now be expressed in terms of Φ, the cumulative distribution function of the standard Normal distribution, as shown in Eq. 2-8. This function is available in tabulated form in many statistics texts and can also be accessed using the NORMSDIST function in Microsoft Excel.

$$p_f = P(R - S \le 0) = P(Z \le 0) = \Phi\left(\frac{0 - \mu_Z}{\sigma_Z}\right) = \Phi\left(\frac{0 - (\mu_R - \mu_S)}{\sqrt{\sigma_R^2 + \sigma_S^2}}\right) \qquad\qquad \textbf{Eq. 2-8}$$

Cornell (1969) defined the reliability index, or safety index, as shown in Eq. 2-9, as the mean of the safety margin divided by the standard deviation of the safety margin. This formulation of the reliability index is referred to as the Cornell reliability index. In this formulation β can be interpreted as the distance between the mean of the safety margin and the point of failure, measured in terms of the standard deviation of the safety margin. This is shown in Figure 2-3.

$$\beta = \frac{\mu_Z}{\sigma_Z} \qquad\qquad \textbf{Eq. 2-9}$$

Cornell's definition of β holds even if the safety margin is a function of more than two variables, as long as the failure surface is linear. The definition of β has been extended to cover other cases, see Melchers (1999) and Madsen et al.(1986). However, for all definitions, the basic concept of β remains the same; it is a measure of the distance between the most likely state of the structure (mean) and the most likely failure point, in terms of the variation.
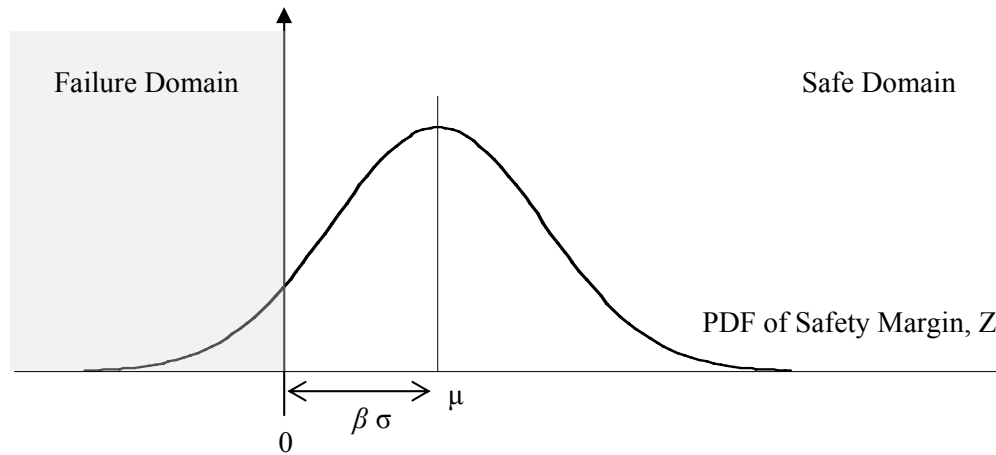
Figure 2-3 Interpretation of β in Terms of the Safety Margin

Though it is only exact in the case of Normally distributed variables and a linear limit state function, β is often approximately related to the probability of failure through Eq. 2-10, which is a generalization of Eq. 2-8. Table 2-1 shows values of β corresponding to several probabilities of failure based on this approximate equation.

$$p_f = \Phi(-\beta)$$

Eq. 2-10

Table 2-1 Probabilities of Failure and Corresponding βs

p_f	β
0.5	0
0.1	1.28
0.01	2.33
0.001	3.09
0.0001	3.72
0.00001	4.27

2.2.2.5 Methods of Computing the Reliability Index

In some cases the probability integral in Eq. 2-3 may be solved using numerical integration. However, this integral is an *n*-fold integral where *n* represents the number of design variables, and thus the complexity rapidly increases as variables are added to the problem. Several other methods have been developed to calculate the probability of failure, or the reliability index directly. The following brief summary of some of the most popular techniques is based on Melchers (1999), Madsen et al. (1986), Haldar and Mahadevan (2000), and Conte (2004). In Section 2.2.2.10 the specific methods used for this report and the reasons why they were selected will be discussed.

2.2.2.5.1 First-Order, Second-Moment Reliability Index

This formulation of the reliability index is an extension of the Cornell reliability index. β_{FOSM} is still defined as the mean of the safety margin divided by the standard deviation of the safety margin and still requires only the mean and standard deviation of the design variables for calculation. However, to allow for non-linear limit state functions, the mean and standard deviation of the safety margin are computed by linearizing the safety margin using the linear terms of a Taylor series expansion. The value of β_{FOSM} depends on the point that is chosen for linearization of the limit state function. A common choice is the point where each random

variable takes on its mean value, resulting in the mean-value, first-order, second-moment reliability index. Though this method is very simple, it has several drawbacks. The most significant drawback is that the value of β_{FOSM} is not invariant with respect to the limit state formulation; two mechanically equivalent formulations of the same limit state can produce different values for the reliability index.

The ambiguity of β_{FOSM} caused by the formulation of the limit state function can be removed by choosing a point on the limit state surface as the expansion point. The point used for expansion is called the design or checking point. When all variables and the limit state function are transferred to standard Normal space the design point is found through a minimization procedure as the point on the limit state surface with the shortest distance to the origin. The reliability index found in this manner is sometimes referred to as β_{HL}, the Hasofer-Lind reliability index (Hasofer and Lind, 1974). This measure of reliability is invariant with respect to the limit state formulation, but it uses only second-moment information about the variables and is not comparable because it does not depend on the curvature of the limit state function at the design point. The generalized reliability index introduced by Ditlevsen makes use of a weighting function to overcome the lack of comparability (Madsen et al., 1986).

2.2.2.5.2   First- and Second-Order Reliability Methods (FORM and SORM)

The first-order reliability method is very similar to the first-order, second-moment method. The limit state function is still linearized using a first-order approximation about the design point. The significant difference between these two methods is that the first-order, second-moment reliability index only uses second moment information about the design variables. FORM uses knowledge of the full distribution of the design variables. The distributions of the design variables are transformed into standard Normal space using

appropriate techniques, such as the Normal tail transformation for independent variables or the Rosenblatt transformation for dependent variables (Melchers, 1999). β_{FO} can then be found using the same optimization techniques used in calculation of β_{FOSM}. To find the probability of failure, Eq. 2-10 may be used to give a first-order approximation.

SORM makes use of non-linear expansions of the limit state function. Determining the probability content of these non-linear surfaces is complicated, and approximate techniques must be used to estimate p_f. The accuracy of both of these techniques depends on the ability of the approximating surface to represent the true limit state.

2.2.2.5.3 Monte Carlo Simulation (MCS)

Monte Carlo Simulation is a technique with applications to many different problems (Rubinstein, 1981). In general the Monte Carlo technique involves using random sampling to generate a large set of artificial data that may be analyzed. In application to structural reliability, a random value is generated for each design variable based on the statistical distribution of that variable, and the random values are used to check the limit state equation. If the limit state function is less than zero, the structure is considered to have "failed". This process is repeated a large number of times, and the probability of failure is estimated as the number of failed samples divided by the total number of simulations. This approach is very robust and can be applied to almost any limit state formulation. However, the accuracy of this approach depends on the number of simulations, and for small failure probabilities the required computing time can be very demanding. With additional knowledge about the failure region, variance reduction techniques, such as importance sampling, can be used to concentrate the simulations in the region of interest and reduce the necessary number of simulations.

2.2.2.5.4 Other Techniques

In some cases a hybrid approach combining simulation with FORM or SORM is used. This may be the case when convergence cannot be reached using all the variables in FORM. This approach was taken by Plevris et al. (1995). The statistical description of resistance of a strengthened member was determined using Monte Carlo Simulation, and then FORM was used with distributions for load to compute the structural reliability.

Response surface techniques can be used when the limit state function is not in an explicit functional form, such as when structural behavior is modeled using finite element analysis. This technique is based on evaluation of the implicit limit state at a limited number of points, and then fitting a function to these points. This functional form can then be directly used with first-order second-moment methods or FORM/SORM.

2.2.2.6 Levels of Reliability Methods

The structural reliability methods described above have been grouped into different levels defined by the types of information they use and the types of calculation they imply (Madsen et al., 1974; Melchers, 1999). These levels are now briefly described in order to illuminate the relation between reliability computation techniques and the LRFD format.

Level 1 methods are the simplest techniques, and are used to provide safety in the design of structures. These techniques rely on just one value to describe each design parameter. ASD, LRFD and other code-level techniques are examples of Level 1 methods.

Level 2 methods make use of two values describing each design parameter (most often the mean and variance) along with a description of the correlation between parameters to calculate a reliability index. These methods are more approximate in their estimate of the probability of failure than methods such as FORM or simulation. The first-order, second-moment reliability index is an example of this level.

Level 3 methods are those methods that seek the best possible estimate of the probability of failure by making use of full distributions to describe the design variables. Examples of this level include FORM/SORM and Monte Carlo Simulation.

Level 4 methods combine consideration of the structure from the previous levels with economic data and seek to provide a cost-benefit analysis. These methods can provide a rational basis for decision-making.

The goal of the study is to develop factors for a LRFD design procedure for FRP strengthening. The design format itself is an example of Level 1 reliability methods; however, the design factors will be calibrated based on Level 2 techniques for computing the reliability.

2.2.2.7 Component vs. System Reliability

The first-order second-moment, FORM, and SORM methods described above are all capable of predicting the probability of failure for a particular member with respect to a particular mode of failure. In reliability analysis this is referred to as component reliability. However, most structural elements are susceptible to failure in several different modes, for example a beam must resist both flexural and shear loads. Furthermore, nearly all structures are composed of many members. The probability of failure of a single element in one of several different mechanisms or the probability of failure of an entire structure are both problems of system reliability. Computation of system reliability is significantly more difficult than computation of component reliability. Monte Carlo Simulation is an option if a model of the complete system can be developed. Or the reliability of a system can be computed based on the reliability of individual components, often relying on simplifying approximations such as assuming the system is a series system or a parallel system. However, the resulting methods remain too complicated for use in calibration of a reliability-based design procedure. Design factors are therefore based on the reliability of a single member

with respect to a particular limit state. This would directly correspond to the weakest link analogy when considering the reliability of the complete structure; however, due to the indeterminate nature of most structures, the reliability of the structure as a whole is usually much higher than the reliability of individual components. This fact must be kept in mind when selecting a target reliability for code calibration. More information on system reliability may be found in Madsen et al. (1986) and Melchers (1999).

2.2.2.8 Time-dependent Reliability

When the statistical description of load or resistance (as for a deteriorating structure) changes with time, these changes must be considered through the use of time-dependent reliability techniques. The most rigorous approaches involve the use of stochastic processes, and the probability of failure is determined as the first passage probability, i.e. the probability that the limit state will be violated for the first time during the time period in question. Direct solution of these theoretical formulations is often intractable except for the simplest cases, and thus numerical or simulation based approaches are necessary (Melchers, 1999). Researchers studying degradation of concrete structures have formulated the reliability problem as seen in Eq. 2-11. In this equation p_f represents the probability of failure, $R(t_i)$ is the time-dependent resistance, and S_i are independent random loading events during the life of the structure. This equation has been solved using simulation for deterministic loading increments (Stewart 1998), as well as stochastic load processes (Mori 1993).

$$p_f = 1 - P[R(t_1) > S_1 \cap R(t_2) > S_2 \cap ... \cap R(t_n) > S_n]$$

Eq. 2-11

While the form of Eq. 2-11 is far easier to handle than dealing directly with out-crossing rates (the probability of leaving the safe domain from a certain point weighted with the probability of being at that point), this equation is still quite demanding from a calibration

standpoint. The commonly used approach in development of reliability-based codes is referred to as the time-integrated approach (Melchers, 1999). In this method, the complete lifetime (or at least the lifetime of interest) of the structure is considered to be a single unit. All random variables must be related to this period of time by choosing appropriate statistical descriptions. This approach has been used in the calibration of previous reliability-based codes. For example, the service life considered in development of the *AASHTO LRFD Bridge Design Specifications* is 75 years, and thus the code is calibrated based on an estimated distribution of the 75-year maximum loading (Nowak, 1999). In this case, deterioration of the structure was not considered, so the resistance distribution remained constant.

2.2.2.9 Limitations of Reliability Methods

The reliability estimates made by the procedures described in the preceding sections are only as good as the information that goes into the procedures. Quantifying all sources of uncertainty is a daunting task, especially in the face of limited data. Formulation of limit states requires abstraction from reality. Material variability can be based on past testing, but the choice of a proper statistical distribution remains open to question. The "tail sensitivity problem" refers to the fact that the distribution chosen to represent even one of the design variables can have a significant effect on the calculated probability of failure (Melchers, 1999). Significantly the effect of human error is not included in reliability calculations.

The accuracy of results obtained through these methods cannot be verified for three reasons, as identified by Lind (1996). One, civil structures are each unique in design, construction, and loading history, so it is not possible to compute a failure frequency of a given structural type. Two, the reliability calculations are conducted with a specific design life in mind; in order to assess the validity of the prediction, you must wait until the end of the design life at which point the knowledge becomes irrelevant. And three, structures are

maintained and will be kept in use as long as they can be made serviceable, without regard to the design life. It may be possible to validate the methods used to generate reliability statements; however the statements themselves cannot be validated. Thus, reliability predictions are subject to change due to the models used to assess reliability and the predictions themselves cannot be verified. This does not seem like firm footing for a design procedure. However, as Melchers (1999) summarizes Matheron (1989) "The justification and acceptance of these methods does not stem from them being able, necessarily, to provide correct descriptions of reality. On the contrary, it stems from the fact that they can give reliable, consistent and satisfactory solutions for practical problems." However, a challenge is to communicate with non-engineers. Thus despite all of their limitations, reliability methods are still useful because they provide a rational approach to solving problems.

2.2.2.10 Reliability Methods Used for This Report

The most frequent reliability tool used during the course of this research has been Monte Carlo Simulation. This procedure was chosen for several reasons: it is very robust, generally simple to implement, and can accommodate many variables without causing convergence concerns. But perhaps most importantly, this procedure can directly assess system reliability. Though the intent of this work was to calibrate based on component reliability, the limit state chosen for explicit consideration herein is the flexural limit state. Flexural failure of a reinforced concrete beam strengthened with FRP can actually occur in three different modes: yielding of the steel followed by debonding or rupture of the FRP, yielding of the steel followed by crushing of the concrete, or, for heavily reinforced sections, crushing of the concrete without steel yielding. Thus, to make use of other reliability methods would require assessing the reliability against three different failure modes and using principles of system reliability to calculate the overall reliability. Monte Carlo Simulation can

consider all three failure modes simultaneously based on the particular random values of a given trial and provide the total reliability against flexural failure.

For some examples, and for the final calibration work, a hybrid approach was adopted. MCS was used to evaluate the mean and standard deviation of the resistance, and then first-order reliability methods were used to compute the reliability index. This method was chosen in large part to save computation time; the number of simulations required to asses the mean and standard deviation of resistance was substantially less than that required to resolve the probability of failure. This procedure is consistent with the methods used by Nowak (1999) in calibration of the *LRFD Bridge Design Specifications*. Section C.6.2.1 of Appendix C shows a comparison of reliabilities calculated with direct MCS and the hybrid approach.

In order to assess time-dependent reliabilities the time-integrated approach (Melchers, 1999) was selected. This is the standard technique for calibrating reliability-based design codes; however past codes have not explicitly considered material degradation. For the present case of FRP strengthening, it was desired to include degradation of the FRP and continued deterioration of the existing structure in the reliability calculations. The time-integrated approach was feasible for this example because the degradation in member resistance was not a function of the applied loading history, but only depended on the time in service and the assumed environmental exposure. If the resistance was dependent on the load history, i.e. damage accumulated due to loading, the random load process would need to be modeled explicitly.

To use the time-integrated approach while considering degradation, the distribution of the minimum resistance during the time period is needed in addition to that for maximum loads. By computing the reliability of the structure based on minimum resistance and maximum loads, the predicted reliability of failure is theoretically conservative. This

conservatism results because it is unlikely that the maximum load and minimum resistance will occur at the same time. The degree of conservatism in a particular case cannot be known without explicitly computing the time-dependent reliability using one of the more sophisticated methods in Section 2.2.2.8. In the case of strengthening design for bridges, where the amount of traffic and weight of trucks are both generally increasing over time, the assumptions of the time-integrated approach may not be as conservative as for the case where the distribution of load is known to be strictly constant.

Thus, time-integrated reliability is not the most accurate approach when time-dependent loads and resistances are considered, but it is consistent with the available load data (see Section 2.6) and it provides a conservative assessment of reliability. Later portions of this report will expand on the limitations of this approach and the research necessary to improve the consideration of time-dependent behavior.

2.3   Previous Development of LRFD

Load and Resistance Factor Design has been applied to a number of different materials. A brief history of the development of reliability-based design procedures in the United States can be found in Ellingwood (1994 and 2000b).

2.3.1   Steel

LRFD was first implemented for design of steel structures. Work sponsored by the American Iron and Steel Institute was initiated in 1969 and carried out at Washington University by Ravindra and Galambos (1978). In 1986 the first LRFD specification for steel design was published by the American Institute for Steel Construction (AISC) (Ellingwood, 2000b).

The reliability index used in calibration of the load and resistance factors for steel is a first-order, second-moment index, which is formulated using the safety margin shown in Eq. 2-12 wherein R is the structural resistance and Q is the load effect. The reliability index is shown in Eq. 2-13, here R_m and Q_m are the mean resistance and load effect and V_R and V_Q are the coefficient of variation of the resistance and load, respectively (Ravindra and Galambos, 1978).

$$Z = \ln\left(\frac{R}{Q}\right)$$ **Eq. 2-12**

$$\beta \cong \frac{\ln\left(\frac{R_m}{Q_m}\right)}{\sqrt{V_R^2 + V_Q^2}}$$ **Eq. 2-13**

2.3.2 Loads

Probabilistic load requirements for building loads were developed in 1979 for inclusion in ANSI Standard A58, which is today known as ASCE Standard 7 (Ellingwood, 2000b). The load factors were developed so as to be independent of the type of construction material being used. The procedure used to develop these load standards is described in Galambos et al. (1982) and Ellingwood et al. (1982). A survey of existing design practices for steel, concrete, masonry, and timber was undertaken to identify approximate target reliability levels. Based on those reliability levels and judgment as to the range of load and resistance factors that would be accepted by professional practice, load factors and load combinations were developed to provide relatively consistent levels of reliability. Though selection of specific resistance factors was left to the appropriate professional and industrial groups, guidance was provided for the selection of consistent factors. First-order reliability methods were used in determination of these factors. Despite the fact that this study was not conducted until after

the first draft of the steel LRFD specification was completed, these factors were still incorporated into the steel design manual.

2.3.3 Engineered Wood

The first LRFD specification for design of engineered wood construction was published in 1996 through a joint effort of the American Forest and Paper Association and the American Society of Civil Engineers (AF&PA, 1996). Due to the unique structural behavior of wood this code considers more than just load and resistance factors. Adjustment factors on the reference strength are used to consider specifics of the service environment and preparation of the timber. Factors include the wet service factor, the temperature factor, the size factor for visually graded sawn lumber of round timber members, the preservative treatment factor and the fire-retardant treatment factor. Additionally, member resistance must be reduced by the time effect factor, which is used to consider reduction in member strength under sustained load. Because the degradation depends on the type of loading, this factor is dependent on the controlling load combination. The load combinations are those from ASCE Standard 7.

2.3.4 Bridges

The *AASHTO LRFD Bridge Design Specifications* (AASHTO, 1998 and 2004) were developed under the National Cooperative Highway Research Program Project 12-33. A thorough discussion of the calibration procedures is provided by Nowak (1999). The code was calibrated for girders under positive moment, negative moment, and shear to a target β of 3.5. This target was selected based on analysis of bridges designed following the existing *Standard Specifications for Highway Bridges* (AASHTO). Only dead, live, and impact loads were considered during the calibration. As part of the calibration procedure a new LRFD design load model was developed, the HL-93 model. This load model was developed to provide a more consistent relationship between actual bridge loading and the model used in

43

design. A description of the load model is given in Section 2.6.2. Statistical models for resistance of steel, reinforced concrete, and prestressed concrete girders were developed in addition to the statistical models of loads. The first-order reliability method was used for calculation of reliability indices.

More recently, a reliability-based specification was developed for bridge rating. The *Manual for Condition Evaluation and Load and Resistance Factor Rating (LRFR) of Highway Bridges* (AASHTO, 2003) is based on a calibration target of 2.5. This target was chosen to represent the operating level of the current bridge inventory. Only certain limit states are considered for evaluation. Two sets of live load factors are used to assess bridges, the LRFD factors are used to check at the "inventory" level, and a less demanding set of factors is used to check against the lower "operating" reliability target. Table 2-2 compares the live load factors for the inventory and operating levels for the limit states that include the HL-93 live load model. Site-specific adjustments may be made to the load factors for permit and legal loads based on traffic levels. Additional factors on resistance to consider material uncertainty after some time in service and system level effects are also used (Moses, 2001).

Table 2-2 Comparison of Live Load Factors for Inventory and Operating Levels

Bridge Type	Limit State*	Inventory	Operating
Steel	Strength I	1.75	1.35
	Service II	1.30	1.00
	Fatigue	0.75**	
Reinforced Concrete	Strength I	1.75	1.35
Prestressed Concrete	Strength I	1.75	1.35
	Service III	0.80	
Wood	Strength I	1.75	1.35

* As defined on *AASHTO LRFD Bridge Design Specifications* (AASHTO 1998 and 2004)
** Optional Checks

44

2.3.5 Concrete

Though concrete design as governed by ACI 318 has used limit states design with factors on load and resistance since the 1963 edition of the code, these factors were not specifically calibrated with modern reliability methods but were instead selected based mainly on judgment (Ellingwood, 1994).   In the 2002 edition of the building code ACI finally moved to a reliability-based code and joined the movement to common load and load combinations for all building materials. Statistics of resistance were developed and resistance factors were calibrated using first-order, second-moment methods to go with the ASCE Standard 7 load combinations (Nowak and Szerszen, 2003; Szerszen and Nowak, 2003).

2.3.6 Aspects of Existing Codes Considered in this Work

The two existing LRFD codes which have had the greatest impact on the design procedure for FRP strengthening presented in this report are the LRFD manuals for engineered wood (AF&PA, 1996) and for bridges (AASHTO, 2002). The wood code has been an important source of inspiration because FRP is similar to timber in that the installation and service environment can have profound effects on the in-situ properties of the FRP. From this code the idea of a reference condition with modification factors for project-specific circumstances was developed. The wood code also makes use of a time-effect factor; however, unlike wood, time-dependent degradation of the FRP is assumed to be independent of the loading history.

Given the specific focus of this report on bridge structures, the *LRFD Bridge Design Specifications* (AASHTO, 2004) and their calibration report (Nowak, 1999) have been a vital source of information regarding loading (as seen in Section 2.6).   In this respect these documents have proven vital to development of the particular example problem chosen for consideration. The calibration report has also been a valuable source of guidance with regard

to how reliability-based codes are calibrated. This report provides examples of many probabilistic techniques. While not all of the techniques have been used for the current work, this report remains a valuable starting point.

2.4 Previous Work on Reliability of FRP in Civil Infrastructure

2.4.1 FRP for Strengthening

The first study on the reliability of FRP strengthened, reinforced concrete members was conducted by Plevris et al. (1995). These authors recognized that deterministic approaches to design of FRP strengthening could not account for the statistical variation in the design variables. The study was conducted on reinforced concrete beams strengthened in flexure subjected to typical building loads. Resistance of strengthened members was characterized using Monte Carlo Simulation considering three modes of failure: steel yielding followed by CRFP rupture, steel yielding followed by concrete crushing, and for over-reinforced sections, catastrophic crushing of the concrete. Debonding of the CFRP was not considered. Statistical descriptions of the design variables were drawn from the literature. A Weibull distribution was derived to model the rupture strain of the CFRP. In order to see the relative importance of different design variables with respect to the resistance, two different nominal values were chosen for each variable. The concrete compressive strength was found to be a significant factor in both the mean resistance and the coefficient of variation of resistance.

In the study by Plevris et.al. (1995), resistance factors were calculated to achieve a target reliability of 3.0 using the design equation shown in Eq. 2-14. In this equation ϕ is a general resistance factor applied to the full nominal resistance, R_n; ϕ_{fc} is a resistance factor specific to the rupture strain of the composite, ε_{fc}^*; γ_D and γ_L are load factors on the dead, D, and live, L, loads respectively. The case where ϕ_{fc} is set equal to 1 (effectively having no FRP specific factor) was also considered. Though the target β was achieved over the entire design

space with reasonable accuracy, in order to match the target reliability very closely, the design space was divided into three types of designs based on specific combinations of values for certain design variables, and separate factors were calibrated for each type of design. The effect of different variables on the reliability index was also studied.

$$\phi R_n (..., \phi_{fc} \varepsilon_{fc}^*, ...) \geq \gamma_D D + \gamma_L L$$

Eq. 2-14

Reliability-based design of flexural strengthening was studied by Okeil, El-Tawil and Shahawy (2002) for reinforced concrete bridge girders and by El-Tawil and Okeil (2002) for prestressed bridge girders. Though these two studies considered different types of girders, they followed very similar procedures. In each study three, representative, simply-supported, interior girders were designed following AASHTO LRFD provisions. Three different damage levels were assumed for each girder corresponding to a loss of 10, 20, and 30 percent of the steel. CFRP strengthening was then designed to return each girder to its original design strength. The moment-curvature response of the strengthened girders was calculated using a model wherein the cross-section is divided into a number of layers, and a uniaxial stress-strain relation is then used to model material behavior within each layer. Response is determined using an iterative procedure that ensures equilibrium and compatibility. Resistance factors for the design of strengthening were calibrated using first-order reliability methods. The design factors were calibrated to a target of β =3.75. This is the target used by AASHTO, 3.5, plus 0.25. The reliability index was increased following the work of Allen (1992) (see Section 2.8.4.1) in an effort to account for the loss of ductility that occurs when FRP is applied to a concrete member. For both the reinforced and prestressed concrete girders the reliability was found to increase as the percentage of load carried by the FRP was increased. This increase was attributed to the very low COV assumed for the composite rupture strain, 0.022. For the

47

reinforced concrete girders one optimum value for ϕ was chosen. For the prestressed girders a function of the ratio of moment carried by the FRP to the moment carried by the prestressing was proposed to calculate ϕ.

Val (2003) studied the reliability of reinforced concrete columns wrapped with FRP. His study considered short, circular columns with primarily only small eccentricities in load. Existing empirical models describing the effect of FRP confinement on reinforced concrete columns were used to predict the strength of the wrapped columns. The uncertainty associated with these models was considered in reliability analysis by considering the constant parameters in these models as random variables. Statistics for these variables were derived based on published results of other studies. The reliability of columns confined with FRP was compared to that of unconfined columns and was found to decrease as the confinement ratio increased. A modification to the strength reduction factor for unconfined columns was proposed to make the factor applicable to columns confined with FRP. The intent of the adjusted factor is to ensure that the reliability of confined columns is at least as high as that for unconfined columns. The effect of several design ratios, such as the confinement ratio, reinforcement ratio, load eccentricity ratio, and live to dead load ratio, on the reliability index was also considered.

Monti and Santini (2002) proposed a more general approach to calibration of material partial safety factors that would apply no matter what type of strengthening application was in question. Their approach is based on computing the probability that the increase in demand is greater than the increase in capacity following strengthening. The optimization problem that results from their formulation is very difficult to solve and was simplified through the use of a simulation procedure. The authors demonstrated the use of their formulation on flexural strengthening. However they also advocated that the material partial factor should be the

same for all types of strengthening, which would require simultaneous calibration over several limit states. In their example, a PDF for the material partial safety factor was computed, leaving the question as to what percentile of the distribution should be selected for use in design. In the simulation procedure, concrete strength, steel yield strength, the neutral axis depth, and the additional load were considered as random variables. Properties of the FRP were not considered as random, but two different values were considered in a deterministic fashion.

2.4.1.1   Limitations of Existing Studies

Several features of these previous studies make them inappropriate for direct application to design. First and foremost, they all consider just one or two different types of FRP, not the full range of available products. With the exception of Val's study of strengthened columns, all of these studies imply that the material used was bonded, prefabricated FRP strips. Therefore these studies do not consider the high degree of variability that may result from field manufacture. Nor do they consider how the FRP design value is determined and how it relates to the in-situ properties of the FRP. Without a specific definition of the design value and a relation between the design value and the distributions used for reliability analysis, the calibrated design factors are meaningless. These studies do not include deterioration of the FRP due to environmental exposure or continued degradation of the structure. The studies of the flexural limit state all assume that adequate anchorage is provided to allow the FRP to reach rupture without giving any details of the anchorage mechanism. Thus, while these studies are important attempts at considering statistical variability in the design of strengthening, they do not address many of the practical issues that are involved in strengthening design and therefore are not directly applicable to future designs.

2.4.2   FRP for New Construction

Reliability-based design has also been considered for design of new structures using prefabricated FRP materials. Example applications of reliability principles to new design include FRP bridge decks, columns, and beams. These areas of application are briefly discussed below; however, as this is not the topic of the present report, the presentation is limited and should not be considered complete.

Carman (2003) studied issues associated with the reliability of prefabricated FRP bridge decks. Monte Carlo Simulation was used to evaluate the reliability of a particular bridge deck geometry. The deck was analyzed using ABAQUS with randomly generated material properties. Two limit states were examined: deflection and first-ply failure. Environmental degradation of the composite was considered with parameters based on durability testing. Due to the extreme computational demands of MCS using finite element software, the probability of failure of the deck was not computed. Instead attention was focused on the change in the probability distributions of the strength ratio and deck deflection as aging of the composite was simulated. Specific guidance for design of such bridge decks was not created; however, many issues for further consideration were identified.

Alqam, Bennett and Zureick (2004) investigated reliability-based design of concentrically-loaded FRP compression members. These authors recognized the numerous sources of variability affecting the construction of composite members and developed resistance factors based on the coefficient of variation of the composite properties. Buckling limit states were investigated for slender members, and material failure limit states were investigated for shorter members. The target reliability was set at 3.0 for buckling and 3.5 for material fracture. COVs of composite properties ranging from 0.05 to 0.25 were considered. First-order reliability methods were used to evaluate the reliability. Expressions for design of

different types of members were provided. The calibrated resistance factors decreased as the COV of the composite properties increased. For different limit states, the COV of different properties was used, depending on which property was most significant to member response.

Schniepp (2002) studied the performance of double web composite beams for use in development of a manufacture's design manual. The 914.4 mm (36 in) deep beam was tested in four-point bending at several different lengths to determine its stiffness characteristics. Special attention was given to the effect of shear on the deflection behavior of the composite. A and B basis allowables, typically applied to composites in aerospace engineering, were derived using the Weibull distribution for composite properties. There was, however, no specific calibration effort to achieve a desired reliability.

2.4.2.1   General Design Standards

Reliability-based standards for design using pultruded FRP shapes have been or are under development. In Europe, the *EUROCOMP Design Code and Handbook* (Clarke, 1996) utilizes a limit states approach to design with pultruded glass fiber composites. Little information was found regarding the reliability basis of this code; however one of the fundamental requirements for design is stated as, "A structure shall be designed and constructed in such a way that: with acceptable probability, it will remain fit for the for the use for which it is required, having due regard to its intended life and its cost" (Clarke, 1996). An older paper announcing the formation of EUROCOMP, the European Structural Polymeric Composites Group, to develop a design code for the use of polymer composites in construction, states that a level 1 reliability approach will be adopted for design, but level 2 methods will be used in development (Quinn and Godfrey, 1991).

Efforts are also underway in the United States. The Pultrusion Industry Council of the Society of Plastics Industry, Inc. has retained the American Society of Civil Engineers

51

(ASCE) to develop standards for structural design, fabrication, and erection of FRP structural components, including pultruded sheet, rod, and structural shapes (Chambers, 1997). The first phase of this work was the development of an outline for the prestandard to help guide further work. The LRFD philosophy was adopted for design. The outlined approach was based on LRFD standards for timber and steel because the material behavior is similar in some ways to that of wood, while the member shapes are closely related to steel shapes. These existing models were drawn upon to help designers learn the new design standard. It was recognized that additional, complementary standards would be needed, such as an ASTM standard for material characterization. No evidence of further work on this standard was found, suggesting that the project may have stalled. Ellingwood (2003) provided a review of the current state of knowledge regarding the basis for reliability-based design with pultruded FRP shapes. This review summarized some progress that has been made, but primarily identified the areas still requiring further research. Databases of material properties are needed for developing statistics of resistance and ASTM standards are needed to provide testing and analysis requirements for property determination. The nature of FRP materials means that serviceability concerns may be a greater issue than for traditional materials; other LRFD codes have not handled serviceability checks very well, and this problem must be remedied for FRP design. Also, a reliability target for calibration must be selected.

2.5   Statistical Descriptors for Resistance Variables

Reliability analysis requires descriptors of statistical variation for all of the variables included in design. Often reliability analysis is conducted on the basis of load and resistance; however, enough data is not currently available to characterize the resistance of FRP strengthened members at the member level. Therefore, the analysis herein will be based on descriptions of the variables affecting the member resistance. The FRP is characterized in

Chapter 3 of this report. Descriptions for all other variables are based on data available in the literature.

2.5.1 Concrete

A comprehensive analysis the random variables affecting the strength of normal weight reinforced concrete members has been provided by Mizra and MacGregor (1976). Many sources contribute to variation in concrete properties. During construction exact material proportions and properties, as well as methods of mixing, transporting, placing, and curing can all affect the end properties. Variation will also exist between properties in test specimens and properties in the structure due to the specific test conditions and the procedures for making test samples.

Mirza and MacGregor (1976) defined three levels for describing the COV of concrete: 0.10-0.15 for good control, 0.15-0.20 for average control and above 0.20 for poor control. The standard deviation and COV were found to depend on the strength of the concrete. The COV is approximately constant for concrete strengths up to about 20.68-27.58 MPa (3000-4000 psi). Beyond this range the standard deviation is approximately constant with values of 2.76, 4.14, and 5.52 MPa (400, 600, and 800 psi) for good, average and poor control, respectively. This implies that the COV decreases as the strength increases, an unsurprising result since higher control is needed to obtain higher strengths.

The Normal distribution is appropriate for modeling concrete compressive strength for COV values up to 0.15-0.20. Beyond this range the Lognormal distribution provides a better fit for the tail regions (Mirza and MacGregor, 1976). The mean compressive strength of the concrete in the structure can be predicted from the design strength using Eq. 2-15, where f_c' is

the design compressive strength of the concrete in psi.[1]   If cylinder test data is available, the COV of the concrete in-situ can be predicted using Eq. 2-16, otherwise a value must be assumed based on the level of control.

$$\overline{f_{cstructure}} = 0.675 f_c' + 1100 \leq 1.15 f_c' \, psi \qquad\qquad \textbf{Eq. 2-15}$$

$$COV_{cstructure} = \sqrt{0.10^2 - 0.04^2 + COV_{cylinders}^2} \qquad\qquad \textbf{Eq. 2-16}$$

The modulus of elasticity of the concrete is related to the compressive strength. Eq. 2-17 and Eq. 2-18 show the mean and COV of the initial tangent modulus based on the compressive strength in the structure (Mirza and MacGregor, 1976). This variable may be modeled with a Normal distribution. The secant modulus can be computed from the initial tangent modulus by assuming a parabolic stress-strain curve with a horizontal tangent at the maximum stress. The variation of the secant modulus is computed as shown in Eq. 2-19

$$\overline{E_{ci}} = 60{,}400 \, \overline{f_{cstructure}}^{\,1/2} \, psi \qquad\qquad \textbf{Eq. 2-17}$$

$$COV_{E_{ci}} = \sqrt{0.07^2 + \frac{COV_{cstructure}^2}{4}} \qquad\qquad \textbf{Eq. 2-18}$$

$$COV_{E_{cs}} = \sqrt{0.12^2 + \frac{COV_{cstructure}^2}{4}} \qquad\qquad \textbf{Eq. 2-19}$$

A more recent analysis of concrete properties was conducted by Nowak and Szerszen (2003) as part of calibration work for the ACI 318 building code. For ordinary ready-mix concrete a Normal distribution was assumed. This work was based on test data obtained from concrete companies. It was found that the bias factor (ratio of mean to nominal) was greater

---

[1] All data in Mirza and MacGregor (1976) was provided in U.S. Customary units. Dimensions have been converted to SI, however equations are left as presented in the original document.

than 1 and that the COV was approximately 0.10. An equation was provided for calculating the bias factor; however there must have been an error when the equation was published because it produces large negative values for the bias factor. This work did not consider the difference between cylinder test properties and in-situ properties. For this reason, as well as the fact that the girders used for the sample calibration described later were mainly constructed during the 1950s and 1960s, the work of Mizra and MacGregor will be used as reference for further work in this study.

2.5.2   Reinforcing Steel

Mirza and MacGregor (1976) also studied the variation in reinforcing bars. Yield strength varies from bar to bar, and mill to mill. It is also affected by the testing speed used at mills. A Normal distribution was found to fit the mid range of the data but did not fit especially well at the tails. Therefore, a modified Lognormal distribution, the Pearson Main Type I distribution, and Beta distributions were also fit to the data. The Pearson and Beta distributions were found to be appropriate for the full distribution for Grade 40 bars; only the Beta distribution was deemed a good fit to the whole range of data for Grade 60 bars.

For Grade 40 bars the Beta PDF shown in Eq. 2-20 was derived to describe steel yield strength in ksi. The Grade 40 data had a mean of 336.5 MPa (48.8 ksi) and COV of 0.107.

$$pdf(f_y) = 3.7138 \left(\frac{f_y - 36}{32} \right)^{2.2105} \left(\frac{68 - f_y}{32} \right)^{3.8157}$$

Eq. 2-20

$$(36 \leq f_y \leq 68 \ ksi)$$

For Grade 60 bars a Beta distribution with the PDF shown in Eq. 2-21 was recommended. This data had a mean of 489.8 MPa (71.04 ksi) and COV of 0.093.

$$pdf(f_y) = 7.1562\left(\frac{f_y - 57}{51}\right)^{2.0204}\left(\frac{108 - f_y}{51}\right)^{6.9545}$$

Eq. 2-21

$$(57 \le f_y \le 108 \; ksi)$$

The reduction in yield strength due to static loading should be assumed Normal with a mean of 24.1 MPa (3.5 ksi) and COV of 0.134. The modulus of elasticity of steel may be modeled as a Normal variable with a mean of 201.3 MPa (29,200 ksi) and a COV of 0.024 (Mirza and MacGregor, 1976).

Nowak and Szerszen (2003) found that steel yield strength followed a Normal distribution with a recommended bias factor of 1.145 and COV of 0.05. Mirza and MacGregor (1976) specifically discussed the use of data from a number of sources; however, Nowak and Szerszen make no mention of the source of their data. If the data of Nowak and Szerszen was all from one mill, this may account for the higher COV found by Mirza and MacGregor. Or newer manufacturing techniques may have tighter controls. In either case, the data of Mirza and MacGregor may be slightly more appropriate for older bridges in need of rehabilitation and will therefore be used herein.

2.5.3 Dimensions

Variations in the as-constructed dimensions can also affect the resistance of structures. Data on dimensional uncertainty specific to bridges was not found; the values presented here are based on general cast-in-place reinforced concrete construction, most likely from buildings. As before, the descriptions provided by Mirza and MacGregor (1976) are used in the sample calibration presented later.

2.5.3.1 Area of Steel

Mirza and MacGregor (1976) found that for bars ranging from 9.5 mm to 35.0 mm in diameter (#3 to #11 bars) the ratio of the measured area of steel to the nominal value can be modeled with a Normal distribution truncated at 0.96 and 1.06, with a mean of 0.97 and COV of 0.024. Nowak and Szerszen (2003) used a Normal distribution with a bias of 1.0 and COV of 0.015.

2.5.3.2 Slab Dimensions

Mirza and MacGregor (1976) recommend Normal distributions with the means and standard deviations shown in Table 2-3 for slabs. Nowak and Szerszen (2003) used a bias of 0.92 and COV of 0.12 for the effective depth of cast-in-place slabs.

Table 2-3 Distribution Properties for Slab Dimensions

Dimension		Nominal Range mm (in.)	Mean Deviation from Nominal mm (in.)	Standard Deviation mm (in.)
Thickness		101.6 - 203.2 (4 – 8)	+ 0.8 (+ 1/32)	11.91 (15/32)
Top Reinforcement	Effective Depth	101.6 - 203.2 (4 – 8)	- 19.05 (- 3/4)	15.89 (5/8)
	Concrete Cover		+ 19.84 (+ 25/32)	19.84 (25/32)
Bottom Reinforcement	Effective Depth	101.6 - 203.2 (4 – 8)	- 7.94 (- 5/16)	15.89 (5/8)
	Concrete Cover		+ 8.73 (+ 11/32)	10.32 (13/32)

2.5.3.3 Beam Dimensions

Mirza and MacGregor (1976) again recommend Normal distributions for variation of beam dimensions. Means and standard deviations are shown in Table 2-4. It should be noted that the recommended description of concrete cover is based on a nominal that is smaller than

57

that typically used for bridge girders. The data set they had for cover in the range of 50.8-63.5mm (2-2.5 inches) showed a standard deviation of approximately 8.38 mm (0.33 inches). Nowak and Szerszen (2003) used a bias of 1.01 and COV of 0.0004 for the width of cast-in-place beams and a bias of 0.99 and COV of 0.0004 for the effective depth.

Table 2-4 Distribution Properties for Beam Dimensions

Dimension		Nominal Range mm (in.)	Mean Deviation from Nominal mm (in.)	Standard Deviation mm (in.)
Width		279.4 – 304.8 (11-12)	+ 2.38 (+ 3/32)	4.76 (3/16)
Depth		457.2 – 685.8 (18-27)	- 3.18 (- 1/8)	6.35 (1/4)
Top Reinforcement	Concrete Cover	38.1 (1 ½)	+ 3.18 (+ 1/8)	15.89 (5/8)
	Effective Depth		- 6.35 (- 1/4)	5.67 (9/16)
Bottom Reinforcement	Concrete Cover	19.05 – 25.4 (3/4 – 1)	+ 1.59 (+ 1/16)	11.11 (7/16)
	Effective Depth		- 4.76 (- 3/16)	12.7 (1/2)

2.5.4 Modeling Uncertainty

Depending on how the reliability problem is formulated it may be appropriate to include a random variable that considers the error between the model used to describe the resistance and results from actual member tests. If the statistics of resistance are derived based on test results there is no need to consider error in the modeling process because no model is used. However, when the statistics of resistance are based on probability distributions of the variables contributing to resistance and analytical or empirical models relating those variables to the resistance, a random variable considering the accuracy of the model should be used.

The random variable describing model error can be derived by comparing test results to the calculation model in question. MacGregor, Mirza and Ellingwood (1983) formulated the model error as a Normal random variable with a mean value equal to the average value of the ratio of the tested resistance to the calculated resistance. The COV of model error is calculated using Eq. 2-22 where $COV_{T/C}$ is the coefficient of variation of the ratio of tested to calculated strengths, COV_{test} is the uncertainty in the measured loads during testing and COV_{spec} is due to errors from strength differences between the test cylinders and the test structure and variations in dimensions of the test structure. These authors used a COV_{test} of 0.02 and COV_{spec} of 0.04 for reinforced concrete beams.

$$COV_m = \sqrt{COV_{T/C}^2 - COV_{test}^2 - COV_{spec}^2}$$

Eq. 2-22

With model error formulated in this manner the limit state function can be formulated as shown in Eq. 2-23 where M is the random variable representing model error, R is the resistance random variable, and S_i are the random variables representing load.

$$g(x) = MR - \sum S_i$$

Eq. 2-23

Model error has not been considered in the current work. There have been many studies of strengthened beams upon which to base such a statistic. However, these studies have so many differences that collecting a group of representative statistics based on similar testing and calculation principles is very difficult. Determining an accurate value for model error is further complicated by the difficulty of determining the exact FRP properties in the test specimen from sample coupons. Without knowing the exact FRP properties or at least having a consistent method for computing in-situ properties, the modeling error would be

including many additional sources of error. Given the large number of assumptions already used in this work, it was not desirable to add more where not absolutely necessary.

2.6   Description of Load Variables

A basic component of any reliability analysis is a statistical description of the loads acting on the structure. In general many different types of loads act on structures simultaneously, making load combinations important in determining the maximum load acting on a structure. When considering combinations, it is highly unlikely that two different types of loading will achieve their maximum value at the same time, thus other techniques must be used to determine the maximum value of total load (Melchers, 1999). In this work only the combination of dead, live, and impact load will be considered. This is the combination of loads against which the resistance factors were calibrated for the LRFD design code (Nowak, 1999). Furthermore, the impact load will be considered as an equivalent static load that is added to the live load, and the value of the impact load will be calculated as a percentage of the live load (Nowak, 1999). Determination of the maximum load for dead and live-plus-impact loads is quite simple. The dead load is assumed constant throughout the life of the structure, and thus the maximum load occurs when that dead load is added to the maximum value of the live-plus-impact load.

Generally, a large amount of data is collected to predict the amount of variation in load components. The variation in dead loads is quantified by considering variation in member dimensions and unit weights of materials. The distribution of maximum live load during a given time period can be based on historical data. In cases where a long history of data is not available, the distribution of maximum loading for a shorter time period (for example a year) could be used to derive a distribution over a longer time period based on extreme value theory (Benjamin and Cornell, 1970). Other methods may be used to estimate the variation in the

impact load based on the dynamic properties of the structure. For the present work descriptions of both dead and live-plus-impact loads for are taken from *NCHRP Report 368* (Nowak, 1999), the report describing the calibration of the *AASHTO LRFD Bridge Design Specifications* (AASHTO, 1998). Though there are many limitations of these load descriptions, including a rather old truck weight survey and an apparent discrepancy between live loads referenced to different time frames, these load models were used to provide consistency with the LRFD specifications for new design, and because they were the most comprehensive models available.

2.6.1 Dead Load

The dead load for bridge elements is divided into four components by Nowak (1999), based on the level of variation in the loads. The four components are the weight of factory made elements, the weight of cast-in-place concrete members, the weight of the wearing surface, and miscellaneous weight such as railings and lighting. T-beam reinforced concrete bridges are composed entirely of cast-in-place concrete and no data is available regarding the weight of miscellaneous additions, therefore only the cast-in-place weight and wearing surface weight are considered. Both of these load components are modeled with a Normal distribution. The cast-in-place component has a bias factor of 1.05 and a COV of 0.10. The wearing surface is assumed to have a mean thickness of 89 mm (3.5 inches) and COV of 0.25.

2.6.2 Live and Impact Loads

As a limit states design procedure, LRFD compares the resistance capacity of a structural element with regard to a particular mode of behavior to the load *effects* acting on the element in that mode. Therefore, for example, the shear capacity is compared to the shear effect produced by the design loads. The statistical models for live load presented in Nowak (1999) are based on the relation between the true load effect caused by heavy vehicles moving

across the bridge and the load effect predicted by the models used for design. Two load models for design are discussed in the calibration report: the HS-20 model, which is used by the AASHTO Standard Specifications to model truck loads, and the new HL-93 load model, which was developed during the calibration process for use in the new LRFD specifications. Aspects of these models significant to the calculation of maximum positive moment (the limit state considered in the calibration example) are shown in **Table 2-5** and Figure 2-4. Many different parameters, such as the span of the bridge, total weight of vehicles, configuration of vehicle weight, position of vehicles, the possibility of multiple vehicles and the properties of the structure, affect the computation of load effects on bridges. The HL-93 model was adopted because it gives a more uniform relation between design loads and actual loads for different span lengths (Nowak, 1999).

Table 2-5 Comparison of HS-20 and HL-93 Load Models for Calculation of Maximum Positive Moment

	HS-20 (AASHTO, 2002)	HL-93 (AASHTO, 1998 and 2004)
Width of Traffic Lane	3600 mm (10 ft)	3600 mm (10 ft)
Maximum Load Effect	-Design Truck (see Figure 2-4) *or* -Lane loading with concentrated load (meant to simulate truck loads, but simplify computation) *or* - Alternate Military Loading	- Design Tandem plus Design Lane Load *or* -Design Truck (see Figure 2-4) plus Design Lane Load
Lane Load	9.3 N/mm (0.64 kip / ft) uniformly distributed longitudinally	9.3 N/mm (0.64 kip / ft) uniformly distributed longitudinally
Concentrated Load	Used in combination with lane loading -80,000 N (18 kip) when calculating moment -116,000 N (26 kip) when calculating shear	N/A
Alternate Military Loading / Design Tandem	Two 110,000 (24 kip) axles spaced 1200 mm (4 feet) apart	Two 110,000 N (25 kips) axles spaced 1200 mm (4 feet) apart with transverse wheel spacing of 1800 mm (6 feet)
Impact	$I = \dfrac{50}{L+125}$ I = impact fraction (max 0.3) L = span length in feet	33% this is not applied to the lane load portion of the live load

Notes:
- For both load models, the loads shall be positioned so as to induce the maximum load effect, and axles that do not contribute to the extreme load effect shall be neglected.
- HL-93 quantities are straight from the specifications for both sets of units; the HS-20 units were originally in U.S. Customary units but were converted and rounded.
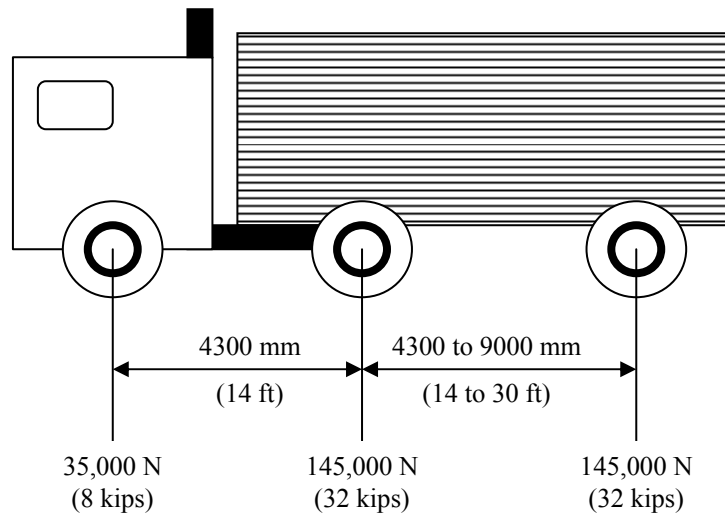
The transverse wheel spacing is 1800 mm (6 ft)

Figure 2-4 Design Truck for HS-20 and HL-93 Load Models

The load effects studied in Nowak (1999) are those acting on girders and include the maximum positive moment in simple spans, the maximum negative moment for two equal continuous spans, and the maximum shear. (Due to limitations in the analytical models for shear strengthening, only flexural strengthening is considered in this work. Strengthening in negative moment regions cannot be achieved through the wet layup process and therefore is not considered herein. Thus only load effects for positive moments are used.) Based on truck survey data, load effects for many different span lengths were computed and then compared to the load effect predicted for that span by the load model used for design, HL-93. Normal distributions were fit to the ratio of the truck moment to the design moment and extrapolated to provide distributions of loading for extended time periods. The study then examined the effect of multiple trucks, either side by side or following each other, using simulations to compute maximum moments and shears. The ratios of the mean maximum load effects for different lengths of time to the load effects predicted using the HL-93 load model were computed as a function of the span length of the bridge. Values of these ratios for positive

moment on simple spans for lengths and time periods of possible interest in this study are shown in Table 2-6.

Table 2-6 Ratio of Mean Maximum Moments to HL-93 Moments

Span Length m (ft)	1 year	5 years	50 years	75 years
9.14 (30)	1.19	1.26	1.35	1.35
12.19 (40)	1.23	1.28	1.35	1.35
15.24 (50)	1.22	1.25	1.33	1.33
18.30 (60)	1.21	1.24	1.32	1.32
21.34 (70)	1.21	1.25	1.31	1.31
24.38 (80)	1.21	1.25	1.32	1.32

The values in Table 2-6 are for the moment per girder based on girder distribution factor equations developed by Zokaie, Osterkamp, and Imbsen as part of NCHRP Project 12-26 (Nowak, 1999). The original equations were developed based on a wheel line (rather than lane load) and the multiple presence factors used in the *Standard Specifications for Highway Bridges* (AASHTO, 2002). These equations were then adjusted to apply to the new conditions in the LRFD standards and can be found in their adjusted form in Table 4.6.2.2.2b-1 of the *AASHTO LRFD Bridge Design Specifications* (AASHTO, 2002) for moment in interior beams (Zokaie, 2000).

The maximum load anticipated for certain lengths of time depends on the amount of traffic crossing the bridge. The values in Table 2-6 are representative of average daily truck traffic (ADTT) equal to 1,000 vehicles in one direction. For ADTT of 5,000 these factors should be increased by 5% and for ADTT of 500 they should be reduced by 5% (Nowak, 1999).

It is anticipated that strengthening projects will have a range of required service lives. It is unlikely that strengthening will be expected to last as long as new construction, and maximum efficiency can be achieved by designing to meet the appropriate service life. In particular, design lives of 10, 20, 30, 40, and 50 years are considered in this report. These time spans were not considered by Nowak in calibration of the LRFD standards, and thus are not included in *NCHRP Report 368* (Nowak, 1999). A brief summary of the difficulties encountered with the derivation of time-span specific load models follows, a more detailed account is provided in Appendix A.

An attempt was made to derive distributions for the intermediate time spans based on the one-year distribution and simple use of extreme value theory; however this attempt did not produce results consistent with the load models presented by Nowak (1999). For example when the one-year distribution of the live load bias factor was used to predict the five-year distribution, the mean value of the fitted Normal distribution was 1.40 compared to 1.25 provided by Nowak. The predicted COV was 0.075 compared to approximately 0.12 reported in the calibration report. Furthermore, the LRFD calibration conducted by Nowak was based on the use of a Normal distribution to model the 75-year maximum loading. If the one-year distribution is modeled as a Normal variable, then, based on extreme value theory, when it is used to predict the 75-year distribution, the 75-year distribution should approach a Gumbel distribution, not a Normal distribution (Bury, 1999). Given these difficulties with defining a load model, a comparison of three different techniques for modeling load was conducted to assess their effect on the final reliability. In one method, the reliability at fifty years was estimated using the one-year distribution and the reliability technique shown in Eq. 2-11; however this result was not consistent with that computed using the time-integrated fifty-year loads in the calibration report. A simple solution to these inconsistencies was not readily

apparent. It was decided to use the data that was directly available in the calibration report, to provide consistency between the design of new and strengthened girders. Therefore the distribution for 50-year maximum loading is used to represent the load variation for all design lives. This contributes further to the conservatism of the time-integrated reliability procedure and suggests that load model development for different design lives should be a subject of considerable future research.

The dynamic load acting on bridges is modeled as an additional static load equal to a certain percentage of the live load. During LRFD calibration extensive simulations considering truck configuration, dynamic properties of the truck and bridge, and road surface roughness were used to assess the value for the dynamic impact factor (Nowak, 1999). As a result of these simulations, the mean value of the dynamic load as a percentage of the live load was taken as 0.10 for two trucks and 0.15 for one truck, with a COV of 0.80 for both cases. These values were used for the reliability calculations underlying the development of the design code. A conservative value of 0.33 applied only to the truck effect of the HL-93 model was proposed for design (Nowak, 1999).

The combined live and impact loads are modeled as a Normal distribution. The mean value is equal to the value of maximum moment predicted for the span by the HL-93 load model multiplied by the appropriate bias factor in Table 2-6 and by the dynamic load factor of 1.1. The COV of these combined loads is computed considering the variation in the live load, the live load analysis factor (which considers error present in using girder distribution factors), and the impact load. For two-lane bridges the value of COV is equal to 0.18 for most spans (Nowak, 1999).

2.7 Consideration of Continued Degradation

2.7.1 Modes of Reinforced Concrete Degradation

Several different phenomena may contribute to the deterioration of strength capacity in reinforced concrete structures. As identified in Bertolini et al. (2004), the concrete itself can be subject to damage from physical, mechanical, structural, chemical, or biological attack. Examples of these different types of attack are shown in Table 2-7.

Table 2-7 Causes of Deterioration of Concrete (Bertolini et al., 2004)

Sources of Degradation	Example
Physical	Freeze-thaw cycling, fire
Mechanical	Abrasion, erosion, impact, explosion
Structural	Overloading, settlement, cyclic loading
Chemical	Alkali-aggregate reactions, acid attack, sulfate attack, attack by pure water
Biological	Biogenic attack, fouling

Degradation of the reinforcement can also cause a loss of structural strength. Corrosion weakens the structure by reducing the cross-sectional area of the steel, causing spalling and delamination of the concrete, and reducing the bond between steel and concrete (Gulikers, 2005). Corrosion and concrete deterioration are closely related. Degradation of the concrete can expose the steel to corrosive environments by eliminating cover and/or reducing the protective characteristics of the concrete. Corrosion of steel creates expansive products that can cause cracking and delamination of the concrete (Betrolini et al., 2004). According to Gulikers (2005) "There is general agreement that corrosion of the reinforcement steel is the most prevalent form of deterioration of the infrastructure necessitating vast amounts of money for rehabilitation and repair."   Due to the importance of corrosion as a deterioration

mechanism and the availability of analytical models for the effect of corrosion on reinforcement, this is the only type of bridge deterioration that will be considered in this work.

2.7.2   Corrosion of Steel in Concrete

The interior pores of cured concrete are generally filled with a highly alkaline pore solution. This solution has a pH over 12.5, and in this environment a thin, passive oxide layer is developed on the surface of the reinforcing steel (Bertolini et al., 2004; Hunkeler, 2005). As long as this layer is maintained the steel is immune to further corrosion. The steel may be depassivated by a drop in the pH caused by carbonation of the concrete cover, or by chloride attack (Bertolini et al., 2004, Hunkeler, 2005). A well-known and generally accepted model of corrosion of steel in concrete was developed by Tuutti (1982). In this model there are two stages of corrosion: initiation and propagation. The initiation stage spans from the time of construction until the reinforcement is depassivated, and the propagation stage extends from the time of depassivation until some limit of performance is reached.   This model is shown schematically in Figure 2-5
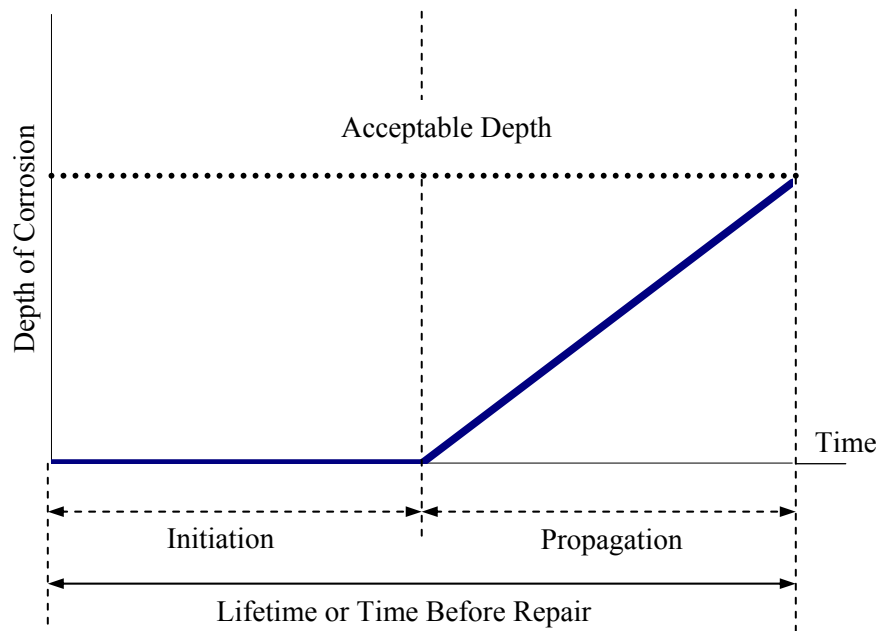
Figure 2-5 Tuutti's (1982) Model for Sequence of Steel Corrosion in Concrete

Corrosion is an electrochemical process that can be simply expressed by Eq. 2-24 (Bertolini et al., 2004).

$$iron + oxygen + water \rightarrow products\ of\ corrosion$$

Eq. 2-24
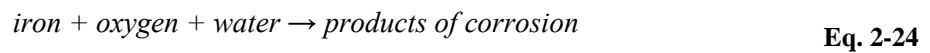
The process of corrosion can be described through four partial processes (Bertolini et al., 2004; Hunkeler, 2005).

- An anodic reaction occurs at the surface of the metal when the passive layer breaks down. This process frees electrons from the iron, producing iron ions.

- A cathodic process occurs at another region of the metal where oxygen is reduced in the presence of water, consuming the electrons freed at the anode.

70

- Electrons are transported through the metal from the anode to the cathode.

- To complete the circuit, the concrete between the cathode and anode must be conductive (provided by ions in the pore solution).

These processes must all occur at the same rate; therefore the partial process with the highest level of resistivity will control the flow of current and thus the rate of corrosion (Bertolini et al., 2004). The steel reinforcement is highly conductive; therefore the transfer of electrons through the metal is never the rate controlling process. The process at the anode is slow during the time when the passive layer is intact, but is not a controlling factor after depassivation. The cathodic process is controlled by the availability of oxygen, and the conductivity of the concrete is primarily controlled by the moisture content. Therefore, once corrosion has been initiated, moisture content is generally the dominant factor in determination of the corrosion rate. In very dry conditions the concrete has a high resistance, slowing corrosion, and in saturated conditions oxygen diffusion to the level of the rebar is very slow, limiting the cathodic process. Peak corrosion conditions are usually near a relative humidity of 95% (Bertolini et al., 2004). However, many other factors contribute to both the initiation time and the corrosion rate, including the porosity of the concrete, which is affected by the type of cement and water-cement ratio, the thickness of cover, and the ambient temperature (Tuutti, 1982; Bertolini et al., 2004).

2.7.2.1 Carbonation-Induced Corrosion

Concrete becomes carbonated through the reaction of the alkaline components of the cement and carbon dioxide from the atmosphere (Hunkeler, 2005). This process begins at the surface of the concrete and gradually moves toward the interior. As the process proceeds the pH of the pore water is reduced to somewhere in the range of 6-9 (Hunkeler, 2005). At these pH levels the passive layer on the steel is no longer stable and corrosion can begin (Bertolini

et al., 2004). Carbonation usually affects large areas of the steel reinforcement, resulting in general corrosion throughout the structure.

2.7.2.2   Chloride-Induced Corrosion

Corrosion of steel reinforcement is frequently caused by the presence of chlorides. Chlorides promote corrosion in 4 ways: they destroy the passive film on the rebar, they reduce the pH of the pore water, they increase the moisture content through the hygroscopic properties of salts, and they increase the conductivity of the concrete (Hunkeler, 2005). In order for chloride-induced corrosion to occur, the chloride content of the concrete at the level of the steel must reach a threshold value. This threshold depends on several factors; however the ability of oxygen to reach the reinforcement seems to be particularly important (Bertolini et al., 2004). Chlorides can be introduced to the concrete through the constituents used to manufacture the concrete (such as aggregates taken from the ocean or as an admixture to promote accelerated setting of the concrete) or through external exposures, such as marine environments or de-icing salt application (Bertolini et al., 2004). Now that the dangers of chlorides are understood, significant steps are taken to limit their introduction at the manufacturing stage, but they remain a concern for older structures.   Chloride-induced corrosion generally produces more localized effects, often called pitting corrosion.

2.7.2.3   Rates of Corrosion

The most important parameter for describing corrosion propagation is the corrosion rate, which is often expressed as a current density. Using Faraday's law of electrochemical equivalence, a corrosion current density of 1 $\mu A/cm^2$ (6.45 $\mu A/in^2$) can be found equivalent to a uniform penetration of 11.6 $\mu m/yr$ (4.567 x 10^{-4} in/yr) (Val 2000). Many researchers have presented approximate values of corrosion rates representing different situations and different

levels of severity. The rates shown in Table 2-8, and typical conditions corresponding to these

rates are provided in (Bertolini et al., 2004).

Table 2-8 Rates of Corrosion Penetration of Steel in Concrete (Bertolini et al., 2004)

Level of Corrosion	Rate μm/yr (in/year)	Typical Conditions
Negligible	< 2 (< 7.874 x 10^{-5})	Concrete non-carbonated and without chloride or contaminated concrete that is saturated or dry (R.H. < 50% for chlorides, R.H. < 70% for carbonation)
Low	2-5 (7.874 x 10^{-5} – 1.968 x 10^{-4})	Concrete with chloride contamination R.H. = 50-80%
Moderate	5-10 (1.968 x 10^{-4} – 3.937 x 10^{-4})	Carbonated concrete R.H. = 70-90%
Intermediate	10-50 (3.937 x 10^{-4} – 0.001968)	Concrete with chloride contamination R.H. = 80-90% Carbonated concrete R.H. = 90-95%
High	50-100 (0.001968 – 0.003937)	Concrete with chloride contamination R.H. = 90-95% Carbonated concrete R.H. = 95-98%
Very High	>100 (>0.003937)	Concrete with chloride contamination R.H. = 95-98%

Roelfstra et al. (2004) suggest corrosion rates for chloride-induced corrosion based on

the quality of the concrete cover and the exposure environment. These rates are shown in

Table 2-9.   Three classes of cover are defined, A, B, and C, by their water and chloride

diffusion coefficients, with A being the most impermeable and C being the most permeable.

The exposure is also divided into three categories, mist, splash, and direct, based on the

contact the surface would have with water during rainfall. The suggested penetration rates are

based on current densities found in a study of pitting corrosion by González et al. (1995).

Table 2-9 Rates of Corrosion Penetration Based on Concrete Cover and Exposure Condition

Concrete Cover Class	Corrosion Penetration Rate μm/yr (in/yr) Exposure Zones		
	Mist	Splash	Direct
A	4 (1.575 x 10^{-4})	20 (0.000787)	20 (0.000787)
B	4 (1.575 x 10^{-4})	20 (0.000787)	20 (0.000787)
C	20 (0.000787)	80 (0.00315)	80 (0.00315)

Gulikers (2005) presents both empirical and electrochemical based models for corrosion behavior. However, both types of models require extensive knowledge of the environmental conditions and electrochemical behavior of the materials, making them impractical for use in a general study of corrosion.

2.7.3 Previous Work Modeling Corrosion-Induced Degradation in Bridges

Corrosion in reinforced concrete is a topic of extensive and ongoing research far beyond the scope of this particular report. However, several researchers have studied the effect of corrosion on the reliability of reinforced concrete structures, particularly bridges. Some authors have approached this topic from a pure reliability standpoint, generally selecting a few variables affecting corrosion for particular study. Val and Melchers (1997) considered a simple slab bridge subject to either uniform or pitting corrosion. Their model considered loss of bond between the concrete and reinforcement in the case of general corrosion and the variability in pit depths for pitting corrosion. Based on their modeling assumptions they found that generalized corrosion is more detrimental to the structure at earlier lifetimes, but at approximately 50 years following initiation, pitting corrosion becomes more critical. In 1998 Stewart and Rosowsky considered the effect of chloride exposure through application of deicing salts or proximity to marine environments. They modeled chloride transport through the concrete through both diffusion and flexural cracking on a three-span, concrete slab bridge

(Stewart and Rosowsky, 1998a). By considering the diffusion of the chlorides or the time to development of critical crack widths, this study took into account the initiation time in considering the change in reliability of the structure over time. In another paper, these authors also examined how knowledge of the occurrence of spalling or past successful service could be used to update the reliability of the structure regarding a strength limit state, as well as the influence of concrete cover and compressive strength on the reliability (Stewart and Rosowsky, 1998b). In 2000 Val, Stewart, and Melchers considered the effect of corrosion on the probability of reaching strength and serviceability limit states and provided a method to update the statistical distributions of resistance variables based on data collected during a bridge inspection. Vu and Stewart (2000) advanced the reliability analysis of deteriorating bridge decks by using a corrosion model based on properties of the concrete (water-cement ratio and amount of cover) and using distributions of resistance updated based on previous survival of the structure. Stewart and Val (2003) analyzed the effect of loss of concrete section due to spalling, by modeling cracking due to production of corrosion products, and considered the life-cycle costs of maintenance on deteriorating structures. Stewart (2004) also studied the effect of spatial variability of pitting corrosion, since the location of very deep pitting may not necessarily coincide with the location of maximum load effect.

Other authors have examined bridge reliability in the context of developing bridge management systems, which attempt to prioritize maintenance spending to maximize the benefit to a given bridge network. Frangopol has worked with many other authors to develop bridge management strategies based on reliability theory. A brief summary of the reliability-based approach to bridge management is presented in Frangopol et al. (2001). In specifically considering the effect of corrosion on bridge reliability Enright and Frangopol (1998a) modeled corrosion with a resistance degradation function and used system reliability methods

75

to assess the effect of resistance variables on the reliability of bridge decks. These authors also studied the effect of different variables on the time to corrosion initiation (Enright and Frangopol, 1998b). Stewart, Estes, and Frangopol (2004) considered life-cycle costs of concrete bridge decks subject to corrosion and compared the present value of repairs due to violations of both strength and serviceability limit states. They found that when serviceability limits are included in the analysis, repair costs are higher than when only strength limit states are included. Though Roelfstra et al. (2004) did not explicitly consider the reliability of bridges, they did attempt to probabilistically model corrosion-induced degradation for use in existing bridge management software. A typical procedure in bridge management systems is to define condition states of a bridge and use Markov chains to predict the transition of bridge members from one condition state to another. These authors modeled degradation due to corrosion using models of chloride diffusion and corrosion propagation and then fit Markov chain parameters to the modeled degradation.

2.7.4 Corrosion Models Used in this Report

In this report corrosion is modeled simply as an example of a mechanism causing continued deterioration of strengthened structures. The work described herein has not sought to advance the state of knowledge regarding corrosion, but rather to draw from existing models and theories to provide an example of structural degradation. With this objective in mind, many simplifying assumptions have been made based on practical considerations of modeling corrosion. Mathematical expressions for corrosion that are based on simple design variables have been chosen.

2.7.4.1 Major Assumptions for Corrosion Modeling

Later sections of this work are based on an assumed deficit of reinforcing steel. Three different deficit levels are chosen as examples. Two cases of continued degradation are then

considered for each deficit level. One case assumes that the steel deficit was either not due to corrosion or that remediation has occurred, effectively slowing the corrosion rate to zero. The other case assumes that corrosion continues after the application of strengthening. Based on this scenario, it is assumed that when strengthening is applied the corrosion process has already been initiated. Therefore the initiation phase of the corrosion process is neglected completely.

In this work the effect of corrosion is considered only in terms of the loss of steel area at the critical cross-section. Loss of steel/concrete bond and the effect of spalling are ignored. This assumption can be justified to some extent based on the specific example of flexural strengthening used for this work. Val, Stewart, and Melchers (1998) found that complete loss of bond had little effect on the reliability in the ultimate flexural limit state, however may be significant in consideration of serviceability limit states. Furthermore, the beams considered in this work are subject to strengthening only in positive moment regions, and corrosion is assumed to occur only in bottom reinforcing bars. (Negative moment regions are not considered due to the difficulties of placing FRP in these areas.) This implies that spalling of concrete may be neglected because spalling at the bottom surface will not reduce the compressive capacity of the section.

An important aspect of this work has been in explicitly considering different possible service lives for the strengthening. For purposes of the current example, lifetimes of 10, 20, 30, 40, and 50 years have been considered. Val, Stewart, and Melchers (1998) only considered the propagation phase of corrosion and found that localized pitting corrosion did not severely affect the reliability until after approximately 50 years. In a small example calibration conducted as part of the current work to judge the effect of including corrosion (described in Section C.8 of Appendix C), it was found that general corrosion caused a greater

77

loss in steel cross-sectional area for the time periods in question. General corrosion is also likely to be more severe for the current example due to the relatively larger bar sizes used in bridge construction. Based on these facts, only general corrosion is modeled in this work. Because general corrosion is assumed, the effect of spatial variability as studied in (Stewart, 2004) is ignored. Furthermore, it is assumed that corrosion affects all bars of the bottom reinforcement equally. This ignores the possibility that only the bottom-most layer of bars is corroding or that a macrocell has formed corroding an active bar and actually protecting a passive bar (Bertolini et al., 2004).

2.7.4.2 Mathematical Models for Corrosion

The particular model chosen for predicting the current density, i_{corr}, in the current work is provided in Vu and Stewart (2000) and shown in Eq. 2-25, where w/c is the water-cement ratio of the concrete and the cover is expressed in mm (this was incorrectly stated to be cm in the paper by Vu and Stewart).

$$i_{corr} = \frac{37.8(1 - w/c)^{-1.64}}{cover}(\mu A/cm^2)$$
<div align="right">**Eq. 2-25**</div>

Though Vu and Stewart modeled a decrease in the corrosion rate with time, for the present work the corrosion rate is assumed constant for the full time period under consideration. Furthermore, no model error for this equation is included in the present reliability study.

For probabilistic modeling purposes, the water-cement ratio may be considered directly correlated to the compressive strength of the concrete. Bolomey's formula, as presented in Vu and Stewart (2000) is shown in Eq. 2-26. In this equation f'_{cyl} is the compressive strength of a standard cylinder expressed in MPa.

$$w/c = \frac{27}{f'_{cyl} + 13.5}$$

<div align="right">**Eq. 2-26**</div>

A website describing the concrete mix design process lists approximate water-cement ratios for different concrete strengths; these values are shown in Table 2-10 (Ghalyand Almstead, 2005).

Table 2-10 Approximate Relation between Concrete Strength and Water-Cement Ratio

Concrete Strength MPa (ksi)	Water-Cement Ratio
41.37 (6)	0.41
34.47 (5)	0.48
27.58 (4)	0.57
20.68 (3)	0.68
13.79 (2)	0.82

Both of these approximate relations between the concrete compressive strength and water-cement ratio are plotted in Figure 2-6. The trends are similar, however the website data has generally lower values for *w/c*.
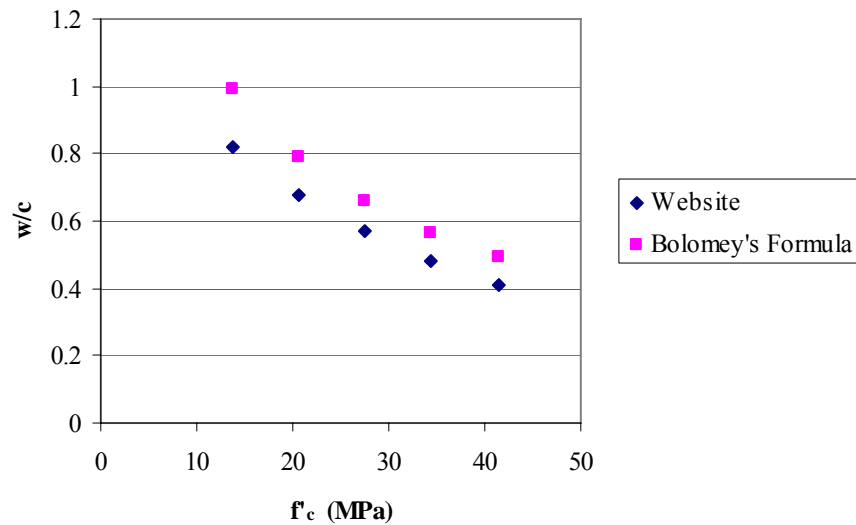
Figure 2-6 Relation between Concrete Compressive Strength and Water-Cement Ratio

Both of these sources provide reasonable estimates of the water-cement ratio for concrete of moderate strength. However, the bridge girders used in the calibration example described in Chapter 5 were all constructed of nominally 22.4 MPa (3.25 ksi) concrete. At these low strengths the predicted water-cement ratio is very high. The high water-cement ratios did not appear representative of actual concrete construction; and they also produced higher levels of corrosion than were desired for this work when used in Eq. 2-25. Therefore the water-cement ratio was assumed to be an independent, Normally distributed random variable with a mean of 0.45 and COV of 0.05. Since all of the concrete girders used in the calibration example had the same strength concrete and nearly all had the same amount of cover, effectively only one corrosion rate is considered in the calibration example.

From the random corrosion rate the new area of reinforcing steel is computed deterministically based on the nominal diameter of the steel bars. Corrosion is considered as a uniform loss in diameter, therefore the diameter after corrosion is calculated as shown in Eq.

2-27, where D_o is the initial diameter, P_{av} is the uniform penetration rate in units of length per time (calculated from i_{corr} using Faraday's law of electrochemical equivalence), and t is the time since corrosion initiation expressed in consistent units of time. The new area is then used to assess the remaining capacity of the member at the critical section.

$$D_{bar} = D_o - 2 \times P_{av} \times t$$

Eq. 2-27

2.8 Target Reliability Index

The reliability target is a key element in calibration of design factors. The task of selecting a target reliability is complicated by the fact that the reliability methods described in Section 2.2 consider only statistical variation in loads and material resistances, while in fact most structural failures result directly from human actions. Melchers (2001) has identified three main causes of structural failure: undetected errors during design, documentation, or construction; an organizational (accidental) error or deficiency occurring during design, construction, or use of the structure; or intentional (illegal) loading or overloading of the structure. Because the effect of human error is not included in reliability calculations, the observed probability of structural failure, while still very low, is much higher than that predicted by reliability methods, which is often referred to as the nominal or notional probability of failure. Due to the limitations of reliability methods, the target reliability selected for use in design cannot be chosen as the allowable probability of failure. Furthermore, the target chosen for code calibration must allow for the fact that the code will apply to a whole class of structures and must consider the approximations that will be necessary to make the code accessible to the general designer (Melchers 2001). There are many approaches to selection of a target reliability index, β_T. These different approaches are briefly discussed before the target reliability for the remainder of this work is set.

2.8.1 Comparison to Other Acceptable Levels of Risk

One suggestion has been to determine acceptable levels of structural failure by studying levels of risk considered acceptable for other human activities. Table 2-11 shows some common risks as well as typical annual probabilities of collapse for buildings and bridges (Ellingwood, 1994).

Table 2-11 Comparison of Common Risks and Structural Failure Probabilities

Action	Typical Risk of Death Per Year
Cigarette Smoking	3.6×10^{-6}
Motor Vehicle Accidents	2.4×10^{-4}
Homicide	1.0×10^{-4}
Fires	1.4×10^{-5}
Building Collapse	1.0×10^{-6}
Bridge Collapse	1.0×10^{-4}

Setting the target reliability in this manner is difficult because there is no accepted method to compare risks due to different sources, and this method does not consider the difference between notional and actual failure probabilities (Ellingwood, 1994). Furthermore, calibration for design code procedures is based on failure, not of a complete structure, but of a particular structural member in a particular mode. For example, calibration of resistance factors for design of bridge girders was conducted for positive moment, negative moment, and shear loads (Nowak, 1999). Relating an acceptable risk of structural failure to the corresponding risk in a particular element is virtually impossible for realistic structures. Thus, while this approach may suggest a general range for consideration, it is not really suitable for choosing a target for design purposes.

2.8.2 Optimization of Cost-Benefit

A rational approach to selection of a target reliability index is to consider it as a parameter subject to optimization (Madsen et al., 1986). In this case the target reliability can be chosen as the value providing an optimum balance between the marginal cost of increasing safety and the marginal reduction in the risk-associated costs of failure. This type of optimization is practical when the costs associated with failure are primarily economic and not related to loss of life or injury (Madsen et al., 1986). However, in reality there is almost no data available upon which to base such an optimization (Szerszen and Nowak, 2003). This method is particularly difficult since reliability-based design is conducted at the member level while optimization might be conducted at the structural level. This may be the way safety levels are determined in the future, but is not yet feasible.

2.8.3 Empirical Approaches

Based on analysis of other risks, some empirical approaches have been suggested for determining a target probability of failure. One method was proposed by the Construction Industry Research and Information Association (CIRIA) in 1977 (Melchers, 1999). The notional target probability of failure can be determined from Eq. 2-28. In this equation μ is a social criteria factor (equal to 0.005, 0.05, and 0.5 for places of public assembly and dams; domestic, office, trade, and industrial buildings; and bridges, respectively), t_L is the structural design life in years, and n is the average number of people within or near the structure when it is in use.

$$p_{fN} = 10^{-4} \mu t_L n^{-1}$$

Eq. 2-28

Using μ equal to 0.5, sample probabilities of failure for bridges and corresponding reliability indices (based on the Normal approximation) are found, as shown in Table 2-12.

Table 2-12 Target Failure Probabilities and Reliability Indices Based on CIRIA

p_f		t_L				
		10	25	50	75	100
	25	0.00020	0.00050	0.00100	0.00150	0.00200
n	50	0.00010	0.00025	0.00050	0.00075	0.00100
	75	0.00007	0.00017	0.00033	0.00050	0.00067
	100	0.00005	0.00013	0.00025	0.00038	0.00050

β		t_L				
		10	25	50	75	100
	25	3.54	3.29	3.09	2.97	2.88
n	50	3.72	3.48	3.29	3.17	3.09
	75	3.82	3.59	3.40	3.29	3.21
	100	3.89	3.66	3.48	3.37	3.29

From these results several general reliability principles are apparent. As the number of people near the structure increases, the allowable probability of failure should decrease. Structures with shorter design lives should have a lower probability of failure during their lifetime. In the case shown here, the average annual probability of failure for all design lives is approximately equal, however the lifetime probability of failure is much smaller for the structure with a design life of only 10 years compared to that for 100 years.

Another method has been proposed by Allen (1981). The target probability of failure suggested by this method is calculated as shown in Eq. 2-29.

$$p_{fN} = 10^{-5} A W^{-1} t_L n^{-1/2}$$

Eq. 2-29

Here A is the activity factor, W is the warning factor, and the other variables are as defined earlier in the CIRIA method. The activity factor is taken as 3.0 for normal activities

on bridges. The warning factor is 0.1 for gradual failure with some warning likely, 0.3 for gradual failure hidden from view, and 1.0 for sudden failure with no previous warning. The nominal probabilities of failure proposed by Allen's method are shown in Table 2-13 for $W =$ 0.1. The results follow similar trends to those seen the CIRIA method; however the allowable probabilities of failure are generally higher. Both methods suggest reliability indices smaller than the value of 3.5 used for the AASHTO LRFD calibration; although, if more people were assumed to be in the vicinity of the bridge, the target indices in both cases would increase.

Table 2-13 Target Failure Probabilities and Reliability Indices Based on Allen (1981) W=0.1

p_f W=0.1		t_L				
		10	25	50	75	100
n	25	0.00600	0.01500	0.03000	0.04500	0.06000
	50	0.00424	0.01061	0.02121	0.03182	0.04243
	75	0.00346	0.00866	0.01732	0.02598	0.03464
	100	0.00300	0.00750	0.01500	0.02250	0.03000

β		t_L				
		10	25	50	75	100
n	25	2.51	2.17	1.88	1.70	1.55
	50	2.63	2.30	2.03	1.85	1.72
	75	2.70	2.38	2.11	1.94	1.82
	100	2.75	2.43	2.17	2.00	1.88

Lifetime reliability levels based on the type of failure and the consequences of failure were proposed in 1978 by the Nordic Committee on Building Regulations (Sarveswaran and Roberts, 1999). These criteria are shown in Table 2-14.

Table 2-14 Target Reliability Levels and Corresponding Lifetime Probabilities of Failure from Nordic Report

Failure Consequences	Ductile Failure with Reserve Strength	Ductile Failure without Reserve Strength	Brittle Failure
Not Serious	3.09 (10^{-3})	3.71 (10^{-4})	4.26 (10^{-5})
Serious	3.71 (10^{-4})	4.26 (10^{-5})	4.75 (10^{-6})
Very Serious	4.26 (10^{-5})	4.75 (10^{-6})	5.20 (10^{-7})

These empirical approaches can provide guidance for selecting the general range of the target reliability. They may be especially valuable for new applications where there is little other information upon which to base such a decision.

2.8.4 Calibration to Safety Levels Implied by Existing Codes

Most of today's LRFD codes have been calibrated based on the reliability indices implied by existing design codes. Representative members designed using the older design specification (usually in the allowable stress format) are chosen, and their reliability is calculated using the same assumptions and models that will be used to determine the reliability-based design factors. Usually there is quite a range of indices, and a subjective "average" is typically chosen as the target reliability. This approach is very attractive because, when β is used as a strictly comparative measure, issues with modeling of random variables are not as significant, i.e. the tail sensitivity problem is largely reduced or eliminated (Melchers, 1999). This has been shown to be a very robust calibration method (Moses, 2001). Even if changes are made to the statistical modeling assumptions, those changes are applied to determining the target β as well as calibrating the new factors. Since the changes are applied everywhere, the calibrated design factors are relatively stable. This would not be the case for a target β that was chosen on a subjective basis alone. The problem encountered with FRP strengthening is that there is no long-standing history of successful designs upon which to

base the target reliability. The target reliabilities used in current design can be used as an indicator, but it is important to remember that in this case β cannot be used as a strictly comparative measure.

2.8.4.1 Reliability Indices from Other LRFD Codes

A target value for β may be determined by comparison to the target used for other reliability-based codes. Table 2-15 shows a comparison of reliability targets currently used for design with different materials. In addition to having different reliability targets, different codes also have different assumed structural lifetimes. To facilitate comparison the estimated average annual probability of failure is also provided. This estimate is based on the assumption that the annual probability of failure is the same for each year, a reasonable assumption if the variation in loading is relatively more significant than the variation in material properties (Ellingwood, 2000b). Since the intent behind the use of FRP is the extension of service-life of an existing structure care needs to be taken to ascertain the desired service-life of the rehabilitated structure and whether reduced reliability levels are acceptable based on location, type of use, and required remaining service-life.

Table 2-15 Target Reliability Indices and Corresponding Annual Probabilities of Failure for Other Structural Design Codes

Material and /or Structural Type	Target β	Design Life	Annual Probability of Failure
Wood Members in Flexure (AF&PA, 1996)	2.4	50 years	1.646×10^{-4}
Steel (braced compact beams in flexure, tension members at yield) members (AISC, 1998)	2.6	50 years	9.343×10^{-5}
Steel (braced compact beams in flexure, tension members at yield) connections (AISC, 1998)	4.0	50 years	6.337×10^{-7}
AASHTO, design (calibrated for girders) (AASHTO, 1998)	3.5	75 years	3.105×10^{-6}
AASHTO, evaluation (calibrated for girders) (Moses, 2001)	2.5	5 years	1.245×10^{-3}
RC Beams in shear and flexure (Szerszen and Nowak, 2003)	3.5	50 years	4.653×10^{-6}
RC Slabs (cast in place) (Szerszen and Nowak, 2003)	2.5	50 years	1.246×10^{-4}
RC Columns (Szerszen and Nowak, 2003)	4.0	50 years	6.337×10^{-7}

The target βs used for wood members and RC slabs of 2.4 and 2.5, respectively, are quite low. These relatively low values are considered acceptable because the target reliability is for a single member and does not include system-level effects. When a structural member is part of a parallel system the reliability of the system is higher than that of a single member, because even if one member is relatively weaker, other members can compensate for its contribution to the system resistance. Wood members are often used in parallel systems, for example floors and roofs. The 2.5 target for RC slabs is based on analysis of a 0.305 m (1

foot) wide strip. The slab structure as a whole will have a higher reliability than the individual strips (Szerszen and Nowak, 2003).

The target reliability used for bridge evaluation is also quite low. This lower target is justified based on economic considerations. The relative cost of additional material at the design stage is much less than the costs associated with postings, rehabilitation, or replacement, and therefore the reliability target used for evaluation is not as conservative as that used for new design (Moses, 2001). The target used in rating is also based on a short time span of loading, 5 years. This corresponds to the maximum allowable interval between bridge inspections. This reliability target is specified for load rating of bridges. Load factors derived based on this target are used to evaluate bridges in service to ensure they have an adequate probability of acceptable performance until the next evaluation period. However, no guidance is given on the target to be achieved if the bridge is strengthened.

In another paper by Allen (2001), the Canadian approach to bridge evaluation is discussed. A base value of 3.5 for a reference period of 1 year is chosen as the target reliability. This corresponds to an annual probability of failure of 2.33 x 10^{-4}. Adjustments are made to this target value based on specifics of the bridge in question. The equation used for adjustments is shown in Eq 2-30. Table 2-16 shows the values for Δ_E, Δ_S, Δ_I, and Δ_{PC}. Higher reliability indices are suggested for cases where the bridge is significant to the traffic network.

$$\beta = 3.5 - [\Delta_E + \Delta_S + \Delta_I + \Delta_{PC}] \geq 2.0$$
Eq. 2-30

Table 2-16 Adjustments to Target Reliability for Canadian Bridge Evaluation

Δ_E Adjustment for element behavior	
Sudden loss of capacity with little or no warning	0.0
Sudden failure with little or no warning but retention of post-failure capacity	0.25
Gradual failure with probable warning	0.50
Δ_S Adjustment for system behavior	
Element failure leads to total collapse	0.0
Element failure probably does not lead to total collapse	0.25
Element failure leads to local failure only	0.5
Δ_I Adjustment for inspection level	
Component not inspectable	-0.25
Component regularly inspected	0.0
Critical component inspected by evaluator (0.0 if Δ_E = 0.0)	0.25
Δ_{PC} Adjustment for traffic category	
All traffic categories except PC (permit controlled and supervised vehicles)	0.0
Traffic category PC	0.6

Based on this formulation, a value of 3.0 would likely be used for evaluation of strengthened bridges. "Sudden failure with little or no warning but retention of post failure capacity" (Δ_E = 0.25) would characterize a FRP debonding failure, assuming that the steel has already yielded, and this type of failure would probably not lead to total collapse of the bridge (Δ_S = 0.25).

2.8.5 Selection of Target β for this Work

The selection of a target reliability index for the remainder of this work is complicated by the nature of strengthening design. Strengthening typically does not require the extended service life of new designs. Therefore the intent is to provide designers with the ability to choose design factors appropriate to a range of different possibilities for the desired service

life of the strengthened structure. This requires choosing a reliability target for each time span. Should this target remain the same no matter the design life (i.e. the probability of failure during the life of the structure is constant regardless of the length of service)? Or should the annual probability of failure be approximately constant, resulting in much higher reliability indices for designs intended for shorter durations?

Strengthening is also different from new design in that the addition of material as strengthening is much more expensive than the addition of material at the initial design stage. Based on a qualitative cost-benefit analysis this would suggest a lower reliability index for strengthening than for new design. At the stage of strengthening, one would hope for a higher level of knowledge about the structure implying that less conservatism would need to be built into selection of the target reliability. In fact, due to degradation of the structure, this may not be the case.

The nature of FRP itself provides other considerations for the reliability index. Debonding of FRP is a brittle failure mode without the warning or ductility provided in elements reinforced strictly with steel. This loss of ductility would suggest the use of a higher reliability index.

Based on the above considerations, a single target could not be set before seeing the results of the calibration example. Therefore the calibration example will use target reliabilities of 2.5, 3.0, and 3.5, spanning the range of reliabilities used for evaluation of existing bridges to design of new bridges. The same target will be used for all time periods. The selection of the same target for all time periods implies a higher annual probability of failure for shorter time periods. This is deemed acceptable because a much higher level of certainty is associated with the structural properties for shorter time spans. Thus, while the annual probability of failure may be higher, there is a higher degree of confidence that the

structure will actually meet that level. For designs of longer life there is less certainty in the properties as time progresses, making the lower annual probability of failure desirable.

To make the suggestions for strengthening design provided by this work applicable to real design, a firm set of resistance factors must be set. This selection will be based on the judgment of experts in the fields of composites and bridge design. In selecting the design factors they find most appropriate for design, these experts will in effect be selecting the target reliability.

2.9   Discussion of Background Data

In this chapter techniques for computing reliability, statistically modeling uncertainty in design variables, and modeling structural degradation through the corrosion process have been discussed. All three of these topics are similar in that there is no one "right" way to approach the problem. In the case of reliability analysis, even exact computational techniques are limited by the accuracy of the statistical models for the design variables. Statistical models are often based on limited data, and to provide for practical usage, they are often very generalized. Corrosion is a phenomenon that is hard to generalize because the exact manner in which it will affect a structure is entirely related to the local circumstances.

Without a "right" answer to these problems, this work has depended on suitable answers. The hybrid reliability approach chosen is compatible with the types of data available and is more computationally feasible than full MCS. Using statistical models developed in the past ensures that there will at least be some degree of comparability between this work and previous studies. The selected approach to corrosion considers at least some of the variability it can introduce, while maintaining a level of detail compatible with the intent to create a procedure for general reliability-based design of strengthening. The approach to describing composite properties described in Chapter 3 is also a suitable approach. There are many

different ways that statistical models and design values could be developed; those selected

strive to be as accurate as possible while retaining the simplicity needed for use in design.

Chapter 3. Characterization of Composite Properties for Reliability Analysis and Design

3.1 Introduction

Reliability-based design with any material requires a statistical description of material properties and their variation, a definition of the design value, and a relationship between the statistical description and the design value in order to allow for the evaluation of reliability. This chapter develops these three aspects with respect to the most significant composite properties for the design and analysis of strengthening, namely the ultimate tensile strength, longitudinal modulus, and thickness of unidirectional laminates. The ultimate strain is also an important characteristic. However, in this work, linear elastic behavior is assumed for the composite, and therefore the ultimate strain can be computed from the ultimate stress and elastic modulus.

Two types of variation are witnessed in the testing of composite properties: stochastic variation, which is inherent to all materials, and systematic deviations from design values, which are due primarily to how the design value was computed and specifics of the composite processing technique. In this chapter results from tensile coupon testing of many different wet layup composite materials are analyzed in order to describe how both types of variation affect material properties. The random variation is first described statistically, producing models for use in reliability analysis to compute resistance factors. Later, the systematic variation and the time-dependent material behavior are considered in developing a procedure to calculate the design value. Throughout this chapter attempts are made to address several of the objectives stated in Chapter 1. Specific efforts are made to provide applicability to a large range of materials, allow for the simple incorporation of new data, and explicitly consider the time-dependent response.

3.2   Description of Data Sets

3.2.1   Testing Procedures

Each data set consists of numerous coupons tested in tension following ASTM D3039 – Standard Test Method for Tensile Properties of Polymer Matrix Composite Materials (ASTM, 2000). In some cases different sets were subject to slight differences in the testing procedure, for example two different test machines were used for tensile testing. This could cause some variation between sets; however care was taken to keep tests as consistent as possible within a given set of coupons. The wet layup specimens were cut to approximately 25.4 mm (1 in) in width and 254 mm (10 in) in length. Prior to testing, width and thickness measurements were taken at five locations along the length of each coupon. The average dimensions for the coupon were used in the calculation of stress. During each test the force and extension were recorded at regular intervals. Following testing, the ultimate stress was calculated using the average composite cross-section and the ultimate force recorded by the testing machine. Modulus was calculated by fitting a straight line to the stress versus strain data over the range from 0.2 to 0.4 percent strain. The ASTM standard recommends that the range from 0.1 to 0.3 percent strain be used for this calculation; however strain results from the extensometer were highly variable at the beginning of the test, and therefore the calculation range was shifted to a more uniform portion of the data.

3.2.2   Wet Layup Composites

Several different sets of wet layup coupons made uniformly were used in an effort to discover consistent relations that are applicable to a variety of specific materials. All coupons were unidirectional laminates, and testing was conducted in the longitudinal direction. The following paragraphs describe each data set in some detail. The sets are summarized in Table 3-1.

Set A is composed of carbon epoxy sample panels constructed in the field during the rehabilitation of the Watson Wash Bridge on Interstate 40 in the Mojave Desert (Lee, 2005). This rehabilitation was conducted with the SCCI C-2 fabric system, a 610.4 g/m^2 (18 oz./sq. yd), 24 k tow, unidirectional carbon fabric (using T700 fibers). The matrix used for this application was SCCI Fiber Matrix I, a two-component epoxy system. There are three subsets to Set A: Set A1 consists of one-layer samples, Set A2 consists of two-layer samples, and Set A3 consists of three-layer samples. The different numbers of layers replicate the different numbers of layers that were used to strengthen different locations on the bridge. The samples were constructed at the beginning and end of each working day.

Set B is also composed of carbon epoxy panels constructed during a rehabilitation project. In this case the rehabilitation was conducted in the labs at UCSD as part of a research project investigating shear strengthening. The fabric system used was Hexcel fabric style GA090. This fabric has a weight of 302 g/m^2 (8.91 oz./sq. yd) and is composed of 12 k tow. The epoxy resin is the same as that used for Set A, SCCI Fiber Matrix I. Set B is composed of four subsets. All sets were constructed in the outdoor lab. Construction of the samples occurred at various stages during the rehabilitation, depending on manufacturer convenience. Sets B1, B2, and B3 were all laid up on a horizontal surface, with the number referring to the number of layers. Set BV was laid up on the vertical surface of the beam (as done for shear strengthening); however, it was prevented from bonding to the concrete through the use of a plastic film and peel-ply. This set had three layers of fabric and was intended to investigate the effect of laying composites up on non-horizontal surfaces.

Set C comes from the rehabilitation of the Golden Gateway Apartment Complex in San Francisco, California. The rehabilitation was conducted with the SCCI C2-06 fabric system, a 678.2 g/m^2 (20 oz/sq. yd) unidirectional carbon fabric (using T300 fibers). The fabric was

impregnated with a two component Delta Plastics epoxy using a wet bath/drip impregnation machine. This data set contains 177 one-layer samples.

Set D is a set of two-layer carbon epoxy samples. This set was also derived from sample panels constructed during rehabilitation in the field. They were manufactured using Tyfo® SCH-41 fabric with Tyfo® epoxy. This is the largest set with 260 data points.

Set E is composed of four sub sets. Sets E1, E2, E3, and E4 are carbon epoxy samples with the set number referring to the number of layers in the composite. These panels were manufactured specifically for use in this study by Fyfe Co. and are composed of Tyfo® SCH-41 fabric and Tyfo® S Epoxy.

Set F is similar to Set E in that it has four subsets and was manufactured for this study by Fyfe Co. These samples are, however, glass epoxy composites composed of Tyfo® SEH-51A fabric and Tyfo® S Epoxy.

Table 3-1 Summary of Wet Layup Data Sets

Data Set	Number of Samples	Number of Layers	Materials	Description
A	49	1	Carbon Epoxy	Field-manufactured concurrent with a rehabilitation
	50	2		
	20	3		
B	29	1	Carbon Epoxy	Manufactured as part of a strengthening project in the laboratory
	29	2		
	29	3		
	29	3		Laid up on a vertical surface
C	177	1	Carbon Epoxy	Field-manufactured concurrent with a rehabilitation
D	260	2	Carbon Epoxy	Field-manufactured concurrent with a rehabilitation
E	27	1	Carbon Epoxy	Manufactured specifically for this research
	28	2		
	29	3		
	27	4		
F	30	1	Glass Epoxy	Manufactured specifically for this research
	30	2		
	30	3		
	30	4		

3.3   Characterization of Random Variation

3.3.1   A Note on the Effect of Thickness

Variation in thickness poses a difficult question in design of wet layup based strengthening approaches. The cross-section of a FRP composite strip is not homogeneous; the section is composed of distinct regions of impregnated fabric and polymer. When a composite is loaded in the longitudinal direction nearly the entire load is carried by the fibers. Therefore, when excess resin is applied during fabrication, the cross-section of the composite will increase without significantly affecting the load carrying capacity. The result is that, for a given type of fabric, thicker composites generally have a lower ultimate stress and modulus

because, though they have approximately the same load capacity, they have a larger cross-sectional area. The relationship between stress and thickness is shown in Eq. 3-1 where σ is the stress, P is the applied load, A is the cross-sectional area of the composite, t is the thickness, and w is the width.

$$\sigma = \frac{P}{A} = \frac{P}{tw}$$

<div align="right">Eq. 3-1</div>

The effect of thickness variation on strength and modulus can be eliminated to some extent by normalizing results to a standard thickness. However, normalized values can be misleading for design because they often imply that the FRP can sustain a higher stress, but this stress is only applicable to the nominal thickness used for normalization. The variation in thickness can also be considered by working with a force or stiffness per unit width. This approach is, however, a significant deviation from traditional design procedures. Therefore, the approach taken herein is to quantify the variation in strength and modulus without normalization and to create designs based on nominal values of strength, modulus, and design thickness. As seen in later sections, the variability of thickness is considered in the derivation of design values. This approach seeks to account for thickness variation while remaining within the traditional design framework.

3.3.2 Basic Statistics

Basic statistical descriptors were computed for each data set. Table 3-2 shows the descriptors for strength, including mean, standard deviation, coefficient of variation (COV), maximum, and minimum. The COV is defined as the standard deviation divided by the mean. Table 3-3 and Table 3-4 show these same statistics for the modulus and thickness, respectively. From the data in these tables it is apparent that there is a large amount of spread within a single set for all three properties. In many cases the maximum value is nearly double the minimum

value. This large range of values makes apparent the need to consider possible variations in properties at the design stage.

Table 3-2 Descriptive Statistics for Ultimate Tensile Strength

Data Set	Mean MPa (ksi)	Standard Deviation MPa (ksi)	COV	Minimum MPa (ksi)	Maximum MPa (ksi)
A1	1043.74 (151.38)	125.98 (18.27)	0.12	806.04 (116.91)	1308.48 (189.78)
A2	1100.58 (159.63)	133.86 (19.42)	0.12	782.05 (113.43)	1396.68 (202.57)
A3	1008.39 (146.25)	137.11 (19.89)	0.14	696.34 (101.00)	1153.55 (167.31)
B1	936.30 (135.80)	195.94 (28.42)	0.21	526.20 (76.32)	1340.43 (194.41)
B2	1096.63 (159.05)	137.45 (19.94)	0.13	815.60 (118.29)	1413.39 (205.00)
B3	1056.31 (153.20)	155.20 (22.51)	0.15	754.18 (109.39)	1469.23 (213.09)
BV	1033.96 (149.96)	153.89 (22.32)	0.15	576.89 (83.67)	1343.26 (194.82)
C	556.28 (80.68)	127.96 (18.56)	0.23	175.86 (25.51)	834.91 (121.09)
D	748.75 (108.60)	95.26 (13.82)	0.13	452.16 (65.58)	926.45 (134.37)
E1	618.31 (89.68)	76.53 (11.10)	0.12	442.16 (64.13)	734.59 (106.54)
E2	587.39 (85.19)	54.62 (7.92)	0.09	451.65 (65.51)	696.41 (101.01)
E3	492.75 (71.47)	82.73 (12.00)	0.17	339.01 (49.17)	611.40 (88.68)
E4	421.41 (61.17)	57.91 (8.40)	0.14	312.80 (45.37)	507.78 (73.65)
F1	412.41 (59.82)	60.61 (8.79)	0.15	299.11 (43.38)	522.59 (75.79)
F2	409.27 (59.36)	37.69 (5.47)	0.09	311.97 (45.25)	479.13 (69.49)
F3	428.81 (62.19)	68.99 (10.01)	0.16	274.54 (39.82)	533.40 (77.36)
F4	406.76 (59.00)	37.76 (5.48)	0.09	311.61 (45.20)	470.10 (68.18)

In considering the strength data it is clear that different material systems produce different average properties; therefore the design procedure under development must be able to accommodate a range of material property values. Furthermore, the average ultimate stress for a single material type (represented in Table 3-2 by a specific letter) is not constant as additional layers are added to the composite. The addition of a second layer seems to improve the strength of the composite, while additional layers beyond two cause the composite strength to decrease. The increase seen between one- and two-layer composites may be attributable to difficulties in testing the often thin and flexible one-layer composites or changes in the thickness due to compaction of layers. The coefficient of variation is seen to range from a low of 0.09 to a high of 0.23.

Table 3-3 Descriptive Statistics for Longitudinal Modulus

Data Set	Mean GPa (ksi)	Standard Deviation GPa (ksi)	COV	Minimum GPa (ksi)	Maximum GPa (ksi)
A1	70 (10206)	9 (1370)	0.13	50 (7286)	94 (13659)
A2	79 (11452)	7 (1045)	0.09	62 (8995)	100 (14516)
A3	80 (11594)	8 (1100)	0.09	70 (10147)	103 (14879)
B1	58 8404	16 (2281)	0.27	40 (5756)	103 (14943)
B2	67 (9708)	18 (2676)	0.28	41 (5963)	125 (18188)
B3	72 (10410)	19 (2734)	0.26	33 (4737)	122 (17719)
BV	68 (9814)	13 (1914)	0.20	45 (6496)	96 (13913)
C	67 (9773)	19 (2705)	0.28	31 (4540)	148 (21438)
D	66 (9540)	7 (1052)	0.11	42 (6052)	89 (12870)
E1	53 (7677)	9 (1254)	0.16	37 (5371)	74 (10748)
E2	48 (6942)	9 (1332)	0.19	30 (4374)	64 (9267)
E3	52 (7614)	9 (1246)	0.16	36 (5275)	72 (10464)
E4	53 (7662)	13 (1826)	0.24	36 (5209)	80 (11531)
F1	23 (3327)	3 (422)	0.13	18 (2582)	27 (3969)
F2	26 (3759)	4 (568)	0.15	20 (2928)	34 (4998)
F3	25 (3605)	3 (494)	0.14	20 (2829)	33 (4855)
F4	25 (3665)	2 (306)	0.08	22 (3148)	31 (4467)

The modulus data again shows differences across material types and for different numbers of layers. In this case the modulus generally increases as the number of layers

102

increases. The coefficient of variation for the modulus is generally slightly higher that that for

strength, ranging from 0.09 to 0.28.

Table 3-4 Descriptive Statistics for Thickness

Data Set	Mean mm (in)	Standard Deviation mm (in)	COV	Minimum mm (in)	Maximum mm (in)
A1	1.1014 (0.0434)	0.0486 (0.0019)	0.04	1.0033 (0.0395)	1.1735 (0.0462)
A2	1.8760 (0.0739)	0.0562 (0.0022)	0.03	1.7610 (0.0693)	1.9855 (0.0782)
A3	2.7407 (0.1079)	0.1245 (0.0049)	0.05	2.4723 (0.0973)	3.0056 (0.1183)
B1	0.5855 (0.0231)	0.0661 (0.0026)	0.11	0.4604 (0.0183)	0.7380 (0.0291)
B2	1.0891 (0.0429)	0.1007 (0.0040)	0.09	0.9000 (0.0354)	1.2940 (0.0509)
B3	1.5523 (0.0611)	0.1769 (0.0070)	0.11	1.2580 (0.0495)	2.1260 (0.0837)
BV	1.5226 (0.0599)	0.1303 (0.0051)	0.09	1.3440 (0.0529)	1.9140 (0.0754)
C	1.5131 (0.0596)	0.1982 (0.0078)	0.13	1.1430 (0.0450)	2.5654 (0.1010)
D	2.1964 (0.0865)	0.2591 (0.0102)	0.12	1.8593 (0.0732)	3.2200 (0.1268)
E1	1.4768 (0.0581)	0.0828 (0.0033)	0.06	1.2800 (0.0504)	1.6420 (0.0646)
E2	3.0184 (0.1188)	0.1745 (0.0069)	0.06	2.7180 (0.1070)	3.3000 (0.1299)
E3	4.5344 (0.1785)	0.3338 (0.0131)	0.07	4.0680 (0.1602)	5.3600 (0.2110)
E4	5.9272 (0.2334)	0.5786 (0.0228)	0.10	5.1740 (0.2037)	6.8560 (0.2699)
F1	1.3325 (0.0525)	0.1617 (0.0064)	0.12	1.0280 (0.0405)	1.7740 (0.0698)
F2	2.5080 (0.0987)	0.1433 (0.0056)	0.06	2.2180 (0.0873)	2.7920 (0.1099)
F3	3.6123 (0.1422)	0.2999 (0.0118)	0.08	3.2280 (0.1271)	4.2260 (0.1664)
F4	4.6583 (0.1834)	0.2069 (0.0081)	0.04	4.0040 (0.1576)	4.9880 (0.1964)

The thickness shows differences across systems, a characteristic of the different fabrics used. The average thickness of multilayer composites is not simply the average thickness of the one-layer composite multiplied by the number of layers, but is generally smaller, suggesting that compaction has occurred. This will be considered in selection of design values for composite properties. The coefficient of variation of the thickness is generally smaller than that of either strength or modulus, with a high value of 0.13 and a low of 0.03.

3.3.3 Statistical Distributions for Representing Composite Properties

Many researchers have studied theoretical derivation of probability distributions for composite properties, particularly strength, based on flaws in the material (Sutherland and Soares, 1997). Theoretical derivations are somewhat limited in that they cannot account for the many sources of variability that may affect composite properties, particularly those manufactured through wet layup. Also, many are based on a "weakest-link" approach that is not directly applicable to composites because, even when the weakest fiber fails, the remaining fibers still carry load (Oh, 1979). Therefore, the emphasis of this work is not on theoretical derivations, but in accurately describing the variation in composite properties as tested.

3.3.3.1 Distributions

Four statistical distributions were fit to each data set. The distributions used - Normal, Lognormal, Weibull, and Gamma - were selected because they are common distributions used in engineering and are often appropriate for modeling material properties. The Normal, Lognormal, and Weibull distributions have all been used in the past to model composite variation (Rust et al., 1989), with the Weibull being a very popular choice (Sutherland and Soares, 1997). Each distribution may be described by its probability density function (PDF) or cumulative distribution function (CDF).

The Normal distribution has many desirable properties including the availability of closed form reliability solutions. This distribution is generally better understood than most distributions and is often used to describe engineering quantities, even in situations where it is not the most appropriate choice. Limitations of the Normal distribution for describing engineering quantities include the possibility of negative values in its sample space and its symmetric nature - when in fact many engineering quantities show some skewness (Bury, 1999). The PDF of a Normal distribution has the form of Eq. 3-2, where μ is the mean of the distribution and σ is the standard deviation. In this work, the Normal distribution was fit to data sets by computing the sample mean and standard deviation and using these values as the distribution parameters.

$$f(x) = \frac{1}{\sigma\sqrt{2\pi}}\exp\left\{-\frac{1}{2}\left(\frac{x-\mu}{\sigma}\right)^2\right\} ; \quad \sigma > 0, \quad -\infty < x, \mu < \infty$$

Eq. 3-2

The Lognormal distribution is closely related to the Normal distribution, and also possesses many closed form solutions. However, it has a skewed shape that is often more appropriate for engineering quantities and a purely positive sample space (Bury, 1999). Eq. 3-3 shows the PDF of the Lognormal distribution. In this equation, λ is the mean of the set of natural logs of x, and ζ is the standard deviation of the natural logs of x. In this work the Lognormal distribution was fit by computing λ and ζ for the sample set and using these values as the distribution parameters.

$$f(x) = \frac{1}{x\zeta\sqrt{2\pi}}\exp\left\{-\frac{1}{2}\left(\frac{\ln(x)-\lambda}{\zeta}\right)^2\right\} ; \quad x > 0, \zeta > 0, \quad -\infty < \lambda < \infty$$

Eq. 3-3

The Weibull distribution is a type III extreme value distribution of minima (Bury, 1999). It has often been used in describing material strength, including composite strength.

The Weibull distribution also has a positive sample space and possesses flexibility in the shape of its distribution depending on the parameters chosen (Bury, 1999). The general form of the Weibull PDF is given in Eq. 3-4. This model is a three-parameter model where α is the shape parameter, β is the scale parameter, and γ is a location parameter that serves as a threshold value (Bury, 1999). When γ is set equal to zero, the remaining function is the PDF of the two-parameter Weibull model. The three-parameter model is considered more robust and may more accurately describe the data (Alqam et al., 2002). However, it is more difficult to fit three parameters, and the two-parameter Weibull model has been found to acceptably model composite properties (Alqam et al., 2002). In this work the two-parameter Weibull distribution was fit through an error minimization procedure. An empirical CDF was created for each data set by ranking the data from lowest to highest and then associating with each point a cumulative probability, which was calculated as the rank of the data point divided by the total number of data points plus one. The SOLVER routine in Microsoft Excel was used to select values for α and β such that the sum of squared errors between the empirical distribution and the fitted Weibull distribution was minimized.

$$f(x) = \frac{\alpha}{\beta}\left(\frac{x-\gamma}{\beta}\right)^{\alpha-1}\exp\left\{-\left(\frac{x-\gamma}{\beta}\right)^{\alpha}\right\}; \ \ x \geq \gamma, \ \ \alpha, \beta \geq 0$$

Eq. 3-4

The final distribution is the Gamma distribution. This distribution was originally developed as a sampling distribution of several statistics; however its flexible shape and positive sample space have led to its use as a general model for engineering (Bury, 1999). The PDF of the Gamma distribution is shown in Eq. 3-5, where α is the shape parameter, β is the scale parameter, and Γ represents the gamma function. This distribution was fit using the same error minimization technique used to fit the Weibull distribution.

$$f(x) = \frac{1}{\beta \Gamma(\alpha)} \left(\frac{x}{\beta} \right)^{\alpha - 1} \exp\left\{ -\frac{x}{\beta} \right\}; \quad x \geq 0, \ \alpha, \beta > 0$$

Eq. 3-5

3.3.3.2 Distributions Fit to Wet Layup Composite Data

All four of the described distributions were fit to each set of strength, modulus, and thickness data. The resulting distribution parameters are shown in Table 3-5 for strength, Table 3-6 for modulus, and Table 3-7 for thickness.

Table 3-5 Distribution Parameters for Ultimate Tensile Strength

Data Set	Normal		Lognormal		Weibull		Gamma	
	μ MPa (ksi)	σ MPa (ksi)	λ MPa (ksi)	ζ	α	β MPa (ksi)	α	β MPa (ksi)
A1	1043.6 (151.382)	126.0 (18.272)	6.943 (5.012)	0.122	8.648	1096.2 (159.010)	55.031	19.068 (2.765)
A2	1100.5 (159.626)	133.8 (19.415)	6.996 (5.065)	0.127	9.881	1158.3 (168.011)	74.149	15.039 (2.181)
A3	1008.3 (146.254)	137.1 (19.886)	6.906 (4.976)	0.146	8.830	1078.9 (156.506)	55.452	18.661 (2.707)
B1	936.3 (135.799)	195.9 (28.419)	6.819 (4.889)	0.217	5.827	998.5 (144.827)	23.683	39.862 (5.781)
B2	1096.6 (159.052)	137.5 (19.936)	6.992 (5.062)	0.127	8.881	1150.9 (166.928)	54.198	20.363 (2.953)
B3	1056.3 (153.205)	155.2 (22.510)	6.952 (5.022)	0.145	9.014	1098.5 (159.320)	50.723	20.811 (3.018)
BV	1033.9 (149.963)	153.9 (22.320)	6.929 (4.998)	0.162	7.872	1091.3 (158.285)	49.027	21.239 (3.080)
C	556.3 (80.682)	128.0 (18.559)	6.289 (4.358)	0.269	5.280	606.3 (87.942)	21.462	26.528 (3.8476)
D	748.771 (108.600)	95.3 (13.816)	6.610 (4.679)	0.135	8.980	792.6 (114.962)	59.167	12.838 (1.862)
E1	618.3 (89.678)	76.5 (11.099)	6.419 (4.488)	0.128	8.488	652.0 (94.570)	55.105	11.327 (1.643)
E2	587.4 (85.194)	54.6 (7.921)	6.371 (4.441)	0.097	15.080	610.8 (88.588)	170.013	3.503 (0.508)
E3	492.7 (71.467)	82.7 (11.999)	6.186 (4.255)	0.172	5.582	529.0 (76.725)	24.453	20.305 (2.945)
E4	421.7 (61.167)	57.9 (8.399)	6.035 (4.104)	0.142	7.041	449.3 (65.164)	36.160	11.780 (1.708)
F1	412.4 (59.815)	60.6 (8.790)	6.011 (4.080)	0.154	7.578	439.8 (63.791)	42.311	9.916 (1.438)
F2	409.3 (59.360)	37.7 (5.466)	6.010 (4.079)	0.095	12.364	423.4 (61.403)	126.359	3.247 (0.471)
F3	428.8 (62.193)	69.0 (10.006)	6.048 (4.117)	0.167	5.888	458.9 (66.560)	28.254	15.275 (2.215)
F4	406.8 (58.996)	37.8 (5.476)	6.004 (4.073)	0.098	15.311	423.7 (61.450)	175.971	2.349 (0.341)

Table 3-6 Distribution Parameters for Longitudinal Modulus

Data Set	Normal		Lognormal		Weibull		Gamma	
	μ GPa (ksi)	σ GPa (ksi)	λ GPa (ksi)	ζ	α	β GPa (ksi)	α	β GPa (ksi)
A1	70.36 (10205)	9.44 (1369)	4.245 (9.222)	0.132	8.604	72.839 (10564)	60.138	1.161 (168.261)
A2	78.52 (11451)	6.59 (1044)	4.360 (9.342)	0.089	14.104	80.164 (11668)	154.805	0.067 (73.337)
A3	79.94 (11594)	7.59 (1100)	4.377 (9.354)	0.091	15.560	81.422 (11809)	161.331	0.488 (71.413)
B1	57.94 (8404)	15.72 (2281)	4.027 (9.004)	0.255	4.101	61.319 (8904)	13.146	4.329 (627.893)
B2	66.93 (9708)	18.45 (2676)	4.173 (9.150)	0.241	6.018	68.20 (9891)	28.198	2.285 (331.474)
B3	71.77 (10410)	18.85 (2734)	4.240 (9.217)	0.269	4.600	76.48 (11092)	16.615	4.301 (623.772)
BV	67.67 (9814)	13.19 (1914)	4.196 (9.173)	0.196	5.066	72.54 (10520)	20.399	3.325 (482.332)
C	67.38 (9773)	18.64 (2704)	4.177 (9.154)	0.252	5.953	67.00 (9827)	24.732	2.598 (376.948)
D	65.78 (9540)	7.25 (1051)	4.180 (9.157)	0.113	11.969	68.120 (9880)	103.890	0.013 (92.149)
E1	52.93 (7677)	8.65 (1254)	3.956 (8.933)	0.166	7.222	55.875 (8104)	38.208	1.394 (202.203)
E2	47.86 (6942)	9.18 (1332)	3.850 (8.827)	0.200	5.400	51.519 (7472)	22.415	2.160 (313.326)
E3	52.50 (7614)	8.59 (1246)	3.948 (8.925)	0.163	7.375	54.928 (7967)	42.105	1.244 (180.393)
E4	52.83 (7662)	12.59 (1826)	3.941 (8.918)	0.228	4.187	56.027 (8126)	15.583	3.321 (481.702)
F1	22.94 (3327)	2.91 (422)	3.125 (8.102)	0.130	7.443	24.332 (3529)	42.001	0.550 (79.844)
F2	25.92 (3759)	3.92 (568)	3.244 (8.221)	0.148	7.961	26.757 (3881)	45.026	0.569 (82.578)
F3	24.86 (3605)	3.40 (494)	3.204 (8.181)	0.136	7.886	25.993 (3770)	46.991	0.528 (76.625)
F4	25.27 (3665)	2.11 (306)	3.226 (8.203)	0.083	13.262	25.994 (3770)	133.244	0.189 (27.485)

Table 3-7 Distribution Parameters for Composite Thickness

Data Set	Normal		Lognormal		Weibull		Gamma	
	μ mm (in)	σ mm (in)	λ mm (in)	ζ	α	β mm (in)	α	β mm (in)
A1	1.10 (0.043)	0.049 (0.002)	0.095 (-3.139)	0.044	23.428	1.10 (0.044)	397	0.0027 (0.0001)
A2	1.88 (0.074)	0.056 (0.002)	0.629 (-2.606)	0.030	54.450	1.90 (0.075)	390	0.0048 (0.0002)
A3	2.74 (0.108)	0.124 (0.005)	1.007 (-2.228)	0.045	23.250	2.79 (0.110)	394	0.0070 (0.0003)
B1	0.58 (0.023)	0.066 (0.003)	-0.054 (-3.776)	0.113	9.324	0.609 (0.024)	64.4	0.0091 (0.0004)
B2	1.09 (0.043)	0.101 (0.004)	0.082 (-3.154)	0.093	11.016	1.130 (0.044)	91.6	0.0119 (0.0005)
B3	1.55 (0.061)	0.177 (0.007)	0.434 (-2.801)	0.110	11.067	1.595 (0.063)	93.6	0.0165 (0.0006)
BV	1.522 (0.060)	0.130 (0.005)	0.417 (-2.818)	0.083	12.740	1.559 (0.061)	129.6	0.0117 (0.0005)
C	1.52 (0.060)	0.203 (0.008)	0.406 (-2.829)	0.127	8.882	1.572 (0.062)	60.3	0.0254 (0.0010)
D	2.18 (0.086)	0.279 (0.011)	0.780 (-2.454)	0.111	10.973	2.235 (0.088)	96.6	0.0228 (0.0009)
E1	1.48 (0.058)	0.083 (0.003)	0.388 (-2.846)	0.057	18.749	1.511 (0.059)	250.6	0.0059 (0.0002)
E2	3.02 (0.119)	0.174 (0.007)	1.103 (-2.132)	0.058	16.227	3.100 (0.122)	198	0.0153 (0.0006)
E3	4.53 (0.179)	0.334 (0.013)	1.509 (-1.726)	0.072	13.327	4.641 (0.183)	260	0.0172 (0.0007)
E4	5.93 (0.233)	0.579 (0.023)	1.775 (-1.460)	0.097	9.133	6.177 (0.243)	69.9	0.0846 (0.0033)
F1	1.33 (0.052)	0.162 (0.006)	0.280 (-2.955)	0.118	9.510	1.374 (0.054)	251	0.0052 (0.0002)
F2	2.51 (0.099)	0.143 (0.006)	0.918 (-2.317)	0.057	16.449	2.570 (0.101)	223	0.0112 (0.0004)
F3	3.61 (0.142)	0.300 (0.012)	1.281 (-1.954)	0.082	11.370	3.729 (0.147)	106.7	0.0337 (0.0013)
F4	4.65 (0.183)	0.207 (0.008)	1.538 (-1.697)	0.046	34.118	4.741 (0.187)	250	0.0187 (0.0007)

For each set of data the empirical cumulative distribution may be plotted with the fitted CDFs. An example of such a plot is shown in Figure 3-1. From this plot it is clear that all of these distributions are able to fit the general trend of the data, and it is not possible to select the best fitting distribution by mere visual inspection. These observations are true of nearly all the data sets; therefore goodness-of-fit tests were used to compare the distributions and select the best distribution for reliability analysis.
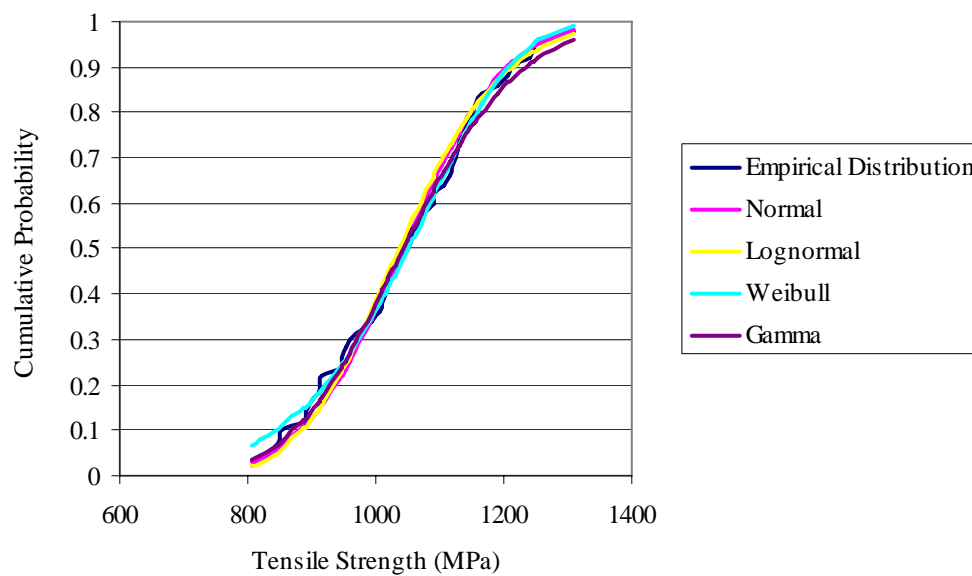
Figure 3-1 Plot of Cumulative Distribution Functions for Set A1 Strength

3.3.4 Best Fitting Distributions

Three different goodness-of-fit tests, Chi-Squared, Kolmogorov-Smirnov (K-S), and Anderson-Darling (A-D), were used to assess the ability of the four different distributions to model the stochastic variation in composite properties. These tests are described in Appendix B.

3.3.4.1 Strength

The results of the Chi-Squared test as applied to the strength data are shown in Table 3-8. The test statistic with the smallest value, representing the best fitting distribution, is highlighted for each data set. The results from this test are inconclusive. The Weibull distribution has a slight advantage because it is the most commonly selected distribution by 1 set, and it is the best distribution for both of the very large data sets, Sets C and D.

Table 3-8 Chi-Squared Goodness-of-Fit Results for Strength

Data Set	Number of Specimens	Number of Bins	Test Statistic			
			Normal	Lognormal	Weibull	Gamma
A1	49	7	4.10	3.43	2.29	1.43
A2	50	7	4.88	7.96	2.08	6.56
A3	20	5	4.00	3.50	4.00	8.00
B1	29	5	1.17	1.86	0.14	1.52
B2	29	5	3.93	5.31	3.24	3.93
B3	29	5	4.97	4.97	4.97	4.97
BV	29	5	1.86	2.55	2.21	1.17
C	177	10	8.59	23.85	7.24	13.34
D	260	12	22.74	41.48	14.06	37.97
E1	27	5	0.22	0.22	0.59	0.96
E2	28	5	4.14	4.14	1.64	1.64
E3	29	5	3.24	3.24	6.34	2.21
E4	27	5	0.06	1.70	2.07	2.07
F1	30	5	0.67	2.00	1.67	1.67
F2	30	5	1.00	0.33	3.67	1.00
F3	30	5	7.33	5.33	7.67	3.67
F4	30	5	5.67	8.00	7.33	8.33

For the K-S and A-D tests, different distributions have different acceptance criteria; therefore the test statistics cannot be directly compared to assess the significance level at which different hypothesized distributions pass the test. These tests are further limited in that tabulated percentage points are only available for certain standard significance levels. In order to compare distributions using these tests, the tests for all distributions are conducted at a

given significance level, and the occurrence of acceptance or rejection is analyzed. Table 3-9 shows the results of the K-S test for the distributions for which test criteria could be found at a significance level, α, of 0.10. The shaded cells labeled FAIL are the tests where the hypothesized distribution should be rejected based on the K-S test. Table 3-9 shows that the Weibull distribution is generally a better representation of strength variation because it was found to be an acceptable fit in all cases at the 0.10 significance level.

Table 3-9 Kolmogorov-Smirnov Goodness-of-Fit Results for Strength, α=0.10

Data Set	Normal	Lognormal	Weibull
A1	PASS	PASS	PASS
A2	PASS	FAIL	PASS
A3	PASS	FAIL	PASS
B1	PASS	PASS	PASS
B2	PASS	PASS	PASS
B3	PASS	PASS	PASS
BV	PASS	PASS	PASS
C	PASS	FAIL	PASS
D	FAIL	FAIL	PASS
E1	PASS	PASS	PASS
E2	FAIL	FAIL	PASS
E3	FAIL	FAIL	PASS
E4	PASS	PASS	PASS
F1	PASS	FAIL	PASS
F2	PASS	PASS	PASS
F3	PASS	PASS	PASS
F4	FAIL	FAIL	PASS

Results from the Anderson-Darling test at a significance level of 0.25 are shown in Table 3-10. At this high significance level there are several cases where the Weibull distribution does not pass the test; however it still has more passing results than any of the other three distributions. Based on the results of these three goodness-of-fit tests, the Weibull

distribution is selected as the best distribution for representing the variability of ultimate strength in wet layup composites.

Table 3-10 Anderson-Darling Goodness-of-Fit Results for Strength, α= 0.25

Data Set	Normal	Lognormal	Weibull	Gamma
A1	PASS	PASS	PASS	PASS
A2	FAIL	FAIL	PASS	FAIL
A3	FAIL	FAIL	FAIL	FAIL
B1	PASS	PASS	FAIL	PASS
B2	PASS	PASS	PASS	PASS
B3	FAIL	PASS	FAIL	PASS
BV	PASS	FAIL	PASS	PASS
C	FAIL	FAIL	PASS	FAIL
D	FAIL	FAIL	FAIL	FAIL
E1	PASS	PASS	PASS	PASS
E2	FAIL	FAIL	PASS	FAIL
E3	FAIL	FAIL	FAIL	FAIL
E4	FAIL	FAIL	PASS	FAIL
F1	FAIL	FAIL	PASS	FAIL
F2	PASS	PASS	PASS	PASS
F3	FAIL	FAIL	FAIL	FAIL
F4	FAIL	FAIL	FAIL	FAIL

3.3.4.2   Modulus

Goodness-of-fit results for modulus are less conclusive than those for strength. Based on the Chi-Squared results shown in Table 3-11 the Weibull or Lognormal distribution appears well suited to modeling longitudinal modulus. Table 3-12 shows the results of the K-S test at a significance level of 0.10. In this case the Lognormal distribution appears slightly better than the Weibull distribution. The results of the A-D test are presented in Table 3-13. These results suggest that the Lognormal and Gamma distributions are best.   As it is one of the best fits in each of these three tests, and because it is a simple distribution to work with, the Lognormal distribution is chosen to model variation in longitudinal modulus of wet layup composites.

Table 3-11 Chi-Squared Goodness-of-Fit Results for Modulus

Data Set	Number of Specimens	Number of Bins	Test Statistic			
			Normal	Lognormal	Weibull	Gamma
A1	49	7	7.71	4.57	10.00	7.71
A2	50	7	8.24	7.68	12.16	6.28
A3	20	5	6.00	3.89	1.79	1.79
B1	29	5	1.17	1.17	0.14	0.48
B2	29	5	10.83	1.17	0.48	0.83
B3	29	5	4.62	1.17	1.86	0.14
BV	29	5	1.17	1.86	1.17	1.17
C	177	10	63.96	27.80	50.18	34.02
D	260	12	34.42	33.63	20.88	28.76
E1	27	5	4.30	6.89	0.96	4.30
E2	28	5	0.93	0.21	0.57	0.93
E3	29	5	1.64	0.93	0.93	0.93
E4	27	5	4.30	6.89	0.96	4.30
F1	30	5	3.00	3.00	3.00	3.00
F2	30	5	1.33	1.00	1.67	1.67
F3	30	5	0.67	0.67	1.67	1.00
F4	30	5	0.67	0.33	0.67	1.67

Table 3-12 Kolmogorov-Smirnov Goodness-of-Fit Results For Modulus, α=0.10

Data Set	Normal	Lognormal	Weibull
A1	PASS	PASS	FAIL
A2	FAIL	PASS	FAIL
A3	PASS	PASS	PASS
B1	PASS	PASS	FAIL
B2	FAIL	PASS	PASS
B3	PASS	PASS	PASS
BV	PASS	PASS	PASS
C	FAIL	FAIL	FAIL
D	FAIL	FAIL	FAIL
E1	PASS	FAIL	PASS
E2	PASS	PASS	PASS
E3	PASS	PASS	PASS
E4	FAIL	PASS	PASS
F1	FAIL	FAIL	FAIL
F2	FAIL	PASS	PASS
F3	PASS	PASS	PASS
F4	PASS	PASS	PASS

Table 3-13 Anderson Darling Goodness-of-Fit Results for Modulus, α=0.10

Data Set	Normal	Lognormal	Weibull	Gamma
A1	FAIL	PASS	FAIL	PASS
A2	FAIL	FAIL	FAIL	FAIL
A3	FAIL	PASS	FAIL	FAIL
B1	FAIL	PASS	FAIL	PASS
B2	FAIL	FAIL	FAIL	FAIL
B3	PASS	PASS	PASS	PASS
BV	PASS	PASS	PASS	PASS
C	FAIL	FAIL	FAIL	FAIL
D	FAIL	FAIL	FAIL	FAIL
E1	PASS	PASS	PASS	PASS
E2	PASS	PASS	PASS	PASS
E3	PASS	PASS	FAIL	PASS
E4	FAIL	PASS	FAIL	PASS
F1	FAIL	FAIL	FAIL	FAIL
F2	PASS	PASS	FAIL	PASS
F3	PASS	PASS	PASS	PASS
F4	PASS	PASS	PASS	PASS

3.3.4.3   Thickness

The results of the Chi-Squared, K-S, and A-D goodness-of-fit tests for thickness are shown in Table 3-14, Table 3-15, and Table 3-16, respectively. In all cases the Lognormal distribution is seen to be slightly superior to the other distributions. Therefore, the Lognormal distribution is chosen to represent the variability in the thickness of wet layup composites.

Table 3-14 Chi-Squared Goodness-of-Fit Results for Thickness

Data Set	Number of Specimens	Number of Bins	Test Statistic			
			Normal	Lognormal	Weibull	Gamma
A1	49	7	3.43	1.43	3.71	4.00
A2	50	7	23.08	23.08	4.88	30.08
A3	20	5	7.50	7.50	14.00	8.50
B1	29	5	0.45	0.45	0.76	0.45
B2	29	5	1.43	2.57	2.86	3.14
B3	29	5	1.59	0.41	1.59	1.00
BV	29	5	2.06	3.31	8.94	1.44
C	177	10	11.73	5.24	17.85	22.17
D	260	12	81.54	57.23	104.31	65.92
E1	27	5	0.22	0.22	2.44	1.33
E2	28	5	7.00	7.00	2.36	3.07
E3	29	5	4.62	5.66	7.38	3.59
E4	27	5	3.59	3.59	3.93	2.55
F1	30	5	2.67	2.67	2.67	7.67
F2	30	5	2.67	2.67	6.67	1.33
F3	30	5	1.17	0.50	4.50	1.17
F4	30	5	2.33	4.00	4.00	15.00

Table 3-15 Kolmogorov-Smirnov Goodness-of-Fit Results for Thickness, $\alpha=0.10$

Data Set	Normal	Lognormal	Weibull
A1	PASS	PASS	PASS
A2	FAIL	FAIL	FAIL
A3	PASS	PASS	PASS
B1	PASS	PASS	PASS
B2	PASS	PASS	PASS
B3	FAIL	PASS	PASS
BV	PASS	PASS	FAIL
C	FAIL	FAIL	FAIL
D	FAIL	FAIL	FAIL
E1	PASS	PASS	PASS
E2	PASS	PASS	PASS
E3	FAIL	FAIL	FAIL
E4	PASS	PASS	FAIL
F1	FAIL	FAIL	FAIL
F2	PASS	PASS	PASS
F3	FAIL	FAIL	FAIL
F4	FAIL	FAIL	PASS

Table 3-16 Anderson-Darling Goodness-of-Fit Results for Thickness, α= 0.25

Data Set	Normal	Lognormal	Weibull	Gamma
A1	FAIL	PASS	FAIL	FAIL
A2	FAIL	FAIL	FAIL	FAIL
A3	PASS	PASS	PASS	PASS
B1	FAIL	FAIL	FAIL	FAIL
B2	PASS	PASS	PASS	PASS
B3	FAIL	PASS	FAIL	PASS
BV	FAIL	FAIL	FAIL	FAIL
C	FAIL	PASS	FAIL	FAIL
D	FAIL	FAIL	FAIL	FAIL
E1	PASS	PASS	PASS	PASS
E2	PASS	PASS	FAIL	FAIL
E3	FAIL	FAIL	FAIL	FAIL
E4	FAIL	FAIL	FAIL	FAIL
F1	FAIL	PASS	FAIL	FAIL
F2	FAIL	PASS	FAIL	PASS
F3	FAIL	FAIL	FAIL	FAIL
F4	FAIL	FAIL	PASS	FAIL

3.3.4.4 Summary of Distributions for Reliability Analysis

Based on the description of goodness-of-fit tests provided in Appendix B and their application to the distributions fit to represent composite data described above, it is clear that selection of the best fitting distribution is in no way deterministic, nor completely objective. There is significant opportunity for error in distribution selection, and given the variety of composites and applications it may be impossible to select a single distribution type for all cases. Further study of the variation in composite properties may find improved representations for composite variation. *However, based on the available data, the Weibull distribution is chosen to model ultimate strength of composites and the Lognormal distribution is chosen to model modulus and thickness.* These distributions have been consistently implemented throughout the remainder of this work.

118

3.3.5 Correlation between Variables

To this point, strength, modulus, and thickness have all been treated as independent variables; however the interaction between variables can have a significant impact on structural reliability if this interaction does exist. Correlation between variables is commonly expressed in terms of a normalized parameter, ρ, called the correlation coefficient. This coefficient describes the degree of linear correlation between variables. For variables that are perfectly correlated such that when plotted as an (x, y) plot they form a line with positive slope, the correlation coefficient is equal to 1. For a negative sloping line the coefficient is equal to negative 1. A value of zero implies no linear correlation. For purposes of reliability analysis, when the absolute value of ρ is less than 0.2 the variables can be treated as uncorrelated and when it is greater than 0.8 the variables can be assumed perfectly correlated (Melchers, 1999). When working with the correlation coefficient it is important to remember that small values of ρ do not necessarily imply no relation between variables; non-linear interaction may still be present. Other types of interaction can be detected by plotting the variables on an (x, y) plot.

Correlation coefficients between strength and thickness, strength and modulus, and modulus and thickness are shown in Table 3-17. It is immediately obvious that there is a high degree of variation in the amount of correlation between variables from set to set. This observation is confirmed by the COVs of the correlation coefficients shown in the bottom row of the table. However, certain trends do stand out. For example, it is clear that the strength and thickness, as well as modulus and thickness, correlation coefficients tend to be negative, implying that higher values of strength (or modulus) are associated with lower values of thickness, and vice versa. This is an expected result since both strength and modulus are stress-based quantities and, as shown in Eq. 3-1, as the thickness decreases the cross-sectional

119

area also decreases, increasing the stress for a given force. This negative correlation may also be related to manufacture: for wet-layup samples a thinner sample is often an indication of better manufacturing techniques, as there is less excess resin. Strength and modulus tend to be positively correlated with each other.

The average value for each of the three correlation coefficients shows that, in general, there is some weak correlation between the variables. However based on these results it is very difficult to choose an appropriate representation of correlation for a general study of composite strengthening reliability. For further work on this project the three variables describing composite properties will be assumed independent. This effectively means that ρ is assumed equal to zero for all three combinations of strength, modulus, and thickness. This assumption is made only in the context of this limited information; better characterization of correlation between composite properties remains an important topic for further investigation.

Table 3-17 Correlation Coefficients for Wet Layup Composites

Data Set	Strength and Thickness	Strength and Modulus	Modulus and Thickness
A1	-0.710	0.101	-0.318
A2	-0.113	0.232	-0.267
A3	0.513	0.058	0.011
B1	-0.488	0.377	-0.360
B2	-0.473	0.337	-0.335
B3	-0.545	0.048	-0.623
BV	-0.427	-0.010	-0.393
C	-0.491	0.291	-0.414
D	-0.567	0.219	-0.197
E1	-0.773	0.611	-0.564
E2	-0.262	0.277	-0.426
E3	-0.821	-0.099	0.156
E4	-0.924	0.572	-0.614
F1	-0.812	0.768	-0.866
F2	-0.429	0.520	-0.430
F3	-0.917	0.478	-0.455
F4	-0.734	0.467	-0.389
AVG	-0.517	0.313	-0.362
STDEV	0.351	0.229	0.230
COV	0.680	0.731	0.635

3.4   Design Values for Composite Materials

3.4.1   Current Approaches to Selection of Design Values

Establishment of design provisions requires specification of material properties for use in design.   There are currently several different design guidelines for the use of FRP in strengthening. These guidelines all use a similar approach to specifying composite properties for design. They generally neglect the modulus, most merely implying that the mean value should be chosen, while a few specify modulus-specific safety factors, and instead place emphasis on the ultimate tensile strength or strain.

The general approach to determine a design value for composite strength is to define the "characteristic value" as a certain percentile of test results, with most guidelines specifying a minimum of 20 to 30 tests. Factors that vary by guideline but that are intended to account for environmental effects, manufacturing specifics, or testing procedures are then applied to this characteristic value to reach the final value for design. Often, instead of specifying a percentile, guidelines give an equation similar to Eq. 3-6 where the characteristic value, x_c, is calculated as the mean, μ_x, less a constant, n, times the standard deviation, σ_x. Eq. 3-7 is an alternative form expressed in terms of the COV.

$$x_c = \mu_x - n\sigma_x$$

<div align="right">**Eq. 3-6**</div>

$$x_c = \mu_x(1 - nCOV_x)$$

<div align="right">**Eq. 3-7**</div>

The constant, n, varies by specification; however by assuming a distribution for the data, the percentile of the distribution specified by Eq. 3-6 or the value of n implied by a certain percentile can be computed, allowing direct comparison of the different guidelines. Table 3-18 shows this comparison for ultimate tensile strength. When necessary a Normal distribution is used to relate the specified percentile to a value of n. As FRP is assumed to have linear-elastic behavior, these relations would apply equally to the ultimate rupture strain, assuming that the modulus has a constant value.

Table 3-18 Different Ways of Specifying the Characteristic Value for FRP Strength

Guideline	n	n Specified or Calculated
ACI 440 (ACI, 2002)	3	Specified
TR 55 (The Concrete Society, 2000)	2	Specified
CHBDC (CSA, 2006)	1.64	Calculated from 5th percentile
Täljsten (2002)	1.64	Calculated from 5th percentile
ISIS Canada (Neale, 2001)	3	Specified
Japanese (Maruyama, 2001)	3	Specified
fib (International, 2001)	1.64	Calculated from 5th percentile

3.4.1.1 Reliability Implications of Current Design Approach

The intent of this research is to develop a reliability-based design procedure for FRP strengthening that provides a uniform level of reliability across a variety of design situations. All aspects of the design procedure contribute to the final reliability of designs, not just the calibrated load and resistance factors.   Therefore it is important to consider the design value from a reliability standpoint. The design value is composed of the characteristic value and any factors applied to that value. All of the existing design guidelines mentioned in Table 3-18 use a different system of safety factors to account for various aspects of FRP design, including degradation and manufacture. Later these factors will be investigated and new factors proposed. Currently, focus is placed on appropriate representation of the characteristic value.

The current method, described above, for determining the characteristic strength provides for a certain probability that the FRP strength will fall below that characteristic value. For example, choosing the lower 5th percentile as the characteristic strength means that the composite has a 5 percent probability of being less than the characteristic value. As the value of n used in Eq. 3-6 increases, the probability that the composite strength will fall below the

characteristic strength decreases. In the case of n equal to 3, the probability of an under-strength composite is 0.0013 based on a Normal distribution. The intent of this approach is to fix the probability of structural failure by fixing the probability that the composite falls below the characteristic value. This approach neglects the fact that the reliability of a structure is determined by the interaction of load and resistance, not by resistance alone. Since the reliability is determined by interaction, the shape of the distributions becomes important, not just the percentiles.

The shape of a variable's distribution is controlled by the type of probability distribution chosen to model the variable and by the amount of spread in the variable. If a certain type of distribution is chosen to model a variable, for example strength, the shape of the distribution is then controlled solely by the amount of variation in that variable. For a material such as steel the variation is fairly uniform from project to project and thus the shape of its distribution is relatively constant. This means that for a given load distribution there will be little change in the resistance distribution, and just one value of the resistance factor can successfully position the resistance curve such that the probability of failure meets the target. However, in the case of composites, there is the potential for large changes in the degree of variation between materials (wet layup versus prefabricated) and between projects (due to manufacturing differences). In this case the shape of the resistance distribution will change as the variation (measured in terms of the COV) changes. Thus, for design with FRP, there are many possible shapes for the resistance distribution, and theoretically each different resistance distribution could require its own value for the resistance factor in order to meet the target reliability. This creates the possibility that a single resistance factor will not be adequate, and that a reliability-based design procedure for FRP will require resistance factors that change as the amount of material variability changes.

A composite with a high degree of variability would generally be considered as an inferior composite and therefore would be expected to have a smaller, more conservative value for its resistance factor than a composite with lower variability. However this was not found to occur in the case of a simple example conducted as a preliminary part of this research. The example was taken from ACI 440 (2002), and consisted of a simple beam strengthened with wet layup composites so as to increase its live load capacity by fifty percent. Designs were created following the ACI 440 design procedure using the characteristic value calculated from Eq. 3-6 with the value of *n* equal to 3. The material assumed for design was a model composite with the properties shown in Table 3-19. Because the characteristic value is based on the level of variation, a different design was created for each value of the strength COV. The distributions shown in Table 3-19 were used in Monte Carlo Simulation (MCS) to evaluate the reliability of the designs. Thickness was modeled as a Weibull variable because only preliminary coupon results were available at that time. Full details of the MCS procedure used in this example are given in Atadero and Karbhari (2004). Results are shown in Table 3-20.

Table 3-19 Properties of Model Composite

Property	Mean	Coefficient of Variation	Distribution
Tensile Strength	1000 MPa (145 ksi)	10%, 15% and 20%	Weibull
Modulus	70 GPa (10153 ksi)	12%	Lognormal
Thickness	1 mm (0.04 in)	5%	Weibull

Table 3-20 Reliability of Designs Using Different COVs for Strength

COV of Strength	Estimated Probability of Failure	Generalized Reliability Index
0.10	0.00171	2.93
0.15	0.00120	3.04
0.20	0.00060	3.24

These results show that as the COV of material strength is increased, the reliability also increases. For design this would imply that composites with higher variation would also have higher, less conservative resistance factors. This counterintuitive result is attributed to the conservatism that is introduced to the characteristic value when three standard deviations are subtracted from the mean value. In cases where the variability is high, subtracting three standard deviations results in very small characteristic values, producing designs with high quantities of FRP. This effect is described in terms of the reliability integral in Atadero and Karbhari (2005). This is an undesirable result for use in a probability-based code. Designers using the code would see that as the COV goes up, the resistance factor also goes up, without necessarily knowing the full background. This would give no incentive for using higher quality materials and could result in lax quality control standards.

Another issue related to the selection of characteristic value has been identified not only when materials of different variability are used to apply a given level of strengthening, but when the same material is used to apply different levels of strengthening. Once again the example beam taken from ACI 440 is used to demonstrate this point. In this case the beam is assumed to be deficient due to a loss of steel. Steel losses of ten, twenty, and thirty percent are considered. Designs are created following the ACI 440 procedure to return the beam to its original load capacity. The material properties shown in Table 3-19 are again used for this example. Figure 3-2 shows the results of the reliability evaluation for this example. As the percent of steel degradation increases, the reliability also increases for all three materials. Some increase is expected because as more of the tensile load is shared between the steel and FRP there is more opportunity for one material to compensate for weaknesses in the other material. However, the FRP with a COV equal to 0.20 not only shows higher overall reliability, but steeper increases in reliability as the percent of steel degradation is increased.

This result is again attributed to the conservatism in the definition of the characteristic value. The bias factor for steel is roughly 1.1, (or the mean strength of steel is approximately 1.1 times the design strength). The bias factor for the composite ranges from 1.45 for a COV of 0.10 to 2.5 for a COV of 0.20, and this bias only considers the ratio of mean strength to characteristic strength, neglecting any additional design factors that may be applied. As the percent of steel degradation increases, the amount of load carried by the FRP is increased. As a result of the conservatism used in defining the composite strength, as the composite is designed to carry more load, the whole system gains reserve strength due to the high composite bias factor, and the reliability is increased. The result is designs that may be too conservative, using more material than required. Providing uniform reliability in this case would require unique factors not only for different values of composite strength COV, but also for different amounts of strengthening.
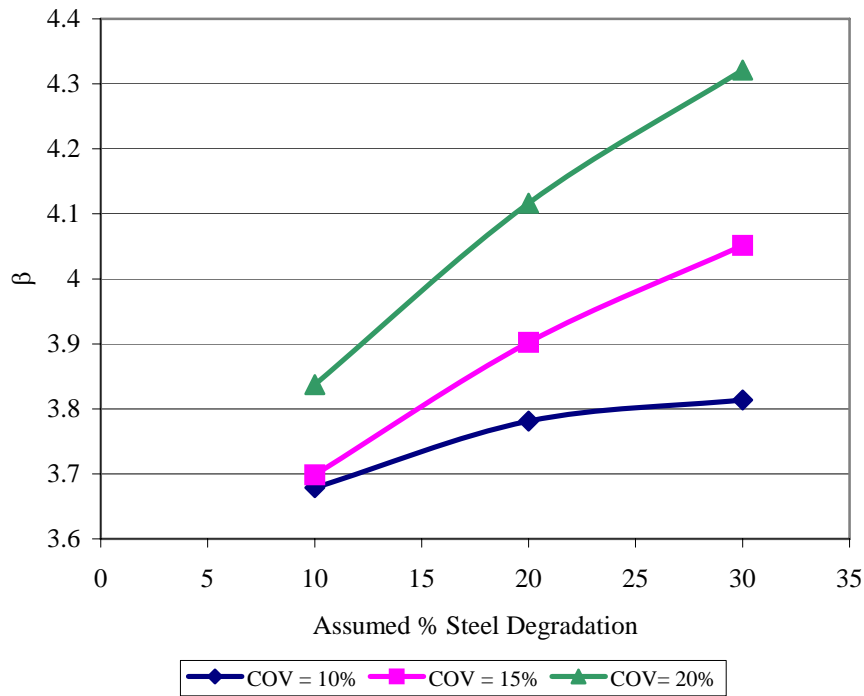
Figure 3-2 Changes in β with Additional Required Strengthening

3.4.2 Proposed Approach to Design Values

The discussion in Section 3.4.1.1 clearly outlines issues that affect the ability of a design procedure to achieve a uniform level of reliability given the current definition of characteristic values. Another complication of having characteristic values that depend on the amount of variation is that every material, with every level of variation, must be treated uniquely. In the interest of developing a procedure applicable to a variety of composite systems and limiting the number of different resistance factors, a new approach is now proposed.

3.4.2.1 Accounting for Material Variability

The current definition of characteristic value attempts to account in some way for material variability by selecting a percentile of the property distribution. This may be convenient when a material has a relatively uniform amount of variation; however this is not

the case for wet layup FRP. The range of possible COVs for composite materials requires that the resistance factor must change as the composite COV changes in order to maintain uniform reliability. Trying to account for different levels of variability in both the characteristic value and the resistance factor adds an unnecessary layer of complexity. Resistance factors are specifically intended to account for variability; therefore it is proposed to use a characteristic value that is independent of material variation.

Rather than altering the traditional resistance factor, ϕ, to account for FRP variability, another, composite specific factor, ψ, is proposed. ϕ will be used to account for variability in the existing structure as well as uncertainty in the design models. ψ is applied only to the FRP contribution of resistance. ψ is specified as a function of the COV of the composite property that is most significant to the limit state in question. For example, when the ACI 440 (2002) bond model is used to assess flexural reliability (as in the previous example), the reliability is found to be sensitive to changes in the amount of variation in the ultimate tensile strength. In contrast, serviceability limit states may be more sensitive to the amount of variation in the modulus.

The LRFD checking equation is now expressed as shown in Eq. 3-8, where γ_i and Q_i are the load factors and load effects, respectively, R is the nominal resistance and x_{FRP} is the FRP contribution to the resistance. This is a break from traditional LRFD implementation but is similar in some ways to the partial factor formats used in other parts of the world, such as Europe and Canada.

$$\sum \gamma_i Q_i \leq \phi R(..., \psi x_{FRP})$$

Eq. 3-8

3.4.2.2 Use of the Mean as the Characteristic Value

The characteristic value in this proposed procedure will be the mean of property test results. The same procedure for determining design values will be applied to both strength and modulus. The mean is chosen to mitigate both issues previously identified with the current characteristic value. Use of the mean will prevent the counterintuitive result that designs created with FRP of higher variability have higher reliability. It will also make the FRP bias factor equal to 1, preventing the buildup of excess capacity as more of the load is carried by the FRP. Though it will be impossible to eliminate differences in reliability due to differences in the amount of remaining steel, it is hoped that this representation of the characteristic value will at least reduce the large increases in reliability when composites of high variability are used. These objectives might have been met by choosing a less demanding percentile of the test results than that specified by ACI 440; however the intent of this format is to segregate the effects of material variation from the selection of the characteristic value. It is believed that this separation will make it more straightforward to accommodate different FRP materials and different manufacturing techniques in one unified design procedure. Isolating the design value from the variation will also streamline the calibration process, because one design value may be associated with several different levels of variation.

Use of the mean is a significant deviation from the traditional design procedures used for a variety of materials. Any differences from current practice will raise objections and cause hesitation in adoption of this procedure; thus change should be made only with good reason. In addition to the important considerations already discussed, there are other compelling reasons for this choice. The mean of a data set can be determined with a high degree of confidence with many fewer samples than would be required for estimation of small

percentiles. Having a high degree of accuracy in design values is important in ensuring structural safety while at the same time limiting the conservatism of design factors. Given the limited database of material properties for the types of composite materials used in civil engineering, limiting the number of test specimens is an important advantage to civil design firms who do not routinely test materials as part of design, and it may make them more willing to work with composites. As discussed in Section 3.4.2.4, the mean was also chosen for its role in a procedure intended to promote reliability-based design.

3.4.2.3 Factors for Systematic Variation and Time-Dependent Behavior

The final aspect of the proposed composite design value is a system of factors to account for the systematic variations that are introduced during design and manufacture and to consider time-dependent behavior of the composite. The factors for systematic variation are referred to as Application Factors because their values depend on the specific circumstances of a particular application. These factors are developed in Section 3.5. Time-dependent composite behavior, including environmental degradation and degradation due to sustained and fatigue loading, is considered in Section 3.6.

3.4.2.4 Promoting Reliability-Based Design

Though substantial justification has already been provided for the features of the proposed design value, further motivation can be found in the intent of the author to promote reliability-based design. Currently, reliability-based design for other materials is slowly gaining ground in design firms. Its use is limited partially by the fact that design engineers do not want to learn a new design approach, but also because they do not understand the clear advantages of reliability-based design and in some cases may not believe it is safe. In the past, efforts have been made to hide the reliability aspects of these new codes from designers as much as possible. The most visible differences between LRFD codes and ASD codes are due

to the limit states design approach of LRFD, not the probabilistic basis of LRFD. As a result of these efforts, many designers still do not understand the basics of reliability-based design and therefore cannot understand its advantages or how it provides for structural safety. Without this understanding designers have no incentive to switch design philosophies in practice.

Aspects of the proposed design procedure highlight differences in reliability-based design without significantly adding to the complexity of implementation. By adopting a format where resistance factors are specific to the variability in the material, designers will be able to directly see the effect of material variability on design safety. This is just a preliminary step in increasing the understanding of the general design community, but by slowly incorporating more and more reliability knowledge into design codes, eventually the basics of reliability theory will be standard knowledge among structural engineers, opening the door for still more sophisticated design techniques. Using the mean as the design value facilitates the clarity of COV dependent resistance factors. It also makes it possible to include factors that account for the systematic differences between the mean predicted by laboratory tests and the mean witnessed in field-manufactured materials without excessively reducing composite properties. The factors for reducing the predicted mean to a value more representative of the field properties, developed in Section 3.5, are based on testing and actually represent changes in properties, not just conservative knock-down factors. Having factors that are specifically related to phenomena witnessed in the field is another way to help designers understand how the code works. It also allows designers to make adjustments to the factors if changes are justified by unique circumstances. Implementing these small changes in a state-of-the-art FRP design code has the potential to significantly advance awareness of

reliability-based design because there is no existing ASD code for FRP, forcing designers to use the newer LRFD procedure.

3.5 Characterizing and Accounting for Systematic Differences between Laboratory Derived Design Values and In-Situ Properties

Properties of composites, particularly wet layup composites, can be very sensitive to specifics of the manufacturing process. In order to determine an accurate value for use in design, it is important that the different issues affecting as-constructed properties are taken into account. It is impractical to expect designers to test specimens that replicate all aspects of field manufacture; therefore a system of "Application Factors" is proposed to assist designers in determining property values that are representative of field conditions. Based on the presently available data sets, preliminary values for some factors are developed.

3.5.1 Currently Used Factors

Each existing guideline for design of composite rehabilitation has its own set of design factors. In some cases the intent of the factors is to account for specifics of manufacture; in other cases the proposed factor is merely an empirical factor of safety. Some guidelines offer a set of partial factors, while other guidelines make use of only one factor. Nearly all guidelines include a factor for environmental degradation of the FRP, and many have limitations on cyclic and sustained stresses to prevent fatigue or stress-rupture failures. These time-dependent provisions are considered in detail in Section 3.6. Presently, a brief summary of factors not related to time-dependent behavior is provided.

ACI 440 only makes use of an environmental reduction factor when computing the composite design value (ACI, 2002). However, in computing the factored resistance an additional resistance factor on the FRP contribution is included. This multiplicative factor has a value of 0.85 for bond critical situations and 0.95 for contact critical situations.

The guideline produced by the International Federation for Structural Concrete (fib) makes use of only one FRP material safety factor; however the value for the factor, γ_f, depends on the type of fiber and the application conditions (International, 2001). This suggests that the factor is intended to account for long-term performance as well as manufacturing conditions. The factor is applied by dividing the FRP strength by the factor. Larger values of the factor are used for wet-layup systems or in situations where the site has difficult working conditions.

TR 55, published by The Concrete Society (2000), uses two partial factors on the FRP strength. One factor depends on the fiber type and the second depends on the manufacturing process. For manufacturing processes the factors are quite specific including values for different types of plate manufacture as well as wet layup. This guideline also provides a factor for long-term behavior of the modulus.

The ISIS Canada (2001) guideline uses only one factor and does not specify a specific value to be used, rather it gives suggestions made by several researchers, leaving the selection of value up to the design engineer. The Canadian Highway Bridge Design Code (CSA, 2006) uses a partial material factor for the FRP that depends on the type of material, the type of application, and the method of composite manufacture. The type of application is considered because the code includes provisions for FRP used as internal reinforcement and prestressing tendon, as well as rehabilitation.

The Japanese Society of Civil Engineers' design recommendations are intended for use with carbon and aramid fibers (Maruyama, 2001). They suggest a material factor of 1.2-1.3 for projects intended for safety and restorability and 1.0 for projects where serviceability is a concern.

The guideline written by Täljsten (2002) has perhaps the most complicated system of factors. Three primary factors are considered: η accounts for the systematic differences between a test body and a construction, γ_n considers the consequences of failure, and γ_m is a factor for material properties. γ_m is itself a combination of up to six other factors accounting for differences between test properties and in-situ properties, uncertainties in calculation models and existing dimensions, the type of failure, the level of quality control, the duration of loading, and the manufacturing process.

Karbhari (2000) has also suggested a system of partial factors for the use of composite materials in civil infrastructure. These factors are not specifically chosen with regard to strengthening; however, unlike many of the other guidelines, they consider specific sources of deviation between laboratory properties and field-manufactured properties. The factors proposed by Karbhari include ϕ_{mat} to account for how the material properties were determined (from direct testing, from lamina level testing, or from constitutive properties), ϕ_{proc} based on the type of manufacture, ϕ_{cure} based on curing conditions of the composite (ranging from autoclave to ambient), ϕ_{loc} to account for the location of manufacture, and ϕ_{degr} to account for material degradation. For each of these factors a range of possible values is given.

From this brief overview it is clear that many existing guidelines do not use separate factors to account for the random variation of composite properties and the systematic deviation of field values from the values upon which design is based, predicted through laboratory testing or mechanics based equations. Typically, the guidelines with just one factor assume that the testing procedure will replicate the systematic deviations, and the factor is included for random variation or as a general safety factor. The assumption that laboratory testing will account for systematic manufacturing differences that occur in the field is a naïve

assumption on the part of these authorizing agencies, particularly when the testing is conducted by manufacturers who cannot be familiar with the specific circumstances of a particular rehabilitation project. The proposed code format is based on the use of a FRP specific resistance factor, ψ, to account for random variation. The amount of random variation may well depend to some extent on the manufacturing process; however the systematic differences due to testing and manufacturing conditions must be considered as well. This is especially true since the proposed format will use the mean property value as the characteristic value, removing some of the conservatism built into current guidelines.

3.5.2   Types of Systematic Variation

The intent of the Application Factors is to account for all of the reasons why the properties observed in the field may not be equal to the predicted composite properties. These factors only consider differences at the stage of initial manufacture. Several sources for differences have been identified. A substantial source of deviation is the way the predicted composite value was determined. For example, prediction methods based on mechanics of materials and using the constitutive properties of the fibers and matrix are well known for over-predicting strength, even though they can be quite accurate for modulus. Properties taken from manufacturer data often represent ideal conditions that are very hard to achieve in the field. Lamina level tests are a far better prediction technique; however they cannot account for the effect of additional layers. Laminate level tests are the most accurate, but the number of layers used in the design may not be known at the time of testing. Another source of differences between tested and field properties is the curing conditions in the field. Cure in the field may be at lower or higher temperatures or humidity levels than laboratory cure. Depending on the resin system, this can impact the properties of field-cured resins. A final key factor is the level of workmanship achieved in the field. Field workmanship may suffer in

comparison to laboratory workmanship due to different levels of worker experience or due to difficult conditions in the field. Other sources may contribute to differences between laboratory- and field-manufactured FRP properties; however, the method of prediction, number of layers, curing environment, and workmanship are believed to be the most significant.

These reasons for variation account only for differences in coupon level test results. In general there is a difference between properties as tested in coupon level tests and the properties exhibited as part of the structure. This effect will not be explicitly considered, as it is very difficult to test.

3.5.3 Proposed Set of Application Factors

The mean value has been chosen as the characteristic value for design. The mean used as the characteristic value is the predicted mean, with the value predicted through any of the methods described in the previous section. To reach the final design value, appropriate partial factors are applied to the characteristic value to make it more representative of the mean property value that would be expected in the field. In general there are four partial factors to be considered: λ_{pred} is based on the accuracy of the prediction method, λ_{layers} is applied to wet layup composites to consider the effect of additional layers, λ_{cure} provides for differences in temperature and humidity from a reference condition, and λ_{work} is based on workmanship. The partial factors are applied to the predicted mean as shown in Eq. 3-9, where x_{design} and $x_{predicted}$ are the property value for design and as predicted, respectively. The design values for strength and modulus will both be determined with this equation; however the value of specific factors will likely be specific to which property is being considered.

$$x_{design} = \lambda_{pred} \lambda_{layers} \lambda_{cure} \lambda_{work} x_{predicted} \qquad \textbf{Eq. 3-9}$$

Although the present work focuses on wet layup materials, it is anticipated that a similar system of factors could be applied to prefabricated materials with a few key differences. For example, λ_{layers} would not be needed for pultruded strips and λ_{cure} might refer to the adhesive used to bond the composite strip to the concrete, rather than the matrix material of the composite itself. The general development of the system of Application Factors has been considered for both wet layup and prefabricated composites. Currently, specific factor development has been limited to wet layup materials. Table 3-21 shows the specific factors to be considered. X marks locations where a factor must be derived. For wet layup composites, values of λ_{pred} for prediction based on constitutive material properties, manufacturer data, and lamina level tests relate the predicted value to the field value of a one-layer composite. λ_{layers} is then applied to relate the field one-layer value to the field two- or three-layer value. For prefabricated composites and wet layup composites tested at the laminate level, λ_{layers} is not necessary and can be neglected or considered equal to 1. Values for λ_{cure} are likely to be very resin specific and will probably need to be provided by manufacturers. Although prefabricated composites are subject to manufacturer controlled cure and workmanship, values for these factors can still be considered applicable to the bonding agent used to apply the composite to the structure.

Table 3-21 Basic Description of System of Application Factors

Type of Factor	Wet Layup Composites	Prefabricated Composites
Property Prediction Method		
Properties of Constitutive Materials	X (use in conjunction with factors for number of layers)	X
Manufacturer Data	X (use in conjunction with factors for number of layers)	X
Lamina Level Tests	X (use in conjunction with factors for number of layers)	
Laminate Level Tests	X	X
Number of Layers		
Two-Layers	X	
Three-Layers	X	
Four-Layers	X	
Cure		
Humidity	X	X (Applies to adhesive)
Temperature	X	X (Applies to adhesive)
Workmanship	X	X (Applies to Adhesive)

3.5.4 Values of Factors for Wet Layup Composites

Based on Sets A, B, E, and F of the current testing program, values are determined for many of the proposed Application Factors. These sets were chosen because fiber and matrix properties, as well as samples for volume fraction testing, were available. Several data sets were included in the testing program with the intent of determining wide-ranging factors. However, it is clear that these sets represent only a small fraction of the available composite systems and further refinement of these factors will likely be necessary.

3.5.4.1 Consideration of Thickness

Since thickness can have a significant impact on the values calculated for strength and modulus (as discussed in Section 3.3.1), it is important that the design values of all three material properties are consistent. As seen in Table 3-4 the average thickness of multilayer composites is not equal to the number of layers multiplied by the one-layer thickness. This fact suggests that the factors of Table 3-21 should be derived for thickness, as well as strength and modulus. However, this is considered to be confusing from a design standpoint, so a different approach is used to account for systematic differences in thickness. The design thickness is defined as the one-layer thickness multiplied by the number of layers. The variation in thickness due to the addition of layers is considered in the derivation of the strength and modulus factors by considering the force and stiffness per unit width rather than the stress and modulus. This concept will be clarified as the factors are actually derived.

3.5.4.2 Values for λ_{pred}

3.5.4.2.1 Predicted Value Based on Constitutive Properties

Equations based on basic principles of mechanics are available to predict numerous properties of composite materials. Of present interest are the predictions for longitudinal strength and modulus. The predictive equation for strength is shown in Eq. 3-10, where $(\sigma_1^T)_{ult}$ denotes the ultimate tensile strength in the longitudinal direction; $(\sigma_f)_{ult}$ is the ultimate strength of the fibers; V_f and V_m are the volume fractions of the fiber and matrix, respectively; $(\varepsilon_f)_{ult}$ is the ultimate strain of the fibers; and E_m is the modulus of elasticity of the matrix.

$$\left(\sigma_1^T\right)_{ult} = \left(\sigma_f\right)_{ult} V_f + \left(\varepsilon_f\right)_{ult} E_m V_m \qquad \textbf{Eq. 3-10}$$

The mechanics based prediction for modulus is shown in Eq. 3-11. Here E_1 denotes modulus in the longitudinal direction, E_f is the longitudinal modulus of the fibers and the other variables are as noted for Eq. 3-10.

$$E_1 = E_f V_f + E_m V_m$$

Eq. 3-11

Both equations rely on the properties and volume fractions of the constitutive materials. Fiber and matrix properties were gathered for the materials of each data set. The properties necessary for prediction are summarized in Table 3-22.

Table 3-22 Properties of Fibers and Matrices for Prediction of Strength and Modulus

Data Set	Fiber			Matrix
	Ultimate Strength MPa (ksi)	Ultimate Strain	Modulus GPa (ksi)	Modulus MPa (ksi)
A	4964 (720)	0.021	232 (33600)	2068 (300)
B	4275 (620)	0.0187	228 (33100)	2068 (300)
E	4964 (720)	0.021	232 (33600)	3178 (461)
F	3241 (470)	0.045	228 (10500)	3178 (461)

Volume fractions were determined for each test panel using acid digestion at elevated temperature and pressure for carbon samples and burn off for glass samples. One sample per panel cannot account for localized variations that may have affected the properties of individual coupons; however an effort was made to select a representative section of the panel for cutting of the sample. In all cases there were several panels that contributed to one set of coupon data. Coupon data from a particular panel was compared to the predicted strength based on the V_f for that panel. Table 3-23 shows the average fiber volume fraction, average ratio of tested strength to predicted strength, and the coefficient of variation of the ratio for each data set. The same values are shown for modulus in Table 3-24. As the predictions are made independent of thickness, thickness is not considered in the derivation of this particular factor.

Table 3-23 Mean and COV of Ratio of Tested Values to Values Predicted Using Properties of Fiber and Matrix for Strength

Data Set	Mean V_f	Mean Tested/Predicted	COV Tested/Predicted
A1	0.36	0.58	0.14
A2	0.34	0.65	0.18
A3	0.32	0.62	0.19
B1	0.36	0.60	0.17
B2	0.33	0.77	0.12
B3	0.38	0.67	0.19
BV	0.36	0.66	0.06
E1	0.27	0.47	0.12
E2	0.28	0.43	0.03
E3	0.29	0.34	0.18
E4	0.27	0.31	0.04
F1	0.19	0.67	0.17
F2	0.30	0.43	0.06
F3	0.34	0.39	0.11
F4	0.35	0.36	0.07

Table 3-24 Mean and COV of Ratio of Tested Values to Values Predicted Using Properties of Fiber and Matrix for Modulus

Data Set	Mean V_f	Mean Tested/Predicted	COV Tested/Predicted
A1	0.36	0.84	0.09
A2	0.34	0.99	0.14
A3	0.32	1.05	0.08
B1	0.36	0.69	0.16
B2	0.33	0.87	0.11
B3	0.38	0.83	0.25
BV	0.36	0.78	0.11
E1	0.27	0.83	0.16
E2	0.28	0.72	0.11
E3	0.29	0.79	0.12
E4	0.27	0.80	0.06
F1	0.19	1.40	0.12
F2	0.30	1.10	0.08
F3	0.34	0.93	0.06
F4	0.35	0.92	0.04

Table 3-23 shows that for a given type of material (sets with same letter) the fiber volume fraction is fairly uniform, with the notable exception of Set F where the one-layer fiber volume fraction is substantially lower than that for two, three and four layers. The ratio of the tested strength to the predicted strength varies for a given material as different numbers of layers are used. Since all sets within a material have roughly the same fiber volume fraction, this variation is attributed to the differences caused by using layered composites. The value of λ_{pred} is intended to relate the predicted strength to the one-layer field property. Therefore the value of λ_{pred} appropriate when strength is predicted using constitutive properties is the ratio of the one-layer tested strength to the predicted strength. The values seen here are 0.58 for Set A1, 0.60 for Set B1, 0.47 for Set E1, and 0.67 for Set F1. Set E1 shows a slightly lower fiber volume fraction than Sets A1 and B1, which have fiber volume fractions similar to each other, but a much lower value of the ratio of tested to mean properties. The lower accuracy shown for Set E is attributed to the poor quality of the composite samples. These samples showed large areas of voids on the surface and between layers, which most likely caused reduced strength during testing. In contrast, Set F1 has the lowest average fiber volume fraction by far, but has the highest value of the ratio between tested and predicted properties. Based on the present data, no strong relationship could be found between fiber volume fraction and the accuracy of the prediction equation for strength. Figure 3-3 shows a plot of the ratio of tested to predicted strength against the fiber volume fraction for the one-layer sets. Each point in this plot represents one panel; therefore each set is represented several times by the different panels that composed it. This graph shows that there is not a clear relation between the fiber volume fraction and the accuracy of the prediction. Visually, there does seem to be a slight orientation of the points suggesting that the prediction method is

more accurate for lower fiber volume fractions. However, due to outlying points this visual assessment is not at all confirmed with a linear fit.
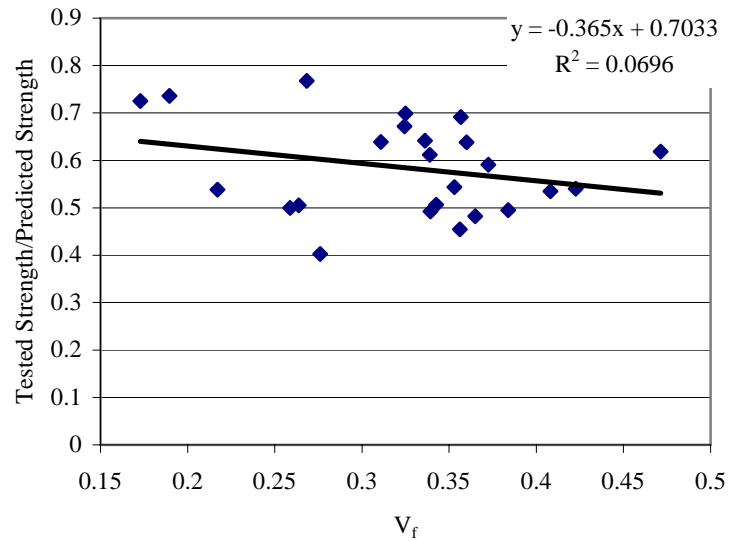
Figure 3-3 Ratio of Tested Strength to Predicted Strength vs. Fiber Volume Fraction for One-Layer Samples

If the points associated with Set E1, the poorly manufactured carbon set, are removed from this plot, the relation does become slightly stronger, as seen in Figure 3-4.
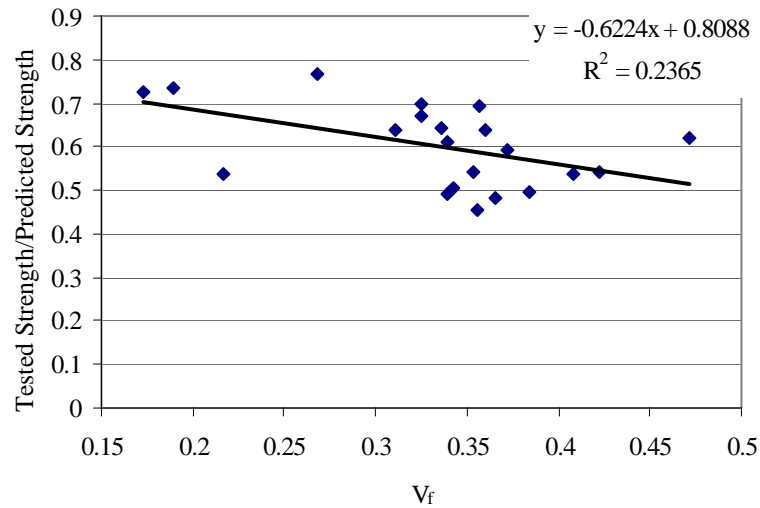
Figure 3-4 Ratio of Tested Strength to Predicted Strength vs. Fiber Volume Fraction for One-Layer Samples Without Set E1

Sets A1 and B1 both have one-layer fiber volume fractions of approximately 0.35. This value is near the upper limit anticipated for wet layup composites without the use of a press or vacuum bag. Based on the slight tendency for the prediction to become better as the fiber volume fraction decreases, it seems conservative to take the ratio of tested to predicted strength at the upper limit of fiber volume fractions as the value of λ_{pred} for this prediction method. The values of this ratio for Sets A1 and B1 are both approximately 0.6. Therefore, 0.6 is chosen as a preliminary value of λ_{pred} for strength for the case of prediction through mechanics of materials equations.

In considering modulus, the ratio of tested to predicted values shown in Table 3-24 tends to increase as the number of layers increases, following the general trend in modulus witnessed earlier. The values of the ratio for the one-layer properties are 0.84 for Set A1, 0.69 for Set B1, 0.83 for Set E1, and 1.4 for Set F1. Once again, Set F1 shows a very high value

for the ratio of tested to predicted values, with this high value attributable to the low fiber volume fraction of Set F1. Figure 3-5 shows a plot of the relation between the ratio of tested to predicted modulus to the fiber volume fraction. This plot shows a stronger trend of increasing ratio as the fiber volume fraction decreases. Therefore the decision is made to treat the value of λ_{pred} for modulus much like that for strength. A test versus prediction ratio appropriate for high values of fiber volume fraction is chosen and assumed to be conservative for lower fiber volume fractions. A straight average of Sets A1, B1, and E1 gives a value of 0.79, this is rounded up to 0.8.

The plot shows the equation:

$$y = -2.4855x + 1.6685$$
$$R^2 = 0.5425$$
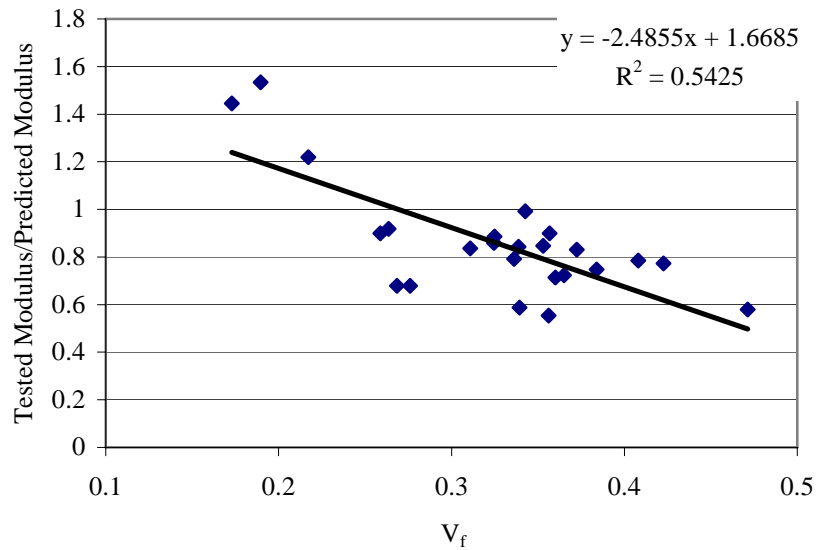
Figure 3-5 Ratio of Tested Modulus to Predicted Modulus vs. Fiber Volume Fraction for One-Layer Samples

Thickness is not considered in the prediction equations, but is an important component to the end design. In design, the stress is multiplied by the thickness to determine a force per unit width. Eq. 3-12 shows the force relationship that should hold for the design force to equal the true force.

$$\lambda_{pred}(predicted\ stress)(predicted\ thickness)=(true\ stress)(true\ thickness) \qquad \textbf{Eq. 3-12}$$

The value of λ_{pred} derived in this section relates the predicted stress to the true stress, but does not explicitly account for differences in thickness. In order for this relation to strictly hold, the predicted thickness must equal the true thickness, a situation that cannot be met without testing. Therefore, for conservatism in design, it is recommended to select the smallest reasonable value of predicted thickness, so that the predicted force per unit width will be less than or equal to the true value witnessed in the field.

3.5.4.2.2 Predicted Value Based on Manufacturer Data

Two of the available data sets were manufactured using an entire composite system (resin and fibers) from a single manufacturer. For these two data sets, Sets E and F, properties were available from the manufacturer. Properties available included typical test values and design values for tensile strength and longitudinal modulus, as well as the laminate thickness on which the calculation of these properties was based. These properties are shown in Table 3-25.

Table 3-25 Manufacturer Properties for Sets E and F

Data Set	Ultimate Tensile Strength MPa (ksi)		Longitudinal Modulus GPa (ksi)		Thickness mm (in)
	Test	Design	Test	Design	
E	876 (127)	745 (107.95)	72.4 (10,500)	61.5 (8,900)	1.0 (0.04)
F	575 (83.4)	460 (66.72)	26.1 (3,790)	20.9 (3,030)	1.3 (0.05)

As previously discussed, for composite materials calculation of ultimate stress and longitudinal modulus is highly dependent on the thickness used in calculations; thus direct comparison of tested stress to manufacturer-reported stress is only accurate when the tested

thickness and manufacturer thickness are nearly equal. The average tested thickness of Set E1 was 1.47 mm (0.058 in), substantially higher than the reported value of 1.016 mm (0.04 in). The average for Set F1 was 1.32 mm (0.052 in), much closer to the reported value of 1.27 mm (0.05 in), but still enough of a difference to be significant. Due to these differences, the comparison between tested and manufacturer properties is made based on force per unit width (stress multiplied by thickness) and stiffness per unit width (modulus times thickness). Table 3-26 shows the computed ratios of tested force and stiffness to manufacturer-reported properties for all layers of Sets E and F.

Table 3-26 Ratio of Tested Properties to Manufacturer-Reported Properties

	Typical Test Value		Manufacturer Design Value	
	Force Ratio	**Stiffness Ratio**	**Force Ratio**	**Stiffness Ratio**
E1	1.03	1.06	1.21	1.25
E2	1.00	0.98	1.17	1.16
E3	0.84	1.08	0.98	1.27
E4	0.70	1.06	0.83	1.26
F1	0.75	0.92	0.94	1.15
F2	0.70	0.98	0.88	1.22
F3	0.71	0.90	0.88	1.13
F4	0.65	0.89	0.81	1.11

The force ratios between tested properties and properties reported by the manufacturer are very different for Sets E and F. Without further data it is impossible to determine if these differences are caused by differences in the material (Set E is carbon reinforced and Set F is glass reinforced) or some other factor. At the one-layer level (which is used for selection of λ_{pred}) the typical test value seems to be a good predictor for the carbon strength, while the design value appears more appropriate for the glass samples. In general, the values of this ratio will be very sensitive to the testing and reporting procedures of individual manufacturers. No consensus value of this ratio can be selected; instead a design firm may need to conduct a

series of tests in order to determine appropriate values of this ratio for the materials commonly specified by the firm.

From these data sets it appears that manufacturers generally report values of modulus that are quite close to the mean value seen in independent testing. The differences between Sets E and F are still witnessed, though to a lesser extent. As mentioned, the value of λ_{pred} in this case is very sensitive to the manufacturer; however these results suggest that a value of 1 may be a reasonable first approximation for λ_{pred} for modulus predictions based on manufacturer test properties. A value of 1.1-1.2 is a reasonable starting point for modulus predictions based on manufacturer design properties.

Since the value of λ_{pred} in this case is based directly on comparison of force or stiffness per unit width, possible differences in thickness are implicitly considered; and the manufacturer specified one-layer thickness should be used as the design thickness.

3.5.4.2.3   Predicted Value Based on Lamina or Laminate Level Tests

In the case where composite properties are based on testing at the lamina level, there is no factor required to adjust the predicted value to the one-layer mean. λ_{pred} in this case should be set equal to 1. Other factors such as λ_{layers}, λ_{cure}, or λ_{work} may be required to adjust the properties of laboratory test specimens to those more representative of field specimens. In the case of laminate level tests, λ_{pred} and λ_{layers} should both be set equal to 1. The average tested thickness should be used as the design thickness in both cases.

3.5.4.3   Values for λ_{layers}

Though much of the difference in properties witnessed between composites with different numbers of layers can be related to the compaction of fibers that occurs when more than one layer is included, changes in strength and modulus are not purely thickness related.

The addition of layers creates regions between the layers where excess resin can collect or voids can form. With each additional layer it also becomes more difficult to keep the fibers perfectly aligned. λ_{layers} is intended to account for the differences in properties caused by these phenomena.

λ_{layers} is intended to relate the mean value of one-layer properties to the mean of two-, three-, and possibly four-layer properties. The one-layer mean is achieved through use of one of the prediction methods previously discussed and λ_{pred}. In order to account for the variations in thickness, as well as strength and modulus, comparisons will again be made on the basis of force and stiffness per unit width. λ_{layers} for strength is computed for each material using Eq. 3-13, where n refers to the number of layers. This same equation can be used to find λ_{layers} for modulus by replacing the force terms with the stiffness per unit width.

$$\lambda_{layers,n} = \frac{n - layer\, force}{n \times one - layer\, force}$$

Eq. 3-13

The values found for λ_{layers} are shown in Table 3-27 for both strength and modulus. Some trends are visible in this table. λ_{layers} for strength generally shows a significant decrease as the number of layers is increased. However, for modulus, λ_{layers} remains relatively stable and close to 1. This suggests that the stiffness per unit width is not substantially affected as the number of layers is increased.

Table 3-27 λ_{layers} for Strength and Modulus

	Data Set	2 layers	3 layers	3 layers vertical	4 layers
Force Ratio	A	0.90	0.81		
	B	0.91	0.97	0.95	
	E	0.97	0.81		0.67
	F	0.93	0.93		0.86
Stiffness Ratio	A	0.96	0.94		
	B	1.05	1.06	1.00	
	E	0.92	1.07		0.98
	F	1.06	0.97		0.96

For design purposes, generally applicable values of λ_{layers} are desired. Based on Table 3-27, λ_{layers} for modulus is set equal to 1 for all number of layers. For strength, the values of λ_{layers} are generalized as shown in Table 3-28.

Table 3-28 Generalized λ_{layers} for Design

	2 –layers	3-layers	4-layers
λ_{layers}	0.9	0.80-0.85	0.7-0.75

3.5.4.4 Values for λ_{cure}

Curing conditions in the field that differ from those used in the prediction of composite properties for design can affect the accuracy of the prediction method. Environmental factors that may affect cure include temperature and humidity. The suggested approach to this problem is to define a reference condition with a standard range of temperature and humidity. For composites cured within the reference range the value of λ_{cure} would be equal to 1. For other conditions, the value of λ_{cure} could once again be found using a comparison of force or stiffness per unit width. Eq. 3-14 shows this calculation.

$$\lambda_{cure} = \frac{force\ for\ cure\ environment}{force\ for\ reference\ cure} \qquad \textbf{Eq. 3-14}$$

λ_{cure} is intended to account only for differences in the cure environment and therefore would be expected to depend only on the specific curing environment, not on the thickness of the composite. However, composites of different numbers of layers or different amounts of resin may be affected differently by changes in cure conditions. For this reason it is suggested that the comparison in Eq. 3-14 be made on the basis of force and that testing for the determination of λ_{cure} should include composites of various numbers of layers in addition to a variety of curing environments.

It is also anticipated that λ_{cure} will depend substantially on the system in question. Manufacturers could be asked to specify values for this factor, or once again design firms may need to conduct a series of tests to determine appropriate values for the resin systems and curing environments they encounter most often in design.

3.5.4.5 Values for λ_{work}

The final factor to be considered is λ_{work}, a factor to account for differences in workmanship between test panels manufactured in a laboratory and composites manufactured in the field. Values of this factor could possibly depend on two different sources of variability: the experience of the workers and/or the difficulty of manufacture in the field as compared to manufacture in the laboratory. If all workers are assumed to be experienced in the manufacture of wet layup composites, λ_{work} is only related to the difficulties of field manufacture.

The vertical panels of Set B (Set BV) were manufactured with the intent of studying the effect of a vertical layup versus a basic horizontal layup. This set was manufactured with

three layers, and can therefore be compared to set B3. The basic statistics of these two different sets are shown in Table 3-1, Table 3-2 and Table 3-3. It can be seen that the vertical panels have slightly lower average values of strength and modulus as well as a smaller average thickness. When the force and stiffness per unit width are compared, Set BV shows approximately 96 percent of the force and 92 percent of the stiffness of Set B3. The COVs of the vertical set are less than or equal to those of the horizontal set. Based on this preliminary data it appears that values of λ_{work} slightly less than 1 may be appropriate for vertical lay ups. However, vertical layup is not anticipated to have a significant impact on the COV used to calculate ψ. Further investigation of this factor, including more data sets and layups on inverted surfaces, is merited before final values are chosen.

3.5.4.6 Summary of Factors for Systematic Variation of Wet Layup Composites

Table 3-29 summarizes the preliminary values determined for the Application Factors, which are meant to account for systematic differences between predicted values of composite properties and the values actually seen in the field. These values are based on a limited amount of data and will be subject to revision as more data becomes available.

Table 3-29 Preliminary Values of Application Factors for Wet Layup Composites

Factor	Strength	Modulus
λ_{pred}		
Properties of Constitutive Materials	0.6	0.8
Manufacturer Data	Depends on Manufacturer	
Lamina Level Tests	1	1
Laminate Level Tests	1	1
λ_{layers}		
Two-Layers	0.90	1
Three-Layers	0.8-0.85	1
Four-Layers	0.7-0.75	1
λ_{cure}		
Humidity	Depends on Resin System	
Temperature		
λ_{work}	0.95	0.9

3.5.4.7   Assessment of Factor Accuracy

The factors in Table 3-29 are based on a broad generalization of the results obtained from testing. As a preliminary check of their accuracy (particularly when two or more factors are used together) the properties predicted by these factors are now compared to the actual test results. The comparison is made by predicting a strength and modulus for each set of data and using the predicted value with the design thickness to determine a predicted force and stiffness per unit width. The actual force or stiffness for each sample in a particular set is then divided by the predicted value for the set. For all comparisons made below, λ_{layers} is taken as 0.8 for three layers and 0.7 for four layers.

Table 3-30 shows the mean and COV of the ratio of the tested force per unit width to the force per unit width predicted using Eq. 3-10 and the factors of Table 3-29 to predict strength.   The fiber volume fraction and design thickness used for prediction were the respective means of the one-layer samples. In Table 3-30 mean values of the ratio greater than

154

1 indicate that the tested values are on average greater than the predicted values. Values equal to 1 indicate that the predicted mean is equal to the tested mean. For Set A the prediction appears to be very accurate but slightly unconservative. Sets B and F show generally increasing conservatism as the number of layers increases, suggesting that the values assumed for λ_{layers} may be slightly too small for these sets. Set E shows very unconservative results. This is attributed to the low quality of Set E, which causes the value of λ_{pred} (derived from all data sets) to be too high to accurately predict test values of the one-layer lamina. The degree of variation in the ratio of tested to predicted is reasonable with an average value slightly over 0.10.

Table 3-30 Mean and COV of Ratio of Tested to Predicted Force per Unit Width
(Prediction Based on Constitutive Properties)

Data Set	1 layer		2 layer		3 layer		3 layer vertical		4 layer	
	Mean	COV	Mean	COV	Mean	COV	Mean	COV	Mean	COV
A	0.97	0.09	0.97	0.12	0.99	0.15				
B	1.00	0.18	1.20	0.12	1.23	0.14	1.26	0.13		
E	0.78	0.09	0.84	0.09	0.79	0.12			0.75	0.06
F	1.09	0.09	1.15	0.09	1.29	0.09			1.36	0.07

A similar comparison of tested and predicted values is shown in Table 3-31 for the stiffness per unit width. Once again Set A shows very good agreement between the predicted and tested values. The factors of Table 3-29 generally over-predict the modulus for Set B. In contrast to the strength predictions, Set E shows generally good agreement between tested and predicted stiffness. Set F is significantly under-predicted in this case; this is attributed to the very low fiber volume fraction of the one-layer specimens. If the fiber volume fraction used in Eq. 3-11 is increased from 0.19 for the one-layer samples to 0.30, which is more representative of the multi-layered composites in this material set, the mean values of this ratio

of tested to predicted drop to 1.20, 1.28, 1.18, and 1.16 for the one-, two-, three-, and four-layer samples, respectively. This higher fiber volume fraction, however, would cause the strength to be significantly over-predicted for all number of layers. In general, the COV of the modulus predictions is significantly higher than that for the strength predictions. This is not unexpected since the modulus test results themselves showed higher variation than the strength results.

Table 3-31 Mean and COV of Ratio of Tested to Predicted Stiffness per Unit Width
(Prediction Based on Constitutive Properties)

Data Set	1 layer		2 layer		3 layer		3 layer vertical		4 layer	
	Mean	COV	Mean	COV	Mean	COV	Mean	COV	Mean	COV
A	1.05	0.13	1.01	0.09	1.00	0.10				
B	0.87	0.25	0.93	0.25	0.93	0.22	0.98	0.18		
E	1.03	0.14	0.96	0.18	1.11	0.34			1.02	0.19
F	1.73	0.06	1.86	0.13	1.72	0.12			1.68	0.08

Comparisons between tested and predicted properties were also made for predictions based on testing of the one-layer samples (lamina level testing). The comparison for the strength ratios is shown in Table 3-32. In general there is very good agreement for all sets. Set A is no longer slightly over-predicted. Sets B and F again show increasing conservatism with an increase in the number of layers. The most significant improvement is in Set E, which is no longer severely over-predicted.

Table 3-32 Mean and COV of Ratio of Tested to Predicted Force per Unit Width
(Prediction Based on Lamina Properties)

Data Set	2 layer		3 layer		3 layer vertical		4 layer	
	Mean	COV	Mean	COV	Mean	COV	Mean	COV
A	1.01	0.12	1.02	0.15				
B	1.20	0.12	1.23	0.14	1.44	0.13		
E	1.08	0.09	1.01	0.12			0.96	0.06
F	1.04	0.09	1.17	0.09			1.24	0.07

Table 3-33 shows the modulus comparisons for predicted properties based on one-layer test results. In most cases the values are quite close. Set A shows some over-prediction. Predictions for Set B are slightly conservative in all cases. Sets E and F are slightly above or below 1 depending on the number of layers.

Table 3-33 Mean and COV of Ratio of Tested to Predicted Stiffness per Unit Width
(Prediction Based on Lamina Properties)

Data Set	2 layer		3 layer		3 layer vertical		4 layer	
	Mean	COV	Mean	COV	Mean	COV	Mean	COV
A	0.96	0.09	0.95	0.10				
B	1.06	0.25	1.07	0.22	1.12	0.18		
E	0.92	0.18	1.08	0.34			0.98	0.19
F	1.07	0.13	0.99	0.12			0.97	0.08

Both sets of comparisons are made between predictions based on factors and the actual data that was used to derive those factors. Therefore, they only really demonstrate that an acceptable generalization of the data has been made in selection of these values. However, as the composites studied here were diverse, the values derived in this work are accepted as reasonable first approximations to the factors relating laboratory properties to field properties. The suggested values of λ_{layers} have been shown to be conservative for some sets for higher

157

numbers of layers. Though the high degree of conservatism is not desirable, it is preferable to over-predicting, which would occur for the other data sets if λ_{layers} was increased. Another consideration is the fact that the one-layer samples, which were used as the basis of prediction for the comparisons in Table 3-32 and Table 3-33, were manufactured in the same conditions as the samples with multiple layers. Thus λ_{cure} and λ_{work} were implicitly included in the analysis. No testing has yet been conducted on the derivation or application of these factors. In general, using a system of factors to account for differences between the laboratory and field requires that even if different methods are used for manufacture in the two locations, the techniques for a given location are consistent. Drastic differences from normal procedures could be accommodated through λ_{work}, but it is vital that differences be observed and included in design.

These factors (and the conservatism they introduce) are not specifically included in the calibration of design factors described in Chapter 4. There are two reasons for this. Firstly, these factors are very preliminary, and therefore there is no general sense of the degree of conservatism they will introduce. In order to make the calibrated resistance factors widely applicable, a general sense of this bias would be needed. Secondly, and most importantly, the intent of these factors is to *accurately* predict field properties so that no bias is needed. It is believed that with further testing the accuracy of these factors can be significantly improved, substantially eliminating any bias that might be introduced. In fact, the intent is to have a code that is calibrated over a range of material property values without respect to how those particular values were derived. This allows for continuing research regarding the impact of field manufacturing conditions without the need to recalibrate the reliability-based resistance factors.

3.6 Time-Dependent Degradation of FRP Properties

Three phenomena are known to contribute to the long-term degradation of FRP material properties: fatigue loading, sustained loading, and environmental exposure. The typical approach to considering these different contributions is to provide limits on the FRP material stress due to sustained or fatigue loading while applying a material reduction factor to account for environmental effects. A similar approach is adopted herein. Discussion will begin with a brief overview of how long-term performance of FRPs is included in current specifications and some limitations of the current approach. The proposed method will then be discussed.

3.6.1 Current Approaches to Considering Time-Dependent Behavior of FRP Properties

3.6.1.1 Environmental Exposure

Nearly all of the guidelines used as background to this work consider time-dependent degradation of FRPs in some fashion. Current design approaches typically use a factor that is dependent on the fiber type to consider degradation due to environmental effects.

The factor used in ACI 440 (2002) is specifically intended to account for the long-term decrease in FRP ultimate strength. The environmental reduction factor, C_E, is selected based on the type of fiber and three different exposure environments: interior, exterior, and aggressive, and is applied to the composite strength and rupture strain. This is the only guideline surveyed that considered the type of environmental exposure.

Many other guidelines do not have a specific factor for material degradation but do include partial factors that depend in part on the fiber type. Often these factors place a severe penalty on glass fiber composites suggesting that they are intended to consider long-term behavior. One of the two partial factors used by TR 55 depends on the material type. This factor has a value of 1.4 for CFRP, 1.5 for AFRP and 3.5 for GFRP, clearly indicating the

conservatism applied to glass fiber composites (The Concrete Society, 2000). TR 55 also includes a partial factor for the composite modulus, which, according to the document itself, is provided to consider the change in modulus with time.

The Canadian Highway Bridge Design Code also uses material reduction factors that depend on the type of fiber (CSA, 2006). The ISIS guideline gives no specific factor for property reduction due to environmental exposure (Neale, 2001). The fib guideline has a thorough discussion of the environmental conditions that may affect composite properties but does not suggest any environment-specific factors to account for possible degradation (International, 2001). The material reduction factors in this guideline do depend on the fiber type; however the differences are quite small. For example, for wet layup systems the factor for carbon is 1.35 and that for glass is 1.50. In the design factors developed by Täljsten (2002) one of the many partial factors considers the type of fiber and the duration of loading, but no consideration is given to specific environmental effects.

As can be seen from this brief survey, the majority of current guidelines do not consider the specific environment to which the FRP will be exposed in service. Prediction of long-term properties cannot be accurate without knowledge of the exposure environment. Furthermore, these guidelines do not explicitly consider the required service life of the strengthened material. Often, strengthened structures are not expected to have the extended lifetime of new construction. Knowledge of the service life is necessary to predict the amount of degradation that will occur during that lifetime. Factors developed without explicitly considering the environmental and service life demands on the strengthening are likely to be highly conservative in most cases but may not provide enough reduction in cases of extreme exposure or extended service life. The proposed design approach will consider both of these influences in development of time-dependent factors.

3.6.1.2 Sustained and Fatigue Loading

As opposed to consideration of environmental degradation where a factor is used, degradation caused by high sustained or cyclic loads is typically accounted for through the use of a stress limitation. ACI 440 (2002) considers fatigue and sustained loading simultaneously by imposing a limit on the stress in the FRP due to the sustained load, as well as the maximum of the cyclic load. This limit is expressed as a percentage of the ultimate design strength of the FRP. These limitations are also referenced in ISIS (Neale, 2001). In addition to checks of the original structure for sustained and fatigue loading, the Canadian Highway Bridge Design Code limits the stress in the FRP due to all dead loads and sustained live loads to a percentage of the ultimate design strength (CSA, 2006). TR 55 has a stress limit on the FRP stress due to service loads to prevent stress rupture and a different limit on the maximum stress range to prevent fatigue failures (The Concrete Society, 2000). Again, these stress limitations are expressed as a percentage of the design ultimate FRP strength. The stress limitations provided in ACI 440, CHBDC, and TR 55 are shown in Table 3-34 for different types of fibers.

Table 3-34 Stress Limitations as Percentage of Ultimate Strength

Fiber Type	ACI Stress Limit	CHBDC Stress Limit	TR 55 Stress Limit on Sustained Loading	TR 55 Stress Limit on Cyclic Stresses
Carbon	55%	65%	65%	80%
Aramid	30%	35%	40%	70%
Glass	20%	25%	55%	30%

The fib guideline (International 2001) does not provide any specific guidance on design against stress rupture or fatigue failure. It does note that fatigue behavior of strengthened beams is typically controlled by the fatigue strength of the existing steel reinforcement, and therefore the strengthening should be designed so as to limit the stress range in the reinforcing

bars. Täljsten (2002) and ISIS (Neale, 2001) also note that prevention of fatigue failure in strengthened structures depends primarily on the original structure. However, Täljsten additionally suggests that the FRP may be considered adequate in fatigue if the actual strain in the fibers is limited to seventy percent of the fibers' failure strain.

3.6.2 Proposed Method for Consideration of Time-Dependent Degradation of FRP Properties

The approach proposed herein is similar to existing design methods in that limitations on stresses are used to prevent failures due to sustained and fatigue loading, while reduction factors are used to account for environmental exposure. However, the factors developed herein consider the reliability, exposure environment, and intended service life of the strengthening.

3.6.2.1 Factor for Environmental Degradation

As discussed in Section 2.2.2.10 the time-integrated approach has been deemed appropriate for calculation of time-dependent reliability. In this method, the reliability of a structure over a given time period is evaluated using the distribution of the maximum load during that period and the distribution of minimum resistance. An important goal of this work is to have factors for environmental degradation that are related to the expected service life of the strengthening. To accomplish this goal, the reliability of the strengthening at various time increments (for example, every ten years) is considered during calibration. This requires distributions of load and resistance that are relevant to the time span in question.

A prime advantage of the present design format is observed in consideration of environmental degradation. The minimum resistance of the structure will occur at the end of the time period in question, when the full degree of degradation has occurred. Neglecting further deterioration of the existing structure, the minimum resistance of the member may be

computed by using the degraded properties of the FRP. Thus, for reliability purposes, the distribution of minimum resistance may be simulated by replacing the distributions describing initial FRP strength and modulus by distributions describing the degraded state. An appropriate distribution type has been determined for each composite property. It will be assumed that the distributional form does not change as the composite degrades. Thus, to further describe the distribution of degraded properties only the mean and variation at the degraded state are needed. But, in order to make this code applicable to a variety of composite systems, a wide range of mean values will be considered as part of the calibration process anyway. Furthermore, the composite specific resistance factor, ψ, is a function of the COV and will be calibrated for a range of COV values. In the time-dependent reliability calculations, the degraded state will be described by a mean value and a COV, but the calibration range for the code already includes a wide range of possible values for mean and COV, so no extra reliability work will be necessary. In order to consider time-dependent degradation in the present framework, the mean value of composite properties used for design must be adjusted to match the mean value after degradation, and the COV after degradation must be used to determine the resistance factor, ψ.

This design framework is based on use of the true field mean as the design value. Previously, adjustments have been made to the predicted mean value in order to account for the differences witnessed between laboratory- and field-manufactured samples. Now the mean must be adjusted to match the degraded state. As shown in Eq. 3-15, a time-dependent factor, η, is now included in Eq. 3-9.

$$x_{design} = \eta \lambda_{pred} \lambda_{layers} \lambda_{cure} \lambda_{work} x_{predicted}$$

Eq. 3-15

The value of η can be quite simply derived from data as the average percent retention of properties. In order to consider both the expected service life and the service environment, η must depend on these two factors. To some extent, η will also depend on the materials subject to degradation, although it is hoped that some consistency in values will be found for a given fiber type.

The research necessary to determine values of η is largely undeveloped. Though durability studies have been conducted on FRP, the FRP tested has generally been of an aerospace or marine quality, rather than the type used for civil applications. Due to the differences in processing and quality control between these composites and those likely to be used in civil applications, the results of these studies cannot be directly applied to the design of strengthening (Karbhari, 2003). Despite the critical nature of data regarding degradation of FRPs applied as external reinforcement, this data is largely unavailable or inaccessible according to a gap analysis conducted on durability data regarding composites used in civil infrastructure (Karbhari, 2003).

Some data is, however, becoming available. A recent work by Abanilla (2004) made use of an accelerated testing program and Arrhenius rate relation to predict the percent retention of both tensile strength and modulus for two- and six-layer carbon fiber composites immersed in deionized water at 23°C. The composites used in this study were manufactured via wet layup and cured at ambient conditions so as to be representative of the composites typically used in strengthening of civil infrastructure. The predictive equations found in this work are shown in Table 3-35.

Table 3-35 Predictive Equations for Property Retention Based on an Arrhenius Rate Relation (Abanilla, 2004)

Property	Percent Retention of Properties (t is expressed in days)
2-layer strength	% = -3.366 ln(t) + 106.07
2-layer modulus	% = -0.4182 ln(t) + 106.07
6-layer strength	% = -5.2543 ln(t) + 106.07
6-layer modulus	% = -2.9626 ln(t) + 106.07

The exposure condition used in this study, immersion in deionized water at 23°C, is not representative of a typical environment for FRP used in rehabilitation. However, these results are representative of the kind of durability data that are needed. With degradation data in this format, η may be determined for any desired service life. For example, for a two-layer composite exposed for ten years, the first equation shown in Table 3-35 can be used to predict 78.5% retention of strength. The value of η is therefore 0.785 when designing for a ten-year service life in this exposure environment. While η is available for any time using equations of this format, reliability is also a function of the load distribution and this distribution may only be available for certain periods of time.

3.6.2.1.1   Advantages of this Approach

The approach to handling time-dependent degradation in composite properties presented herein has several advantages over other approaches currently in use. Foremost is the fact that this approach allows explicit consideration of the expected time in service and the expected service environment. By considering the exact conditions to which the composite will be subjected, this approach allows for the full utilization of composite properties without excessively conservative knockdown factors, yet is still calibrated to provide adequate safety. Any environment and any composite system may be considered; the only limitation is the

availability of data. This approach is also advantageous in that it allows for the incorporation of new data without the need to recalibrate the resistance factors. New data can be directly applied to computation of the degraded resistance properties, and as long as the degraded values fall into the range of properties over which the code is calibrated, no recalibration is necessary. The use of load distributions appropriate for different time periods will likely require an adjustment in the design factors. In order to maintain the simple application of the percent retention as the value of η, it may be best to provide different load factors for different design lives. This topic, however, requires further investigation from a reliability standpoint. A final advantage of this approach is that it is intuitive and direct from the viewpoint of designers. This contributes further to the goal of creating a design format that is understandable and will be accepted by engineers without extensive reliability knowledge. Having factors with a clear meaning also enables designers to adjust the factors slightly in situations where they feel the change is appropriate.

3.6.2.1.2   Limitations of Proposed Approach

The proposed approach to time-dependent degradation of FRP strengthening was specifically developed in consideration of the limited amount of durability data for these materials. Given the current state of knowledge regarding FRP, more sophisticated approaches are not yet justified. However, there are several limitations to the ideas presented here. Perhaps the most significant drawback preventing immediate application of this design procedure is the unavailability of data. This approach is tailored to easily accept new data, but this assumes that data is available and research is continuing. The equations presented by Abanilla (2004) are ideal for use in this design methodology; however, while they allow for time specific factors, only one exposure environment is considered, thus environment specific factors are still on the horizon. Another issue is that this approach does not explicitly consider

166

the effect of the initial condition of the composite on the degree of degradation it experiences. This could be considered in the testing process to determine η, but is not handled by the design procedure itself.

3.6.2.2   Stress Limitations for Sustained and Fatigue Loading

3.6.2.2.1   Sustained Loading

A search of the literature found no studies specifically considering the effect of sustained loads on FRP composites applied as external reinforcement. With no additional data, the recommendations of existing guidelines, which are based on the sustained loading behavior of unbonded FRPs, are the best information available. The Canadian Highway Bridge Design Code (CHBDC) provides one of the newest sets of limits, and thus these are suggested for design (CSA, 2006). To prevent failure due to stress-rupture, the stress in CFRP, AFRP, and GFRP due to sustained loads should not exceed 65%, 35%, or 25%, respectively, of the ultimate composite strength (CSA, 2006). In the CHBDC this limit is applied to the specified tensile strength provided by the manufacturer, which is defined as the lower fifth percentile of test results. This specified strength does not include a reduction factor for environmental effects or manufacturing differences. Though the lower fifth percentile may be substantially lower than the mean value for a highly variable material, the consideration of manufacturing and environmental exposure included in the procedure proposed herein should bring the design mean into this lower range. Therefore, for the current approach, it is recommended to apply the CHBDC stress limitations to the design value of ultimate stress including the environmental reduction factor.

3.6.2.2.2   Fatigue loading

Several studies conducted on the fatigue loading of FRP strengthened, reinforced concrete members in flexure have found that the structural behavior is controlled by the

fatigue performance of the existing steel reinforcement (Barnes and Mays, 1999; Aidoo et al., 2004). This was found to be true for relatively small beams, with a length of 2.3 m (7.55 feet) (Barnes and Mays, 1999) as well as a 62% scaling of actual T-beam bridge girders, with a length of 6.1 m (20.0 feet) (Aidoo et al., 2004). For a similar range of loading between the strengthened and unstrengthened beams, the application of FRP can significantly improve the fatigue life of a member by reducing the stress range experienced by the steel (Barnes and Mays, 1999). This was found to be true even for beams that had lost steel due to corrosion before the FRP was applied (Masoud et al., 2005). This would suggest that for repair work FRP would be expected to extend the fatigue life. However, Barnes and Mays (1999) also found that the fatigue capacity as a percentage of the ultimate capacity was slightly lower for a beam with external FRP plates, suggesting that some care may be necessary when the design is intended to significantly increase the load carrying capacity.

Aidoo et al.(2004) found that the fatigue behavior was sensitive to the bond between the FRP and concrete. They noted that as debonding started from cracks at midspan load was unable to be transferred to the FRP, thus increasing the stress in the steel at midspan and returning the fatigue behavior to that of the unstrengthened section. In their study all of the strengthened girders failed through fracture of reinforcing steel, followed by a secondary complete debonding of the FRP in one direction from midspan (Aidoo et al., 2004). Ferrier et. al. (2005) specifically looked at the fatigue behavior of the FRP/concrete bond using single and double lap FRP-concrete specimens to assess the loss in bond shear strength. They found that the bond performance depends on the properties of the polymer matrix. Polymers with higher glass transition temperatures exhibited better bond performance; this was attributed to the potential for polymers with lower glass transition temperatures to suffer a loss in mechanical properties due to heating caused by the fatigue loading. This loss of mechanical

properties is critical to the crack initiation stage of bond failure through fatigue. Though their study did specifically consider the fatigue characteristics of bonded joints, their work should be extended to consider how the loss of bond strength affects the fatigue life of the reinforcing steel.

As the FRP itself appears to have little impact on the fatigue life, no limiting stress range for the composite material is suggested for design. This recommendation also seems justified based on the fact that when strengthening is applied the existing steel has already been subjected to numerous cycles, while the FRP is brand new. However, the characterization of fatigue behavior for the overall member, found in these studies, should be considered in design. Though the application of FRP can result in significant extensions in fatigue life by lowering the stress range experienced in the steel, this reduction in the stress range is only possible in the presence of effective bonding between the FRP and concrete. Given the significance of the FRP / concrete bond and its uncertain characteristics, it would seem prudent not to count on the extended fatigue life provided by composites until the degradation of bond under fatigue loading is better understood. Therefore, it is proposed that the existing structure should be evaluated for fatigue, based on the relevant standards, without considering the FRP contribution. (This evaluation could perhaps be conducted with slightly relaxed safety factors since the FRP should provide some contribution.) This would suggest that FRP composites are not a recommended repair strategy for structures that are critical in fatigue, unless some method can be found to guarantee the effectiveness of the FRP / concrete bond.

3.7 Summary

This chapter has developed the information and procedures necessary to model the statistical variation of the composite and to calculate a design value based on the

manufacturing conditions and expected exposure environment. Importantly, the Application Factors and environmental factors are not based on reliability calculations. This allows research on these factors to continue without requiring recalibration of the resistance factors. Chapter 4 will further develop the reliability procedure by conducting a large example calibration. With the calibrated resistance factors resulting from Chapter 4, a full design example will be presented in Chapter 5 utilizing the design values and COV dependent resistance factors advocated in this chapter.

Chapter 4. Calibration of Resistance Factors for Flexural Strengthening of Bridge Girders

4.1 Introduction

Chapters 2 and 3 of this report have laid most of the groundwork for the consideration of reliability-based factors for FRP strengthening. Chapter 2 discussed reliability methods and available statistical models for the existing structure and the loads acting on it. It also laid out the model chosen to represent continued degradation of the structure. Chapter 3 developed models of statistical variation of the FRP and a system of factors for use in computing the design value. This chapter builds on that foundation by calibrating preliminary resistance factors for the design of flexural strengthening of bridge girders.

This chapter begins by describing the calibration procedure. Then conclusions from numerous smaller calibration examples, which were used to assess the effect of different variables in the reliability calculation process before this large calibration was undertaken, are briefly discussed. These examples are described in detail in Appendix C. Following this discussion the calibration process is followed step-by-step to derive the resistance factors needed for design. The results obtained during the calibration process are analyzed, and conclusions are drawn regarding the direction of future development. Finally, following these results, a subset of the calibration range is used to investigate certain assumptions made during the calibration process.

4.2 Procedure for Calibration of Resistance Factors

In certain simplified cases, load and resistance factors can be determined based on purely analytical considerations using Mean-Value First-Order Second-Moment (MVFOSM) reliability methods (described in Section 2.2.2.5.1) (Melchers, 1999). However, these approaches are limited to specific formulations of the limit state function and the use of all

Normal or all Lognormal variables. They also do not consider additional design factors such as the composite specific factor, ψ, proposed in this report. Therefore, a more general trial and error procedure is implemented. In principle, this procedure follows the technique detailed in the Transportation Research Circular, *Calibration to Determine Load and Resistance Factors for Geotechnical and Structural Design* (Allen et al., 2005).Figure 4-1 shows a flowchart of the calibration procedure. The basic idea of the procedure is to define the range of cases to which the calibrated factors will be applicable, create many trial designs spanning the range of applicability with assumed values of the resistance factors, evaluate the reliability of the designs, and then select the set of factors, ϕ and ψ, that minimizes the differences between the evaluated reliabilities (β) and the target reliability (β_T). The procedure shown below assumes that the load factors have already been selected or determined and is used to calibrate resistance factors compatible with those load factors.
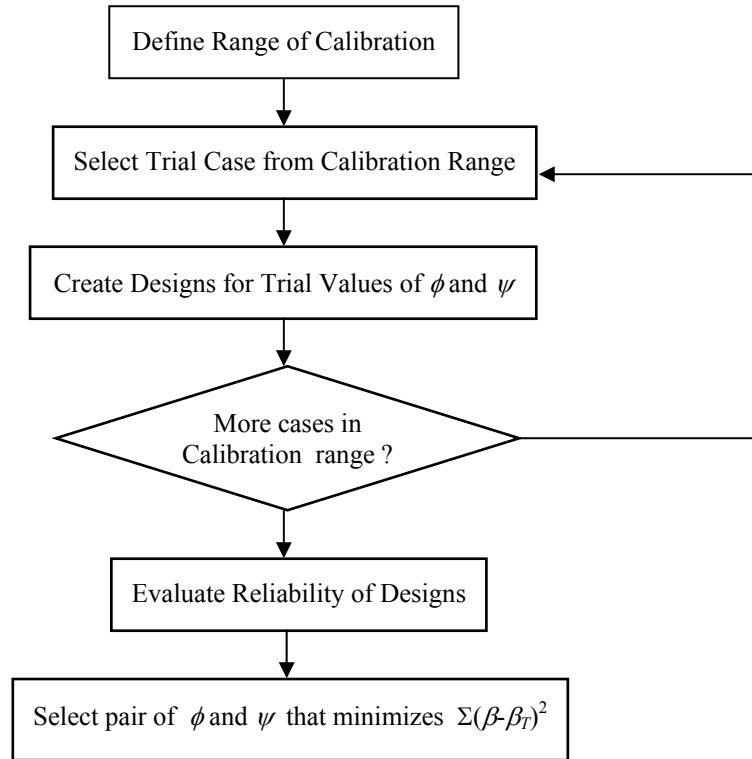
Figure 4-1 Basic Flowchart for Calibration Procedure

To calibrate design factors for a given limit state a range of calibration must be first chosen. This range defines the cases to which the resulting design factors will be applicable. In this report the range of calibration is defined by the properties of the composite materials, the states of FRP degradation, the geometries of representative members for strengthening, the prospective design lives, and the state of the reinforcement at the time of strengthening as well as that anticipated due to further corrosion. (The loss of reinforcement cross-section due to corrosion is the only form of continued structural deterioration considered in this work.) The range of calibration for this work is described in detail in Section 4.4.

The next step in the calibration process is to create designs of strengthening for the trial cases based on assumed values of the resistance factors. For this work the value of ψ has been allowed to vary from 0.95 to 0.50 in increments of 0.05. In most of the initial work (described in Appendix C) the value of ϕ was held constant at 0.9. For this final calibration, this factor too was allowed to change, taking on values of 0.85, 0.9, and 0.95. The designs are created based on the loads and load factors specified for the design code and the selected strengthening design procedure. The specific models and procedures as well as the simple computer program used to create the trial designs are described in Section 4.5.

After designs are created, their reliability must be assessed. The reliability of each design is evaluated using the reliability method and statistical models chosen for use in calibration. The statistical descriptions of random variables and the procedures and programs used for reliability calculation in this calibration example are described in Section 4.6.

Finally, the resulting set of reliability data must be analyzed to choose the set of resistance factors that minimizes the difference between the target reliability and the actual reliabilities calculated from the designs. The errors are squared so that large positive and negative values of error are not able to counteract each other. Analysis of the results and recommended values of resistance factors are presented in Section 4.7.

This procedure must be repeated for each case requiring a resistance factor. For example, separate factors need to be calibrated for different limit states, such as shear and flexure. In the design procedure proposed herein, different resistance factors will be calibrated for different values of the COV of composite properties. Since this design procedure makes use of characteristic (and thus design) values that are independent of the amount of variation, new trial designs do not have to be created for each level of COV. However, the reliability of designs must be evaluated for different statistical descriptions of the FRP properties, and

different values of the resistance factor will be found to minimize the error between the computed reliability and the target reliability for different COVs. This somewhat simplified calibration process is one of many arguments for use of the mean value as the design value.

4.3 Summary of Previous Calibration Work

Before work began on this large calibration, numerous smaller examples were conducted to isolate the impact of key variables and to identify general trends in reliability. These examples and their results are described in detail in Appendix C. What follows here is a brief summary of the different examples conducted and the major conclusions drawn from them. These conclusions have influenced how the final calibration was conducted.

For all of the following examples a sample girder was designed following the *AASHTO LRFD Bridge Design Specifications* (AASHTO, 1998[1]). This girder is described in Section C.2 of Appendix C. The strengthening was designed using sectional analysis following the procedure described in Section C.3 and Appendix D.

4.3.1 Load Factors for Strengthening Design (Section C.5)

The first example considered which set of load factors should be used in the design of strengthening. A major goal of this work is to create a design procedure for strengthening that is compatible with the existing procedures for new design; therefore, it was initially assumed that the load factors would be the same as those specified in the *AASHTO LRFD Bridge Design Specifications* (AASHTO, 1998 and 2004). However, as small examples were conducted, it became apparent that designs created to meet the factored load demand following the LRFD specifications had reliabilities significantly higher than the projected target range of 2.5 to 3.5. Thus, a less demanding set of load requirements was desired. In an

---

[1] Two different versions of the AASHTO LRFD specifications are referenced in this work. The 1998 version was used for U.S. Customary Units, and the 2004 version was used for SI units. Nearly all calculations were initially conducted in U.S. Customary Units.

effort to tie the strengthening procedures to existing AASHTO requirements, the load factors from the *Manual for Condition Evaluation and Load and Resistance Factor Rating (LRFR) of Highway Bridges* (AASHTO, 2003) were considered. The sample girder was assumed to have suffered a 20% loss in steel, and repairs were designed to allow the girder to meet the LRFD and LRFR factored loads. The results of this example showed that the reliability of designs created using the LRFR factors were much closer to the target range. Therefore, the resistance factors in the final calibration will be calibrated to work with the LRFR load factors to meet the target reliability. The LRFR load factors for the Strength I limit state are shown in Table 4-1. This limit state corresponds to "normal vehicular use of the bridge without wind," (AASHTO, 1998), and is the only limit state considered for calibration of resistance factors in this work.

Table 4-1 LRFR Load Factors for Design of Strengthening (AASHTO, 2003)

Load Component	Load Factor
Cast-in-place Dead load	1.25
Wearing Surface	1.5
Live + Impact Load	1.35

It should be noted that the LRFD specification makes use of a term, η, to modify the factored loads. This factor is intended to consider the ductility, redundancy, and operational importance of the structure. This term is not used in the LRFR manual and therefore is not considered elsewhere in this chapter.

4.3.2 Large Example Calibration without Corrosion (Section C.6)

A relatively large example was conducted to consider a number of issues, including different ways of calculating the reliability index, different FRP properties and different amounts of variation in those properties, different amounts of steel remaining at the time of

strengthening, and the time specific load models provided in Nowak (1999). The conclusions drawn from this example are:

- The hybrid reliability method, which combines Monte Carlo Simulation of resistance statistics with FORM evaluation of the reliability index, appears to produce reasonable predictions of reliability. Furthermore, it is much faster to implement and will allow for the consideration of numerous cases in the final calibration.

- The amount of remaining steel is significant to the resulting reliability. Though this value cannot be accurately assessed in the field, a design procedure that does not at least consider the change in reliability resulting from different percentages of steel loss will likely be highly conservative.

- The distributions of maximum live load taken from *NCHRP Report 368* (Nowak, 1999) appear to have some inconsistencies; thus a simplified description of live load as described in Section 2.5 of Chapter 2 will be used.

- Small differences in composite materials appear to have relatively little effect on the reliability. This example considered six different sample materials with varying properties representing the range of values anticipated from wet layup carbon reinforced composites, and generally only small differences were observed in the reliability. However, several different materials will still be used in the final calibration.

- Changes in the composite modulus COV have a limited impact on the final resistance factor for the bond model used in these examples.

4.3.3 Example with Corrosion (Section C.8)

A final example was used to better understand the models available for describing corrosion. A design procedure was proposed whereby the amount of steel remaining at the end of the desired service life was estimated, and the amount of FRP required for strengthening was calculated based on this amount of steel. The estimate of remaining steel for design was based on general corrosion; however the reliability was assessed for both general and pitting corrosion. General corrosion was found to more severely affect the reliability for the time periods and rebar sizes under consideration. Therefore, this final calibration is conducted using general corrosion to describe deterioration of the steel.

4.4 Range of Calibration

The reliability of a strengthening design depends on many different factors. Some of these factors include the material properties, the geometry and properties of the existing structure, and the amount of load carried by the FRP. As each situation is unique, it is impossible to select a set of design factors that will allow the target reliability to be reached for all cases. Therefore, it is very important to define the range of designs over which the code is applicable. The design factors can then be calibrated so that designs within the selected range will be reasonably close to the target reliability. If certain types of design are more common than others, given knowledge of these designs, the selection process can be weighted so that the most common designs will have reliabilities very close to the target.

In selecting the range of calibration for this project, specific goals and limits as to the type of designs, materials and limit states to be considered were set. The selected range of calibration - including the materials, levels of FRP degradation, sample girders, time periods, and corrosion states of the existing structure - is described in detail in the following sections. An extensive range of calibration was selected in an attempt to answer many of the questions

about reliability-based design of strengthening and in order to produce resistance factors applicable to real situations. However, it is important to remember that this is just an example case, and the reliability procedures developed throughout this report can be applied to many different situations, extending or changing completely the range of calibration.

4.4.1   Composite Materials

4.4.1.1   Initial Properties

Five different sample materials were considered for this example. The properties of these materials are shown in Table 4-2. These properties are slightly different than those used for previous examples. The properties chosen previously were selected by looking at the general range of properties seen in the test results described in Chapter 3 without regard for the composite thickness. For selection in this final example, the property values were based on a one-layer thickness of 1.27 mm (0.05 in), and the properties seen in test results were normalized to this thickness. Therefore, for example, the average 1-layer strength of Set A, 1043.7 MPa (151.38 ksi), with an average thickness of 1.1 mm (0.0434in), was normalized to a value of 906.0 MPa (131.4 ksi) for a thickness of 1.27 mm (0.05 in). The properties chosen were meant to represent general composites, thus the value was rounded to 896.3 MPa (130 ksi). Other values in Table 4-2 are close to values obtained by normalizing other materials tested. Set B was constructed with a very thin fabric that would be unlikely to produce a composite with a one-layer thickness of 1.27 mm (0.05 in); therefore its low normalized value of 432.3 MPa (62.7 ksi) was not chosen. The values of modulus were chosen based on the normalized strengths to produce some variety in the ultimate strain of the composite for different materials. The strains shown in Table 4-2 are representative of typical ultimate strains found in wet layup composites.

179

Table 4-2 Generalized Composite Properties Used for Calibration

Material	Ultimate Strength MPa (ksi)	Modulus GPa (ksi)	1-Layer Thickness mm (in)	Ultimate Strain mm/mm (in/in)
1	620.5 (90)	51.7 (7500)	1.27 (0.05)	0.012
2	689.5 (100)	61.4 (8900)	1.27 (0.05)	0.011
3	758.4 (110)	58.6 (8500)	1.27 (0.05)	0.013
4	827.4 (120)	59.3 (8600)	1.27 (0.05)	0.014
5	896.3 (130)	68.9 (10000)	1.27 (0.05)	0.013

As noted at the end of Section 3.4.5.7 of Chapter 3, the Application Factors derived in Chapter 3 are not explicitly considered in this calibration example. These factors are meant to remain outside the reliability calculations to allow for the easy inclusion of new research. Thus the values shown in Table 4-2 assume that any necessary Application Factors have already been applied and that the values in the table are design values. The implications of this assumption are described further in Section C.4 of Appendix C.

4.4.1.2 States of FRP Degradation

Three different states of FRP degradation were considered. The first state was no degradation of material properties with time. The second state was dependent on the time in service and was modeled using the Arrhenius rate equations developed by Abanilla (2004), which are described in Section 3.6.2.1 of Chapter 3. Following this work, the percent retention of tensile strength for two-layer composites can be predicted with Eq. 4-1, where *t* is the time of exposure expressed in days. Eq. 4-2 can be used to predict the retention in composite modulus; however this equation does not indicate deterioration of the modulus until times beyond the 50-year range considered in this study. Therefore, this equation was not used, and the percent retention of modulus was taken as one hundred percent.

$$\textit{\% retention in strength} = -3.366\ln(t) + 106.07 \qquad \textbf{Eq. 4-1}$$

$$\textit{\% retention in modulus} = -0.418\ln(t) + 106.07 \qquad \textbf{Eq. 4-2}$$

Eq. 4-1 and Eq. 4-2 were derived based on data collected from composite samples subjected to constant immersion in deionized water. It was thought that this exposure environment might be too harsh to represent field conditions; therefore the third degradation state was chosen to represent a less severe environment. For this state, the Arrhenius rate equations were again used, but the degradation was assumed to occur five times slower. For example, to predict the state of degradation after 20 years of exposure, for the case of slower degradation t was set equal to 1460 days (4 years). Since the same model was used, but slowed by a factor of five, the modulus was again assumed to have one hundred percent retention of properties for the full time span in question. These three different degradation states were generally referred to as ND, for no degradation, AD, for Arrhenius rate degradation, and SD for slower degradation model.

In Section 3.6.2.1 of Chapter 3, material values for the calculation of time-dependent reliability are discussed, and the theory is proposed that the resistance factors need only to be calibrated for an acceptable range of material values without explicitly considering degradation. In this example, time-dependent environmental degradation of the composite is specifically included to test this hypothesis.

4.4.2 Representative Members for Calibration

The members considered in this example application were all plain reinforced concrete T-beams. In order to determine typical dimensions for these members, a survey was conducted of approximately one hundred T-beam bridges in the Caltrans bridge network based on plans provided by Caltrans. The bridges surveyed represented many different situations; however highway overpasses were probably the most common. The quality of different plans

varied significantly. In many cases it was not possible to assess all the quantities of interest. Some of the plans were incomplete, referencing other documents. Some of the pdf files were difficult to read, and not all dimensions could be determined. Some plans described two bridges (for example, for different directions of traffic on a divided highway), and in this case typically just one of the two bridges was assessed. There were also many plans describing widening projects; since each widening project was unique it was difficult to assess common features. However, in some cases the original bridge plans were included with the drawings for the widening project, and this allowed the dimensions of the original bridge to be assessed and included in the survey. For each bridge plan as many of the quantities shown in Table 4-3 as possible were noted. The center of the longest span was deemed the critical location for positive moments and quantities at this location were noted. Interior girders were surveyed because they typically bear a higher distribution of loads. The dimensions collected from the full set of bridge plans studied are provided in Appendix G.

Table 4-3 Bridge Quantities Surveyed to Determine Common Values for Calibration

Bridge Quantity	Assessment Notes
Span	Longest span on the bridge
Deck width	Assumes uniform width, includes sidewalks, etc.
Roadway width	Assumes uniform width, does not include sidewalks, curbs, railings, etc.
Number of girders	For expansion projects this was usually considered as the original number of uniform girders
Girder Spacing	Center-to-center distance between girders
Overhang	Amount of deck protruding past exterior girders
Slab thickness	Designs did not seem to specify any additional thickness for wearing
Depth of T-beam	Depth including the thickness of the deck When the depth varied, the depth at the center of the span was taken
Width of T	Taken as width away from diaphragms
Cover of Reinforcement	Top and bottom of slab as well as at bottom of girders (when available)
Concrete Strength	Most often specified as an allowable stress used in design
Steel Yield	Most often specified as an allowable stress used in design
Area of steel, girder	Taken at center of span in interior girders Temperature and shrinkage steel along the side of the girders was not considered.
Area of steel, slab	Was generally found to have same spacing top and bottom

After all of the plans had been examined, key dimensions were analyzed in an attempt to gain an understanding of the range of typical values. Each plan is unique and rather than develop generic designs with average quantities, typical values were identified and then plans roughly meeting these values were selected from the inventory of available plans.

4.4.2.1 Typical Bridge Dimensions

In choosing bridges for calibration, emphasis was given to the length of spans and typical numbers of girders. Some consideration was also given to the deck width. For the other quantities some variation was sought, but no special effort was made to match the range of values observed in the bridge survey.

Figure 4-2 shows a histogram of the bridge spans surveyed. The bars are centered over the span length shown on the horizontal axis and range 1.52 m (5 ft) on either side. Clearly the vast majority of bridge spans fall within the range from 10.7 - 25.9 meters (35-85 ft). Figure 4-3 shows a histogram of the number of girders. Four, five, and six girders are most common, with seven and eight also showing significant frequency. Finally, Figure 4-4 shows the histogram of deck widths. Again, the widths shown on the horizontal axis represent the center of the range; in this case the spread is 1.22 m (4 ft) on either side. The majority of decks surveyed are less than 14 meters (46 ft) wide, with another small peak near 17.7 meters (58 ft).
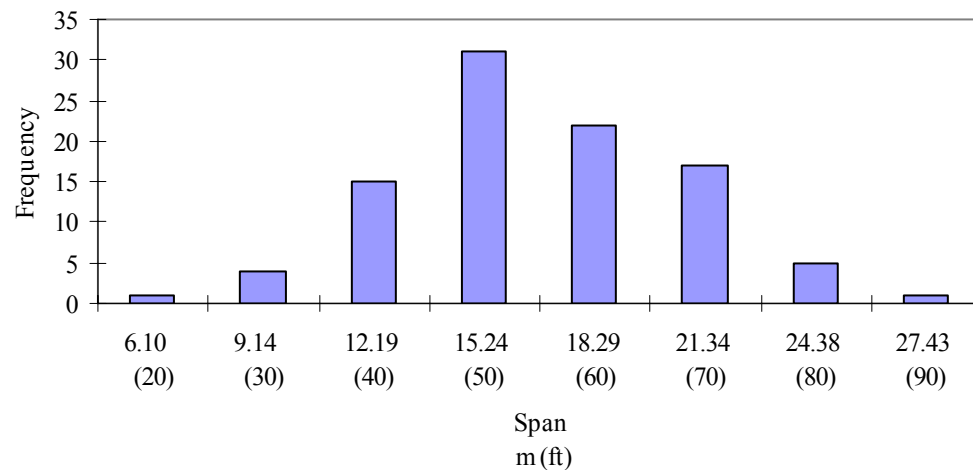
Figure 4-2 Histogram of Bridge Spans
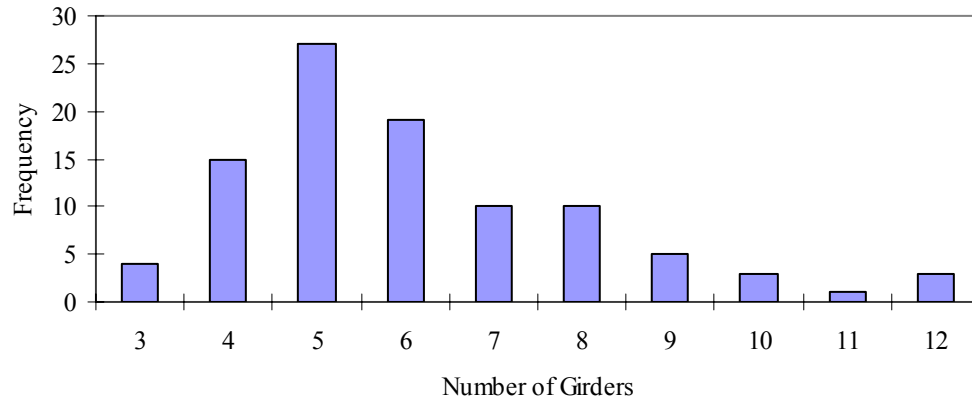
Figure 4-3 Histogram of Number of Girders
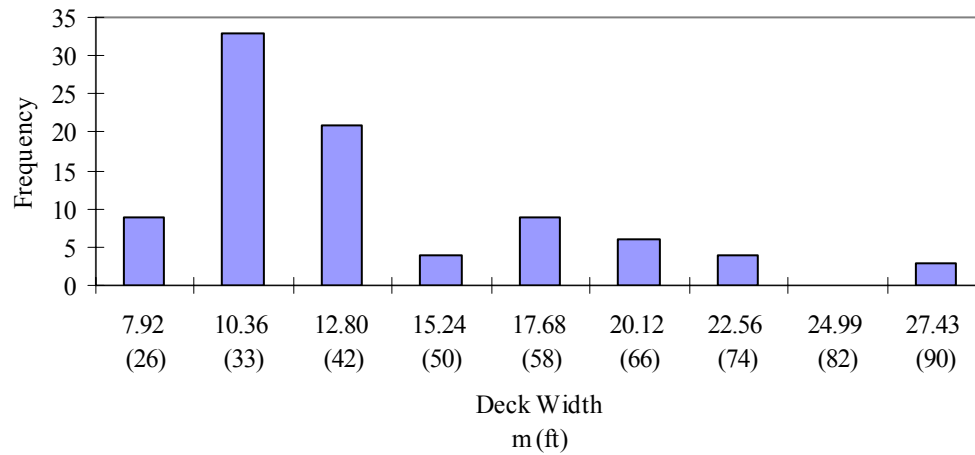
Figure 4-4 Histogram of Deck Width

4.4.2.2   Selected Girders

Based on the general range of significant values identified in the previous section, originally ten bridge plans were selected from the inventory.   After preliminary analysis identified two bridges that were significantly under strength, ten additional girders were selected, with an emphasis on older bridges. In addition to the range of dimensions

represented, other criteria were also important in the selection of bridges for calibration. Plans were chosen that were as complete and readable as possible. Bridges with more complicated geometry, such as curves or changes in elevation of the road deck, were avoided. Bridges that were not roughly uniform throughout their length were also avoided. Many bridges had some degree of skew; this was not used as a selection factor, because skew was ignored during calibration work. Table 4-4 shows key geometric quantities of the bridge decks chosen for further calibration work. Table 4-5, Table 4-6, and Table 4-7 show a comparison between the bridges selected and the complete sample of bridges surveyed in terms of population percentages for the span length, number of girders, and deck width, respectively. These tables show that the selected bridges are able to represent the range of values exhibited in the full sample fairly well, particularly with respect to the span length and number of girders.

Table 4-4 Geometry of Representative Bridges for Calibration

Bridge Number	Caltrans Bridge ID	Year of Construction	Span m (ft)	Deck Width m (ft)	Number of Girders	Girder Spacing m (ft)
1	290247R	1976	12.2 (40)	13.0 (42.5)	5	2.7 (9)
2	290032G	1967	13.4 (44)	12.5 (41)	6	2.2 (7.25)
3	120156L	1966	14.0 (46)	10.4 (34)	5	2.3 (7.5)
4	120152L	1964	15.8 (52)	13.6 (44.75)	7	2.1 (6.83)
5	110071L	1966	16.8 (55)	12.1 (39.66)	6	2.2 (7.33)
6	290174L	1968	17.0 (56)	18.2 (59.66)	8	2.4 (7.83)
7	290159	1959	18.2 (59.64)	17.2 (56.29)	7	2.6 (8.66)
8	260007	1960	19.8 (65)	10.4 (34)	4	2.8 (9.33)
9	110062	1966	20.4 (67)	10.4 (34)	5	2.2 (7.25)
10	570115	1953	22.9 (75)	10.3 (33.66)	4	2.7 (9)
11	570427L	1963	13.3 (43.5)	12.1 (39.67)	6	2.1 (7)
12	540500L	1968	13.4 (44)	10.1 (33.33)	4	2.7 (9)
13	120106	1960	14.2 (46.58)	10.4 (34)	5	2.3 (7.5)
14	540429R	1957	14.6 (48)	18.1 (59.33)	8	2.1 (7)
15	570219	1941	15.8 (52)	10.6 (34.67)	5	2.5 (8.167)
16	120146	1961	17.2 (56.5)	27.0 (88.67)	12	2.3 (7.67)
17	570125	1951	16.8 (55)	10.3 (33.67)	4	2.6 (8.5)
18	110069	1962	20.3 (66.5)	10.4 (34)	5	2.2 (7.33)
19	290064	1953	21.3 (70)	9.9 (32.33)	4	2.7 (9)
20	540483	1956	22.9 (75)	9.9 (32.33)	4	2.6 (8.5)

**Table 4-5 Comparison of Distribution of Span Lengths for Selected Bridges
and All Bridges Surveyed**

Span Length m (ft)	Selected	All Bridges
4.9-7.6 (16-25)	0.0%	1.0%
7.9-10.7 (26-35)	0.0%	4.2%
11.0-13.7 (36-45)	20.0%	15.6%
14.0-16.8 (46-55)	35.0%	32.3%
17.1-19.8 (56-65)	20.0%	22.9%
20.1-22.9 (66-75)	25.0%	17.7%
23.2-25.9 (76-85)	0.0%	5.2%
26.2-29.0 (86-95)	0.0%	1.0%

**Table 4-6 Comparison of Distribution of Number of Girders for Selected Bridges
and All Bridges Surveyed**

Number of Girders	Selected	All Bridges
3	0.0%	4.1%
4	30.0%	15.5%
5	30.0%	27.8%
6	15.0%	19.6%
7	10.0%	10.3%
8	10.0%	10.3%
9	0.0%	5.2%
10	0.0%	3.1%
11	0.0%	1.0%
12	5.0%	3.1%

**Table 4-7 Comparison of Distribution of Deck Widths for Selected Bridges
and All Bridges Surveyed**

Deck Width m (ft)	Selected	Whole Sample
>=9.1 (>=30)	0.0%	10.1%
9.1-11.6 (30-38)	60.0%	37.1%
11.6-14.0 (38-46)	20.0%	23.6%
14.0-16.5 (46-54)	0.0%	4.5%
16.5-18.9 (54-62)	15.0%	10.1%
18.9-21.3 (62-70)	0.0%	6.7%
21.3-23.8 (70-78)	0.0%	4.5%
23.8-26.2 (78-86)	0.0%	0.0%
26.2-28.7 (86-94)	5.0%	3.4%

Nearly all of the bridges selected were designed according to allowable stress principles, and thus their plans provided material properties in terms of the allowable stresses used for design. For reliability analysis the compressive strength of the concrete and the yield strength of the steel were needed. An older version of Chapter 8 of the *Caltrans Bridge Design Specifications* (1993), Reinforced Concrete, was used to interpret design strengths based on the allowable stresses in the plans. Based as much as possible on the plans themselves, but in some cases on the date of construction, all girders except girder 1 were found to be constructed with Grade 40 reinforcement. Girder 1 was from the newest bridge of those selected and was constructed with Grade 60 steel. The minimum compressive strength for concrete was set at 22.4 MPa (3,250 psi) in the design specifications, and this value was

used as the concrete strength for all girders. It is noted that in reality the compressive strength is likely to be higher; however this cannot be confirmed without testing of individual structures. However, Caltrans guidelines such as the SDC do use higher values without tests.

4.4.3   Time Periods Considered

As discussed throughout this report, strengthening projects are not anticipated to have the extended lifetime of a new civil engineering structure. In an effort to prevent overly conservative estimates of degradation, this example will explicitly consider the design life of the strengthening. Periods of 10, 20, 30, 40, and 50 years were selected somewhat arbitrarily as likely design lives. TR 55 discusses a design lifetime of 30 years for strengthening projects (The Concrete Society, 2000).

4.4.4   Cases of Continued Degradation

Knowing the exact state of the existing structure at the time of strengthening is a highly unlikely situation. This work has focused on strengthening required due to a deficiency in the reinforcing steel, a difficult parameter to assess given that the steel is embedded in concrete. In some cases, for example if the deficiency is due to an error at the design stage, it might be possible to have a fairly good estimate of the structural dimensions, including the steel area. In other cases, where the structure is in need of strengthening because it has experienced degradation, the existing state could be entirely unknown because current methods of non-destructive evaluation or health monitoring are not yet capable of accurately predicting the amount of steel remaining. There is also significant uncertainty regarding the progression of continuing degradation. Often a structure may be subject to some repair before strengthening is applied, and this could slow the rate of corrosion. Or a member that was strengthened to replace missing reinforcement could start to corrode some time in the future after strengthening is applied.

It is impossible to consider every possible condition requiring strengthening or every pattern of continuing degradation following the application of FRP in the general sense required for a design code. However, in order to consider a range of possibilities, six different corrosion conditions were considered in this work:

1. 10% steel loss at the time of strengthening and no continuing corrosion

2. 20% steel loss at the time of strengthening and no continuing corrosion

3. 30% steel loss at the time of strengthening and no continuing corrosion

4. 10% steel loss at the time of strengthening *with* continuing corrosion

5. 20% steel loss at the time of strengthening *with* continuing corrosion

6. 30% steel loss at the time of strengthening *with* continuing corrosion

Conditions 1 through 3 could represent a case where strengthening was applied to replace missing steel not lost to corrosion, or possibly a case where an effective corrosion protection scheme was applied to the remaining steel. Conditions 4 through 6 could represent girders with steel lost to corrosion where the corrosion process was not effectively arrested. The continuing corrosion in these cases is modeled with the model of general corrosion described in Sections 2.7.4 of Chapter 2 and Section C.8 of Appendix C.

4.5 Design of Strengthening

After defining the range over which the resistance factors will be calibrated, the next step is to create trial designs for each of the cases to be considered using assumed values of the resistance factors. For this example ϕ was allowed to take values of 0.95, 0.9, and 0.85, while ψ ranged from 0.5-0.95 in increments of 0.05. Given this range of resistance factors

and the range of calibration described in Section 4.4, up to 13,500 trial designs were created for each girder.

4.5.1   Calculation of Design Load

All of the bridge girders selected were designed and constructed as continuous structures. Therefore, the load demands acting on the structure had to be assessed based on this continuous nature. Due to the difficulty of analyzing moving loads, a computer software program was used to analyze the bridges. QConBridge™ is a live load analysis program developed by the Washington State Department of Transportation (2006), and available for free on the department's website. This program analyzes the HL-93 load model (including the impact factor of 0.33), described in Section 2.6.2, on continuous frame structures. The program allows for user-defined distributed and point loads to model sources of dead load and allows hinges to be inserted within spans. The program provides factored load combinations for the Strength I, Service I, Service II, Service III, and Fatigue limit state combinations as defined by AASHTO (1998 and 2004). The user can set the impact factor. The load factors can also be changed by the user; however it was found that the change in load factor was not implemented correctly in the program. Therefore, only the unfactored load components were taken from the program and these were used to compute the factored load demand using the LRFR load factors shown in Table 4-1. Another software program provided by Caltrans, Caltrans Bridge Design System (CT-BDS) is also capable of analyzing moving loads on continuous structures. This program does have some live load models built into the software, but also allows user definition of live loads. Each software program has some advantages over the other program, regarding the ease of use. A comparison of the two programs, as shown in Table 4-8 showed very similar results. All analysis for this work was conducted with QConBridge™ because it had an easy to use graphical application for defining the bridge

geometry, its results were consistently slightly more conservative, and because it was available for use earlier than CT-BDS. More details regarding QConBridge™ and how it was used for this work are available in Appendix H.

Table 4-8 Comparison of QConBridge™ and CT-BDS for Selected Girders

Girder	QConBridge™			CT-BDS		
	Dead kN-m (kip-ft)	Wearing kN-m (kip-ft)	Live kN-m (kip-ft)	Dead kN-m (kip-ft)	Wearing kN-m (kip-ft)	Live kN-m (kip-ft)
2	113.8 (84)	28.5 (21)	726.3 (536)	113.8 (84)	28.5 (21)	718.2 (530)
4	200.5 (148)	46.1 (34)	670.7 (495)	200.5 (148)	46.1 (34)	661.2 (488)
6	257.5 (190)	55.6 (41)	1005.4 (742)	257.5 (190)	55.6 (41)	995.9 (735)
10	666.7 (492)	98.9 (73)	2069.1 (1527)	657.2 (485)	98.9 (73)	2054.2 (1516)

The load analysis models were quite simplified. QConBridge™ was used to model a single girder line. Only major features of the bridges were modeled; hinges as defined in the plans were inserted, and point loads were used to model diaphragm weight (see Appendix H). The dead and wearing loads for a single interior girder were input to the program to calculate the moment effects due to these load components. The live load effect for a single girder due to the HL-93 load model was computed based on live-load distribution factors from the *AASHTO LRFD Bridge Design Specifications* (AASHTO, 1998 and 2004).

Equations for calculating the distribution factors for moment in interior beams for different bridge types and limitations on the range of applicability of the equations are given in Table 4.6.2.2.2b-1 of the AASHTO specifications (1998 and 2004). For T-beam structures the equations for one and two design lanes loaded are shown in Eq. 4-3 and Eq. 4-4, respectively. These empirical equations are provided in both SI (AASHTO, 2004) and customary U.S. units (AASHTO, 1998). These equations do produce slightly different results, due to their

empirical nature, and it should be noted that the equations in customary U.S. units were used

as this work was being conducted.   In these equations S is the spacing between girders in mm

(ft), L is the length of the span in mm (ft), K_g is the longitudinal stiffness parameter in mm[4]

(in[4]), and t_s is the thickness of the slab in mm (in). Calculation of K_g is described in Section

4.6.2.2.1 of the LRFD specifications. This parameter is related to the moment of inertia of the

cross-section; however the description in the specification seems to be geared toward

composite girders with steel beams and concrete decks. No additional information on this

parameter specific to concrete T-beams could be found in the specifications, and therefore the

moment of inertia of the complete T-section was used in calculation. Due to the exponent on

this term, it has a very small effect on the overall distribution factor, and therefore small

differences in K_g have very little impact on the overall factor.

$$g = 0.06 + \left(\frac{S}{4300}\right)^{0.4} \left(\frac{S}{L}\right)^{0.3} \left(\frac{K_g}{Lt_s^3}\right)^{0.1} \quad \text{SI}$$

Eq. 4-3

$$g = 0.06 + \left(\frac{S}{14}\right)^{0.4} \left(\frac{S}{L}\right)^{0.3} \left(\frac{K_g}{12.0Lt_s^3}\right)^{0.1} \quad \text{US}$$

$$g = 0.075 + \left(\frac{S}{2900}\right)^{0.6} \left(\frac{S}{L}\right)^{0.2} \left(\frac{K_g}{Lt_s^3}\right)^{0.1} \quad \text{SI}$$

Eq. 4-4

$$g = 0.075 + \left(\frac{S}{9.5}\right)^{0.6} \left(\frac{S}{L}\right)^{0.2} \left(\frac{K_g}{12.0Lt_s^3}\right)^{0.1} \quad \text{US}$$

When these equations are used to derive the distribution factors, no separate factor is

needed for multiple presence. These distribution factors expressed in terms of a single wheel

line (as opposed to full axles as provided in the AASHTO specification and shown in Eq. 4-3

and Eq. 4-4) were used in calibration of the LRFD specification with the K_g term set equal to 1

(Nowak, 1999). More information about the derivation of these equations and how they compare to finite element analysis of bridges can be found in Zokaie (2000).

Based on the three load components calculated by the software program, the factored LRFR load for strengthening design was calculated as shown in Eq. 4-5. Table 4-9 shows the load components and factored loads for all twenty girders.

$$\sum_i \gamma_i Q_i = 1.25 Dead + 1.5 Wearing + 1.35 g(Live + Impact)$$ **Eq. 4-5**

Table 4-9 Load Components and LRFR Factored Load for Design

Girder	Dead Load kN-m (kip-ft)	Wearing Load kN-m (kip-ft)	Live + Impact Load kN-m (kip-ft)	Distribution Factor (g)	Factored Loads kN-m (kip-ft)
1	202.0 (149.07)	53.5 (39.48)	784.5 (578.95)	0.73	1110.1 (819.23)
2	113.3 (83.60)	27.9 (20.59)	884.3 (652.59)	0.66	972.2 (717.51)
3	126.1 (93.09)	31.9 (23.54)	751.3 (554.43)	0.66	876.5 (646.90)
4	147.1 (147.98)	46.4 (34.22)	841.4 (620.94)	0.62	1025.2 (756.57)
5	228.5 (168.65)	54.0 (39.86)	930.1 (686.43)	0.64	1168.1 (862.09)
6	256.8 (189.49)	55.8 (41.15)	1252.8 (924.56)	0.69	1575.1 (1162.44)
7	308.5 (227.64)	60.0 (44.31)	1073.8 (792.49)	0.76	1577.9 (1164.53)
8	364.0 (268.66)	72.3 (53.38)	1261.9 (931.32)	0.76	1855.0 (1369.01)
9	380.8 (281.06)	74.5 (54.99)	1248.5 (921.37)	0.65	1689.9 (1247.14)
10	666.9 (492.16)	98.3 (72.53)	2539.3 (1874.00)	0.79	3689.6 (2722.94)
11	112.5 (83.01)	29.7 (21.92)	700.4 (516.91)	0.65	796.0 (587.48)
12	165.6 (122.20)	33.6 (24.82)	840.9 (620.60)	0.78	1139.1 (840.70)
13	149.3 (110.17)	34.6 (25.56)	745.9 (550.48)	0.68	919.9 (678.89)
14	142.4 (105.08)	34.2 (25.26)	784.5 (578.94)	0.64	907.6 (669.81)
15	263.8 (194.70)	48.3 (35.66)	894.3 (660.00)	0.72	1269.3 (936.77)
16	246.3 (181.78)	50.1 (37.00)	988.8 (729.74)	0.68	1293.0 (954.28)
17	359.6 (265.39)	52.8 (38.96)	970.6 (716.32)	0.81	1590.0 (1173.48)
18	378.4 (279.27)	72.3 (53.35)	1233.4 (910.24)	0.66	1683.1 (1242.16)
19	490.7 (362.13)	78.1 (57.62)	1430.9 (1056.00)	0.79	2252.8 (1662.60)
20	515.9 (380.74)	83.4 (61.56)	1994.6 (1472.00)	0.74	2754.5 (2032.82)

4.5.2 Calculation of Resistance

The resistance of a strengthened girder was calculated using sectional analysis as described in Appendix D. The basic assumption of plane sections remaining plane under bending was used to justify a linear strain distribution through the depth of the member. The girder was assumed to reach its ultimate capacity when either the concrete or FRP reached a limiting strain value, at which point the steel was assumed to have already yielded. The strain limit for compressive failure in the concrete was set at 0.003 mm/mm, as specified in ACI 318 (1999). For design purposes, the limiting strain in the FRP was calculated as the minimum of 0.9 multiplied by the composite rupture strain or the predicted debonding strain (discussed in detail in the following section). Due to the large compressive area of concrete provided by the deck slab, the limiting FRP strain was the controlling value for design. As the concrete had not yet reached its ultimate capacity, common values of the stress block factors were not able to accurately represent the force carried by the concrete when the FRP was reaching its limiting strain. Therefore equations based on a parabolic stress distribution in the concrete were used to calculate more accurate values for the stress-block factors as a function of the strain in the concrete located furthest from the neutral axis (Collins and Mitchell, 1991). The neutral axis of the girder was found through iteration by enforcing equilibrium and continuity in the presence of the limiting strains. From there, the factored moment equation took the form shown in Eq. 4-6, where ϕ is the resistance factor applied to the total resistance, A_s is the area of steel, f_y is the yield strength of the steel, d is the depth from the compression face to the steel, a is the depth of the assumed rectangular stress block, ψ is the composite specific resistance factor, A_{FRP} is the area of FRP, f_{FRP} is the stress in the FRP at the debonding strain limit, and h is the total depth of the section.

$$\phi M_n = \phi(A_s f_y(d - \tfrac{a}{2}) + \psi A_{FRP} f_{FRP}(h - \tfrac{a}{2}))$$

Eq. 4-6

This method is an approximate approach to calculating the capacity of concrete sections with externally-bonded FRP reinforcement. The stress block factors are intended for use in rectangular sections, rather than the T-sections of the girders used in this calibration. However, this simplifying approximation was still adopted for several reasons. First, the girders were under-reinforced; the amount of tensile reinforcement controlled the capacity of the section, making the exact force carried in the concrete of less importance. Secondly, the neutral axis at ultimate was often found to be in the flange, allowing the section to be exactly modeled as a rectangular section. And finally the *AASHTO LRFD Bridge Design Specifications* (1998) note that "for flanged sections in which the neutral axis is in the web, [the stress block factor] has experimentally been found to be an adequate approximation." Other authors have used models wherein the member cross-section is divided into a number of layers and unidirectional stress-strain relationships are used to describe the behavior of the material composing each layer (Okeil et.al., 2002). This approach was thought to be impractical for design code development because it would require that designers either have access to software implementing this modeling technique or develop their own computer programs.

4.5.2.1 Debonding Model

The small examples discussed in Appendix C all made use of the debonding model proposed in ACI 440 (ACI, 2002). At the present time there is no definitive model for predicting the strain at which FRP will begin to debond from a concrete surface. The ACI 440 model was initially used because it was easy to implement and was published in a well-known source. However, as the present work was progressing, other work being conducted by the research group found that the ACI model often over-predicted the debonding strain for

198

experiments conducted in the laboratory (Ghosh and Karbhari, 2006). Therefore, a different debonding model was used for this final calibration example.

The newer debonding model is based on a fracture mechanics approach to the interface (Niu et al., 2005). Though a complete understanding of debonding behavior depends on the distribution of flexural cracking in the RC beam, a simplified approach has been used here. Based on this simplified analysis, the axial load carried in the FRP when debonding initiates can be calculated as shown in Eq. 4-7, where P_{max} is the axial load, b_{FRP} is the width of the FRP strip, G_f is the interfacial fracture energy, E_{FRP} is the modulus of the FRP, and t_{FRP} is the thickness of the FRP. These equations are derived analytically and may be used with any set of consistent units.

$$P_{max} = b_{FRP}\sqrt{2G_f E_{FRP} t_{FRP}}$$

Eq. 4-7

The strain in the FRP when this axial load is reached can be calculated by dividing the axial load by the cross-sectional area of the FRP and the modulus of the FRP, as shown in Eq. 4-8.

$$\varepsilon_{max} = \frac{P_{max}}{t_{FRP} b_{FRP} E_{FRP}}$$

Eq. 4-8

Eq. 4-7 and Eq. 4-8 can then be combined as shown in Eq. 4-9.

$$\varepsilon_{max} = \sqrt{\frac{2G_f}{E_{FRP} t_{FRP}}}$$

Eq. 4-9

The interfacial fracture energy can be approximately related to the compressive strength of the concrete as shown in Eq. 4-10, where f'_c is the concrete compressive strength expressed in MPa and G_f is in N/mm.

$$G_f = 0.644 f_c'^{0.19}$$

<div align="right">**Eq. 4-10**</div>

This simplified analytical derivation of the strain at which the FRP begins to debond is not able to account for all of the conditions affecting the debonding strain and was found to consistently under-predict debonding strains found in test results. Thus an empirical factor of 1.5 is applied to the predicted debonding strain.

In some cases, particularly when degradation models are applied to the FRP, the predicted debonding strain exceeds the rupture strain of the FRP. For design purposes, the rupture strain multiplied by 0.9 was used as the upper limit on FRP strain. The value of 0.9 is arbitrary and was carried over from the design approach used in ACI 440, where it is likely meant to provide some conservatism in the estimate of composite rupture strain.

4.5.3   Computational Procedure

For the purposes of this work, a strengthening design consists of the width and number of layers of composite to be applied. Given the large range of conditions over which this sample calibration was conducted, a simple program was developed in Java to automate the design process. For a single girder the program was able to consider all calibration conditions by looping through the different resistance factors, materials, FRP degradation models, and levels of steel degradation. Situations where the initial capacity without FRP was already sufficient were identified and marked with "nsn" for no strengthening needed. For all other cases, the required amount of FRP to meet the factored load demand was determined with a much higher degree of accuracy than would be used in actual design. The thickness of the FRP was not allowed to exceed three layers. This value was chosen as the limit based on the rapidly decreasing debonding strain with the addition of layers and the practical difficulty of maintaining good fiber alignment when applying more than three layers.   The fabric width was selected to the nearest 6.35 mm (0.25 in) and was allowed to reach the full width of the

stem of the T-girder. This approach was taken to be very accurate in determining the required resistance factor. During actual design, conservatism will undoubtedly be added by using fabrics in commonly available widths.

If the design strength could not be reached with three layers of FRP applied to the full width of the T-section the case was marked with "np" for not possible. The resulting designs were outputted in a format that could be easily transformed into an input file for the MCS program used to evaluate the statistics of resistance. Each girder had its own unique geometry, and these geometrical values were hard coded into the program. An example of the code for girder 6 is provided in Section F.1 of Appendix F. Please note that design calculations were conducted in the U.S. customary system of units.

4.5.4   Summary of Designs

The number and type of strengthening designs varied widely from girder to girder. There was no consistent relation between the initial capacity of the girder (before assumed steel loss) and the design strength required based on the LRFR load factors. The amount of steel specified at the design stage could have been affected by a number of considerations, including the age of the design, the need to use additional steel to meet serviceability criteria, or the constraints imposed by the use of standard reinforcing bars in discreet bar sizes. As a result, for different girders, designs were needed (and able to be created) for different ranges of the six corrosion conditions. Two of the girders, girder 2 and girder 10, had such low initial capacities that they could not be strengthened to meet the load requirements for any of the corrosion conditions.

4.6   Calculation of Reliability

With designs created for each girder for as many of the calibration conditions as possible, the next step was to evaluate the reliability of the designs. This was conducted using

201

the hybrid procedure, employing both Monte Carlo Simulation and First-Order Reliability Methods, as described in Appendix E.

4.6.1 Description of Load Uncertainty

As specified in *NCHRP Report 368* (Nowak, 1999) Normal distributions were used to model the three components of total load: cast-in-place dead load, wearing surface load, and live load plus impact. The distributions were derived for a specific girder line as described in Section 4.5.1 where the design load was calculated. The distribution parameters for each of these load components were calculated based on bias factors and COVs provided in the report. The bias factor for cast-in-place dead load is 1.05, and the COV is 0.10 (Nowak, 1999). The mean load due to the wearing surface is taken as the value due to a mean thickness of 88.9 mm (3.5 inches), and its COV is 0.25 (Nowak, 1999). The bias factor on the live load depends on the span length of the girder. A factor of 1.1 is used to include the increase in live load due to dynamic impact. A constant value of 0.18 is used for the COV of live plus impact load (Nowak, 1999).

For FORM analysis, these three separate Normal distributions were combined into one Normal distribution to describe the total load. The mean of the distribution of total load is calculated by summing the mean of each of the three separate distributions, as shown in Eq. 4-11. This same equation is shown as a function of the individual load components and their respective bias factors in Eq. 4-12, where D represents the cast-in-place dead load, W represents the load due to the wearing surface at a thickness of 88.9 mm (3.5 in), and L represents the static live load distributed to a single girder.

$$\mu_{load} = \mu_{dead} + \mu_{wearing} + \mu_{live+impact}$$
<div align="right">**Eq. 4-11**</div>

$$\mu_{load} = \lambda_{dead} D + W + \lambda_{live} L(1.1)$$
<div align="right">**Eq. 4-12**</div>

The standard deviation of the total load was calculated following Eq. 4-13. This equation is expressed in terms of the numerical values for COV and the mean of the different load components in Eq. 4-14.

$$\sigma_{load} = \sqrt{\sigma_{dead}^2 + \sigma_{wearing}^2 + \sigma_{live+impact}^2} \qquad \textbf{Eq. 4-13}$$

$$\sigma_{load} = \sqrt{(0.10\mu_{dead})^2 + (0.25\mu_{wearing})^2 + (0.18\mu_{live+impact})^2} \qquad \textbf{Eq. 4-14}$$

Table 4-10 shows the mean of the three separate load components, the live load bias factor, which is a function of the span, and the mean and standard deviation of total load for use in reliability analysis of the girders. The live load bias factors are seen to be quite consistent, even for changing span lengths. This occurs because the HL-93 live load model was used. This model was selected for use in the LRFD code because it gave a more uniform value for the bias than the HS-20 live load model.

Table 4-10 Distribution Parameters of Load for Reliability Analysis

Girder	μ_{dead} kN-m (kip-ft)	$\mu_{wearing}$ kN-m (kip-ft)	λ_{live}	$\mu_{live+impact}$ kN-m (kip-ft)	μ_{total} kN-m (kip-ft)	σ_{total} kN-m (kip-ft)
1	212.1 (156.52)	62.4 (46.06)	1.35	680.0 (501.85)	954.5 (704.43)	125.2 (92.40)
2	118.9 (87.78)	32.5 (24.02)	1.34	706.8 (521.62)	858.3 (633.42)	128.0 (94.49)
3	132.4 (97.74)	34.6 (25.51)	1.34	584.8 (431.54)	751.7 (554.79)	106.4 (78.55)
4	210.5 (155.38)	54.1 (39.92)	1.33	609.1 (449.50)	873.7 (644.80)	112.4 (82.99)
5	239.9 (177.08)	63.0 (46.50)	1.325	691.2 (510.10)	994.1 (733.68)	127.7 (94.23)
6	269.6 (198.96)	65.1 (48.03)	1.325	1014.8 (748.96)	1349.5 (995.95)	185.4 (136.80)
7	323.9 (239.02)	70.1 (51.70)	1.32	940.2 (693.88)	1334.1 (984.60)	173.2 (127.82)
8	382.2 (282.10)	84.4 (62.27)	1.315	1111.1 (819.99)	1577.7 (1164.36)	204.7 (151.07)
9	399.9 (295.11)	86.9 (64.15)	1.31	945.1 (697.51)	1431.9 (1056.77)	176.1 (129.97)
10	700.2 (516.76)	114.7 (84.62)	1.315	2364.8 (1745.25)	3179.3 (2346.63)	432.3 (319.07)
11	118.1 (87.16)	34.3 (25.30)	1.34	667.0 (492.25)	819.4 (604.71)	120.9 (89.26)
12	173.9 (128.31)	33.4 (24.65)	1.34	767.5 (566.40)	974.7 (719.36)	139.5 (102.94)
13	156.7 (115.68)	40.4 (29.82)	1.34	592.6 (437.34)	789.7 (582.83)	108.3 (79.91)
14	149.5 (110.34)	39.9 (29.47)	1.33	585.3 (431.93)	774.7 (571.74)	106.9 (78.87)
15	277.0 (204.44)	52.4 (38.65)	1.33	751.1 (554.35)	1080.5 (797.45)	138.6 (102.31)
16	258.6 (190.87)	58.5 (43.16)	1.325	783.84 (578.48)	1101.0 (812.51)	144.2 (106.41)
17	377.6 (278.66)	61.6 (45.45)	1.325	915.4 (675.57)	135.1 (999.67)	169.7 (125.27)
18	397.3 (293.23)	84.3 (62.24)	1.325	955.3 (705.05)	1437.0 (1060.52)	177.7 (131.18)
19	515.2 (380.24)	91.1 (67.23)	1.31	1312.1 (968.32)	1918.4 (1415.78)	242.8 (179.19)
20	541.7 (399.77)	97.3 (71.82)	1.315	1723.3 (1271.81)	2362.3 (1743.41)	315.8 (233.08)

4.6.2 Description of Resistance Uncertainty

The uncertainty in the resistance of the strengthened girders was characterized by considering the uncertainty in design variables contributing to the total resistance.   Statistical descriptions for nearly all of the design variables were used along with a computational model of resistance in a Monte Carlo procedure to determine the mean and standard deviation of the resistance. Table 4-11 shows the statistical descriptions used for each variable. For properties of the existing structure the origin of these descriptions was discussed in Chapter 2.   The distributions used to describe the FRP were derived in Chapter 3.   The distributions for water/cement ratio and interfacial fracture energy were based on the judgment of the present researchers.

Table 4-11 Statistical Distributions Used in Reliability Analysis

Variable	Statistical Distribution	Mean	COV
Error in width of T (additive)	Normal	2.4 mm (3/32 in)	2
Error in depth to steel (additive)	Normal	-3.2 mm (-1/8 in)	2
Error in total depth (additive)	Normal	-4.8 mm (-3/16 in)	2.667
Error in cover (additive)	Normal	1.6 mm (1/16)	5
Error in slab thickness (additive)	Normal	0.8 mm (1/32 in)	15
Error in initial steel area (multiplicative)	Normal Truncated between 0.96 and 1.06	0.97	0.024
Concrete Compressive Strength	Normal	Depends on nominal f'_c see Section 2.4.1	0.15
Concrete Modulus	Normal	Depends on Compressive Strength, see Section 2.4.1	0.10
Steel Yield Strength	Beta	Depends on steel grade, see Section 2.4.2	Depends on steel grade, see Section 2.4.2
Steel Modulus	Normal	201.3 GPa (29200 ksi)	0.024
FRP Strength	Weibull	Depends on material, see Table 4-2	Allowed to vary from 0.05 to 0.30
FRP Modulus	Lognormal	Depends on material, see Table 4-2	0.20
FRP Thickness (1-layer)	Lognormal	1.27 mm (0.05 in)	0.05
Water / cement ratio	Normal	0.45	0.05
Interfacial Fracture Energy	Normal	Depends on concrete strength, see Eq. 4-10	0.10
Dead Load (for calculation of initial strain)	Normal	Depends on Girder, see Table 4-10	0.10

The model used to compute the resistance of the strengthened section was the same as that used for design, except the arbitrary factor of 0.9 applied to the predicted composite

rupture strain was removed. In the future, a more accurate analysis of the section capacity could be implemented at the reliability evaluation stage. This simple approach was adopted here because features of the analysis process (such as prediction of the debonding strain) are still under development and the main interest of the current project was to consider as many different design cases as possible, which was facilitated by a quick and simple analysis procedure.

4.6.3   Calculation Procedures

4.6.3.1   Simulation of Resistance

The mean and standard deviation of resistance were estimated following the Monte Carlo procedure described in Section E.1 of Appendix E. A simple Java program was developed to conduct the simulation. The design program output included dimensions of the strengthening, the material number, and values of time used to describe the corrosion condition. These parameters were provided to the simulation program as input. The simulation program was specific to each girder and had the girder dimensions hard coded into the program, including the area of steel before continuing corrosion corresponding to the different corrosion cases. It also had values for the material properties hard coded into the program. For a given design, the program automatically looped over the different possibilities for the strength COV. An example of this program for girder 9 is included in Section F.2 of Appendix F.

There are several specifics about the implementation that should be noted. First, there was some concern about the random number generators provided in Java libraries. It was noticed that there were slight differences (less than 1%) in the numerical values of the mean and standard deviation of resistance when the same program was run on different computers. Even with these small differences in the mean and standard deviation, it was found that the

computed value of the reliability index did not change significantly. Nonetheless, all analysis was conducted on a single computer to provide for strict comparability. All calculations in this program were performed in customary U.S. units. This program computes the initial strain at the bottom concrete face. A limit was placed on this initial strain to prevent cases that were not realistic, such as negative values of initial soffit strain. This limit was found to result in almost no change in the final result, but did improve the stability of the simulation, particularly for cases with continuing corrosion. The output of this program was compiled in Microsoft Excel spreadsheets where the FORM procedure as described in Section E.3 of Appendix E was conducted.

4.6.3.1.1 Convergence

In order to determine the number of trials to include in each simulation, a small set of example cases were quickly conducted. girder 17 was chosen for this small test because it was a girder that was capable of being strengthened for all 6 different corrosion cases. The designs used for the test were selected to represent all six different corrosion cases and all five materials, as well as a range of FRP areas. The mean and standard deviation of resistance were estimated for all six different strength COVs for a range of different number of trials. Figure 4-5 shows an example plot of the changes in the computed mean of resistance with the number of trials. This specific example is for corrosion condition 1 and material 3, but it is representative of the results for the other corrosion conditions and materials. Similar results were also observed for the standard deviation.
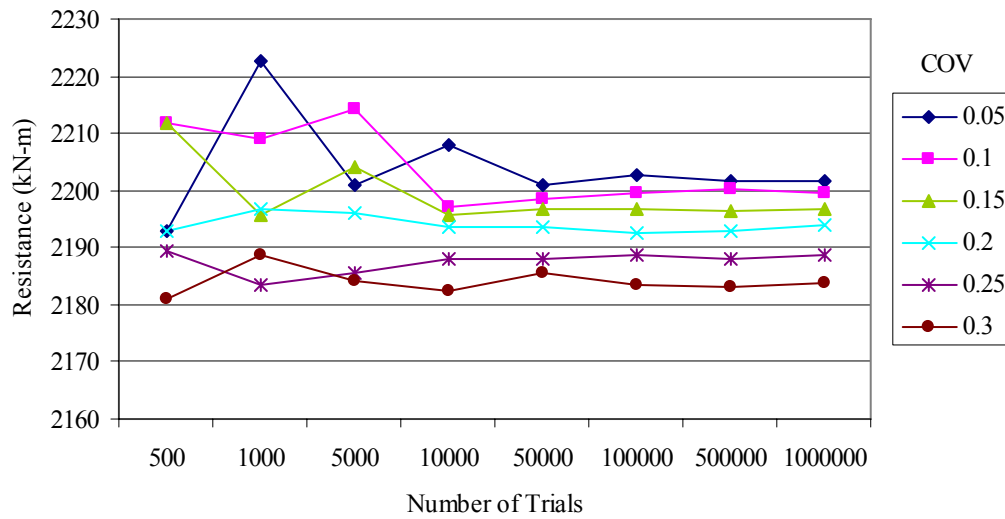
Figure 4-5 Plot of Convergence of Monte Carlo Results as a Function of the Number of Trials

Based on these results 100,000 trials were run for each case. This value was chosen because beyond 100,000 there appeared to be little improvement in convergence.

4.7   Results

4.7.1   Procedures Used to Analyze Reliability Results

After the reliability for all cases had been calculated, the resulting reliability indices were grouped into a series of spreadsheet files. Each file held the reliability indices corresponding to a particular girder and corrosion condition. From these files plots were created to determine the values of ϕ and ψ to achieve each of the three target reliability levels, 2.5, 3.0, and 3.5. An example of such a plot for girder 15, corrosion condition 1, a target reliability of 3.0, and a value of ϕ equal to 0.9 is shown in Figure 4-6. From this figure the value of ψ to meet a target reliability of 3.0 would be selected as 0.8.
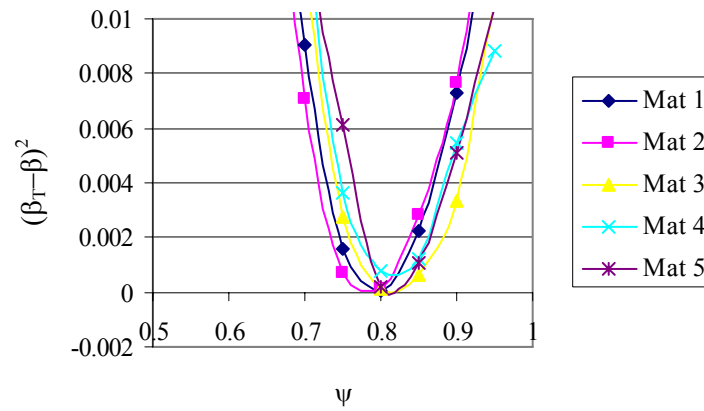
Figure 4-6 Example of Plots Used to Select Calibrated Resistance Factors

This approach to factor selection is slightly different from examples of resistance factor calibration found in the literature, because, though all five different materials are considered, this plot does not truly consider the sum of squared errors between the target and computed reliability for a range of designs (different girders and states of deterioration). Each of the five curves shows only the difference between the target and actual reliability for a single design. The difficulty in determining an appropriate range of designs to sum across will be discussed shortly.

In the following sections, trends seen in the factors will be discussed and recommendations of values for use in design are made. The specific values of the factors should be considered preliminary. The trends witnessed confirm the usefulness of the approach to design values described in Chapter 3. They also highlight some areas in which to pursue future research.

4.7.2 Effect of the Amount of Remaining Steel

As observed in Appendix C, the amount of steel remaining is probably the most important factor in the reliability of RC sections repaired with externally bonded FRP. The girders used for calibration represented a range of different initial conditions. Some girders had enough steel to significantly exceed the capacity demanded by LRFR load factors and did not need strengthening until high amounts (~30%) of the as-originally-designed steel were lost. Other girders were initially very close to the load demand, and for higher percentages of steel loss it was not possible to apply enough FRP (within the geometric constraints of the section) to bring the girder up to the required capacity. Given this range of different girders, comparisons based strictly on the amount of as-originally-designed steel lost (comparing different girders at the same corrosion condition) were uninformative. Thus, a different basis for comparison was required.

In the calibration examples of Appendix C a single girder was used and distinct differences were seen for different levels of steel loss. Since only one girder was used, changes in the amount of steel loss were relative to a common baseline condition. Therefore, for the present calibration, an effort was made to group girders into similar amounts of steel loss relative to a common baseline. This baseline was defined as the amount of steel needed to just meet the LRFR load requirements. For each girder, the amount of steel needed to just meet the LRFR demand was computed, and then the total amount of steel loss was compared to this baseline to compute a percentage of loss below that needed to meet LRFR. Then different girders evaluated at different corrosion conditions could be grouped together based on the amount of steel loss relative to the amount needed to meet LRFR requirements. The girders were grouped in increments of 5% steel loss relative to the LRFR baseline. Table 4-12 shows the baseline areas and the areas for each corrosion condition for all 20 girders in mm^2

(in^2). It also shows the percentage below the baseline area. Negative percentages mean that the amount of steel remaining at that corrosion condition exceeds that needed to meet LRFR requirements. These conditions are shaded grey. The other colors represent the groups ranging from 0% to 30% in increments of 5%. Cells with no shading represent cases where the remaining steel was more than 30% below the baseline area. There were very few cases where it was possible to even create designs for relative losses exceeding 30%, and thus these girders and corrosion conditions were not considered in selection of resistance factors.

Table 4-12 Baseline LRFR Steel Areas and Steel Areas for Each Corrosion Condition in mm² (in.²)
and Relative Percent Loss Groupings by Color

Girder	Baseline Steel Area	Corrosion 1	Corrosion 2	Corrosion 3	Corrosion 4					Corrosion 5					Corrosion 6				
					10	20	30	40	50	10	20	30	40	50	10	20	30	40	50
1	4179 (6.48)	5440 (8.43) -30.2%	4835 (7.49) -15.7%	4231 (6.56) -1.2%	5294 (8.20) -26.7%	5149 (7.98) -23.2%	5007 (7.76) -19.8%	4866 (7.54) -16.4%	4728 (7.33) -13.1%	4698 (7.28) -12.4%	4562 (7.07) -9.1%	4428 (6.86) -5.9%	4296 (6.66) -2.8%	4166 (6.46) 0.3%	4102 (6.36) 1.8%	3975 (6.16) 4.9%	3850 (5.97) 7.9%	3727 (5.78) 10.8%	3606 (5.59) 13.7%
2	4784 (7.42)	3463 (5.37) 27.6%	3078 (4.77) 35.7%	2693 (4.17) 43.7%	3327 (5.16) 30.5%	3194 (4.95) 33.3%	3063 (4.75) 36.0%	2935 (4.55) 38.7%	2810 (4.36) 41.3%	2950 (4.57) 38.3%	2825 (4.38) 41.0%	2702 (4.19) 43.5%	2582 (4.00) 46.0%	2464 (3.82) 48.5%	2574 (3.99) 46.2%	2456 (3.81) 48.7%	2342 (3.63) 51.0%	2230 (3.46) 53.4%	2121 (3.29) 55.7%
3	4910 (7.61)	5440 (8.43) -10.8%	4835 (7.49) 1.5%	4231 (6.56) 13.8%	5294 (8.20) -7.8%	5149 (7.98) -4.9%	5007 (7.76) -2.0%	4866 (7.54) 0.9%	4728 (7.33) 3.7%	4698 (7.28) 4.3%	4562 (7.07) 7.1%	4428 (6.86) 9.8%	4296 (6.66) 12.5%	4166 (6.46) 15.2%	4102 (6.36) 16.5%	3975 (6.16) 19.0%	3850 (5.97) 21.6%	3727 (5.78) 24.1%	3606 (5.59) 26.6%
4	5158 (7.99)	4781 (7.41) 7.3%	4250 (6.59) 17.6%	3719 (5.76) 27.9%	4644 (7.20) 10.0%	4510 (6.99) 12.6%	4378 (6.79) 15.1%	4247 (6.58) 17.7%	4091 (6.34) 20.7%	4121 (6.39) 20.1%	3995 (6.19) 22.6%	3870 (6.00) 25.0%	3747 (5.81) 27.3%	3627 (5.62) 29.7%	3598 (5.58) 30.2%	3480 (5.39) 32.5%	3364 (5.21) 34.8%	3250 (5.04) 37.0%	3137 (4.86) 39.2%
5	5202 (8.06)	5440 (8.43) -4.6%	4835 (7.49) 7.0%	4231 (6.56) 18.7%	5294 (8.20) -1.8%	5149 (7.98) 1.0%	5007 (7.76) 3.7%	4866 (7.54) 6.4%	4728 (7.33) 9.1%	4698 (7.28) 9.7%	4562 (7.07) 12.3%	4428 (6.86) 14.9%	4296 (6.66) 17.4%	4166 (6.46) 19.9%	4102 (6.36) 21.1%	3975 (6.16) 23.6%	3850 (5.97) 26.0%	3727 (5.78) 28.3%	3606 (5.59) 30.7%
6	6880 (10.66)	7253 (11.24) -5.4%	6447 (9.99) 6.3%	5641 (8.74) 18.0%	7058 (10.94) -2.6%	6866 (10.64) 0.2%	6676 (10.35) 3.0%	6489 (10.06) 5.7%	6304 (9.77) 8.4%	6263 (9.71) 9.0%	6082 (9.43) 11.6%	5904 (9.15) 14.2%	5728 (8.88) 16.7%	5554 (8.61) 19.3%	5469 (8.48) 20.5%	5300 (8.22) 23.0%	5134 (7.96) 25.4%	4970 (7.70) 27.8%	4808 (7.45) 30.1%
7	5409 (8.38)	7253 (11.24) -34.1%	6447 (9.99) -19.2%	5641 (8.74) -4.3%	7058 (10.94) -30.5%	6866 (10.64) -26.9%	6676 (10.35) -23.4%	6489 (10.06) -20.0%	6304 (9.77) -16.5%	6263 (9.71) -15.8%	6082 (9.43) -12.4%	5904 (9.15) -9.1%	5728 (8.88) -5.9%	5554 (8.61) -2.7%	5469 (8.48) -1.1%	5300 (8.22) 2.0%	5134 (7.96) 5.1%	4970 (7.70) 8.1%	4808 (7.45) 11.1%
8	7403 (11.48)	10880 (16.86) -47.0%	9671 (14.99) -30.6%	8462 (13.12) -14.3%	10587 (16.41) -43.0%	10298 (15.96) -39.1%	10014 (15.52) -35.3%	9733 (15.09) -31.5%	9456 (14.66) -27.7%	9395 (14.56) -26.9%	9123 (14.14) -23.2%	8855 (13.73) -19.6%	8591 (13.32) -16.0%	8332 (12.91) -12.5%	8204 (12.72) -10.8%	7950 (12.32) -7.4%	7700 (11.94) -4.0%	7454 (11.55) -0.7%	7212 (11.18) 2.6%

Table 4-12 (Continued) Baseline LRFR Steel Areas and Steel Areas for Each Corrosion Condition in mm² (in.²) and Relative Percent Loss Groupings by Color

Girder	Baseline Steel Area	Corrosion 1	Corrosion 2	Corrosion 3	Corrosion 4					Corrosion 5					Corrosion 6				
					10	20	30	40	50	10	20	30	40	50	10	20	30	40	50
9	5803 (8.99)	5696 (8.83) 1.8%	5063 (7.85) 12.7%	4431 (6.87) 23.7%	5537 (8.58) 4.6%	5380 (8.34) 7.3%	5226 (8.10) 10.0%	5073 (7.86) 12.6%	4923 (7.63) 15.2%	4913 (7.62) 15.3%	4766 (7.39) 17.9%	4620 (7.16) 20.4%	4477 (6.94) 22.9%	4336 (6.72) 25.3%	4290 (6.65) 26.1%	4152 (6.44) 28.4%	4017 (6.23) 30.8%	3883 (6.02) 33.1%	3752 (5.82) 35.3%
10	9255 (14.35)	5884 (9.12) 36.4%	5231 (8.11) 43.5%	4577 (7.09) 50.5%	5679 (8.80) 38.6%	5478 (8.49) 40.8%	5280 (8.18) 42.9%	5086 (7.88) 45.0%	4895 (7.59) 47.1%	5037 (7.81) 45.6%	4848 (7.51) 47.6%	4662 (7.23) 49.6%	4479 (6.94) 51.6%	4301 (6.67) 53.5%	4396 (6.81) 52.5%	4219 (6.54) 54.4%	4046 (6.27) 56.3%	3876 (6.01) 58.1%	3710 (5.75) 59.9%
11	4453 (6.90)	5440 (8.43) -22.2%	4835 (7.49) -8.6%	4231 (6.56) 5.0%	5294 (8.20) -18.9%	5149 (7.98) -15.6%	5007 (7.76) -12.4%	4866 (7.54) -9.3%	4728 (7.33) -6.2%	4698 (7.28) -5.5%	4562 (7.07) -2.4%	4428 (6.86) 0.6%	4296 (6.66) 3.5%	4166 (6.46) 6.5%	4102 (6.36) 7.9%	3975 (6.16) 10.7%	3850 (5.97) 13.5%	3727 (5.78) 16.3%	3606 (5.59) 19.0%
12	5729 (8.88)	5439 (8.43) 5.0%	4832 (7.49) 15.6%	4232 (6.56) 26.1%	5290 (8.20) 7.6%	5148 (7.98) 10.1%	5006 (7.76) 12.6%	4865 (7.54) 15.1%	4729 (7.33) 17.5%	4697 (7.28) 18.0%	4561 (7.07) 20.4%	4426 (6.86) 22.7%	4297 (6.66) 25.0%	4168 (6.46) 27.3%	4103 (6.36) 28.4%	3974 (6.16) 30.6%	3852 (5.97) 32.8%	3677 (5.78) 34.9	3606 (5.59) 37.1%
13	4569 (7.08)	4413 (6.84) 3.4%	3923 (6.08) 14.1%	3433 (5.32) 24.9%	4282 (6.64) 6.3%	4152 (6.44) 9.1%	4024 (6.24) 11.9%	3898 (6.04) 14.7%	3775 (5.85) 17.4%	3799 (5.89) 16.9%	3677 (5.70) 19.5%	3556 (5.51) 22.2%	3438 (5.33) 24.8%	3322 (5.15) 27.3%	3316 (5.14) 27.4%	3202 (4.96) 29.9%	3090 (4.79) 32.4%	2980 (4.62) 34.8%	2872 (4.45) 37.1%
14	4252 (6.59)	4413 (6.84) -3.8%	3923 (6.08) 7.7%	3433 (5.32) 19.3%	4282 (6.64) -0.7%	4152 (6.44) 2.4%	4024 (6.24) 5.4%	3898 (6.04) 8.3%	3775 (5.85) 11.2%	3799 (5.89) 10.7%	3677 (5.70) 13.5%	3556 (5.51) 16.4%	3438 (5.33) 19.1%	3322 (5.15) 21.9%	3316 (5.14) 22.0%	3202 (4.96) 24.7%	3090 (4.79) 27.3%	2980 (4.62) 29.9%	2872 (4.45) 32.5%
15	5537 (8.58)	5149 (7.98) 7.0%	4577 (7.09) 17.3%	4005 (6.21) 27.7%	4995 (7.74) 9.8%	4844 (7.51) 12.5%	4695 (7.28) 15.2%	4548 (7.05) 17.9%	4404 (6.83) 20.5%	4432 (6.87) 20.0%	4289 (6.65) 22.5%	4149 (6.43) 25.1%	4011 (6.22) 27.5%	3876 (6.01) 30.0%	3869 (6.00) 30.1%	3736 (5.79) 32.5%	3605 (5.59) 34.9%	3477 (5.39) 37.2%	3351 (5.19) 39.5%
16	5223 (8.10)	5440 (8.43) -4.2%	4835 (7.49) 7.4%	4231 (6.56) 19.0%	5294 (8.20) -1.3%	5149 (7.98) 1.4%	5007 (7.76) 4.1%	4866 (7.54) 6.8%	4728 (7.33) 9.5%	4698 (7.28) 10.1%	4562 (7.07) 12.7%	4428 (6.86) 15.2%	4296 (6.66) 17.8%	4166 (6.46) 20.2%	4102 (6.36) 21.5%	3975 (6.16) 23.9%	3850 (5.97) 26.3%	3727 (5.78) 28.6%	3606 (5.59) 31.0%

Table 4-12 (Continued) Baseline LRFR Steel Areas and Steel Areas for Each Corrosion Condition in mm^2 (in.^{2}) and Relative Percent Loss Groupings by Color

Girder	Baseline Steel Area	Corrosion 1	Corrosion 2	Corrosion 3	Corrosion 4					Corrosion 5					Corrosion 6				
					10	20	30	40	50	10	20	30	40	50	10	20	30	40	50
17	4612 (7.15)	4617 (7.16)	4104 (6.36)	3591 (5.57)	4462 (6.92)	4309 (6.68)	4159 (6.45)	4012 (6.22)	3867 (5.99)	3958 (6.13)	3814 (5.91)	3673 (5.69)	3534 (5.48)	3399 (5.27)	3454 (5.35)	3320 (5.15)	3189 (4.94)	3060 (4.74)	2933 (4.55)
		-0.1%	11.0%	22.1%	3.2%	6.6%	9.8%	13.0%	16.2%	14.2%	17.3%	20.4%	23.4%	26.3%	25.1%	28.0%	30.9%	33.7%	36.4%
18	5779 (8.96)	6352 (9.85)	5646 (8.75)	4940 (7.66)	6171 (9.57)	5993 (9.29)	5817 (9.02)	5644 (8.75)	5474 (8.49)	5476 (8.49)	5308 (8.23)	5143 (7.97)	4980 (7.72)	4821 (7.47)	4781 (7.41)	4624 (7.17)	4470 (6.93)	4319 (6.69)	4170 (6.46)
		-9.9%	2.3%	14.5%	-6.8%	-3.7%	-0.7%	2.3%	5.3%	5.2%	8.1%	11.0%	13.8%	16.6%	17.3%	20.0%	22.6%	25.3%	27.8%
19	6203 (9.61)	5884 (9.12)	5231 (8.11)	4577 (7.09)	5709 (8.85)	5536 (8.58)	5365 (8.32)	5198 (8.06)	5033 (7.80)	5065 (7.85)	4902 (7.60)	4742 (7.35)	4584 (7.11)	4430 (6.87)	4422 (6.85)	4270 (6.62)	4120 (6.39)	3974 (6.16)	3830 (5.94)
		5.1%	15.7%	26.2%	8.0%	10.8%	13.5%	16.2%	18.9%	18.3%	21.0%	23.6%	26.1%	28.6%	28.7%	31.2%	33.6%	35.9%	38.3%
20	8251 (12.79)	8160 (12.65)	7253 (11.24)	6347 (9.84)	7940 (12.31)	7724 (11.97)	7510 (11.64)	7300 (11.31)	7092 (10.99)	7046 (10.92)	6842 (10.61)	6641 (10.29)	6444 (9.99)	6249 (9.69)	6153 (9.54)	5963 (9.24)	5775 (8.95)	5591 (8.67)	5409 (8.38)
		1.1%	12.1%	23.1%	3.8%	6.4%	9.0%	11.5%	14.0%	14.6%	17.1%	19.5%	21.9%	24.3%	25.4%	27.7%	30.0%	32.2%	34.4%

Within each grouping of the relative percent losses, a range of resistance factors was selected to meet each of the three target reliability indices. The values for the resistance factors are shown in Table 4-13. As shown in the previous calibration examples, different values for ψ were found for different levels of the strength COV. The values of ψ shown in Table 4-13 are the average of the higher (corresponding to low COVs) and lower (corresponding to high COVs) values of the ranges of ψ found for the girders and corrosion conditions in a particular group. It is important to recognize that this was a strict average, and therefore it can be expected that in using these factors roughly half of designs will fall below the target reliability and roughly half will be above it. The COVs listed in the table refer to the amount of variation seen in the value of the ψ within a particular group. Though the levels of variation are generally reasonable, it is clear that there were significant amounts of variation between different design conditions falling within a single group. These values are provided to give some sense of the amount of variation within a set of factors for a single group, however are not necessary for use in design.

Table 4-13 Summary of Resistance Factors for Different Target Reliabilities and Different Amounts of Relative Steel Loss

% below steel needed for LRFR	β=2.5	β=3.0	β=3.5
>=5	Generally too high to meet target, or else no strengthening needed	ϕ = 0.9 Avg ψ = 0.778-0.692 COV= 18.0% & 20.2%	ϕ = 0.85 Avg ψ = 0.777-0.717 COV = 13.5% & 13.0%
5< , >=10	18 out of 38 cases are too high or no design ϕ = 0.95 Avg ψ = 0.839-0.732 COV = 10.0% & 13.0%	ϕ = 0.9 Avg ψ = 0.831-0.752 COV = 11.6% &12.7%	ϕ = 0.85 Avg ψ = 0.834-0.787 COV = 9.3% & 9.1%
10< , >=15	21 out of 45 cases are too high or no design ϕ = 0.95 Avg ψ = 0.870-0.782 COV = 9.1% & 9.6%	For 15 out of 45 cases ϕ =0.95 or 0.90 both work. ϕ = 0.9 Avg ψ = 0.864-0.819 COV = 9.7% & 9.9%	17 out of 45 cases are too low or no design possible. The rest are pretty evenly split. ϕ = 0.85 Avg ψ = 0.885-0.840 COV = 7.5% & 7.6% ϕ = 0.90 Avg ψ = 0.662-0.626 COV = 6.9% & 8.3%
15< , >=20	24 out of 48 cases are too high or no design ϕ = 0.95 Avg ψ = 0.912-0.847 COV = 4.2% & 6.4%	For 28 out of 48 cases, ϕ=0.95 or 0.90 both work. The rest are evenly split. ϕ = 0.9 Avg ψ = 0.891-0.856 COV = 6.4% & 6.8% ϕ = 0.95 Avg ψ = 0.689-0.658 COV= 13.7% & 14.5%	34 out of 48 are too low or no design The rest are evenly split, with multiple values of ϕ that work ϕ = 0.85 Avg ψ = 0.890-0.859 COV = 6.4% & 5.5% ϕ = 0.9 Avg ψ = 0.677-0.652 COV = 10.9% & 9.3% ϕ = 0.95 Avg ψ = 0.536-0.518 COV = 4.1% & 4.8%
20< , >=25	24 of 38 cases are too high or no design ϕ = 0.95 Avg ψ = 0.915-0.879 COV = 3.7% & 3.8%	23 of 48 cases are too low or no design ϕ = 0.95 Avg ψ = 0.741-0.709 COV = 5.5% & 5.7% ϕ = 0.9 Avg ψ = 0.923-0.898 COV = 4.6% & 4.8%	33 of 48 cases are too low or not possible The rest are evenly split, with multiple values of ϕ that work ϕ = 0.85 Avg ψ = 0.95-0.905 COV = 0.0% & 2.1% ϕ = 0.9 Avg ψ = 0.768-0.734 COV = 2.5% & 3.3% ϕ = 0.95 Avg ψ = 0.61-0.578 COV = 3.3% & 3.8%

Table 4-13 (Continued) Summary of Resistance Factors for Different Target Reliabilities and Different Amounts of Relative Steel Loss

% below steel needed for LRFR	β=2.5	β=3.0	β=3.5
25< , >=30	28 of 39 cases are too high or no design $\phi = 0.95$ Avg ψ = 0.927-0.899 COV = 2.8% & 2.5%	Mostly too low or no design possible	Mostly too low or no design possible

In general very little change in the value of ψ was observed for COVs from 0.05 to 0.15. For COVs between 0.15 and 0.30, the decrease in value of the resistance factor appeared to be approximately linear. An example of the change in ψ with change in the strength COV is shown for girder 18, corrosion condition 4, with the SD degradation model, a target β of 3.5, and $\phi = 0.85$ in Figure 4-7. Based on these results, in order to use the high and low values of ψ shown in Table 4-13, the high value can be applied when the strength COV is between 0.05 and 0.15, and interpolation between the high and low value can be used to determine the appropriate value of ψ for strength COVs between 0.15 and 0.30.
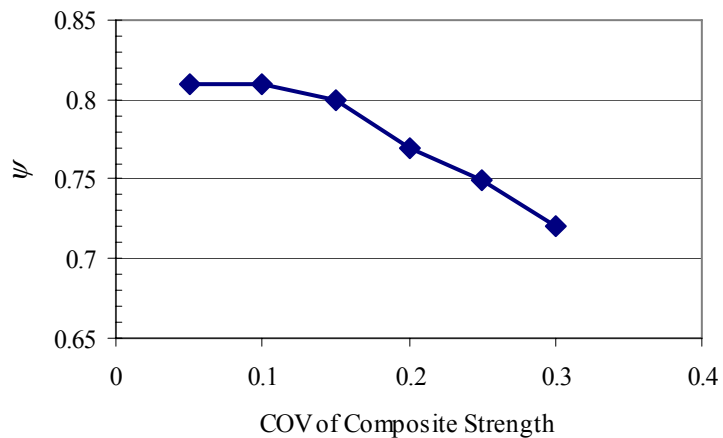
Figure 4-7 ψ vs. Strength COV for Girder 18, Corrosion Condition 4, SD, β_T = 3.5, and $\phi = 0.85$

As with the previous results (see Appendix C), as a larger portion of load is carried by the FRP the reliability of the strengthened section tends to increase. This can be seen in the resistance factors of Table 4-13. For a given target β, as the percentage of steel loss increases the values of the resistance factors also increase. This can be seen for a single value of ϕ in the way the values for ψ increase. It can also be seen in the way higher values of ϕ become possible for designs with increased steel loss.

There is also some sense that as the amount of steel loss increases there is a reduction in the range of values for ψ. This is observed in two senses: 1) the change in ψ seems to be less affected by the COV of strength, closing the gap between the high and low values and 2) the designs for different girders seem to have less variability in the actual values for ψ, as seen in the lower COVs of the factors for increased steel loss. There is no exact explanation for this phenomenon; however it is believed that it can be attributed to the bond model, the addition of layers to provide more FRP to girders with higher steel deficiency, and the smaller debonding strains predicted for thicker composites. This idea will be described in detail in Section 4.7.4 when the different degradation models are compared.

4.7.2.1 Significance

The factors shown in Table 4-13 are all that is needed to complete the design process that was first outlined in Chapter 3. However, currently, application of these factors requires that the designer specify the target reliability index and possess a good estimate of the amount of steel reinforcement remaining in the girder. If this design procedure was adopted as a formal code document, it is highly likely that the code-writing agency would specify the target reliability index, removing this responsibility from the individual designer. Furthermore, it is highly unlikely that a good estimate of the steel area will be available. In fact, it is possible that the amount of uncertainty in the area of steel may overwhelm the variation in the

219

composite, resulting in composite specific factors that are independent of the composite strength COV. Given the dependence of the reliability on the characteristics of the existing structure, better assessment of the existing structure is a topic in need of considerable further study.

The factors shown in Table 4-13 were selected to produce designs meeting the target reliability in the average sense. In general, factors in LRFD codes are selected with a bit more conservatism. For example, the code-writing agency may select resistance factors so that nearly all cases meet the target reliability, accepting the fact that many designs may be overly conservative. Furthermore, the factors are nearly always rounded to the nearest 0.05. The present work has calibrated factors following the procedure outlined in Figure 4-1, but has not conducted a rigorous verification process nor sought to introduce conservatism into the factors. It is felt that this process is best conducted by an agency that can adjust the factors based on a consensus of the design community.

Though the calibrated factors are all that is required for design, by examining further trends in the resistance factors conclusions providing justification of the ideas in Chapter 3 and showing the need for further research can be made.

4.7.3 Effect of No Continuing Corrosion vs. Continuing Corrosion

For corrosion cases 1, 2, and 3 a constant amount of initial steel loss was assumed (10%, 20%, and 30% respectively) and only the effect of FRP degradation was considered in evaluating the reliability of the deteriorating structure at times of 10, 20, 30, 40, and 50 years. In these cases the degradation in FRP properties was considered at the design stage, and therefore it was anticipated that the reliability would remain relatively stable, particularly since the same load description was used for all of the time periods. As an example, Table

4-14 shows the calibrated values of ψ given $\phi = 0.9$ for girder 15 and corrosion case 2, with

the FRP subject to the AD degradation model.

Table 4-14 Example of Calibrated ψ for Girder 15, Corrosion Case 2, with FRP Degradation

COV	Design Life (yrs)				
	10	20	30	40	50
0.05	0.91	0.92	0.92	0.92	0.92
0.10	0.9	0.92	0.92	0.92	0.92
0.15	0.9	0.9	0.91	0.9	0.9
0.20	0.88	0.89	0.89	0.89	0.89
0.25	0.86	0.87	0.87	0.87	0.87
0.30	0.85	0.85	0.85	0.85	0.85

This table clearly shows that with increasing time there is virtually no change in the

required value of ψ to meet the target reliability index (especially considering the subjective

nature of reading values off of graphs similar to Figure 4-6). This result was a general trend

seen across all of the girders for corrosion conditions 1, 2, and 3. This result also held for the

SD degradation model.

Corrosion cases 4, 5, and 6 started with an initial loss of steel (10%, 20%, and 30%,

respectively) but then considered additional loss due to the model chosen to describe general

corrosion. The degradation of the composite due to environmental exposure and the loss of

steel area due to continuing corrosion were both considered at the design stage, and it was

hoped that this would result in consistent reliabilities. However, in these cases, for a given

resistance factor, designs actually became more reliable as the design life increased. This

meant that for a constant reliability target, the value of ψ increased with time. As an

example, the values of ψ for $\phi = 0.9$, for girder 3, corrosion case 5, and the AD model of

degradation are shown below in Table 4-15.

Table 4-15 Example of Calibrated ψ for Girder 3, Corrosion Case 5, with FRP Degradation

COV	Design Life (yrs)				
	10	20	30	40	50
0.05	0.62	0.72	0.75	0.78	0.8
0.10	0.62	0.72	0.75	0.78	0.8
0.15	0.62	0.7	0.75	0.78	0.8
0.20	0.6	0.67	0.72	0.78	0.8
0.25	0.57	0.65	0.72	0.75	0.8
0.30	0.55	0.62	0.7	0.75	0.78

This increase could be partially related to the previously observed increase in reliability with an increase in steel loss. It is also likely that the corrosion model used in design was slightly conservative relative to the statistical model used in reliability analysis. The nominal cover was taken as 50.8 mm (2 in.), and this value was used to predict the amount of remaining steel for design. In computing the reliability, error in the cover dimension was modeled as a random variable with a mean of +1.59 mm (+1/16 in). This larger cover used in reliability analysis could result in an average value of remaining steel slightly greater than the value used for design. The difference between the predicted amount of remaining steel and the amount calculated in the reliability assessment would become greater over time, resulting in higher reliabilities for longer design lives.

4.7.3.1 Significance

The fact that the reliability remained quite stable over time for corrosion cases 1, 2, and 3 confirms the use of the factor for time-dependent degradation of the composite due to environmental exposure, η, as proposed in Chapter 3. The work conducted here is based on the assumption that the model used to calculate η is an accurate representation of the environmental degradation, i.e. no bias between the design degradation and degradation used to compute reliability was included in the reliability calculations. In Chapter 5, a method will

be discussed to include some model uncertainty (for both the Application Factors and the environmental factor) in design calculations, but the design procedure still relies on the assumption that the models are accurate in the mean sense.

The reliability results for Cases 4, 5, and 6 indicate the importance of using accurate models for design or the need to account for differences between design models and those used to represent the actual state of the structure and assess reliability. It is likely that a better model of corrosion, or perhaps of general deterioration of the structure, will be developed in the future, and in this case it may be possible to recalibrate the resistance factors and maintain a more uniform reliability over time. In the meantime, the present model may not be that bad. The model does show increasing conservatism with time; however, some extra conservatism at extended lifetimes may be desirable, as time-dependent models are likely to be less accurate as time increases. There is also some question about using time-dependent load models in the future. This analysis used 50-year loads for all time frames. If it had actually used loads specific to the design life, the designs at 10-40 years may not have required such low resistance factors. Currently it is believed that the design assumptions for corrosion are reasonable and the best course of action is to understand what causes the reliability to change and keep these sources of change in mind during the course of further development.

4.7.4 Effect of Different FRP Degradation Models

The use of models to predict FRP degradation had very little effect on the reliability for corrosion cases 1, 2, and 3 where there was no continuing corrosion. Table 4-16 shows a typical example with the values of ψ for girder 5 and corrosion case 2 with $\phi = 0.9$. This table shows that there is little difference in the calibrated factor for the three different degradation states considered. However, a common trend was for the cases where a

degradation model was used to show a slightly increased range in the values of ψ, usually expressed as lower values for the factor at higher COVs, and in some cases higher values at lower COVs.

Table 4-16 Example of Calibrated ψ for Girder 5, Corrosion Case 2

COV	ND	AD					SD				
		10	20	30	40	50	10	20	30	40	50
0.05	0.82	0.83	0.83	0.83	0.84	0.86	0.82	0.82	0.82	0.83	0.82
0.1	0.82	0.82	0.83	0.83	0.82	0.84	0.82	0.82	0.82	0.83	0.82
0.15	0.82	0.8	0.82	0.82	0.82	0.82	0.81	0.8	0.81	0.81	0.81
0.2	0.81	0.8	0.8	0.8	0.8	0.8	0.8	0.78	0.78	0.79	0.8
0.25	0.8	0.77	0.77	0.77	0.77	0.76	0.77	0.77	0.77	0.77	0.77
0.3	0.77	0.75	0.74	0.73	0.75	0.75	0.75	0.75	0.75	0.73	0.73

This trend was also observed when considering cases with continuing corrosion. An example is shown in Table 4-17 for girder 14 and corrosion level 4 with the target β equal to 3.0 and ϕ equal to 0.90 (results for 10-year designs were below the target of 3.0 used to derive these factors). For 20-year designs with no degradation the composite specific resistance factor ranges from 0.61 – 0.58, but when degradation is included the factor ranges from 0.62-0.55. Also observe how the range of values for ψ is smaller at an extended time of 50 years. This was observed previously in examining the effect of the amount of steel loss.

Table 4-17 Example of Calibrated ψ for Girder 14, Corrosion Case 4

COV	ND					AD				
	10	20	30	40	50	10	20	30	40	50
0.05		0.61	0.72	0.79	0.81		0.62	0.75	0.8	0.8
0.1		0.61	0.72	0.79	0.81		0.62	0.75	0.8	0.8
0.15		0.6	0.72	0.78	0.81		0.61	0.71	0.77	0.8
0.2		0.6	0.72	0.77	0.8		0.58	0.7	0.75	0.78
0.25		0.6	0.71	0.77	0.8		0.57	0.68	0.72	0.78
0.3		0.58	0.7	0.75	0.8		0.55	0.65	0.7	0.77

It is thought that this difference in the way changes in the FRP strength COV affect design factors may be attributable to the bond model and the amount of FRP required for different design lives. The FRP strength COV was allowed to vary in this example; however the model used to predict debonding is largely dependent on the FRP modulus. Therefore the strength COV will have a somewhat limited impact on the debonding strain (and therefore capacity of the girder) except in the cases where the rupture strain controls (where strength variability will directly affect the limiting strain in the FRP). The belief is that a larger range in ψ is observed in cases where the rupture strain is more often acting as the limiting strain in the FRP, where variation in strength has a more direct impact on the capacity of the girder. The rupture strain is more likely to control for 1-layer designs because the bond model imposes significant reductions in the debonding strain with the addition of layers. This would help explain the increased range in ψ for designs with less steel loss. The rupture strain is also more likely to control in cases where a degradation model is used because these models reduce the strength and therefore the rupture strain. This corresponds to the increased range in ψ witnessed for designs with degraded FRP properties.

4.7.4.1 Significance

In Chapter 3 of this report a procedure was proposed for computing composite properties for use in design. This procedure is based on the idea of creating designs with the

mean value that is anticipated in the field. One of the reasons given supporting this choice as a design value was that it would simplify the calibration process by allowing calibration over a range of properties without explicit consideration of design factors specific to a certain project. The intent was to create a design process that could easily accept new information (in the form of improved factors for describing initial conditions and environmental degradation) without requiring the recalibration of reliability-based design factors. Despite the theoretical justification for leaving out all design factors, this example calibration has made use of the factors describing time-dependent degradation as a check on this hypothesis. As seen in Table 4-16 there is a slight difference between the factors found for cases with no degradation and those with degradation included. This difference has been attributed to the drop in rupture strain, which in turn changes the failure mode from composite debonding to composite rupture, that comes with degradation models that primarily affect the ultimate strength of the composite. However, the differences are quite small, and thus the previous hypothesis is confirmed to some extent by this example. Therefore the design factors shown in Table 4-13 have been effectively calibrated over a range of composite strengths from 453 MPa (65.7 ksi), the minimum value of ultimate strength when degradation was included, to 896 MPa (130 ksi), the maximum value considered without degradation.

4.7.5 Effect of Different Materials

For most cases there was little difference in the reliability for the different materials considered in this calibration. In general the curves that were used to select the value of ψ minimizing the difference between the actual reliabilities and the target reliabilities were clumped together. For higher values of the strength COV, there was generally a bit more separation between curves; however the values of ψ for different materials were usually within 0.05 of each other, and an approximate average value was recorded as the factor for

226

design. Though it did not occur for all cases, there did seem to be a tendency for Materials 1 and 2 to be slightly less reliable (requiring a slightly smaller factor) than the other three materials. These are the two lowest strength materials. However, even in cases where there were (small) observable differences between materials, the amount of change in the reliability was quite small in comparison to the effect of other variables, such as the area of steel or corrosion condition.

4.7.5.1   Significance

This finding would imply that further calibration work could depend heavily on the use of only one material and supports the conclusion of Section 4.7.4.1 that the resistance factors may be calibrated over a range of composite properties without having to consider each composite independently.

4.8   Extensions on the Large Calibration Example

4.8.1   Effect of Changes in Modulus COV

In the calibration examples described in Appendix C, changes in the COV of composite strength were observed to have a more significant effect on the reliability index of a strengthened beam than changes in the COV of modulus. Based on this finding the calibration described in the present chapter only considered changes in the COV of composite strength. However, as described in Section 4.5.2.1, a different bond model was used in this calibration from that used in the sample calibrations, and therefore the level of modulus variation may be more significant than previously observed. In order to assess the importance of modulus variation, a subset of 5 girders was analyzed to assess the effect of changes in the modulus COV on the calibrated resistance factor.

Girders 4, 14, 16, 18, and 19 from Table 4-4 were chosen for this study. These girders were chosen because they all had geometries and initial steel areas that allowed for the design

of strengthening for many of the corrosion conditions described in Section 4.4.4.   Since strengthening designs were based on the variation-independent material design values proposed in Chapter 3, no new designs had to be created for this check.   The reliability of each design was assessed using all of the same random variable descriptions given in Table 4-11, except for the composite strength and modulus.   In order to consider the effect of changes in the COV of the modulus, the reliability of the strengthening was evaluated for values of the modulus COV of 0.05, 0.10, 0.15, 0.20, 0.25, and 0.30, while the strength COV was held at 0.20 for all cases.

4.8.1.1   Results

The results of this brief study can be summarized by Table 4-18, which shows the calibrated values of ψ for girder 16 and corrosion condition 4 with a target reliability of 3.5 and $\phi = 0.85$ when both the strength and modulus of the composite were allowed to vary.

Table 4-18 Comparison of Calibrated Resistance Factors with Changes in Strength and Modulus COVs for Girder 16, Corrosion Condition 4, $\beta_T = 3.5$, $\phi = 0.85$

| | COV | ψ | | | | | | | | | |
| | | ND | | | | | AD | | | | |
		10	20	30	40	50	10	20	30	40	50
Changes in Strength COV	0.05	0.72	0.79	0.82	0.85	0.87	0.72	0.8	0.82	0.86	0.86
	0.10	0.72	0.77	0.82	0.85	0.87	0.71	0.8	0.82	0.86	0.86
	0.15	0.72	0.77	0.82	0.85	0.87	0.7	0.78	0.82	0.85	0.86
	0.20	0.7	0.77	0.81	0.85	0.86	0.67	0.76	0.81	0.85	0.85
	0.25	0.7	0.76	0.81	0.85	0.86	0.67	0.73	0.8	0.82	0.85
	0.30	0.68	0.74	0.8	0.85	0.85	0.62	0.71	0.79	0.81	0.85
Changes in Modulus COV	0.05	0.71	0.78	0.82	0.85	0.86	0.7	0.78	0.82	0.85	0.87
	0.10	0.71	0.78	0.82	0.85	0.86	0.7	0.78	0.82	0.85	0.87
	0.15	0.72	0.78	0.82	0.85	0.86	0.7	0.78	0.82	0.85	0.87
	0.20	0.72	0.78	0.82	0.85	0.86	0.7	0.78	0.82	0.85	0.87
	0.25	0.73	0.79	0.83	0.85	0.87	0.7	0.77	0.83	0.85	0.87
	0.30	0.73	0.8	0.83	0.85	0.87	0.7	0.77	0.83	0.85	0.87

This table shows that:

1. The range of values for ψ is very similar whether the strength or modulus COV is changed.

2. The value of ψ shows significant differences as the strength COV increases, but there are only small changes in ψ when the modulus COV increases.

3. In some cases the value of ψ actually increases with an increase in the modulus COV.

4. The above findings are true whether or not degradation of the composite is modeled.

These results are representative of those seen for all of the girders considered here and justify the consideration of only the strength COV when calibrating ψ.

4.8.2 Effect of Different Bond Models

In general, design factors calibrated on the basis of reliability are specific to the exact set of design and reliability analysis assumptions used in calibration of the factors.   The analysis conducted in this report used the same bond model to predict the strain in the FRP at the time of debonding for both design and analysis of reliability. This model was described in Section 4.5.2.1.   Because the same model was used for design and assessment of reliability, no bias related to a change in model was introduced. The question was therefore raised as to whether the calibration results found in this report would be applicable if a different bond model was employed, assuming that the new model was also used for both design and assessment of reliability.

To test this idea, the same subset of five girders used in Section 4.8.1 was again utilized. For this test the only thing changed was the bond model used in design and reliability assessment. The fracture mechanics based model described in Section 4.5.2.1 was replaced by the bond model given in ACI 440 (2002). In this model, the strain at debonding is predicted as shown in Eq. 4-15, where κ_m is the debonding coefficient and $\varepsilon_{FRP,ult}$ is the ultimate strain of the composite.   Eq. 4-16 shows the calculation of κ_m. In these equations n is the number of layers, E_{FRP} is the modulus of the composite, and t_{FRP} is the thickness of a single layer. The equation for κ_m is empirical, and therefore the equation changes when different unit systems are used. Equations for both unit systems are shown below; however the U.S. customary system was used in the analysis.

$$\varepsilon_{debond} = \kappa_m \varepsilon_{FRP,ult}$$

Eq. 4-15

$$\kappa_m = \begin{cases} \dfrac{1}{60\varepsilon_{FRP,ult}}\left(1-\dfrac{nE_{FRP}t_{FRP}}{360,000}\right) \le 0.90 \ \ \text{for} \ \ nE_{FRP}t_{FRP} \le 180,000 \ \text{N/mm} \\[4mm] \hspace{5cm} \text{SI} \\[4mm] \dfrac{1}{60\varepsilon_{FRP,ult}}\left(\dfrac{90,000}{nE_{FRP}t_{FRP}}\right) \le 0.90 \ \ \text{for} \ \ nE_{FRP}t_{FRP} > 180,000 \ \text{N/mm} \end{cases}$$

Eq. 4-16

$$\kappa_m = \begin{cases} \dfrac{1}{60\varepsilon_{FRP,ult}}\left(1-\dfrac{nE_{FRP}t_{FRP}}{2,000,000}\right) \le 0.90 \ \ \text{for} \ \ nE_{FRP}t_{FRP} \le 1,000,000 \ \text{lb/in} \\[4mm] \hspace{5cm} \text{US} \\[4mm] \dfrac{1}{60\varepsilon_{FRP,ult}}\left(\dfrac{500,000}{nE_{FRP}t_{FRP}}\right) \le 0.90 \ \ \text{for} \ \ nE_{FRP}t_{FRP} > 1,000,000 \ \text{lb/in} \end{cases}$$

4.8.2.1 Results

During creation of the trial strengthening designs, the ACI model was observed to generally predict a larger value for the debonding strain than the fracture mechanics based model. This larger predicted debonding strain meant that designs created using the ACI model used a smaller area of composite, and designs were able to be created using the ACI model in cases where designs were deemed not possible (within the three layer limit) using the other bond model.

The calibrated factors were compared for cases where designs were able to be created with both bond models. In some cases the calibrated factors compared very well. For example, for the case of girder 4 with a target of reliability of 3.0, corrosion condition 1, $\phi =$ 0.9, and the AD degradation model the factors were generally quite similar, as seen in Table 4-19. However when girder 4 was again compared with all parameters as before except the corrosion condition was changed to condition 2 (as shown in Table 4-20), the factors for low values of the strength COV remained similar for both models, but the factors for high strength COVs were quite different. The factors calibrated with the ACI model decreased in value very quickly for higher COVs. The ACI calibrated factors did not show the trend witnessed in

the other factors that as the amount of relative steel loss increased the spread between the high and low values of the calibrated factors decreased. In fact the trend was opposite; with greater amounts of steel loss there was a greater drop-off in the calibrated factors for higher levels of COV. Thus, in comparing the results from the two different bond models, it is clear that although the factors are within a similar range of values, a change in modeling assumptions for creating designs or assessing reliability requires recalibration of the resistance factors.

Table 4-19 Example of Calibrated ψ for Girder 4, $\beta = 3.0$, Corrosion Condition 1, $\phi = 0.9$, AD

COV	Fracture Mechanics Model					ACI 440 Model				
	10	20	30	40	50	10	20	30	40	50
0.05	0.8	0.8	0.8	0.81	0.82	0.82	0.82	0.82	0.82	0.82
0.1	0.79	0.8	0.8	0.8	0.8	0.81	0.81	0.82	0.82	0.82
0.15	0.77	0.77	0.78	0.77	0.79	0.8	0.8	0.81	0.8	0.81
0.2	0.75	0.75	0.76	0.77	0.77	0.79	0.79	0.78	0.8	0.79
0.25	0.72	0.73	0.74	0.75	0.74	0.76	0.76	0.75	0.76	0.76
0.3	0.7	0.71	0.71	0.71	0.7	0.73	0.73	0.72	0.72	0.72

Table 4-20 Example of Calibrated ψ for Girder 4, $\beta = 3.0$, Corrosion Condition 2, $\phi = 0.9$, AD

COV	Fracture Mechanics Model					ACI 440 Model				
	10	20	30	40	50	10	20	30	40	50
0.05	0.9	0.9	0.9	0.9	0.9	0.9	0.9	0.9	0.91	0.91
0.1	0.9	0.9	0.9	0.9	0.9	0.9	0.9	0.9	0.9	0.9
0.15	0.9	0.9	0.9	0.9	0.9	0.87	0.87	0.87	0.87	0.88
0.2	0.9	0.89	0.89	0.89	0.89	0.84	0.84	0.85	0.83	0.85
0.25	0.87	0.87	0.87	0.87	0.87	0.8	0.8	0.8	0.8	0.8
0.3	0.87	0.86	0.86	0.86	0.86	0.75	0.75	0.75	0.75	0.75

4.9   Summary

In this chapter preliminary resistance factors for the design of FRP strengthening of RC T-beam bridge girders were calibrated. The factors were calibrated using a variety of representative girders and considering a number of different conditions. Many assumptions contributed to this calibration process, resulting in the preliminary nature of these factors. In

the following chapter, a design example will make use of the material design values described

in Chapter 3 and the resistance factors calibrated here.

Chapter 5. Recommended Design Procedure and Design Example

This chapter draws together the developments of the previous chapters into a proposed procedure for design. The chapter starts in Section 5.1 by outlining the design procedure based on the currently available information. It continues in Section 5.2 with a design example to show the implementation of the procedure as a means of clarifying current implementability.

5.1 Proposed Design Procedure

The proposed design procedure is composed of the following steps:

1. Assess the existing structure

2. Define the objectives and parameters for strengthening

3. Determine design values for the composite

4. Select appropriate resistance factors

5. Calculate the amount of FRP needed to meet the design objectives

6. Perform final checks on the design

7. Specify appropriate quality control measures to be followed during application of FRP

These steps are described in detail in the following sections. Though these steps may be considered as generally applicable to design of any strengthening project, the descriptions below are somewhat tailored to the specific case of RC T-beam bridge girders considered throughout this report.

5.1.1 Assess the Existing Structure

Any strengthening project must start with an evaluation of the structure to be strengthened. At this stage deficiencies in the existing structure and the limit state(s) to be considered are identified. This step likely includes inspection of the structure itself, as well as review of construction documents. The major types of information needed to proceed with design of strengthening include the geometry and material properties of the structure, an assessment of the steel deficiency and likelihood of continuing corrosion (or quantification of other deterioration mechanisms), and definition of the loading applied to the structure. Though not critical to design calculations, other factors, such as the state of the concrete cover, are very important to the successful implementation of strengthening and may require repair before the application of FRP. Existing design guidelines, such as ACI 440 (2002), TR 55 (The Concrete Society, 2000), *Externally Bonded FRP Reinforcement for RC Structures* (International, 2001), and NCHRP 514 (Mirmiran et al., 2004), provide guidance regarding minimal conditions for the existing structure in order to provide a suitable basis for externally bonded FRP.

5.1.2 Define the Objectives and Parameters for Strengthening

After the structure has been assessed, the specific objectives to be achieved through strengthening as well as parameters affecting the strengthening implementation should be defined. Generally, the primary objective of any FRP application will be to restore or add load carrying capacity. However, in some cases there may be other concerns, such as a reduction in deflection. (As described in Section 3.6.2.2.2 FRP is not recommended for the repair of structures deficient in fatigue.) Other parameters of interest at this stage are the anticipated application conditions, required service life, and environmental conditions. This information is required to calculate the appropriate design values for the composite.

The present work has considered only the flexural, Strength I limit state and has been based on the use of the HL-93 live load model as described in Section 2.6.2. Simplified analysis, such as the use of distribution factors described in the *AASHTO LRFD Bridge Design Specifications* (1998 and 2004), can be used to determine the dead, wearing, and live plus impact load acting on the structure. The resistance factors calibrated in Chapter 4 are intended for use with the Strength I load combination at the Operating level as described in the *Manual for Condition Evaluation and Load and Resistance Factor Rating (LRFR) of Highway Bridges* (AASHTO, 2003). The factored load can be calculated as shown in Eq. 5-1, where *D* is the dead load, *W* is load due to the wearing surface, *L* is the live load, and *IM* is the impact load, with all quantities referenced to a single girder line.

$$\sum \gamma_i Q_i = 1.25D + 1.5W + 1.35(L + IM)$$
<div align="right">**Eq. 5-1**</div>

Once the factored LRFR design load has been computed, the amount of steel required to meet this design load can be calculated and compared to the amount of steel that is predicted to be present at the end of the design life. This quantity will be used later in selecting the appropriate values of the resistance factors. Based on the results of Chapter 4, if the amount of steel present is less than 70% of the amount of steel needed to meet the LRFR load demand, it is unlikely that it will be possible to design strengthening to meet the design load using conventional methods of externally bonded FRP repair.

5.1.3 Determine Design Values for the Composite

The selection of a composite material can be influenced by several factors. The type of fiber and resin can be chosen to resist degradation due to the anticipated service environment and load carrying requirements. Cost and availability are other major considerations. This

design procedure does not specifically address composite selection but assumes that an appropriate selection has been made.

Given a specific composite material, calculation of design values is a three-step process. First characteristic values (initial values for the means) of the composite strength and modulus must be determined though any of the methods described in Chapter 3. These methods include calculation based on constitutive properties of the fiber and matrix, use of manufacturer supplied data, and lamina or laminate level testing. Next the Application Factors must be applied to account for the specifics of the field application, as shown in Eq. 5-2. Preliminary values for some of these factors for wet layup composites are provided in Table 3-29 of Chapter 3.

$$x_{design} = \lambda_{pred} \lambda_{layers} \lambda_{cure} \lambda_{work} x_{predicted}$$ **Eq. 5-2**

Finally, the environmental reduction factor, η, is calculated based on the design life and expected environmental conditions and applied as shown in Eq. 5-3.

$$x_{design} = \eta \lambda_{pred} \lambda_{layers} \lambda_{cure} \lambda_{work} x_{predicted}$$ **Eq. 5-3**

These calculations result in design values for both the ultimate composite strength and modulus. Throughout this work the composite has been assumed to behave in a linear-elastic manner. Thus the ultimate composite strain for design can be calculated by dividing the design ultimate strength by the design modulus.

5.1.4 Select Appropriate Resistance Factors

In a general sense, this step in the design process involves selecting the overall resistance factor, ϕ, appropriate to the limit state in question and the composite specific factor, ψ, specific to the FRP variation. Specifying these values for the designer is one of the more

important tasks of a code-writing agency, and generally the designer has a rather limited role. However, the design procedure proposed herein has not gone through the rigorous codification process, and thus selection of the resistance factors currently requires the approval of the owner.

As described in Section 4.7.2 of Chapter 4 the reliability of a strengthening measure is found to be highly dependent on the relative contributions of the FRP and steel to carrying the tensile portion of the flexural load. The calibrated resistance factors are summarized in Table 4-13 based on the percentage of steel deficiency relative to that needed to support the LRFR load. They are also grouped according to the three target reliability indices considered, 2.5, 3.0, and 3.5. In the future it is expected that a code-writing agency will set the target reliability for design, but currently the designer is required to select a reliability target.

For some combinations of the target reliability index and amount of steel loss, the range of values for the composite specific factor, ψ, is significant, and in those cases the value of ψ should be selected based on the COV of composite ultimate strength. For strength COVs of 0.15 or less, the larger value of the factor should be used. For strength COVs greater than 0.15, linear interpolation should be used between the high and low value of the factor with these values corresponding to COVs of 0.15 and 0.30, respectively. It should be noted that changes in the strength COV have been found to most affect the reliability of flexurally strengthened girders, and thus ψ in this work depends on the COV of composite strength. This does not eliminate the possibility that the modulus COV may be a more critical measure of composite variation for other limit states.

The COV of the critical composite property is increased by the contribution of uncertainty from the use of the Application Factors to consider field conditions and by

238

environmental degradation of the composite. Based on a first order approximation, the COV of the composite for use in design can be calculated as shown in Eq. 5-4, where $COV_{characterstic}$ is the value of the composite strength COV found through material tests or estimated based on designer judgment, $COV_{Application}$ is the COV of the ratio of tested values to those predicted using the Application Factors, and $COV_{degradation}$ is for the addition of uncertainty due to the degradation process and the models used to describe the process.

$$COV_{design} = \sqrt{COV_{chaacteristic}^2 + COV_{Application}^2 + COV_{degradtaion}^2}$$ **Eq. 5-4**

If test results are not available to calculate a value for $COV_{characteristic}$, the average, low, and high values for this parameter found during the tests conducted for the present work are shown in Table 5-1. These values should provide an adequate representation for wet layup materials, with the low value only appropriate for cases where extremely good quality control can be ensured.

Table 5-1 Approximate Values for $COV_{characteristic}$ for Wet Layup Composites Based on Testing

Property	Average $COV_{characteristric}$	Low $COV_{characteristric}$	High $COV_{characteristric}$
Strength	0.14	0.09	0.23
Modulus	0.17	0.09	0.28

Based on the Application Factors derived herein, the average value for $COV_{Application}$ is 0.11 for strength and 0.17 for modulus. There is currently no data available for $COV_{degradation}$.

5.1.5 Calculate the Amount of FRP Needed to Meet the Design Objective

Depending on the type of strengthening being considered, different models will be used to calculate the appropriate amount of FRP. For the flexural strengthening considered in this work, the resistance of strengthened sections has been consistently calculated using sectional analysis as described in Appendix D. This is the process that will be used in the design

example described below. Other analysis techniques for calculating flexural capacity could also be implemented; however the effect of different techniques on the calibrated resistance factors should be assessed.

5.1.6 Perform Final Checks on the Design

Design codes frequently prescribe additional requirements to be satisfied. In this particular case, after the required amount of FRP has been determined, the stress in the FRP due to sustained load should be evaluated and checked against the limits described in Section 3.6.2.2.1. The sustained load acting on a bridge will be assumed equal to the service level loads (those used to check deflections, etc. in new design). The total service level load is equal to the sum of the dead, wearing, and live plus impact loads without any load factors.

5.1.7 Specify Appropriate Quality Control Measures to be Followed During Application of FRP

Probably the most important part of the whole strengthening process is to apply the FRP using good techniques and high levels of quality control. Guidance on the appropriate techniques to employ can be found in existing documents discussing the repair of RC structures with FRP. (ACI, 2002; The Concrete Society, 2000; International, 2001; Tälsten, 2002; Mirmiran, 2004).

5.2 Design Example

In the following sections the design procedure just described is used to design a repair scheme for a T-beam bridge girder. This design example uses sectional analysis to determine the resistance of the strengthened girder and assumes models to describe corrosion of the reinforcement and degradation of the FRP. All of these models are used as examples to describe the overall design procedure and could be replaced with other models, though different models could require recalibration of the resistance factors derived in Chapter 4.

240

5.2.1 Structural Assessment

Girder 15 as described previously in Chapter 4 will be used for this example as the member to be strengthened. The dimensions and material properties of this girder needed for strengthening design are shown in Table 5-2.

Table 5-2 Dimensions and Material Properties of Girder 15

Span	15.85 m (52 ft)
Effective Flange Width, b	2.5 m (8.17 ft)
Slab Depth	177.8 mm (7 in)
Width of T	508 mm (20 in)
Depth of T, h	1066.8 mm (42 in)
Depth to Reinforcement, d	940 mm (37 in)
Reinforcement	Seven 32.3 mm diameter (#10) bars
f'_c	22.4 MPa (3.25 ksi)
E_c	22.4 GPa (3249.5 ksi)
f_y	275.8 MPa (40 ksi)
E_s	200 GPa (29000 ksi)
Cover at Bottom of T	50.8 mm (2 in)

For this example it will be assumed that an inspection of the girder has found evidence of corrosion, and it is estimated that approximately ten percent of the initial reinforcement area has been lost to corrosion. The existing shear capacity has been found adequate, and therefore the girder will only be strengthened in flexure. There is no unusual traffic anticipated on the bridge; and FRP will be applied only to increase the reliability of the structure. Furthermore, it is assumed that all necessary preparation, such as filling holes, replacing concrete, and sandblasting the concrete surface, will be taken care of prior to the application of FRP.

5.2.2 Objectives and Parameters for Strengthening

The bridge girder is being strengthened to increase the safety of the structure under normal traffic loads. Therefore, meeting the LRFR factored load is the primary objective of the strengthening project. In Section 4.5.1 of Chapter 4 the LRFR factored load demands for

all of the girders were calculated and the values were provided in Table 4-9. The LRFR factored load for girder 15 is 1269.3 kN-m (936.77 kip-ft).

This factored load must be met with the desired reliability based on the other circumstances of the design. The design life of the strengthening is assumed to be 30 years, and it is anticipated that corrosion of the reinforcement will continue. It will also be assumed that the environmental degradation of the FRP can be modeled using the SD model described in Section 4.4.1.2 of Chapter 4.

5.2.3   Composite Design Values

A carbon-epoxy composite is used for this example. Based on lamina level tests the properties shown in Table 5-3 are found for the composite. (These properties are taken from Set A1 as described in Chapter 3. The strength of this composite is somewhat higher than the range used for calibration; however the composite thickness is less. The reliability of this design will be evaluated at the end of the example, to consider the effect of differing properties.) Assume that the curing environment replicates that anticipated in the field.

Table 5-3 Results from Lamina Level Tests

Property	Mean	Standard Deviation
Ultimate Strength	1073.74 MPa (151.38 ksi)	125.98 MPa (18.27 ksi)
Modulus	70 GPa (10206 ksi)	9 GPa (1370 ksi)
Thickness	1.1024 mm (0.0434 in)	0.0483 mm (0.0019 in)

The equation used to calculate design values, Eq. 5-2, is repeated below.

$$x_{design} = \lambda_{pred} \lambda_{layers} \lambda_{cure} \lambda_{work} x_{predicted}$$ **Eq. 5-2**

Table 5-4 repeats Table 3-29, and shows the preliminary values of the Application Factors. These factors are used in Eq. 5-2 to calculate the anticipated field values of strength and modulus, which are the values used for design.

Table 5-4 Preliminary Values of Application Factors for Wet Layup Composites

Factor	Strength	Modulus
λ_{pred}		
Properties of Constitutive Materials	0.6	0.8
Manufacturer Data	Depends on Manufacturer	
Lamina Level Tests	1	1
Laminate Level Tests	1	1
λ_{layers}		
Two-Layers	0.90	1
Three-Layers	0.8-0.85	1
Four-Layers	0.7-0.75	1
λ_{cure}		
Humidity	Depends on Resin System	
Temperature		
λ_{work}	0.95	0.9

As an initial estimate, it is assumed that two layers of fabric will be necessary. Therefore the design mean for strength can be calculated as shown in Eq. 5-5. Here the value for λ_{pred} is set equal to 1 for lamina level tests; λ_{layers} is set at 0.9 for a two-layer composite; λ_{cure} is equal to 1 because the cure environment matches that anticipated in the field; and λ_{work} is taken as 1 because no specific value is yet available for the overhead layup anticipated for flexural strengthening.

$$f_{frp\,design} = (1)(0.9)(1)(1)(1073.74)$$ **Eq. 5-5**

$$f_{frp\,design} = 966.366 \ \text{MPa} \quad (140.16 \ \text{ksi})$$

The value of FRP modulus for design is found in Eq. 5-6

$$E_{frp\,design} = (1)(1)(1)(1)(70)$$

Eq. 5-6

$$E_{frp\,design} = 70 \text{ GPa } (10206 \text{ ksi})$$

The above values for strength and modulus are the properties anticipated at the time of manufacture and do not yet consider environmental degradation of the composite. The time dependent factor, η, must also be considered as shown in Eq. 5-3, repeated below.

$$x_{design} = \eta \lambda_{pred} \lambda_{layers} \lambda_{cure} \lambda_{work} x_{predicted}$$

Eq. 5-3

The design life of this strengthening is 30 years, and the environmental conditions will be modeled with the SD degradation model described in Section 4.4.1.2. The equations for calculating the percent retention of properties, which is equal to η, are shown in Eq. 5-7 for strength and Eq. 5-8 for modulus. Since the slower degradation model is being used, the time in days is divided by 5 before being used in the equation as t.

$$\% \text{ retention in strength} = -3.366\ln(t) + 106.07$$

Eq. 5-7

$$\% \text{ retention in modulus} = -0.418\ln(t) + 106.07$$

Eq. 5-8

The values of η for strength and modulus are calculated in Eq. 5-9 and Eq. 5-10, respectively.

$$\eta_{strength} = -3.366\ln(2190) + 106.07$$

Eq. 5-9

$$\eta_{strength} = 80.18\%$$

$$\eta_{modulus} = -0.418\ln(2190) + 106.07$$

$$\eta_{modulus} = 102.85\%$$

Since the value of $\eta_{modulus}$ is greater than one hundred percent retention, $\eta_{modulus}$ will be set equal to 1. Therefore, the final design values are calculated in Eq. 5-11 and Eq. 5-12 for strength and modulus, respectively.

$$f_{frp\,design} = (0.8018)(966.366)$$

$$f_{frp\,design} = 774.83 \ \text{MPa} \ (112.38 \ \text{ksi})$$

$$E_{frp\,design} = (1)(70) \ \text{GPa}$$

$$E_{frp\,design} = 70 \ \text{GPa} \ (10206 \ \text{ksi})$$

5.2.4   Selection of Resistance Factors

In order to select the appropriate resistance factors from Table 4-13 the target reliability index and the percent steel deficiency relative to the LRFR load demand are needed. For this example the target reliability will be assumed equal to 3.5.

In order to calculate the percent steel deficiency, first the amount of steel needed to just meet the LRFR requirements is needed. This can be calculated with simple sectional analysis and some iteration, based on failure of the original girder occurring due to steel yield followed by concrete crushing .

1. First an estimated area of steel, $A_{s,LRFR}$, is selected. The area of steel in this girder as designed is 5735.8 mm^2 (8.89 in^2), thus assume a trial value a little less than this, for example 5600 mm^2 (8.68 in^2).

2. Then the depth of the concrete stress block can be calculated as shown in Eq. 5-13, where b is the width of the concrete beam (taken as the effective flange width).

$$a = \frac{A_{s,LRFR} f_y}{0.85 f_c' b} = \frac{(5600)(275.8)}{0.85(22.4)(2500)} = 32.45 \text{ mm} (1.28 \text{ in})$$ **Eq. 5-13**

3. The factored moment capacity can be calculated as shown in Eq. 5-14.

$$\phi M_n = \phi A_{s,LRFR} f_y (d - a/2)$$ **Eq. 5-14**

$$\phi M_n = 0.9(5600)(275.8)(940 - 32.45/2)$$

$$\phi M_n = 12.8407 \times 10^8 \text{ N-mm} = 1284.1 \text{ kN-m} (947.66 \text{ kip-ft})$$

Since the value found in step 3 is greater than the required capacity of 1269.3 kN-m (936.77 kip-ft), a slightly smaller area of steel is needed. Through iteration (repeating steps 1 through 3) the required steel area to just meet the LRFR load requirements can be found equal to 5535.5 mm^2 (8.58 in^2).

Next, the amount of steel remaining at the end of the strengthening design life must be predicted. The steel is assumed to have an initial 10% deficiency, and corrosion is expected to continue for the full design life of 30 years. The initial steel area is calculated in Eq. 5-15 for 7 bars with diameter 32.3 mm (#10 bar).

$$A_{s,design} = 7 * \pi * \left(\frac{32.3^2}{4}\right) = 5735.8 \text{ mm}^2 (8.89 \text{ in}^2)$$ **Eq. 5-15**

The area remaining after 10% loss is 5162.2 mm^2 (8.0 in^2). The bar diameter corresponding to this area is calculated in Eq. 5-16.

$$d_{10\% loss} = \sqrt{\frac{4A_{s,10\% loss}}{7\pi}} = 30.64 \text{ mm} \ (1.21 \text{ in})$$

Eq. 5-16

The rate of corrosion can be predicted based on the water-cement ratio and amount of cover using Eq. 5-17.

$$i_{corr} = \frac{37.8(1 - w/c)^{-1.64}}{cover}$$

Eq. 5-17

The corrosion rate is calculated for a concrete cover thickness of 50.8 mm (2 in) and water-cement ratio equal to 0.45 in Eq. 5-18.

$$i_{corr} = \frac{37.8(1 - 0.45)^{-1.64}}{50.8} = 1.9835 \ \mu A/cm^2 \ (12.80 \ \mu A/in^2)$$

Eq. 5-18

The average penetration per year corresponding to this corrosion rate can be calculated using Eq. 5-19.

$$P_{av} = 0.0116 i_{corr} = 0.0116 * 1.9835 = 0.023 \ \text{mm/yr} \ (0.000906 \text{ in/yr})$$

Eq. 5-19

The diameter of a single bar after a given number of years can be calculated from Eq. 5-20, where d_o is the initial diameter of the bar, and t is the time in years.

$$d = d_o - 2 * P_{av} * t$$

Eq. 5-20

In this case d_o is equal to $d_{10\% loss}$, so the remaining diameter after a 30 year service life is 29.26 mm (1.15 in), as shown in Eq. 5-21.

$$d = 30.64 - 2 * 0.023 * 30 = 29.26 \ \text{mm} \ (1.15 \text{ in})$$

Eq. 5-21

Based on this diameter the area of steel remaining after 30 years is calculated in Eq. 5-22.

$$A_{s,30yr} = 7 * \pi * \frac{29.26^2}{4} = 4706.9 \quad \text{mm}^2 \ (7.29 \ \text{in}^2)$$ **Eq. 5-22**

The percent of steel deficiency relative to the LRFR baseline can be calculated as shown in Eq. 5-23.

$$\%_{deficient} = \frac{A_{s,LRFR} - A_{s,30yr}}{A_{s,LRFR}} = \frac{5535.5 - 4706.9}{5535.5} = 14.9\%$$ **Eq. 5-23**

Based on this steel deficiency and the target reliability index of 3.5, the resistance factors shown in Table 5-5 are selected for use in this example from Table 4-13 in Chapter 4.

Table 5-5 Resistance Factors for Design Example

ϕ	0.85
ψ	0.885 - 0.840

In order to pick the appropriate value of ψ from this range the COV of composite strength is needed. Eq. 5-4, repeated below, is used to include all sources of variation affecting the composite strength. However, currently no data is available for $COV_{degradation}$; therefore this term will not be used.

$$COV_{design} = \sqrt{COV_{chaacteristic}^2 + COV_{Application}^2 + COV_{deg\,radation}^2}$$ **Eq. 5-4**

The COV of the characteristic value can be found as the standard deviation of test results divided by the mean of test results and for this example is equal to 0.12. As listed in Section 5.1.4, the average value for $COV_{Application}$ for strength is 0.11. The strength COV for use in selecting ψ is therefore 0.163 as shown in Eq. 5-24.

$$COV_{strength} = \sqrt{(0.12)^2 + (0.11)^2} = 0.163$$ **Eq. 5-24**

Since this value of the COV exceeds 0.15, the value of ψ for design can be found through interpolation. The high value of ψ should be associated with a COV of 0.15 and the low value with a COV of 0.30. The interpolated value is calculated in Eq. 5-25.

$$\frac{\psi_{high} - \psi_{design}}{\psi_{design} - \psi_{low}} = \frac{0.15 - COV_{design}}{COV_{design} - 0.30}$$

$$\frac{0.885 - \psi_{design}}{\psi_{design} - 0.840} = \frac{0.15 - 0.163}{0.163 - 0.30} \qquad \text{Eq. 5-25}$$

$$\psi_{design} = 0.881$$

For design purposes, it is probably not necessary to go through the interpolation process unless the range for ψ is very large. However it was used in this case to provide a complete example.

5.2.5 Calculating the Required Area of FRP

After calculating the design load, design properties of the FRP, and the resistance factors, the quantity of FRP required to meet the design load can be determined using the sectional analysis procedure described in Appendix D. This process is followed below.

1. **Choose a trial quantity of FRP by specifying the width, *w*, and number of layers, *n*.** The trial quantities are $w = 375$ mm (14.75 in) and $n = 2$ layers.

2. **Calculate the strain limit in the FRP.** The interfacial fracture energy is calculated in Eq. 5-26 and used to find the predicted debonding strain in Eq. 5-27, as described in Section 4.5.2.1 of Chapter 4. The rupture strain limit is calculated in Eq. 5-28.

$$G_f = 0.644 f_c'^{0.19} = (0.644)(22.4)^{0.19}$$

$$G_f = 1.163 \, \text{N/mm} \ (6.64 \, \text{lb/in})$$

$$\varepsilon_{FRP\,debond} = 1.5\sqrt{\frac{2G_f}{E_{FRP}t_{FRP}}}$$

$$\varepsilon_{FRP\,debond} = 1.5\sqrt{\frac{2(1.163)}{(70000)(2*1.1024)}} = 0.00582$$

$$\varepsilon_{FRP\,rupture} = (0.9)\frac{f_{frp,design}}{E_{frp,design}}$$

$$\varepsilon_{FRP\,rupture} = (0.9)\frac{774.83}{70000} = 0.00996$$

The strain limit to prevent debonding is smaller than that to prevent rupture of the FRP, thus $\varepsilon_{FRP\,debond}$ is the controlling strain limit in the FRP.

3. **Select a trial value for the depth to the neutral axis, c.** Start with $c = 101.6$ mm (4 in).

4. **For the trial neutral axis depth check to see if the concrete or FRP controls the design.** The strain at the level of the FRP when the extreme compressive concrete is at the ACI limit for concrete strain, 0.003, is calculated in Eq. 5-29. The initial strain on the soffit, ε_{soffit}, is conservatively estimated as 0.000434 using the remaining steel area, $A_{s,30yr}$ based on elastic analysis of the RC section under dead and wearing loads. See any basic concrete text, for example (Hassoun, 2002), for details.

$$\varepsilon_{FRPcrush} = 0.003\left(\frac{h-c}{c}\right) - \varepsilon_{soffit}$$

$$\varepsilon_{FRPcrush} = 0.003\left(\frac{1066.8 - 101.6}{101.6}\right) - 0.000434 = 0.028$$

Since $\varepsilon_{FRPcrush}$ is greater than $\varepsilon_{FRPdebond}$, debonding of the FRP is the controlling failure mode for this neutral axis depth, and $\varepsilon_{FRPdebond}$ is the limiting strain in the FRP.

5. **Calculate the strain in the reinforcing steel.** This calculation is shown in Eq. 5-30.

$$\varepsilon_s = (\varepsilon_{FRP} + \varepsilon_{soffit})\left(\frac{d-c}{h-c}\right)$$

$$\varepsilon_s = (0.00582 + 0.000434)\left(\frac{940 - 101.6}{1066.8 - 101.6}\right) = 0.00543$$

6. **Calculate the stress in the steel and FRP**. These calculations are shown in Eq. 5-31 and Eq. 5-32 for the steel and FRP, respectively.

$$f_s = E_s\varepsilon_s \leq f_y$$

$$E_s\varepsilon_s = 200000(0.00543) = 1086.0 \text{ MPa}$$

$$f_s = f_y = 275.8 \text{ MPa} \ (40 \text{ ksi})$$

$$f_{FRP} = E_{FRP}\varepsilon_{FRP}$$

$$f_{FRP} = (70000)(0.00582) = 407.4 \text{ MPa} \ (59.09 \text{ ksi})$$

7. **Estimate the stress block factors for the concrete.** The strain in the extreme compressive zone of the concrete is calculated in Eq. 5-33. This value is used to calculate stress block factors, α_1 and β_1 in Eq 5-48 through Eq. 5-50.

$$\varepsilon_{ct} = c\left(\frac{\varepsilon_{soffit} + \varepsilon_{FRP}}{h-c}\right)$$

Eq. 5-33

$$\varepsilon_{ct} = 101.6\left(\frac{0.000434 + 0.00582}{1066.8 - 101.6}\right) = 0.000658$$

$$n = 0.8 + \frac{f_c'}{17} = 0.8 + \frac{22.4}{17} = 2.12$$

Eq. 5-34

$$\varepsilon_c' = \frac{f_c'}{E_c}\frac{n}{n-1} = \frac{22.4}{22400}\frac{2.12}{2.12-1} = 0.00189$$

Eq. 5-35

$$\beta_1 = \frac{4 - \dfrac{\varepsilon_{ct}}{\varepsilon_c'}}{6 - 2\dfrac{\varepsilon_{ct}}{\varepsilon_c'}}$$

Eq. 5-36

$$\beta_1 = \frac{4 - \dfrac{0.000658}{0.00189}}{6 - 2\left(\dfrac{0.000658}{0.00189}\right)} = 0.689$$

$$\alpha_1 = \frac{1}{\beta_1}\left(\frac{\varepsilon_{tc}}{\varepsilon_c'} - \frac{1}{3}\left(\frac{\varepsilon_{tc}}{\varepsilon_c'}\right)^2\right)$$

Eq. 5-37

$$\alpha_1 = \frac{1}{0.689}\left(\frac{0.000658}{0.00189} - \frac{1}{3}\left(\frac{0.000658}{0.00189}\right)^2\right) = 0.446$$

8. **Use equilibrium to calculate a new estimate of the neutral axis.** This calculation is shown in Eq. 5-38, where A_s is equal to $A_{s,30yr}$, and A_{FRP} is equal to the trial width multiplied by the thickness and trial number of layers.

$$c = \frac{A_s f_s + A_{FRP} f_{FRP}}{\alpha_1 \beta_1 f_c' b}$$

$$c = \frac{(4706.9)(275.8) + 2(1.1024)(375)(407.4)}{(0.446)(0.689)(22.4)(2500)}$$ **Eq. 5-38**

$$c = 95.01 \text{ mm} \quad (3.74 \text{ in})$$

9. **Iterate to find the neutral axis.** For the trial quantities above, the neutral axis can be found equal to 98.2 mm (3.87 in).

10. **Find the factored moment capacity of the section.** This calculation is shown for the trial quantities above in Eq. 5-39.

$$\phi M_n = \phi \left[A_s f_s \left(d - \frac{\beta_1 c}{2} \right) + \psi A_{frp} f_{frp} \left(h - \frac{\beta_1 c}{2} \right) \right]$$

Eq. 5-39

$$\phi M_n = 0.85 \left[\begin{array}{c} 4706.9(275.8)\left(940 - \frac{(0.688)(98.2)}{2} \right) \\ + (0.881)(2*1.1024*375)(407.4)\left(1066.8 - \frac{(0.688)(98.2)}{2} \right) \end{array} \right]$$

$$\phi M_n = 1260.7 \text{ kN-m} \quad (930.41 \text{ kip-ft})$$

11. **Adjust the trial values of FRP width and number of layers until the load demand is met.** By repeating the above procedure, it can be found that a slight increase in the width to 390 mm (15.35 in) provides a moment capacity of 1270.93 kN-m (937.96 kip-ft). *Thus the final design is to apply two 390 mm wide layers of*

FRP to the girder.   A summary of the other design quantities for this amount of FRP is provided in Table 5-6.

Table 5-6 Final Design Quantities

$\varepsilon_{FRP\ debond}$	0.00582
$\varepsilon_{FRP\ rupture}$	0.00996
c	98.6 mm (3.88 in)
$\varepsilon_{FRP\ crush}$	0.02903
$\varepsilon_{FRP\ controlling}$	0.00582
ε_s	0.00544
f_s	275.8 MPa (40 ksi)
F_{FRP}	407.6 MPa (59.11 ksi)
ε_t	0.000637
α_1	0.434
β_1	0.688

5.2.6   Check the Stress in the FRP under Sustained Loads

Limits on sustained stress in the FRP were discussed in Section 3.6.2.2.1 of Chapter 3 and are intended to prevent stress-rupture of the composite. The limit from the CHBDC (CSA, 2006) was chosen in Chapter 3. This limit is 65% of the ultimate stress for carbon-reinforced composites. The design strength of the composite was found equal to 774.83 MPa (112.38 ksi), and therefore the FRP stress under sustained loads should be less than 503.64 MPa (73.05 ksi).   The stress in the FRP at the debonding limit, as shown in Table 5-6, is 407.6 MPa (59.11 ksi). This value is less than the sustained load limit, and thus the design meets this criterion.

5.3   Reliability Assessment of Design Example

The engineer using this design procedure will not explicitly calculate the reliability of the designed section. In fact, the primary reason for calibrating design factors is to keep complicated reliability procedures out of the design office.   However, the reliability was calculated in this case in order to see if the calibrated design factors were able to produce a

design close to the target reliability, particularly since a material slightly out of the calibration range was used for design.

The same reliability procedures used for calibration and described in Appendix E were used to assess the reliability of this design. The stochastic variation in the composite was described using the distribution parameters fitted in Chapter 3. These parameters are repeated in Table 5-7. It should be noted that the Java program used for MCS is in U.S. Customary units, and therefore the reliability was assessed in these units.

Table 5-7 Statistical Distributions for Set A1 used in Reliability Analysis

Property	Distribution	Parameters
Ultimate Strength	Weibull	$\alpha = 8.648$ $\beta = 1096.2$ MPa (159.010 ksi)
Modulus	Lognormal	$\lambda = 4.245$ MPa (9.222 ksi) $\zeta = 0.132$
Thickness	Lognormal	$\lambda = 0.095$ mm (-3.139 in) $\zeta = 0.044$

The reliability calculated for this strengthening design example was 3.51, a value that is very close to the target reliability of 3.5. This demonstrates that the calibrated factors are capable of meeting the target reliability, even when a material slightly different from the calibration materials is used. However, despite the closeness of this particular example to the reliability target, it must be remembered that the resistance factors in Table 4-13 were found as the *average* value pertaining to a group of girders with similar amounts of steel deficiency relative to the LRFR requirements.

In another example case, girder 13 (as described in Chapter 4) was selected as the member to be strengthened. The design life was assumed equal to 40 years, with an initial

loss of 10%. This girder had a deficiency relative to LRFR of 14.5%, nearly equal to that found here. The same composite material was assumed, and the reliability target was again set at 3.5. Despite all of the similarities, the reliability of the strengthening designed for this girder was only 3.26.

This suggests that grouping the girders on the basis of steel loss may not be adequate to fully define the different ranges of resistance factors. However, no other trend was readily observable. Furthermore, the resistance factors found in LRFD codes are generally rounded up. In this work, the factors are presented exactly as they were calibrated, and the calibration was conducted to meet the target reliability on average. By adjusting the factors the target reliability could be met or exceeded a higher percentage of the time. These findings suggest that in the future when more information is available and a more rigorous calibration can be conducted, an important part of the process will be to evaluate the designs created with the calibrated factors and adjust the factors if necessary.

5.4   Summary

In this chapter the proposed design procedure was outlined and then used to create an example strengthening design. The procedure discussed herein is based on the information currently available; however it is general in nature, and its framework was selected with the intent to facilitate the inclusion of new information. Models were assumed for calculating resistance and predicting future structural deterioration and composite degradation to demonstrate the use of the proposed procedure, but the models used here are only examples and could be replaced with other models. The next chapter concludes this report with a discussion of topics for further research and identifies the areas of the design procedure that may be subject to future changes or improvements and how these changes would affect the overall design process.

Chapter 6. Conclusions, Recommendations, Areas for Study

6.1   Summary

This report describes the experimental and analytical procedures followed to develop a framework for reliability-based design of FRP strengthening for existing concrete structures. The statistical variation in wet layup composites was characterized for use in reliability analysis based on tensile testing of a number of field-manufactured sample sets. A method for specifying the design value of composite properties was proposed. This method is based on the use of the mean value from laboratory characterization as the characteristic value, a composite specific resistance factor that accounts for the variation in the composite, a system of Application Factors that considers the specifics of field manufacture, and an environmental reduction factor that is specific to the exposure environment and anticipated service life of the composite strengthening.

After the design format was developed, preliminary values of resistance factors were calibrated. The factors were calibrated for a set of reinforced concrete T-beam bridge girders. Possible continued degradation of the structure was considered through corrosion of the reinforcement. Five different FRP materials with assumed properties typical of wet layup composites were used in the calibration. The factors were found to depend on the amount of steel remaining relative to that needed to just meet the LRFR load requirements. An example design was presented to further explain the proposed procedure.

6.2   Areas for Further Study

Reliability-based design for FRP strengthening is an emerging field of research, and as such, this report has only described the initial aspects of LRFD development. The work described herein has produced a sound framework; however there are many gaps remaining to

be filled before the procedure can be considered complete. Often assumptions were necessary because the information needed to answer the questions was just not available. The following sections summarize the major areas identified for further study and describe how advances in these areas would improve or change the proposed design procedure.

6.2.1 FRP Composite Material Properties and Design Factors

The most pressing concern regarding the FRP materials is the limited data upon which this work is based. The data is limited with regard to the number of specimens and samples, the types of composites and manufacturing conditions represented, and the exposure conditions modeled for degradation. This work has specifically sought to develop a design procedure that can accommodate new findings. Presently, it can be considered as the basis for use of LRFD until further data is available.

6.2.1.1   Statistical Description of Properties

In Chapter 3 several different sets of field manufactured wet layup samples were analyzed to determine appropriate statistical models for composite properties. While the data sets were large compared to sets of five or ten that might commonly be used to assess material properties, they were still quite small from a statistical standpoint. It would be desirable to have many larger data sets, representing even more composite materials.

This additional data could be used to verify the distributions chosen to model variation in composite properties or perhaps identify different classes of composites that should be modeled in different ways. More data might also make it possible to select a representation of the correlation between composite properties. This data would be used in future calibration of resistance factors to improve the models of FRP variation.

No matter how much data is collected, thickness and its effect on strength and modulus will remain a concern for wet layup composites. One solution to this problem may be to base

design on force and stiffness per unit width. This is a concept that merits further study, although the advantages it offers may not justify a change in the basic design philosophy of using stress and modulus.

6.2.1.2   Prefabricated Composites

Though the proposed design framework was developed with the intent to have one uniform procedure applying to all types of composite materials, no prefabricated composites were considered in this work. Extending the proposed procedure to include prefabricated materials will require extensive work, considering both the FRP and the adhesive used to bond it to the concrete. Some of these tasks include:

- Development of statistical models to describe the FRP and adhesive.

- Derivation of values for Application Factors specific to strengthening with prefabricated composites.

- Development of models for the environmental degradation of composite and adhesive.

- Use of a bond model that allows for consideration of FRP *and* adhesive variation in calibration.

- Calibration of resistance factors.

Depending on the results of this work, it may be possible to divide composites into two or three broad ranges with different resistance factors applying to each range. Or it may be possible to use just one set of resistance factors, so long as the design value is appropriately calculated.

6.2.1.3   Application Factors

This work proposed a set of four Application Factors; λ_{pred}, λ_{layers}, λ_{cure}, and λ_{work}. Preliminary values for some of these factors were derived herein; however further specification of values for these factors will require extensive study. λ_{cure} is likely to depend on the particular material in question, though some generalizations may be found. It will be hard to analytically study λ_{work}, and this factor may depend heavily on the expert opinion of designers and contractors working in this field. It is emphasized that improvements to these factors will not require recalibration of resistance factors, but will improve the predictions of in-situ property values.

6.2.1.4   Degradation Models

As discussed in Chapter 3, there is currently a severe deficit in data describing the degradation of composite properties due to environmental exposure. The present design procedure was created to be flexible in accommodating new degradation data. As this data is gathered and used to develop models, the prediction of in-service FRP properties will become steadily more accurate. It is particularly important to gather data and develop models that represent conditions that are likely in service, rather than the severe environments used in laboratory durability testing. It is also important to assess the effect of environmental exposure on the variation in composite properties.

6.2.2 Limit States for Evaluation

This work focused exclusively on FRP applied to strengthen members in flexure. This choice was made because the behavior of strengthened members was best understood in flexure. However this is not the only failure mode that FRP is applied to mitigate, and each failure mode must be considered for a complete LRFD specification. Ideally, calibration of resistance factors for different limit states should be conducted concurrently, so that the same

FRP specific factor, ψ, can be applied in all situations, with changes only to the general resistance factor, ϕ.

6.2.2.1   Flexure

The main concern regarding flexural application is preventing the composite from debonding from the concrete. This work made use of a preliminary bond model based on the fracture mechanics of the bond between FRP and concrete. As bond models are improved, it may be necessary to recalibrate factors based on the new model. It may also be possible to use a simple, but conservative, model for design, while using a more accurate and complex model for calibration, in which case recalibration would definitely be required.

Another consideration in flexural strengthening is the use of anchorage mechanisms. Reliability-based design of anchored systems will not be possible until a limit state function can be defined. This function may be implicit (as in a finite element program); however it must be general enough to represent a range of designs before it is suitable for use in design code development.

6.2.2.2   Shear

The ability to define the limit state function is the main limitation affecting reliability-based design of shear strengthening with FRP. Schuman (2004) found that current approaches to calculating the shear capacity of strengthened beams are inaccurate and in fact, unconservative. He found that through the use of anchorage, a certain minimum value of capacity could be predicted. While this could allow for reasonable design of shear strengthening with the use of a safety factor, this is not an acceptable definition of capacity for use in reliability analysis.

6.2.2.3   Slabs

A very desirable use of composites is to strengthen concrete slabs. Though slabs are generally designed as flexural members, their load carrying behavior is often more complex. In order to better apply FRP strengthening in the most effective manner, FRP strengthened slab behavior must be better understood.

6.2.2.4   Serviceability

The application of FRP can add to the stiffness of members and improve their deformation behavior. Some serviceability limit states, such as crack width, may already be exceeded before the FRP is applied. Therefore, in order to consider serviceability limit states in an LRFD specification for strengthening, a clear definition of applicable limit states is necessary.

6.2.2.5   Modeling Error

The analysis conducted in this work did not consider the error present in any of the models assumed for design or reliability analysis, for example those used to predict section capacity or corrosion of reinforcement. There are many issues associated with an accurate assessment of modeling error, including the difficulties associated with assessing material properties within a structure or laboratory specimen. This is an important variable to consider in future reliability analysis and deserves significant study.

6.2.2.6   Interaction of Limit States

Finally, it is important to consider the interaction of different limit states. A significant problem is the interaction of flexure and shear in strengthened beams. A beam initially weak in flexure may become critical with respect to shear after the application of flexural strengthening. Given the more brittle and less predictable behavior of RC members in shear

this is an undesirable event. This interaction can be especially critical when the member being strengthened is a slab and punching shear is a concern.

In general, a better understanding of how FRP affects the failure modes of the existing structure is needed for all FRP applications, and for reliability analysis a statistical description of the modeling error is also desirable.

6.2.3   Statistical Models of Load

Appendix A provides details regarding the limitations of existing models for live loads acting on bridges. There are many questions regarding the live load models used in calibration of the LRFD specification for design of new bridges. These models assume a Normal distribution of load for all time periods, when in fact some other distribution may be more appropriate. The set of distributions provided for different time frames does not seem to be self-consistent. The distributions are based on old load surveys (Nowak, 1999). And finally, the distributions do not consider the gradual increase in load as trucks become heavier and traffic increases.

Further study of loading is vital for reliability-based design of all strengthening measures and even new design. As complete life-cycle costs become more important in bridge management strategies, the ability to assess the reliability over different time periods is vital. The simplicity of the time-integrated approach is very attractive, and new load models should develop a set of distributions for different time frames that are self-consistent. However some forms of structural deterioration depend on the loading history of the structure, and therefore random process models are needed to describe the load for reliability analysis. Development of time-integrated and random process models should be conducted together, so as to provide similar reliabilities for certain reference cases. A standard set of load models would significantly aid the development of reliability-based design, as the work of different

research teams would have greater compatibility and comparability. In considering time-dependent load models, it may also be advantageous to develop design life specific load factors. This would allow for the accommodation of different reliabilities for different design lives, while maintaining constant resistance factors. Another topic of interest for the design of strengthening is the potential to use site-specific data in design.

6.2.4   Modeling Continued Structural Degradation

There are numerous mechanisms by which a structure deteriorates. In this work, one of those mechanisms, loss of steel reinforcement cross-section due to corrosion, was modeled. This mechanism was chosen because it is a significant mode of deterioration, and because models are available to describe it. However, there are other modes that can also affect the integrity of a structure. And, furthermore, despite the efforts herein, it is difficult to define a general model of corrosion. Significant further work is needed to better model the complete deterioration of structural properties and predict the future capacity of structures.

6.2.5   Time-Dependent Reliability

The work conducted in this project hinges on the calculation of reliability. Each method of computing the reliability index is based on its own set of assumptions, and therefore only reliabilities calculated in the same manner can be directly compared. While the relative differences between different techniques for calculating non-time-dependent reliability are quite clear, the differences between time-dependent techniques are not as clear. This is particularly true when considering deteriorating structures and growing load demands. An assessment of these different techniques would be valuable and could serve to encourage the consideration of time-dependent behavior in other design codes. (With the exception of the time effect factor for creep in the engineered wood code (AF&PA, 1996), existing LRFD

264

specifications do not consider the time-dependent behavior of materials or the possibility of designing to different design lives.)

6.2.6   Selection of β_T

Selection of the target reliability index was discussed in Section 2.8 of Chapter 2. There are many factors which complicate the selection: the fact that the designs are not for new construction, the lack of an existing code to use for comparison, the loss in ductility that accompanies the application of FRP, and the desire to consider specific design lives. The question of appropriate reliability targets does not necessarily have a right answer, but a set of consistent targets should be chosen based on an affirmed set of principles. For example, the target reliabilities for different time periods could be set to have approximately the same annual probability of failure or the same lifetime probability of failure. The target could be lower because the design is for a repair, or it could be adjusted upward to compensate for the loss in ductility. Many different options are justifiable, and while the design community has reached a consensus of 3.5 for new design and 2.5 for existing structures the question of differences based on anticipated service-life are still open.

6.2.7   Understanding the State of the Existing Structure

Throughout this report the importance of the amount of steel remaining in the section has been witnessed.   The state of the existing structure (the entire structure, not just the reinforcement) when strengthening is applied, as well as the continuing deterioration characteristics of the structure, will have a significant impact on the reliability of any strengthening scheme. Therefore developing better techniques for assessing and predicting the state of structures is perhaps the most important of all the areas for further research described in this chapter.

6.3 Conclusion

The uncertainty involved in design of FRP strengthening can be considered through a reliability-based design format such as LRFD. This work has developed a framework for the application of LRFD to FRP strengthening and, by employing numerous assumptions, has calibrated design factors. While extensive further research is required to fill out the proposed framework, the design example shown in the previous chapter indicates the approach by which the current results can be implemented to initiate design using the approach.. However, until this data is developed, the current methodology enables engineers to use LRFD principles for design, thereby bringing FRP composites to an equivalent state with conventional materials, vis-à-vis design approach. It is recommended that factors shown in this report for wet layup be adopted till such a time that additional data is available through additional testing by Caltrans.

Appendix A. Live Load Statistics for Specified Design Life

A.1 Introduction to Problem

In *NCHRP Report 368* (Nowak, 1999)*,* the report describing the calibration of the *AASHTO LRFD Bridge Design Specifications* (AASHTO, 1998 and 2004)*,* bias factors are provided to relate the live load effects predicted using the HL-93 live load model to the mean of the anticipated maximum live load based on data taken from traffic surveys. In that report bias factors were provided for time spans of 1 day, 2 weeks, 1 month, 2 months, 6 months, 1 year, 5 years, 50 years, and 75 years. These time spans do not directly correspond to those time periods chosen for consideration in this study, namely 10, 20, 30, 40 and 50 years. Several techniques were studied in an attempt to better understand the available data and use it to estimate the time-dependent reliability, since rehabilitation needs shorter periods of life.

A.2 Attempted Derivation of Extreme Value Distribution

A.2.1 Basic Distribution of the Maximum

The probability distribution of the maximum value of a random variable can be quite simply derived following Castillo et al. (2005).

For a random variable *X*, with PDF *f(x)* and CDF *F(x),* the joint PDF of a sample of independent and identically distributed x_i drawn from *F(x)* can be written as shown in Eq. A-1. The joint CDF is shown in Eq. A-2.

$$f(x_1, x_2,..., x_n) = \prod_{i=1}^{n} f(x_i)$$

Eq. A-1

$$F(x_1, x_2,..., x_n) = \prod_{i=1}^{n} F(x_i)$$

Eq. A-2

From here the CDF of the maximum order statistic, $X_{n:n}$, can be found as shown in Eq. A-3 through Eq. A-6.

$$F_{\max}(x) = \Pr(X_{n:n} \leq x)$$

<div align="right">**Eq. A-3**</div>

$$F_{\max}(x) = \Pr(\max(X_1, X_2, ..., X_n) \leq x)$$

<div align="right">**Eq. A-4**</div>

$$F_{\max}(x) = \Pr(all\ X_i \leq x)$$

<div align="right">**Eq. A-5**</div>

$$F_{\max}(x) = \prod_{i=1}^{n} \Pr(X_i \leq x) = \prod_{i=1}^{n} F(x) = [F(x)]^n$$

<div align="right">**Eq. A-6**</div>

Thus, the CDF of the maximum can be found by raising the original CDF to the nth power. The PDF, as shown in Eq. A-7, can be found through differentiation of Eq. A-6.

$$f_{\max}(x) = nf(x)[F(x)]^{n-1}$$

<div align="right">**Eq. A-7**</div>

A.2.2 Attempted Use of Distribution of the Maximum

Based on Eq. A-6 an attempt was made to derive distributions of the maximum five- and fifty-year live loads from the distribution of one-year maximum live load presented by Nowak (1999) by raising the CDF of the one-year load to the fifth and fiftieth powers, respectively. Five and fifty years were chosen because distributions for these time frames were provided in the calibration report, and thus the derived distribution could be compared to the statistics provided by Nowak (1999). The distributions for all of these time spans were provided in terms of the bias factor and COV. The bias factor represents the mean of the distribution divided by a constant (in this case the value of live load predicted using the HL-93 model). Therefore, the distribution of the bias factor has the same variation as the distribution of maximum live load and is equivalent to the distribution of maximum live load divided by a constant. Thus, extreme value theory was applied to find the distribution of the bias factor for maximum live load for these different time spans.

This task was conducted numerically in Microsoft Excel. The CDF of the one-year maximum live load was defined in terms of the bias factor and COV provided by Nowak (1999). The value of the CDF for a range of possible bias factors was calculated and then raised to the necessary power to find a numerical representation of the CDF for the five- and fifty-year live loads. Nowak's work specified that all distributions were Normal distributions. Therefore, using the error minimization procedure described in Section 3.3.3.1 of Chapter 3, parameters of the Normal distribution were fit to the numerically defined CDFs.

The example case chosen was for a span of 15.2 m (50 ft). The one-year bias factor was 1.22, and the COV was estimated from Figure B-11 of (Nowak, 1999) to be 0.13. Figure A-1 shows a plot of the fitted Normal PDFs of the bias factor for maximum live load for the different time spans considered. It is clear that for extended time periods the mean value of the bias factor is increased substantially and the amount of variation is decreased. Figure A-2 shows the CDFs of these same distributions.
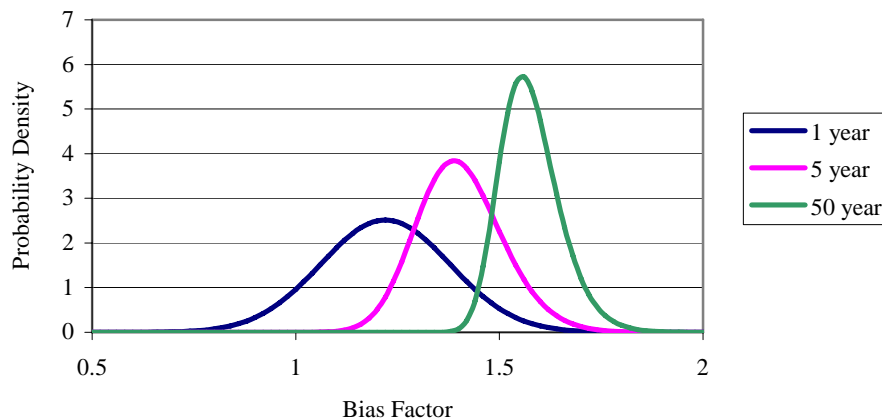
Figure A-1 PDF of Bias Factor for Maximum Load for Different Time Spans
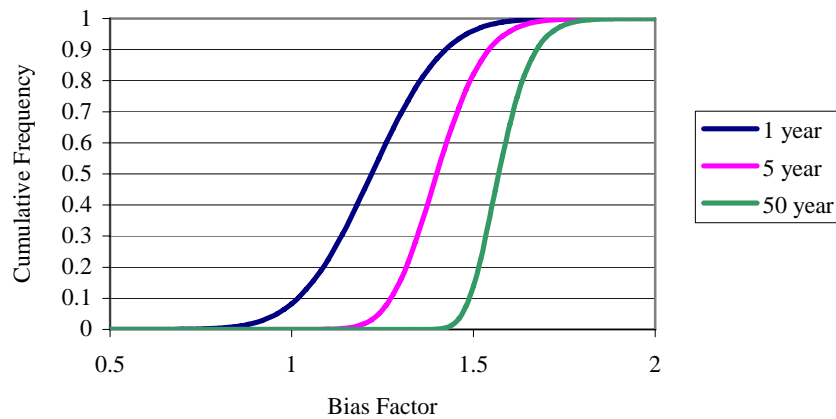
Figure A-2 CDF of Bias Factor for Maximum Load for Different Time Spans

Table A-1 shows a comparison of the numerical values of the mean and COV of the bias factors obtained using extreme value theory and those provided by Nowak. It is clear from this table that the values calculated using extreme value theory are not consistent with the values provided by the calibration report. The distributions estimated from the maximum one-year load describe far more demanding distributions of live load.

Table A-1 Comparison of Estimated Bias Factors and Bias Factors from NCHRP Report 368

Time Period	Estimated with Extreme Value Theory		Provided in NCHRP Report 368 (Nowak, 1999)	
	Mean	COV	Mean	COV
5 years	1.40	0.075	1.25	0.12
50 years	1.57	0.045	1.33	0.11

Nowak (1999) specified that distributions for all time spans could be represented as Normal. However, based on extreme value statistics, for an originally Normal distribution the distribution of the maximum for samples drawn from that distribution should asymptotically approach a Gumbel distribution (Bury, 1999). For purposes of comparison parameters of a

Gumbel distribution were also fit the theoretical distribution. Figure A-3 shows the theoretical PDF as well as the fitted Normal and Gumbel PDFs for the maximum fifty-year live load. Clearly, the theoretical distribution falls somewhere between the two, showing some of the skewness of the Gumbel distribution. This casts some question on the continued use of the Normal distribution to represent live loads for extended time intervals.
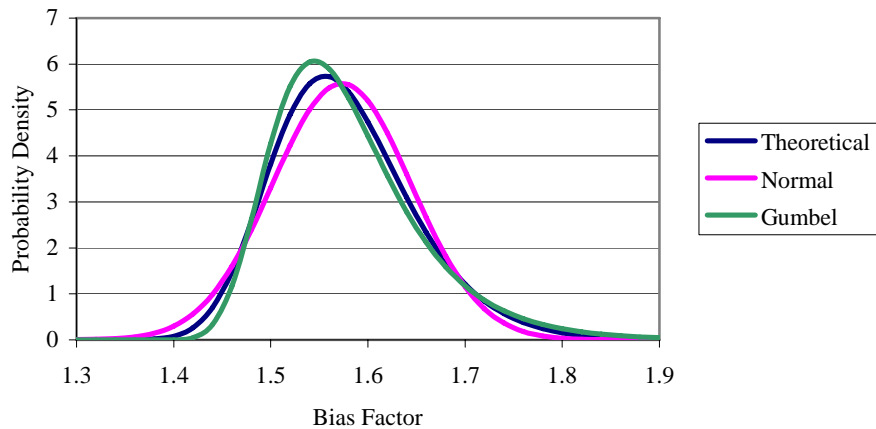
Figure A-3 Comparison of Distributions for Mean Maximum 50-Year Load Bias Factor

Previous studies on strengthening of bridge girders with FRP (Okeil et al., 2002; El-Tawil and Okeil, 2002) have used a normal distribution to describe live loads. However, other studies of bridge reliability have used different models of live load. Park et al. (1998) used an Extreme Type I distribution (a Gumbel distribution) to describe the annual maximum live load. A number of studies (Stewart and Rosowsky, 1998a and 1998b; Val et al., 1998; Val and Melchers, 1998) used a Normal distribution to describe the maximum weight of a single truck, however used Eq. A-6 to find the maximum annual truck load based on the number of occurrences of two trucks crossing side-by-side. They then used this annual model to calculate the probability of failure during a given design life, t_L , as shown in Eq. A-8,

where S_i are independent load events occurring annually, and $R(t_i)$ is the time-dependent structural resistance.

$$p_f(t_L) = 1 - \Pr[R(t_1) > S_1 \cap R(t_2) > S_2 \cap ... \cap R(t_n) > S_n]$$

Eq. A-8

Based on the analysis of live load models conducted here, it was apparent that distributions for the desired time-periods estimated using extreme value theory would not directly correspond to the data provided in *NCHRP Report 368* (Nowak, 1999). This was a concern because this research has sought to create a procedure for design of strengthening that is consistent with the existing provisions for new design, and it was felt that consistency in live load models was important.

A.3 Different Methods Used to Assess Time-Dependent Reliability

Without readily available live load distributions for the time periods of interest and with no clear way to derive distributions consistent with existing data for these time periods, three different definitions of the live load distribution were tested to see how they affected the resulting reliability.

A.3.1 Definition of Trial Conditions

The girder used in this comparison of different time-dependent reliability approaches was the same girder used for most of the preliminary calibration studies. Details of this girder's dimensions can be found in Section C.2 of Appendix C. Strengthening for this girder was designed following the assumptions of Section C.3 of Appendix C for an assumed loss of steel equal to twenty percent of the initial steel area. Some details of this example are given in Table A-2.

Table A-2 Basic Details of Strengthening Example

Initial FRP Properties	Strength	896 MPa (130 ksi)
	Modulus	57 GPa (8267.3 ksi)
	1-layer Thickness	1.016 mm (0.04 in)
Design of Strengthening	Assumed ϕ	0.90
	Assumed ψ	0.75
	Total Factored Design Load	1593.3 kN-m (1175.84 kip-ft)
	Number of Layers	1
	Width of FRP	273 mm (10.75 in)

Degradation of the FRP was included in this example using the model of Abanilla (2004) described in Section 3.6.2.1 of Chapter 3. The reliability of the girder was calculated through the use of direct Monte Carlo Simulation as described in Appendix E.

A.3.2 Trial Calculation Techniques and Results

The reliability of the strengthening design was assessed for five and fifty years using three different approaches, which are summarized in Table A-3. All of these approaches used a Normal distribution to describe the maximum live load because this was the distribution used for calibration of the LRFD provisions (Nowak, 1999). Method 1 made direct use of the distributions provided by Nowak (1999). Method 2 used Normal distributions fit to the theoretical distribution of the maximum as described in Section A.2. The bias factor distributions were slightly different from those derived above because this sample girder had a span of only 12.2 m (40 ft). Despite the difference in spans, the bias factor distributions showed the same trends observed previously between the derived distribution and Nowak's (1999) distribution, and thus the general results of this comparison are not expected to be span dependent. Method 3 was based on Eq. A-8. The reliability was calculated in annual

273

increments based on the distribution of one-year maximum load from Nowak (1999) and included degradation of the FRP. The reliability over the complete time period was calculated from these annual reliabilities using Eq. A-9, where p_{fi} are the annual probabilities of failure. This equation assumes that the maximum load in each year is independent of the maximum load for other years.

$$p_f = 1 - \prod_i (1 - p_{fi})$$

Eq. A-9

Table A-3 Different Methods Used to Calculate Time-Dependent Reliability

Method	Load Description	Resistance Description	Reliability Calculation
1	Loads modeled at 5 and 50 years using Normal distributions and the bias factors and COVs from Nowak (1999)	Resistance calculated using degraded FRP properties at 5 and 50 years	Time-integrated approach MCS
2	Loads modeled at 5 and 50 years using Normal distributions fit to the theoretical distributions of the maximum based on the 1-year distribution from Nowak (1999)	Resistance calculated using degraded FRP properties at 5 and 50 years	Time-integrated approach MCS
3	1-year Normal distribution of load from Nowak (1999) used to compute reliability for each year	Resistance calculated at the end of each 1- year increment using degraded FRP properties	MCS used to compute reliability in yearly increments Overall p_f is calculated using Eq. A-9

The reliability indices resulting for the two different time periods using each of these three techniques are shown in Table A-4.

Table A-4 Comparison of Reliabilities for Different Computation Techniques

Year	Time-Dependent Reliability Method		
	1	2	3
5	3.66	3.54	3.55
50	3.21	2.88	2.79

It can be seen that the reliabilities calculated with Method 1 (directly using Nowak's data) are significantly higher than those calculated with the other two methods, particularly at a time of fifty years. This is not a surprise given the differences in bias factors that were seen in Section A.2.2. This difference suggests that the distributions in Nowak (1999) are not consistent with each other, because the distributions for longer time periods can not be derived from the distributions of shorter time periods. Methods 2 and 3 actually produce quite similar results. These two methods are both based on the one-year distribution (as opposed to Method 1 which used time specific distributions), which could help explain their consistency. This similarity of results suggests that an appropriately selected time-integrated distribution can approximate more rigorous techniques. However, all of these results are troubling in the fact that the time-integrated approach is supposed to provide a conservative estimate of reliability (since it compares the maximum load to the minimum resistance and it is unlikely that they will occur simultaneously), when in fact it is the more rigorous approach that is actually the most conservative. This unexpected result again points out the incompatibility of distributions for different time spans in (Nowak, 1999). It also shows that great care should be used when deriving time-integrated distributions.

Though this example considered just one girder, the results are expected to be representative of a significant range of girders. This is because the change in bias factors for

girders of different spans is very small, especially when compared to the differences between Nowak's models (1999) and the distributions derived with Eq. A-6.

A.4 Conclusions

Though these significant inconsistencies in existing live load data point to the need for further and perhaps enhanced analysis of the statistical models used to describe bridge loading, the development of new live load models was not the intent of this report. Therefore, a decision had to be made as to which model to use: the directly available distributions, even though they did not conform to the specific time frames desired, or derived distributions, which may not be consistent with the load models used in the development of the LRFD specifications. The decision was made to use the distribution of 50-year maximum live loading for all time frames in question. This decision will provide for consistency by allowing the direct usage of Nowak's models (1999). It should also give conservative results for time frames shorter than 50 years. (Nowak's data showed no increase in bias factor between 50 and 75 years so, based on his models, the reliability will also be acceptable for time-periods somewhat longer than 50 years if structural deterioration is neglected.) The time-integrated approach will be used because it is consistent with this format for the live load model.

The fact that this live load model was chosen for the analysis in this report does not replace the need for substantial further study of the statistical models used to describe bridge loading. As structural design continues to evolve, it is highly likely that time-dependent behavior will be explicitly considered more often, and simple methods of evaluating the reliability at different times will be needed. Therefore, it is suggested that statistical models for live loading should be developed such that the time-integrated approach can be directly applied, while still allowing for some consistency between different time frames. A comparison of rigorous analysis techniques to the time-integrated approach for a range of

different structures could aid in selection of accurate time-integrated models. It will also be important to define random process models for loading, which allow for reliability computation when structural damage is a function of the loading history. A set of self-consistent models will greatly aid in the development of future reliability based design codes. There should also be some consideration given to the gradual increase in both truck weight and traffic density on bridges. All of the models discussed above assume that the annual distribution of truck weights remains constant over an extended period of time. This is not an accurate descriptor of real circumstances and suggests that the time-integrated approach of comparing the maximum load to the minimum resistance may not necessarily be a conservative assumption.

Appendix B. Goodness-of-Fit Tests

B.1 Introduction

Three different goodness-of-fit tests were used for comparing the accuracy of the fitted distributions: Chi-Squared, Kolmogrov-Smirnov, and Anderson-Darling. All goodness-of-fit tests are hypothesis tests. They cannot say that a distribution *is* a good fit; they can only indicate when it is unlikely that the hypothesized distribution is a good fit. The significance level of a test gives the criteria for rejecting the hypothesis that the proposed distribution is an acceptable fit (Romeu, 2003). For example, a 0.05 significance level means that when a distribution is rejected, there is a 5% chance that the rejected distribution is actually an acceptable fit. Distributions that fit a set best will pass the test at higher significance levels. For example, at the 0.10 significance level, a distribution that fits the data well has a 10% chance of being rejected, so if it passes the test, it is a better fit than a distribution that only passes at the 0.05 level and only had a 5% chance of being rejected.

B.2 Chi-Squared Test

The Chi-Squared goodness-of-fit test divides the data range into a number of bins, *k*, and compares the actual number of data points in each bin to the number of points predicted by the hypothesized distribution. This test is easy to apply to both discrete and continuous distributions; however when the data is grouped into bins some information about the true distribution is lost (Moore, 1986). This test works best for large samples, but the definition of large depends on the confidence level of the test and the number of bins used. More details can be found in (Moore, 1986).

To apply the test, a test statistic is computed using Eq. B-1, where *k* is the total number of bins, *actual* refers to the number of actual data points that fall into bin *i*, and *predicted* is the

number of points predicted in the bin based on the distribution whose fit is being tested. This statistic is then compared to the approximate χ^2 distribution with *k-1-number of estimated distribution parameters* degrees of freedom evaluated at the desired significance level, α. If the computed statistic is less than $\chi^2_{(k\text{-}1\text{-number of estimated distribution paramters})}(\alpha)$, the assumed distribution is accepted as a reasonable fit for the given significance level (Haldar and Mahadevan, 2000). The results of the test depend to some extent on the bins used. It is suggested that each of the bins have an equal probability under the hypothesized distribution. The number of cells to use can be approximately calculated with Eq. B-2, where n is the total number of data points, though this equation overestimates to some extent (Moore; 1986). The Chi-Squared test uses the same rejection criteria for every distribution; therefore the distribution that passes the test at the highest significance level is the one with the smallest value of the test statistic.

$$\sum_{i=1}^{k} \frac{(actual_i - predicted_i)^2}{predicted_i}$$

Eq. B-1

$$k \approx 2n^{2/5}$$

Eq. B-2

B.3 EDF Tests

The Kolmogorov-Smirnov (K-S) and Anderson-Darling (A-D) tests are both referred to as Empirical Distribution Function (EDF) tests because they measure the vertical difference between the EDF and the distribution being tested. Both of these tests are appropriate for small and large samples (Romeu, 2003). For the purposes of these tests, the empirical distribution function, $F_n(x)$, is defined as shown in Eq. B-3, where n is the total number of observations. These tests both have rejection criteria specific to the distribution being tested.

Furthermore, when distribution parameters are estimated from the data itself the test criteria are subject to modification (Stephens, 1986).

$$F_n(x) = \frac{\text{number of observations} \leq x}{n}$$

Eq. B-3

B.3.1 Kolmogorov-Smirnov Test

The Kolmogorov-Smirnov test statistic can be computed using Eq. B-4 (Stephens, 1986). In this equation D^+ computes the largest vertical distance between the EDF and the distribution being tested when the EDF is greater than the assumed distribution, and D^- computes the largest vertical distance when the EDF is less than the assumed distribution. $F(x_i)$ is the value of the CDF for the distribution being tested evaluated at the ith ordered data point. The value of D is then compared to tabulated percentage points for specific assumed distributions and given significance levels. If D is less than the tabulated values, the distribution being tested is accepted at the significance level of the test. Otherwise the distribution is rejected. Modifications to D based on the number of specimens in the set and percentage points for the test were found in Stephens (1986) for the Normal, Lognormal, and Weibull distributions. Parameters for K-S tests of the Gamma distribution could not be found for the case where the distribution parameters are estimated from the data; thus this test could not be applied to the fitted Gamma distributions.

$$D^+ = \max\{F_n(x_i) - F(x_i)\} \; ; \; D^- = \max\{F(x_i) - F_n(x_{i-1})\} \; ;$$

$$D = \max\{D^+, D^-\}$$

Eq. B-4

B.3.2 Anderson-Darling Test

The Anderson-Darling test statistic is computed as shown in Eq. B-5, where n is the total number of data points and $F(x_i)$ is as previously defined. An advantage of this test is that

it is good at detecting differences between the data and the assumed distribution in the tail regions (Stephens, 1986). This is an important consideration given the sensitivity of reliability calculations to the tail behavior of distributions. Modifications to A^2 based on the number of specimens and percentage points for the test were found in Stephens (1986) for the all four of the distributions.

$$A^2 = -n - (1/n)\sum_{i}^{n}(2i-1)\left[\ln F(x_i) + \ln(1 - F(x_{n+1-i}))\right]$$

Eq. B-5

Appendix C. Preliminary Calibration Examples

C.1 Introduction

During the course of this project numerous small example calibrations were conducted to isolate key variables and identify general reliability trends. This appendix describes the most significant of these small examples as well as the implications drawn from them for further work. Many of the conclusions drawn were previously described in Chapter 2. The intent here is to provide more justification for these decisions. While simple beams were used to investigate the reliability implications of different composite design values (as seen in Chapter 3), for other reliability trials a sample girder was designed. The sample girder and the general strengthening design procedure are common to all of the following cases. Design of the girder is described in Section C.2 and the general strengthening design procedure is described in Section C.3. A discussion of how material properties were specified for the sample composites used in these examples is given in Section C.4. Details of the specific example cases follow these descriptions.

C.2 Sample Girder

In the following examples, a reinforced concrete T-beam, representing an interior girder from a bridge deck, is used as the structure to be strengthened.   The girder was designed using the *AASHTO LRFD Bridge Design Specifications* in Customary U.S. units (AASHTO, 1998) following a textbook example (Barker and Puckett, 1997). For simplicity, the girder was assumed to be simply supported. The assumed dimensions for the bridge are show in Table C-1.

Table C-1 Bridge Deck Dimensions

Span	12.2 m (40 ft)
Girder Spacing (center to center)	2.44 m (8 ft)
Deck Width	8.53 m (28 ft)
Number of Lanes	2

The girder was designed considering the Service I and Strength I limit states from AASHTO LRFD. The materials are Grade 60 reinforcing bar with a yield strength of 413.7 MPa (60 ksi) and 34.5 MPa (5 ksi) concrete. As the span was relatively short and assumed to be simply supported, the design tandem was found to be the governing vehicular load. The load effects are shown in Table C-2.

Table C-2 Load Effects for Girder Design

Component Dead Load	408.97 kN-m (301.67 kip-ft)
Wearing Surface Dead Load	75.88 kN-m (56.0 kip-ft)
Live Load (including impact) Due to Tandem and lane load (multiple presence and girder distribution factor are also included)	717.40 kN-m (529.45 kip-ft)
Factored Moment for Service I Limit State	1202.05 kN-m (887.12 kip-ft)
Factored Moment for Strength I Limit State	1786.22 kN-m (1318.24 kip-ft)

In design of the girder, the serviceability limit state was found to control the amount of rebar in the tension region, requiring eight 32.3 mm diameter (#10) bars, providing a moment capacity of 2275.00 kN-m (1678.97 kip-feet), compared to the Strength I load demand of 1786.22 kN-m (1318.24 kip-feet). The amount of reinforcement to just meet the Strength I limit state was found to be eight 28.6 mm diameter (#9) bars, providing 5161.3 mm^2 (8 in^2) of steel. The intent of these calibration examples was to provide an example for the strength limit state of the girder, but, based on design to meet the serviceability requirements, very

large amounts of steel loss would be required before the strength limit state was violated. Therefore the initial area of steel in the girder was taken as the 5161.3 mm^2 (8 in^2) needed to meet the strength limit state. Dimensions of the girder are provided in Table C-3.

Table C-3 Dimensions of Sample Girder

Effective Flange Width	3.66 m (8 feet)
Web width	508 mm (20 in)
Deck thickness	203.2 mm (8 in)
Depth of T-beam (including deck)	1066.8 mm (42 in)
Depth to Reinforcing Steel	957.6 mm (37.7 in)
Area of Steel	5161.3 mm^2 (8.0 in^2)

C.3 General Procedure for Strengthening Design

Throughout this work the design flexural strengthening is based on sectional analysis following the procedure outlined in Section D.2 of Appendix D. For the examples in this appendix, the limiting strain in the FRP to prevent debonding was calculated using the ACI 440 (ACI, 2002) bond model. In this model a bond-dependent coefficient, κ_m, is calculated based on the rupture strain, modulus, and thickness of the FRP and multiplied by the rupture strain to predict the debonding strain (see Section 4.8.2 of Chapter 4). In the case of a T-beam, there is a very large area capable of carrying compression (the entire tributary slab is able to carry compressive forces), and thus the failure mode seen in this case is yielding of the steel followed by debonding of the FRP. Since the concrete is not at its ultimate stress when the FRP debonds, the common stress block factors do not accurately predict the force carried in the concrete. Therefore, stress block factors based on the strain in the extreme concrete fiber from Collins and Mitchell (1991), which assume a parabolic stress distribution, were used to estimate the force in the concrete.

These examples make use of the proposed design format of Chapter 3 with one factor, ψ, that acts only on the FRP contribution to resistance and one, ϕ, that acts on the total resistance. The factored moment equation takes the form shown in Eq. C-1, where A_s is the area of steel, f_y is the yield strength of the steel, d is the depth from the compression face to the steel, a is the depth of the assumed rectangular stress block, A_{FRP} is the area of FRP, f_{FRP} is the stress in the FRP at the debonding strain limit, and h is the total depth of the section.

$$\phi M_n = \phi(A_s f_y (d - \tfrac{a}{2}) + \psi A_{FRP} f_{FRP} (h - \tfrac{a}{2}))$$

<div align="right">Eq. C-1</div>

In these examples ϕ is given the existing value of 0.9 for flexure (AASHTO, 1998) and ψ is the factor that is calibrated to reach the target reliability. ψ was generally allowed to range from 0.95-0.50 in increments of 0.05. A different required area of FRP was computed for each value of ψ. The strengthening was designed to meet the appropriate factored load. Selection of this load is discussed in detail in Section C.5.

The required amount of FRP to meet the factored load demand was determined with a much higher degree of accuracy than would be used in actual design. Both the number of layers and the width of the fabric were changed. The fabric width was selected to the nearest 6.35 mm (0.25 in) and allowed to reach the full width of the T-girder. This approach was taken to be very accurate in determining the required resistance factor. During actual design, conservatism will be added by using fabrics in commonly available widths.

C.4 Composite Material Properties for Calibration

In general, the different sample calibrations described below all use slightly different values to represent the composite properties. However, the sense in which these values describe the composite properties is the same for all cases. For all cases a constant value is selected to represent the thickness of a single composite layer. Derivation of the Application

factors in Chapter 3 considered the likely degree of compaction between layers, and thus compaction is not considered in determining the design thickness.

The values chosen to represent the FRP strength and modulus are assumed to represent the property values for use in design (i.e. the Application factors have already been applied). It should be remembered from Chapter 3 that the Application factors are not calibrated using reliability methods, but are derived outside of the reliability framework. Thus, they do not need to be explicitly considered at the calibration stage. The intent of this approach is to allow new data regarding the systematic deviation of composites to be easily incorporated without the need for recalibration. The derived Application factors may not perfectly represent the relation between assumed and field properties for all cases. This fact may be considered at a later stage by adjusting the COV of the FRP properties to include the increased variation caused by the use of Application factors.

The properties given in the examples that follow are used for strengthening schemes over a range of thicknesses without considering reductions that would occur due to the addition of layers. This approach is used because the properties are meant to be representative of a range of possible values, not of a single material. The ranges used were considered appropriate for composites of one, two, and three layers. Leaving the reduction factors out at the calibration stage will not have a significant impact on the calibrated factors because the goal of the design value derived in Chapter 3 is to use the anticipated mean field value in design. Thus the value used for design is the same as the mean of the distribution used for reliability analysis. To consider the reduction in properties due to additional layers in calibration would therefore require that the reduction in values be applied to both the design value and the mean used for reliability analysis. As long as the relation between the design value and the mean used for reliability evaluation is consistent, i.e. as long as a change to one

286

affects the other in the same way, the effect of possible reduction factors on reliability may be neglected. For this particular work the design value and the mean are meant to be equal to each other, and this equality must be maintained.   The plan for the final calibration is to use a range of different material values that correspond to the mean of properties found in the field. Once the code is calibrated over this range, any values for the composite properties in the field (found for design purposes by using factors) within this range will be acceptable.

C.5 Load Factors for Use in Strengthening Design

A primary goal of this work is to develop a design procedure for strengthening that is consistent with existing design procedures for new construction, which are provided by the *AASHTO LRFD Bridge Design Specifications* (AASHTO, 1998) for the specific example in question. At early stages of this project it was felt that this interest would be best served by using the same load factors as those used for new construction. As examples were considered to evaluate the impact of specific variables (such as the FRP properties or the amount of remaining steel) on the reliability of designs and the resulting design factors, it became apparent that designing to the factored loads prescribed by the *AASHTO LRFD Bridge Design Specifications* (AASHTO, 1998) for the Strength I limit state resulted in reliabilities much higher than the projected target level. The reliability was often in the range of 4 to 5, whereas the projected target level was approximately 2.5 to 3.5. Initially it was feared that significant errors existed in the models used for load or resistance.   Upon closer examination of the calibration report (Nowak, 1999), it was found that for reinforced concrete girders, a live load factor of 1.7 and resistance factor of 0.9 produced designs with a reliability index near 3.9. Furthermore, the live load factor actually specified by AASHTO is 1.75.   So while small errors surely exist in the load and resistance models developed herein, the conclusion was

287

reached that the primary source of such high reliabilities was the overly conservative live load factor used for new design.

In an effort to use a less conservative live load factor, while still tying the proposed code to AASHTO Specifications, the load factors presented in the *Manual for Condition Evaluation and Load and Resistance Factor Rating (LRFR) of Highway Bridges* (AASHTO, 2003) were investigated in a simple example. The live load factor in this manual is lower than that in the LRFD specification because it was calibrated to a target reliability of 2.5 rather than the 3.5 used for LRFD.

In this example the girder described in Section C.2 was assumed to have 20% steel loss and designs were created following Section C.3 to return the sample girder to the capacity demands of both LRFD and LRFR factored loads. ϕ was held constant at 0.9, while ψ was allowed to vary from 0.95 to 0.4. To ensure a certain degree of generality in the results, three different materials were considered, with mean properties as shown in Table C-4.

Table C-4 Mean Property Values of Sample Composites

Material	Strength MPa (ksi)	Modulus GPa (ksi)	Thickness per Layer mm (in)
1	620.5 (90)	51.7 (7500)	1.016 (0.04)
2	827.4 (120)	68.9 (10000)	1.016 (0.04)
3	1034.2 (150)	86.2 (12500)	1.016 (0.04)

The reliability index of the designs was computed using Monte Carlo Simulation. A detailed description of this process is provided in Section E.1 of Appendix E. Three million trials were used to compute the probability of failure of each design. Following the distributions fit in Chapter 3, the strength of the composite was modeled with a Weibull distribution, while the composite modulus and thickness were modeled as Lognormal

variables. Representative values of variation were selected based on the wet layup tests described in Chapter 3. The strength COV was allowed to range from 0.05 to 0.20. The COVs of the composite modulus and thickness were assumed to be 0.15 and 0.05, respectively. The steel yield strength and concrete compressive strength were also modeled as random variables. All other design variables were considered deterministic. The load components were all modeled as Normally distributed following the models described in Section 2.6 of Chapter 2.

Figure C-1 shows the resulting reliability indices for strengthening designs created with Material 1 and evaluated for different levels of strength variation. The reliabilities of the designs created to meet the LRFD loads are substantially higher than those to meet the LRFR loads. (In fact, for lower values of ψ there were cases where the LRFD designs showed no failed trials, preventing the calculation of the reliability index.) The results for Materials 2 and 3 were virtually identical to these results. The similarity between materials is a common result throughout these calibration examples.
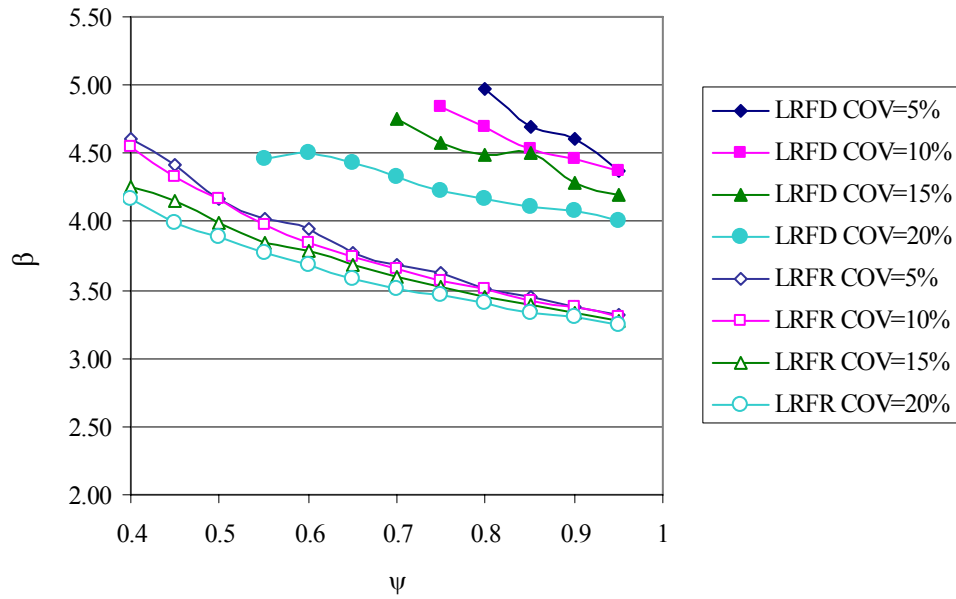
Figure C-1 β vs. ψ for Material 1 Designs to Meet LRFD and LRFR Loads

The reliabilities of the LRFR designs are much closer to the target range, particularly for the range of ψ values that would likely be accepted by the design community, (i.e. values less than 1). Therefore, the LRFR load factors are used for the remaining example cases and are selected for the full sample calibration of Chapter 4. The Strength I load factors used in calibration for this work are shown in Table 4-1 of Chapter 4. Entirely new load factors could have been calibrated, but these factors were chosen to provide some consistency with existing design practice.

C.6 Large Example Calibration without Corrosion

As work progressed, a relatively large sample calibration was undertaken to investigate several different issues:

- What is the effect of different approaches to calculating the reliability index?

- Can this design procedure be applied to a range of FRP properties?

- How does the amount of remaining steel affect the reliability?

- How can time-dependent reliability be assessed with the distributions in Nowak (1999)?

- How do changes in the COV of FRP strength and modulus affect the calibrated resistance factor?

This example did consider degradation of the composite, but not continuing degradation of the structure.

C.6.1   Description of Procedures and Variables

C.6.1.1   Degraded Structure

The girder was assumed to require repair due to a loss in reinforcement. Previous test cases with simple beams (see Figure 3-2 in Chapter 3) have shown that the reliability of members reinforced with externally bonded FRP depends on the percentage of load carried by the FRP. Designs with increased load sharing between the FRP and steel are generally found to be more reliable than designs where one of these two materials is dominant. To more formally investigate this phenomenon, initially 10, 20, and 30 percent loss in the tension steel were to be considered in this example. However, due to the less demanding live load factor in the AASHTO LRFR evaluation manual (AASHTO, 2003), the girder with 10 percent steel loss was found to have adequate capacity without the application of FRP.

C.6.1.2   FRP Properties

One goal of this example was to see how the proposed design procedure would work for different composite materials, requiring a range of different properties. Six sample materials were used to provide this range. The properties of these materials are shown in

Table C-5 and were used in the sense described in Section C.4. It should be noted that the properties of Materials 1, 2, and 3 used in this example are not the same as those used in the previous example. The values for strength were chosen to be representative of the range seen in wet layup CFRP in the testing described in Chapter 3. Materials 1-3 were used to show the effect of constant rupture strain but varying modulus. Materials 4-6 were used to show the effect of constant modulus but changing rupture strain. The thickness for a single layer was set at 1.01 mm (0.04 in).

Table C-5 Mean Property Values of Sample Composites

Material	Strength MPa (ksi)	Modulus GPa (ksi)	Rupture Strain
1	620.5 (90)	47.7 (6923)	0.013
2	827.4 (120)	63.6 (9230)	0.013
3	1034.2 (150)	79.6 (11538)	0.013
4	620.5 (90)	62.1 (9000)	0.010
5	827.4 (120)	62.1 (9000)	0.0133
6	1034.2 (150)	62.1 (9000)	0.0167

C.6.1.3   Degraded Properties

Only degradation of the FRP was included in this example. Degradation of the FRP was considered for 5 and 50 years in service. These time periods were used because load information for these specific time frames is provided in *NCHRP Report 368* (Nowak, 1999). (This example was conducted before the issues with live load modeling described in Appendix A had been fully explored). Degradation of both the strength and modulus was calculated using models for percent retention of composite properties based on the Arrhenius rate relation found by Abanilla (2004), which was described in Section 3.6.2.1 of Chapter 3. In this example degradation was considered at the design stage by using the degraded mean value as the design value, following the procedure proposed in Chapter 3. The percent retention of

properties computed for the two different time frames are shown in Table C-6. The modulus test results used by Abanilla to derive these models did not show degradation, but rather post-curing effects, and thus the model calculated retention values slightly higher than 100%.

Table C-6 Percent Retention of FRP Properties for Different Design Lives

	Strength	Modulus
5 years	80.79	102.93
50 years	73.04	101.96

C.6.1.4 Designs

Strengthening designs were created for both 20 and 30 percent steel loss, using all six of the sample materials shown in Table C-5. Furthermore, for each material three different design values for the FRP were used, representing no degradation and degradation after five and fifty years. A design was created for each combination of the resistance factors. ϕ was held constant at 0.9 and ψ was allowed to vary from 0.95 to 0.5. ψ was not allowed to range all the way down to 0.4 as seen in the previous example because, as shown in Figure C-1, the reliability indices for LRFR designs with $\psi < 0.5$ were close to 4.0 and thus much higher than the range of desired reliability targets.

C.6.1.5 Reliability Analysis

The reliability of each of the designs was evaluated using two slightly different methods. The first method was straight Monte Carlo Simulation. The limit state considered is shown in Eq. C-2, where M_R is the moment capacity of the girder, M_{DC} is the moment due to the cast-in-place dead load, M_{DW} is the moment due to the wearing surface, and M_{LL} is the live load moment including impact.

$$g = M_R - M_{DC} - M_{DW} - M_{LL}$$

Eq. C-2

Random values of the design variables were generated following the distributions described in Section C.6.1.8 and used in the sectional analysis procedure described in Section C.3 and Appendix D to predict the resistance of the strengthened girder. Random values for the three load components were generated following the distributions in Section C.6.1.7. The probability of failure was estimated as the number of limit state violations divided by the total number of simulations (3,500,000 simulations were run for each case). An approximate value of β was then calculated from Eq. C-3.

$$\beta = -\Phi^{-1}(p_f)$$ **Eq. C-3**

The second approach for calculating the reliability index was a hybrid approach, which used of the mean and standard deviation of member resistance found through Monte Carlo Simulation in the FORM method outlined in *NCHRP Report 368* (Nowak, 1999), and described in Section E.3 of Appendix E. This method assumes that the resistance follows a lognormal distribution and the loads follow normal distributions. These two different methods were used so that their results could be compared before selecting a procedure for the final calibration example. A brief comparison of the techniques is shown in Table C-7.

Table C-7 Comparison of Two Different Reliability Procedures

	Monte Carlo Only	Monte Carlo with FORM
Description of Resistance	Defined in terms of the distributions of variables contributing to resistance No distribution is fit to the resistance	Mean and standard deviation are found based on the distributions of contributing variables Lognormal distribution is fit to Resistance
Description of Load	Random values generated from distributions of three components of load	Distributions of three load components are summed into one Normal distribution for load (the resulting distribution should be exact because it is a linear combination of Normally distributed variables)
How is p_f calculated?	$p_f \cong \dfrac{\# \, of \, failures}{total \; simulations}$	β calculated with FORM $p_f \cong \Phi(-\beta)$

C.6.1.6   Time-Dependent Reliability

One goal of this sample calibration was to try out the loads provided for different time frames in the calibration report (Nowak, 1999) and assess how they worked with the time-integrated approach for computing time-dependent reliability.   For this example three different cases were considered. The reliability with undegraded properties was evaluated at the 75-year loads. This corresponds to the method used in AASHTO LRFD where the initial properties are compared to the lifetime maximum load. Additionally, the reliability of the five year degraded structure was evaluated against the distribution of the five-year maximum load; and the structure after 50 years in service was evaluated at the 50-year maximum load. Degradation of the FRP was included at the design stage, so these examples were not necessarily intended to show a decrease in reliability as the age of the structure increased, but rather to assess the effect of using load distributions referenced to different time spans.

C.6.1.7   Load Variables

Two components of dead load were considered: the cast-in place construction component and the wearing surface component. Bias factors, COVs, and assumed statistical

distributions from *NCHRP Report 368* were used to model these load components (Nowak, 1999). Table C-8 describes the statistics of dead load used for this analysis.

Table C-8 Statistical Description of Dead Loads

Load Component	Nominal Value	Distribution Type	Bias Factor	COV	Mean Value	Standard Deviation
Cast-in-place	408.76 kN-m (301.67 k-ft)	Normal	1.05	0.10	429.20 kN-m (316.75 k-ft)	42.9 kN-m (31.675 k-ft)
Wearing Surface	76 mm (3 in) thickness 76 kN-m (56 k-ft)	Normal	NA	0.25	89 mm (3.5 in) thickness 88.52 kN-m (65.33 k-ft)	22.1 kN-m (16.33 k-ft)

The live load statistics were also developed using bias factors and COVs from *NCHRP Report 368*. The bias factor between the LRFD load model (HL-93) and the mean maximum live load effect depends to some extent on the span. The bias factors for a span of 12.19 m (40 feet) for the different time periods considered are shown in Table C-9. The bias factor is applied only to the static portion of the live load (before the impact factor is included). An additional factor of 1.1 is used to account for the dynamic load. The COV for the combined live and impact loads is also shown in Table C-9. (These values are in part based on reading off of a graph, so their accuracy is somewhat questionable.) The mean and standard deviation of live plus impact load for each time span are in the final two columns of Table C-9.

Table C-9 Live Load Statistics for Different Design Lives

	Bias Factor	COV	Mean kN-m (kip-ft)	Standard Deviation kN-m (kip-ft)
75 years	1.35	0.165	847.85 (625.72)	139.73 (103.119)
50 years	1.35	0.165	847.85 (625.72)	139.73 (103.119)
5 years	1.28	0.171	803.88 (593.27)	137.10 (101.183)

For the reliability analysis using just MCS, the three different components of load were each randomly generated from their own distribution. For the hybrid analysis, simple combination rules for adding normal distributions (shown in Eq. C-4 and Eq. C-5 for the mean

and variance, respectively) were used to derive the statistics shown in Table C-10 for the total load. This combined distribution was used in the FORM analysis.

$$\mu_Q = \mu_{cast-in-place} + \mu_{wearing} + \mu_{live+impact}$$ <div style="text-align: right">**Eq. C-4**</div>

$$\sigma_Q^2 = \sigma_{cast-in-place}^2 + \sigma_{wearing}^2 + \sigma_{live+impact}^2$$ <div style="text-align: right">**Eq. C-5**</div>

Table C-10 Statistics of Total Load

	Mean kN-m (kip-ft)	Standard Deviation kN-m (kip-ft)
75 years	1365.58 (1007.806)	147.84 (109.1037)
50 years	1364.58 (1007.806)	147.84 (109.1037)
5 years	1321.61 (975.361)	145.36 (107.2762)

C.6.1.8   Resistance Variables

The variation in resistance was accounted for by considering the material properties as random variables.   The error due to modeling assumptions (the difference between the modeled strength and the actual strength) was neglected. At this stage, all dimensions were modeled as deterministic. The concrete and reinforcing steel strengths were both modeled based on the work of Mirza and MacGregor (1976). The concrete was modeled with a normal distribution with a mean of 30.85 MPa (4475 psi) and a standard deviation of 4.63 MPa (671.25 psi).   The steel was modeled using a beta distribution derived by Mirza and MacGregor. The PDF was shown in Chapter 2 and is repeated here in Eq. C-6.

$$pdf(f_y) = 7.1562 \left(\frac{f_y - 57}{51} \right)^{2.0204} \left(\frac{108 - f_y}{51} \right)^{6.9545}$$
$$(57 \le f_y \le 108 \ ksi)$$ <div style="text-align: right">**Eq. C-6**</div>

The FRP strength was modeled as a Weibull random variable. The reliability was evaluated for strength COVs of 0.5, 0.10, 0.15, 0.20, and 0.25. The modulus was modeled as a lognormal random variable. The reliability was evaluated for modulus COVs of 0.5, 0.10, 0.15, 0.20, and 0.25. This range of COVs for strength and modulus was selected based on the material property tests described in Section 3.3 of Chapter 3, and was used to assess the effect of different levels of variability in material properties on the reliability of designs. The thickness was modeled as a lognormal variable with a mean of 1.016 mm (0.04 in) and COV of 0.05. For all cases the distribution was fit using the method of moments, where the distribution parameters are calculated based on known values of the mean and variance.

C.6.2 Results of Sample Calibration without Corrosion

The results from this sample exercise allowed conclusions to be made on a range of issues affecting calibration. In order to compare calibrated resistance factors, the target reliability for this example was set at 3.5, which is the value used in the *AASHTO LRFD Bridge Design Specifications* (AASHTO, 1998).

C.6.2.1   Effect of Reliability Calculation Method

Given a limit state model and descriptions of the statistical variation in design variables, calculation of reliability through a strict Monte Carlo procedure is the most accurate method, but it is also very time consuming. Therefore, use of a hybrid approach, which uses FORM to compute the reliability from the simulated statistics of resistance and substantially lowers the required computing time, was considered. The hybrid method corresponds to the procedure described in *NCHRP Report 368* (Nowak, 1999). Thus, in addition to saving computer time, use of the hybrid method would also provide another link between the design procedures for new design and strengthening design. This example allowed for comparison of these two reliability techniques before a method was selected for the final calibration.

Noticeable differences between the results of the two different reliability methods were observed. In general, as the COV of strength increased, more difference between different materials was seen. The difference between materials was generally much greater for the case of strict Monte Carlo. In the hybrid results the curves for different materials were often very tightly packed. However, it also appeared that the hybrid results were often slightly conservative as compared to the Monte Carlo results.

An example comparison is shown in Figure C-2 (Monte Carlo) and Figure C-3 (hybrid) below. For the case of 20% steel loss and no FRP degradation the hybrid results shown in Figure C-3 are clearly conservative because they require a smaller value for the resistance factor. In this case the hybrid results do not really show differences between different materials. A similar pattern holds for the results at 5 and 50-year design lives for a steel loss of 20%, although the conservatism is not as clear at 50 years.
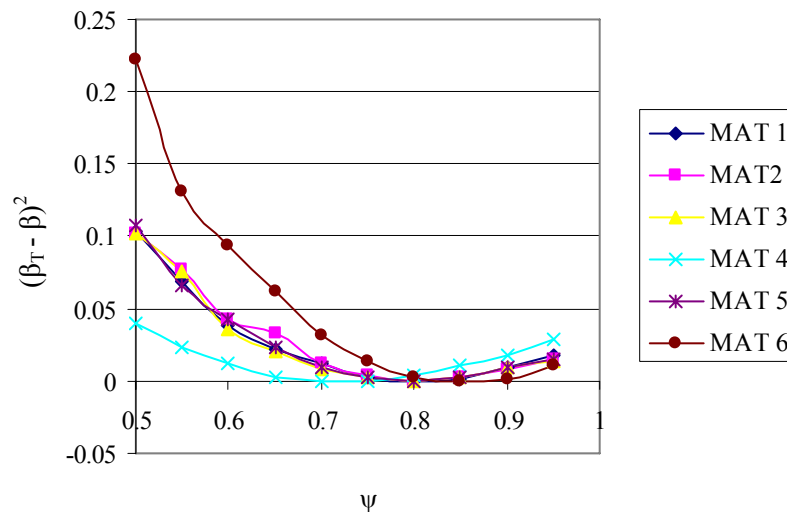
Figure C-2 Monte Carlo Results for 20% Steel Loss, Strength COV = 0.25, Modulus COV =0.05, 0 degradation, 75 year loads
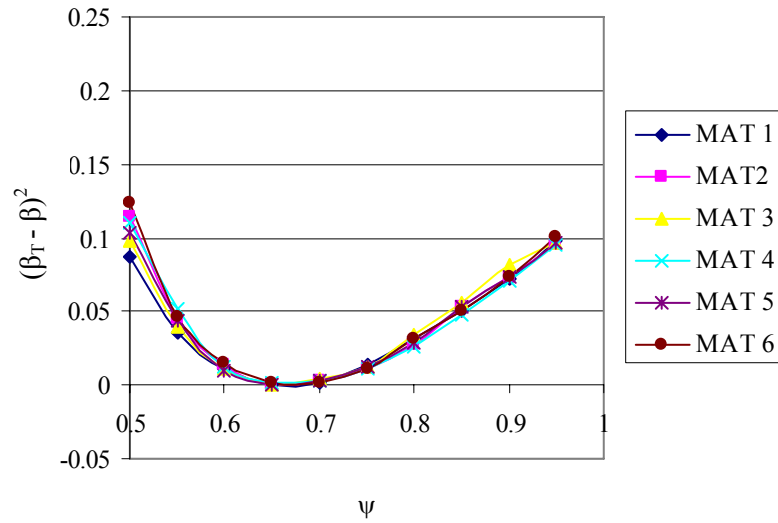
Figure C-3 Hybrid Results for 20% Steel Loss, Strength COV = 0.25, Modulus COV = 0.05, 0 degradation, 75 year loads

For the cases with 30% steel loss, the hybrid results do not show conservatism. Figure C-4 (Monte Carlo) and Figure C-5 (hybrid) show the same conditions as above except the steel loss is set at 30%. In this case the Monte Carlo results are much less smooth, and the hybrid results are not strictly conservative. At the 5 and 50 year time periods the hybrid results are slightly unconservative. However, for all cases with 30% steel loss the hybrid results do show some of the differences between materials and are in the general range of the Monte Carlo results. It makes sense that at the level of 30% steel loss there is a much greater difference between materials because more of the load is carried by the FRP, and thus there is more opportunity for the differences to assert themselves.
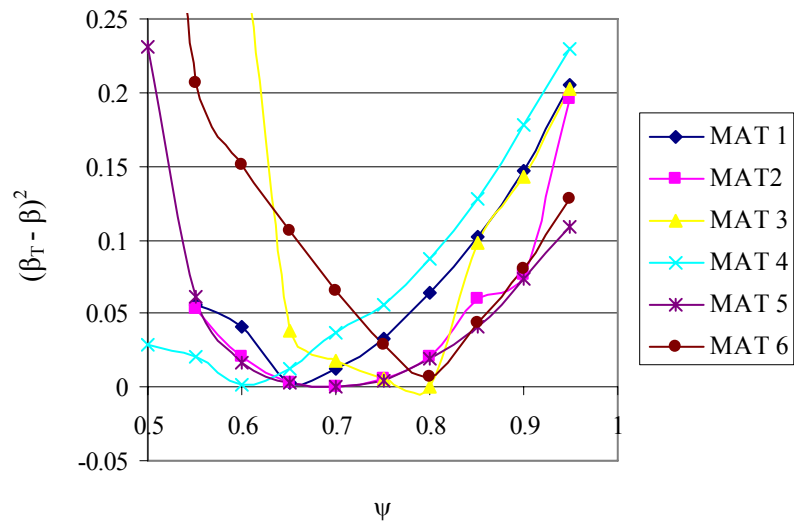
Figure C-4 Monte Carlo Results for 30% Steel Loss, Strength COV = 0.25, Modulus COV = 0.05, 0 degradation, 75 year loads
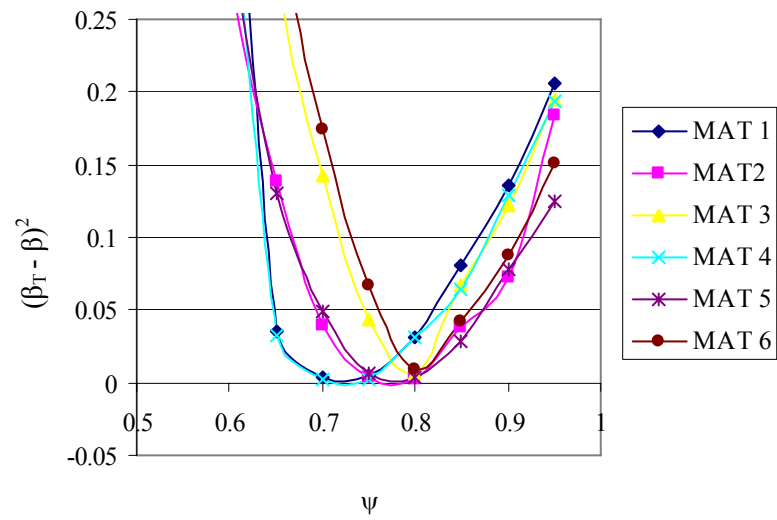
Figure C-5 Hybrid Results for 30% Steel Loss, Strength COV = 0.25, Modulus COV = 0.05, 0 degradation, 75 year loads

Based on these results the hybrid approach appears to be a reasonable and much faster substitute for the more rigorous Monte Carlo Simulation. While some accuracy will be lost, the faster reliability method will allow many more cases to be considered. Given the preliminary nature of this work, the ability to investigate more cases and hopefully identify more reliability trends is considered to be much more important than the absolute accuracy of the reliability calculations. This is especially true when the limitations of the statistical descriptions for design variables are also considered.

C.6.2.2   Effect of Different Amounts of Steel Loss

As stated earlier, one objective of this example was to consider the effect of different amounts of steel loss on the reliability of strengthened sections. When the discrepancy between reliabilities of beams with different amounts of remaining steel was first witnessed (see Section 3.4.1.1) traditional methods of defining the design value had been used and large differences in reliability were seen. This example makes use of the proposed design value, which uses the mean as the characteristic value. This choice of characteristic value was made in part in an attempt to limit the change in reliability as the percentage of steel loss is increased. This example therefore gives an indication of how the new design value works with different amounts of remaining steel.

Figure C-3 shows the hybrid results for 20% steel loss with zero degradation of the composite and Figure C-5 shows results for this same situation except the girder had 30% steel loss. Clearly, in the case of 20% steel loss a lower value of the resistance factor, ψ, is required than for 30% steel loss. This implies that for a given value of the resistance factor the designs for 30% steel loss are more reliable. Cases with 50 years of assumed degradation, evaluated with the 50-year loads also showed this behavior based on hybrid results. The five-

year cases did not show much of a difference between the two levels of steel loss. The less demanding loads for five-year evaluation may not have been large enough to differentiate between 20% and 30% steel loss. The Monte Carlo results generally show that the 20% steel loss cases are more reliable than the 30% loss cases; however the increased spread in the 30% loss cases makes it difficult to compare.

The two different reliability methods both show that there is a difference in reliability between the two different amounts of steel loss. However, they differ on which girder is more reliable. Although they are more approximate, the hybrid results show better agreement with what could theoretically be expected based on the presence of more than one load path and with trends seen in other work studying the reliability of strengthened sections (Okiel et al, 2002). Furthermore, in the previous section the hybrid method was selected as the reliability technique for use in this work in part to provide compatibility with the techniques used by Nowak (1999) in calibration of the LRFD code. Thus, the effect of the amount of steel loss will be assessed based on the hybrid results.

Even with the newly proposed design value, differences exist in the reliabilities of girders with different amounts of steel loss. Due to the nature of reinforced concrete, knowing the exact amount of steel present in a beam after some steel loss has occurred is virtually impossible. This makes it somewhat impractical to base design factors on the amount of remaining steel. However, the change in reliability between girders with different amounts of steel may be substantial, and completely neglecting this effect could be overly conservative. Therefore, the final calibration example will provide design factors referenced to different levels of steel loss in an effort to be as complete as possible. If this work is adapted into a formal code document, the code agency will have the option of defining different factors for approximate ranges of steel loss or could conservatively choose those factors calibrated to

lower levels of steel loss. The more conservative designs for higher levels of steel loss that would result from this approach may be beneficial. Designs with a greater percentage of steel loss will have a lower reserve capacity should anything happen to the FRP; it might, therefore, be a good idea to allow slightly higher reliabilities in designs more dependent on the FRP contribution.

C.6.2.3   Effect of Time Span for Evaluation

Three different time spans were considered in this example; however the load statistics available for 75 and 50 years were identical. For simplicity, the target reliability index was set equal to 3.5 for all time periods in question. This constant target is somewhat misleading. It implies that all members have the same probability of failure during the reference lifetime; i.e. the member evaluated for five-year loads has a 0.000233 chance of failure in five years and the member evaluated for 50-year loads has a probability of failure of 0.000233 in 50 years. Clearly, the member evaluated for five years has a much higher annual probability of failure. This demonstrates one of the many considerations that must go into the selection of the target reliability index.

Figure C-6, Figure C-7, and Figure C-8 show results for no degradation and 75-year loading, five-year exposure and five-year loading, and 50-year exposure and 50-year loading, respectively. The results in Figure C-6 and Figure C-8 are nearly identical. This occurs because the degradation of FRP properties was included at the design stage for the case with 50-year exposure, allowing the change in properties to influence the design, and the same load statistics were used to evaluate both cases. This result suggests that the proposed design value, in which potential degradation is included at the design stage, is able to achieve a uniform reliability when the same loads are used for reliability evaluation. This would imply that degradation does not need to be explicitly considered in the calibration stage; confirming

304

the idea that it is only necessary to select a range of FRP properties for calibration, keeping

degradation in mind so as to calibrate over an appropriate range of properties.
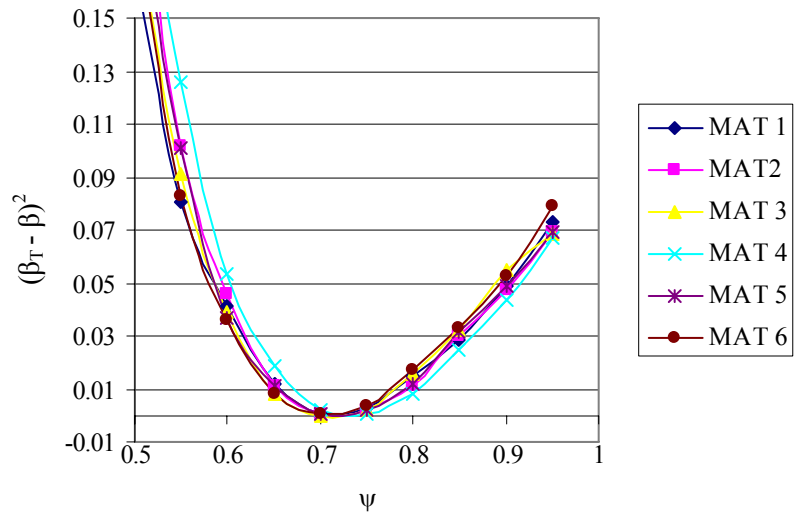
Figure C-6 Hybrid Results for 20% Steel Loss, Strength COV = 0.15, Modulus COV = 0.15, no degradation, 75 year loads
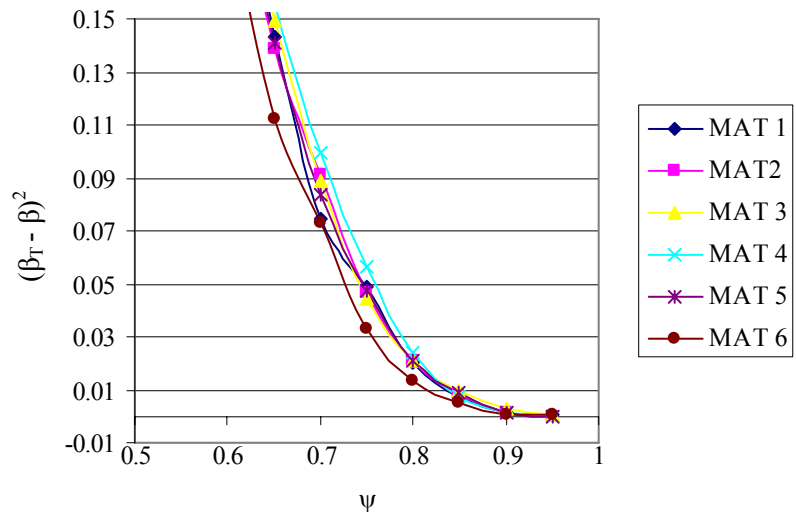
Figure C-7 Hybrid Results for 20% Steel Loss, Strength COV = 0.15, Modulus COV = 0.15, 5-year exposure, 5 year loads
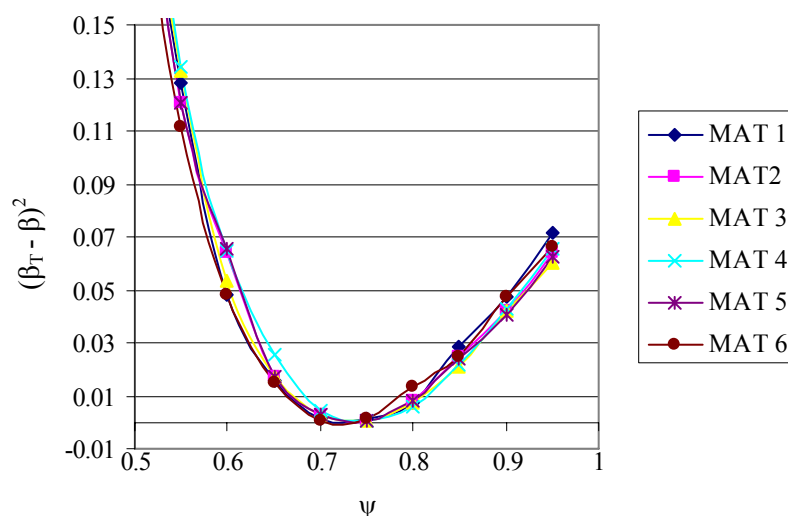
Figure C-8 Hybrid Results for 20% Steel Loss, Strength COV = 0.15, Modulus COV = 0.15, 50-year exposure, 50 year loads

The designs created for five years of exposure and evaluated with the five-year maximum loading (shown in Figure C-7) have a much higher calibrated resistance factor than the designs for 50 and 75 years. This occurs because all three cases are being compared at the same reliability index without considering the differing reference time. The annual probability of failure for $\beta = 3.5$ and a reference time of 75 years is approximately 3.107×10^{-6} (this assumes that the probability of failure in a given year is independent of the probability of failure in other years, a reasonable assumption if the extreme loading is assumed independent from year to year). For a five-year reference period, the β corresponding to this annual probability of failure is approximately 4.16. Figure C-9 shows results for the 5-year case if the target reliability is set at 4.16. This analysis was expected to lower the resistance factor, but not to the full extent shown. It was thought that by using the adjusted reliability target a resistance factor more consistent with those calibrated for no degradation and 50 years of exposure would be found.   However, this much smaller factor served as a first indication that

there may be some inconsistencies in the load distributions derived by Nowak (1999) for different periods of load exposure as discussed in Section 2.6.2 and Appendix A. It also brings to light the complicated interaction between the factors for load and resistance and the target reliability. If, for example, it was decided that the same resistance factors should be used for the FRP regardless of the design life, the calibration process would require careful selection of the reliability target for different design lives and/or load factors that depend on the design life.

Figure C-9 Hybrid Results for 20% Steel Loss, Strength COV = 0.15, Modulus COV = 0.15, 5-year exposure, 5 year loads

The original intent of this work was to use distributions of maximum load that were representative of the anticipated service life in order to prevent excessive conservatism in creating strengthening designs that did not need to last as long as designs for new construction. After seeing the results of this sample calibration this idea was put aside for the present work. This decision was made in part because of the limitations and apparent inconsistencies in available load data, as described in Appendix A. It was also made because

selection of the target reliability index is complicated when designs are referenced to different design lives. Current LRFD standards, including the AASHTO standards for bridge design, do not consider degradation of any materials and do not use reliability indices that are dependent on the design life. Thus previous work in this area could not be identified to provide guidance in the selection of time-dependent reliability targets. Therefore, for the present purposes, the choice was made to use one reference time for loads and calibrate all resistance factors to a single value of the reliability index. (Although three different target reliability indices are used, the calibrated resistance factors are compared only to other factors for the same target and no reference is made to the required service life.) This means that all designs will have the same reliability for the time period to which the loads are referenced, and designs intended for shorter lives will have a higher reliability when referenced to that life. Thus the specific time of exposure is only considered in terms of the FRP properties. Though this approach significantly simplifies the matter, it seems justified given the limited data regarding all aspects of time-dependent structural behavior and loading. Suggestions for future improvements, possibly resulting in designs more precisely calibrated to their design life are provided in Chapter 6.

C.6.2.4   Effect of Differences in Mean Value of FRP Properties

It is known that different levels of composite variation will change the reliability; however the effect of different mean property values is also of interest. This effect can be studied by comparing the reliabilities of designs created with different materials but the same COVs for strength and modulus. As the hybrid results shown above demonstrate, for 20% steel loss there is generally good agreement between all materials. The hybrid results for 30% steel loss show more variation between different materials, as seen in Figure C-5. This is particularly true as the COV of strength and to some extent that of modulus increases.

Furthermore, for 30% steel loss, the case with no degradation of properties shows significant variation between materials, while the results for five years (Figure C-10) show less, and those for fifty years (Figure C-11) even less.
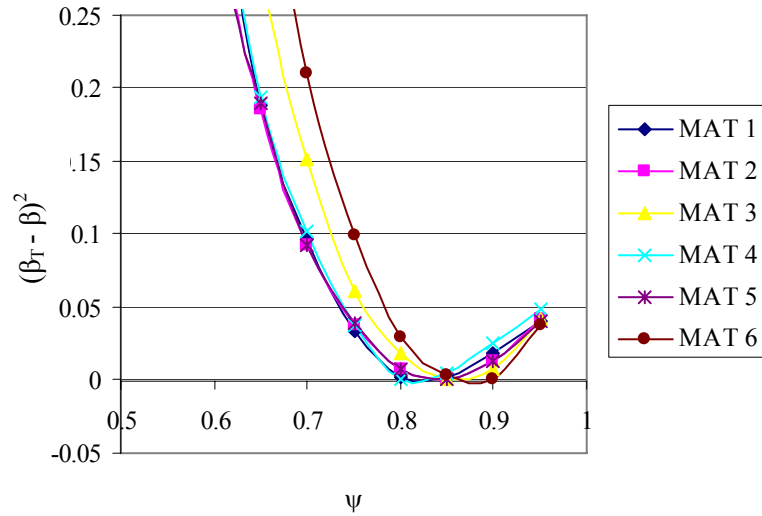
Figure C-10 Hybrid Results for 30% Steel Loss, Strength COV = 0.25, Modulus COV = 0.05, 5-year exposure, 5 year loads
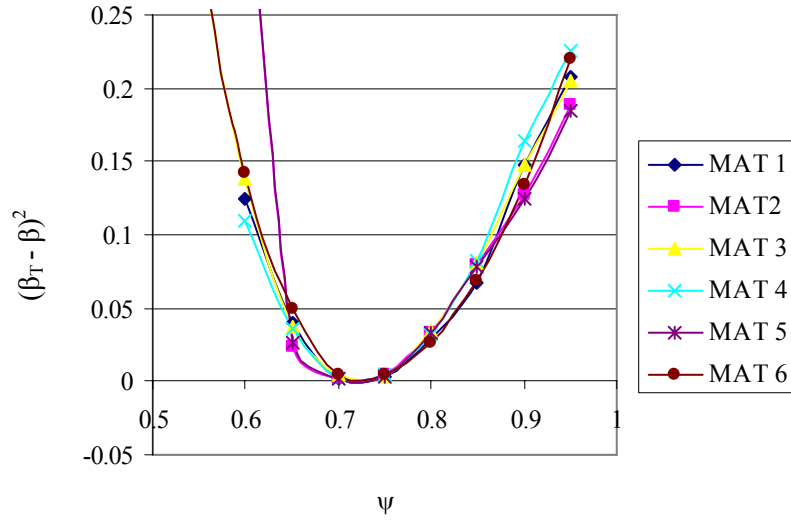
Figure C-11 Hybrid Results for 30% Steel Loss, Strength COV = 0.25, Modulus COV = 0.05, 50-year exposure, 50 year loads

These results seem to be related to how the debonding strain is predicted.   The debonding model in ACI 440 (2002) predicts the debonding strain as the rupture strain of the composite multiplied by κ_m. Eq. C-7 shows how κ_m is calculated. In these equations, ε_{fu} is the ultimate strain of the composite, n is the number of layers, E_f is the modulus of the composite expressed in N/mm^2 and t_f is the thickness of the composite in mm.

$$\kappa_m = \frac{1}{60\varepsilon_{fu}}\left(1 - \frac{nE_f t_f}{360,000}\right) \leq 0.90 \quad \text{for} \quad nE_f t_f \leq 180,000$$

Eq. C-7

$$\kappa_m = \frac{1}{60\varepsilon_{fu}}\left(\frac{90,000}{nE_f t_f}\right) \leq 0.90 \quad \text{for} \quad nE_f t_f > 180,000$$

Clearly, the rupture strain of the composite is an important variable to this debonding model. The percent retention of composite strength and modulus for the different design lives

was shown in Table C-6. The rupture strains calculated from these degraded values are shown in Table C-11.

Table C-11 FRP Rupture Strains at Different Design Lives

Material	No Degradation	5 Years Exposure	50 Years Exposure
1	0.013	0.010	0.009
2	0.013	0.010	0.009
3	0.013	0.010	0.009
4	0.010	0.008	0.007
5	0.013	0.010	0.010
6	0.017	0.013	0.012

Often in this example, the calculated value of κ_m exceeded the limiting value of 0.9, and thus the debonding strain was calculated as 0.9 multiplied by the rupture strain. Table C-11 shows that many of the composites have similar rupture strains, thus when the same debonding criteria, $\kappa_m = 0.9$, is used, the designs produce similar reliabilities. This can explain why some design situations showed great similarities between materials, while other cases did not. Nearly all designs created for 20 percent steel loss used the 0.9 limit on κ_m because these designs only required one layer of FRP, which typically results in large values of κ_m. Even though the designs for 30 percent steel loss were often of multiple layers, the designs for 5 and 50 years still were dominated by cases where $\kappa_m = 0.9$ because these designs had low values of the rupture strain, which also tends to produce high values of κ_m. In contrast, the designs for 30 percent steel loss with no FRP degradation had a great deal of variation in the controlling value of κ_m. Materials 1 and 4 were again controlled by the 0.9 limit, while Materials 2, 3, 5 and 6 were controlled by lower values of κ_m for all cases.

The Monte Carlo results do show more variation between materials for all levels of the COV. It appears that materials with similar rupture strains are often grouped together. This is result that could be anticipated based on analysis of the debonding model just discussed. The case shown in Figure C-2, where materials 1, 2, 3, and 5 are all closely grouped is a typical result for steel loss of 20%. When these groupings are present, for a given value of ψ, Material 6 is usually slightly more reliable, and Material 4 is slightly less reliable. This implies that, for a constant level of COV, FRPs with higher rupture strains produce more reliable designs, an unsurprising conclusion. The 30% steel loss Monte Carlo results resemble the hybrid results with significant spread and with the weaker materials generally being slightly less reliable. Though not as clearly defined as in the case of 20% degradation, material 4 is usually on the less reliable side, and material 6 is usually slightly more reliable.

From these results it can be concluded that differences in composite materials do affect the reliability of designs created with these materials to some extent. However, these differences are generally quite small when the reliability is assessed with the hybrid method. A selection of different materials will again be used in the final calibration example; and slightly more variation in the composite rupture strain will be sought. These results suggest that smaller rupture strains are slightly less reliable, so while using a range of values for calibration is appropriate to prevent an overly conservative design code, it may be a good idea to define a minimum value of rupture strain for designs created with this procedure.

C.6.2.5   Effect of Changes in Modulus Coefficient of Variation

In this example the COV of the modulus was allowed to vary from 0.05 to 0.25 in order to examine the effect that changes in the modulus COV have on the reliability of a design. (The effect due to changes in the strength COV will be examined in Section C.6.2.6.) Figure C-12, Figure C-13, and Figure C-14 show the results for 20% steel loss with five years of

exposure for a strength COV of 0.25 and modulus COV of 0.05, 0.15, and 0.25, respectively. As the modulus COV increases there is some separation between the different materials that occurs, however the value of ψ changes very little. This particular case is representative of the results in general. Therefore, it is recommended to calibrate the resistance factor for just one average value of modulus COV (perhaps 15 or 20%). It must be noted, however, that this conclusion was drawn based on the ACI bond model. The final calibration makes use of another model that is based on fracture mechanics and is described in Section 4.5.2.1 of Chapter 4. This assumption was used for the large calibration example, because the potential impact of the change in bond model was not initially realized. This assumption is tested for the final calibration example, with results shown in Section 4.8.1 of Chapter 4.
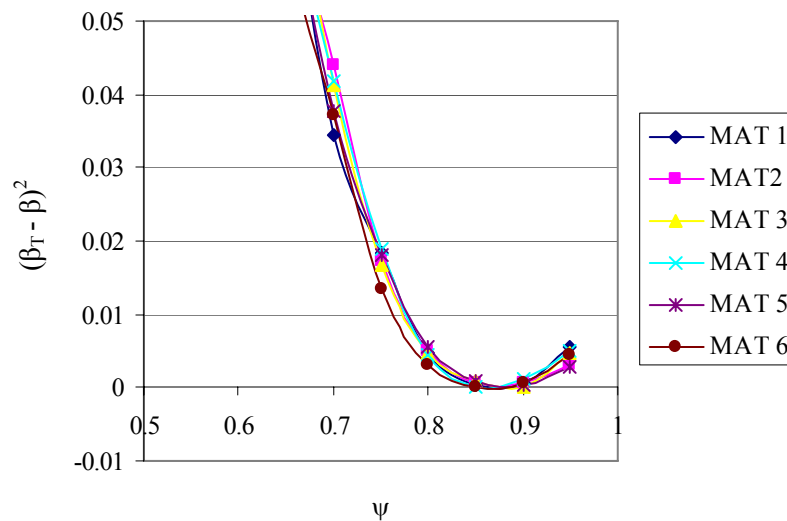
Figure C-12 Hybrid Results for 20% Steel Loss, Strength COV = 0.25, Modulus COV = 0.05, 5-year exposure, 5 year loads
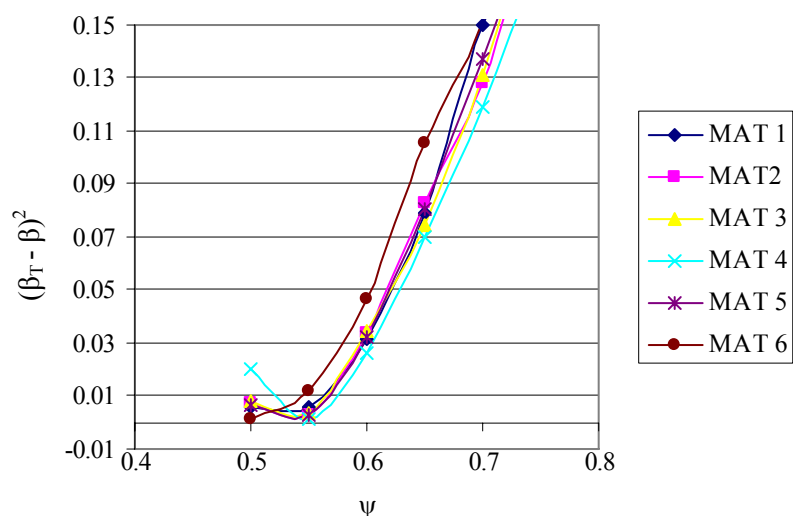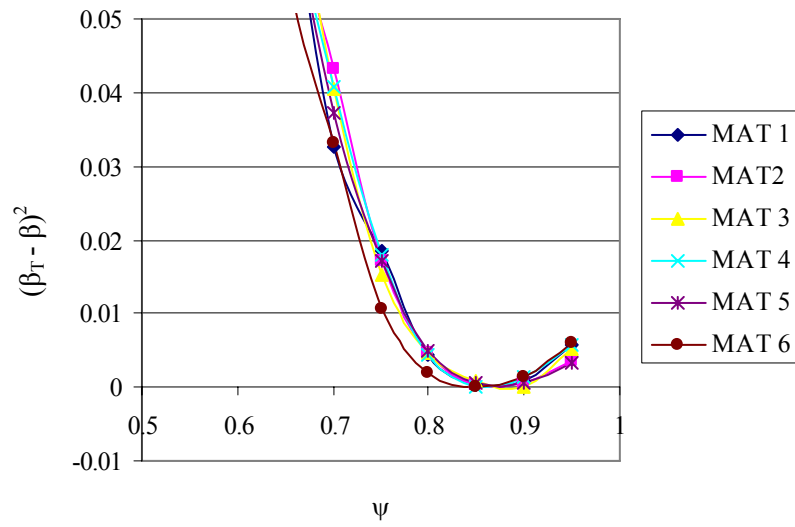
Figure C-13 Hybrid Results for 20% Steel Loss, Strength COV = 0.25, Modulus COV = 0.15, 5-year exposure, 5 year loads
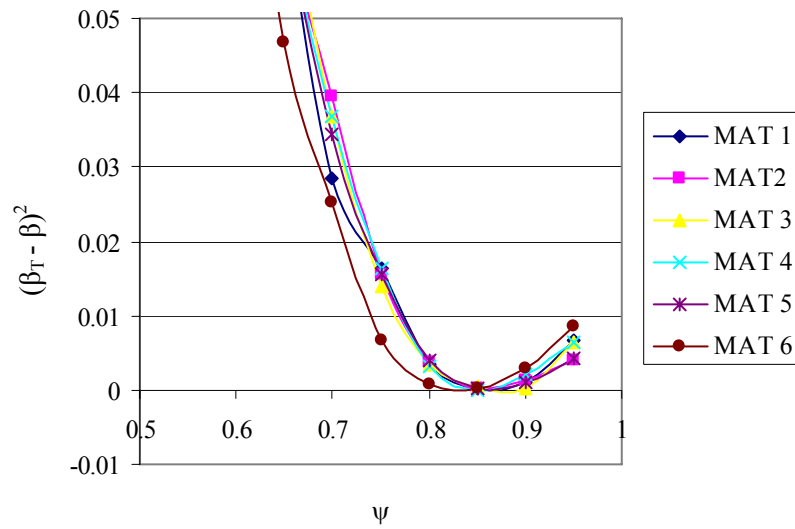
Figure C-14 Hybrid Results for 20% Steel Loss, Strength COV = 0.25, Modulus COV = 0.25, 5-year exposure, 5 year loads

C.6.2.6   Effect of Changes in Strength Coefficient of Variation

Finally, this example sought to confirm the practicality of considering a COV of strength dependent resistance factor. It was indeed found that, for a given design, as the COV of ultimate strength increases the reliability decreases. Thus a smaller value of the resistance factor, ψ, is needed to meet the target reliability. Figure C-15 and Figure C-16 show the relationship between ψ and the COV of composite strength for 20% and 30% loss of steel, respectively. Again, the target reliability index used for factor selection is 3.5. As observed earlier, the required resistance factors are much smaller for the 20% loss. The 5-year factors are clearly very high due to the less demanding 5-year loads. In all cases the relation between ψ and COV is approximately linear (or bi-linear) allowing for a simple function to relate these two variables in the design procedure.
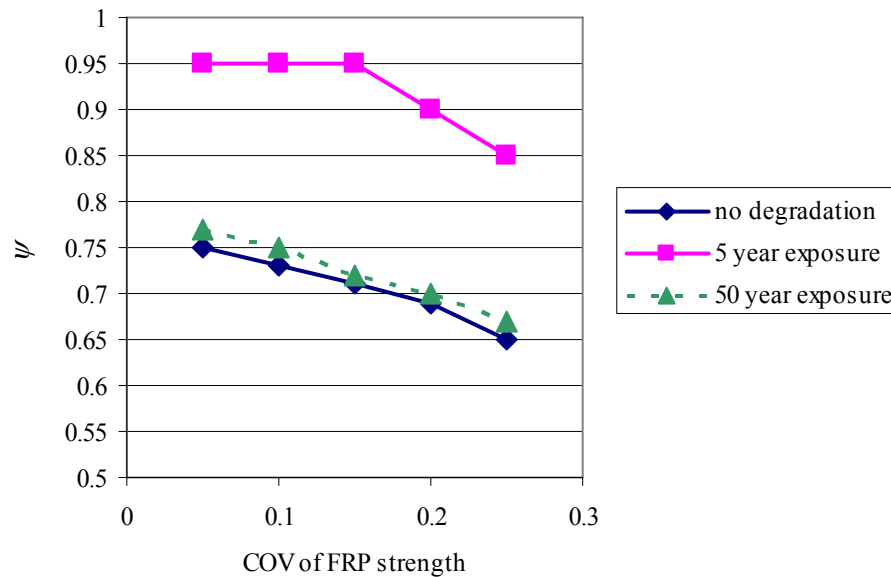
Figure C-15 ψ as a function of Strength COV for 20% Steel Loss and Modulus COV =15%
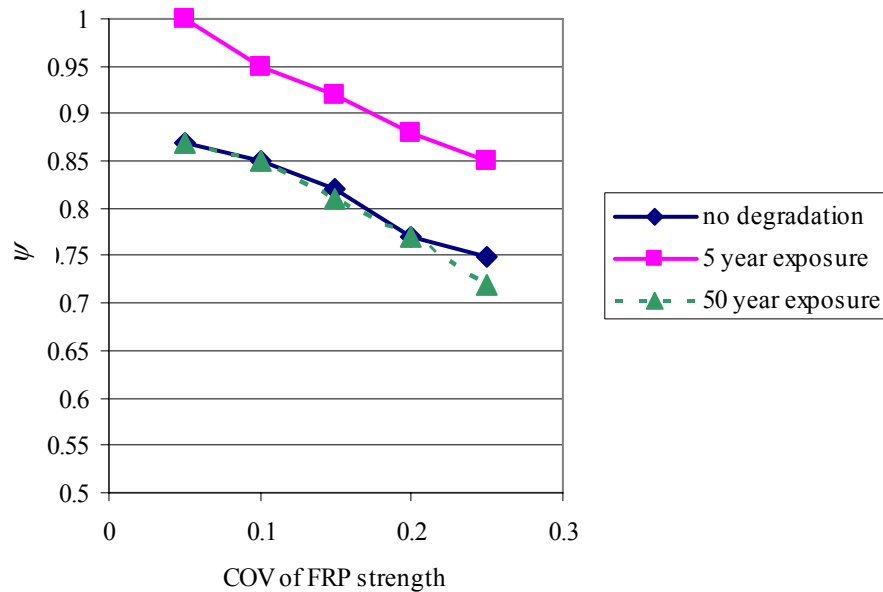
Figure C-16 ψ as a function of Strength COV for 30% Steel Loss and Modulus COV =15%

C.7 Effect of Resistance Variables Considered in Reliability Analysis

Much of the earlier work in this project, including the two previous examples, was conducted considering only the composite properties, steel yield strength, and concrete compressive strength as random variables. Limiting the number of random variables did simplify the computation of reliability to some extent; however it was felt that a small check should be conducted to ensure that the conclusions being drawn from these examples would still be applicable when the reliability was assessed including more random variables.

The previously described sample girder was used for this assessment. Four different cases for reliability analysis were considered. The resistance variables modeled as random variables for each case are listed in Table C-12. The models used for the random variables are described in Chapter 2.

Table C-12 Cases for Assessment of Resistance Variable Effect on Reliability

Analysis Case	Random Variables
1	FRP Strength, Modulus, and Thickness ; Concrete Compressive Strength, Steel Yield Strength
2	Case 1 plus dimensions (depth to steel, width of flange, depth to FRP)
3	Case 1 plus Steel Modulus and Concrete Modulus
4	Case 1 plus dimensions and Modulus of Steel and Concrete

The designs assessed were from the previous large sample calibration. The reliability of designs for Materials 1, 2, and 3 with no material degradation over the range of resistance factors and both levels of steel degradation were computed for all four cases described in Table C-12. It was felt that this range would be sufficient to discern a general trend in the effect of using different random variables in the assessment of reliability.

The resulting reliabilities for the designs with Material 2 are shown in Figure C-17. This graph clearly shows that the reliabilities predicted using Case 2, are significantly lower than those predicted using the other cases. Cases 1 and 3 produce very similar results, with Case 4 reliabilities usually slightly smaller. These same trends were observed for the other materials. These results suggest that fairly accurate reliability assessments can be made using only the FRP properties, the concrete strength, and steel yield strength as random variables. This provides reassurance that the conclusions reached in the previous examples will be valid for more sophisticated reliability analysis. Though this data may justify the use of only select resistance variables in reliability assessment, all variables for which models are available will be used in the final calibration example.
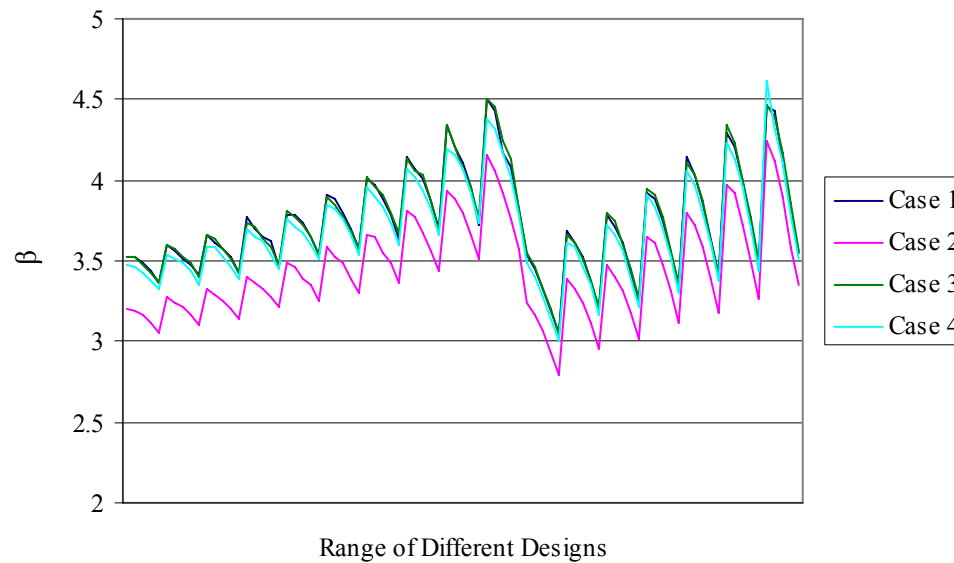
Figure C-17 Effect of Using Different Cases of Random Variables to Assess Reliability for Material 2 Designs

C.8 Example with Corrosion

The final example calibration was conducted to study the effect of including corrosion of the reinforcing steel in the analysis. It was primarily intended to assess the philosophy chosen for design. Additionally, the models selected to predict the effect of corrosion on the area of steel were tested and time-dependent reliabilities were again assessed.

C.8.1 Design Philosophy

The philosophy chosen for design is to predict the amount of steel remaining at the end of the desired service life and design the FRP strengthening (considering degraded properties) to meet the factored loads given this amount of steel. The prediction of the remaining steel area will be made based on an assumption of general corrosion. General corrosion is usually associated with carbonation of the concrete, while corrosion due to chloride ingress is more likely to cause pitting corrosion. It might be anticipated that chloride induced pitting

corrosion would be more likely on a bridge structure; however this type of corrosion is more unpredictable and seems more difficult to consider at the design stage. Therefore, the plan is to base design on general corrosion. This example was also intended to assess the different corrosion models; therefore the effects of general and pitting corrosion are considered at the reliability evaluation stage of this example.

C.8.2 Degraded Structure

The same sample girder was again used in this example; however the degradation level of the structure at the time of strengthening was considered in a slightly different fashion for this example. In Roelfstra et. al. (2004) a basic bridge condition assessment is related to the physical state of the structure. This assessment is shown in Table C-13. Based on this table it was assumed that approximately 10% of the steel section would be missing at the time of FRP application. This was in contrast to the example of Section C.3.5, where it was found that the load-rating factor for 10% loss in steel was greater than 1, suggesting no need for repair. In truth it is very difficult to determine the amount of steel remaining in a structure after corrosion has been initiated, making load-rating calculations difficult. Therefore, this approximate estimate based on a physical assessment of the bridge may be more representative of actual practice. This situation reflects the general uncertainty about the state of the bridges when strengthening is applied and the need for further research in this matter.

Table C-13 Relation of Condition States for Bridge Management Systems to Structural Integrity of Bridge

Condition State	Description	Physical Criteria
1 Good	No visible damage; only thin superficial cracks; no signs of corrosion	< 0.2% free Cl $^-$/mass of cement
2 Acceptable	Visible spots of rust and/or local spalling; thin cracks due to corrosion of the reinforcements and/or humid zones; insignificant mechanical damage	< 50 μm of reinforcement radius loss
3 Damaged	Spalling with visible reinforcement, insignificant loss of section, less than 10% visible reinforcement; cracks and or humid zones	< 10% of reinforcement section loss
4 Bad Condition	Spalling with visible reinforcement, significant loss of section, more than 10% of reinforcement visible; cracks and or humid zones	< 25% of reinforcement section loss
5 Alarming	The structure is in danger, measures are necessary before next principal inspection; immediate measures	> 25% of reinforcement section loss

C.8.3 Prediction of Remaining Steel

The corrosion rate was predicted using Eq. C-8 (Vu and Stewart, 2000). In this equation the corrosion rate is found in μA/cm^2 when the cover is expressed in mm. The corrosion rate was assumed constant during the whole lifetime; although some sources suggest that corrosion may slow as corrosion products build up on the surface of the steel.

$$i_{corr} = \frac{37.8(1 - w/c)^{-1.64}}{cover}$$

Eq. C-8

For this example the water-cement ratio and concrete strength were considered as fully dependent variables. The girder was designed with a concrete strength of 34.5 MPa (5 ksi). A concrete mix design website (Ghaly and Almstead, 2005) listed the approximate water-cement ratios corresponding to different concrete strengths as shown in Table 2-10 of Chapter 2. Based on these values, the rate of corrosion was predicted using a water-cement ratio of 0.5.

Once the corrosion rate was found, the amount of penetration in mm/yr was calculated using Eq. C-9, allowing calculation of the new steel diameter and area.

$$P_{av} = 0.0116i_{corr}$$

<div align="right">**Eq. C-9**</div>

Time spans of 10, 30, and 50 years were considered. The calculated steel areas are shown in Table C-15. The percent loss of area is based on the starting value of 5162 mm^2 (8.0 in^2), and includes the 10% loss at the time of strengthening.

Table C-14 Remaining Steel Area for Various Design Lives

Design Life (yr)	10	30	50
Bar diameter mm (in)	26.571 (1.046)	25.495 (1.004)	24.418 (0.961)
A bar mm^2 (in^2)	554 (0.859)	510 (0.791)	468 (0.726)
A$_s$ mm^2 (in^2)	4432 (6.876)	4080 (6.330)	3744 (5.807)
% loss in Area	13.5	20.4	27

C.8.4 FRP Properties

Only three sample FRP materials were used for this example. They were selected to show a range of strength and modulus, with small differences in the ultimate strain (as opposed to previous examples which had many materials with the exact same rupture strain). The assumed values are shown in Table C-15. Degradation of the FRP properties was considered using the percent retention equations described previously in Section C.6.1.3.

Table C-15 Assumed Properties for Sample Composites

	Strength MPa (ksi)	Modulus GPa (ksi)	Rupture Strain
MAT 1	620.5 (90)	51.7 (7500)	0.012
MAT 2	827.4 (120)	63.4 (9200)	0.013
MAT 3	1034.2 (150)	73.8 (10700)	0.014

C.8.5 Design of Strengthening

Strengthening was designed following the principles of Section C.3. Designs were produced for values of $\phi = 0.95$, 0.9, and 0.85 and values of ψ ranging from 0.95 to 0.5. ϕ was allowed to vary in this example based on the idea that different design lives might result in different levels of variation in the amount of remaining steel, requiring changes to the resistance factor applied to the steel contribution.

C.8.6 Reliability Analysis

The hybrid method combining MCS and FORM was used to evaluate the reliability of designs. The time-integrated approach was used to compute the time-dependent reliability.

C.8.7 Random Variables

Based on the conclusions of Section C.6.2.3, for this example only the distribution of 50-year mean maximum loads from *NCHRP Report 368* was used to model the live load. The resistance was modeled using all of the random variables in Case 4 of Section C.7.

Random variables describing the corrosion process also had to be considered. Eq. C-8 uses the water-cement ratio and rebar cover to predict the current density of corrosion. The water-cement ratio and concrete strength were assumed perfectly correlated, and the water-cement ratio was calculated from the randomly generated value of concrete strength using a linear equation fit to the data in Table 2-10. Using this linear equation in simulation produced water-cement ratios with a mean of 0.55 and COV of 0.12. This mean was higher than the assumed value of 0.5 because the statistical description used for concrete strength predicts a mean value of concrete strength in the structure slightly less than the value specified for design. In simulation, the cover was computed by taking the difference between the random values of h (the depth of the T-beam) and d (the depth to the reinforcement). This resulted in a mean of 106.7 mm (4.2 in.), substantially greater than the 50.8 mm (2 in.) used in design, and

COV of 0.13. Later, the error in this computation was recognized, as d is measured to the center of gravity of the reinforcement, and therefore cannot be directly used to estimate the amount of cover. Based on these input variables of water-cement ratio and rebar cover the rate of corrosion was found to have a mean of 1.4 $\mu A/cm^2$ (9.03 $\mu A/in^2$) and COV of 0.31. (As a point of reference, a corrosion rate of 1 $\mu A/cm^2$ (6.45 $\mu A/in^2$) is generally considered moderate, and 10 $\mu A/cm^2$ (64.5 $\mu A/in^2$) is considered very high.) This mean value was in the target range desired; thus, despite the high water-cement ratio and large cover, these results were deemed representative of a moderate rate of corrosion, which was the desired test case. The COV of the corrosion rate was somewhat higher than the value of 0.20 used in most references surveyed; however it was a direct result of the predictive equation for current density and the amounts of variation in water-cement ratio and cover, all of which seemed reasonable in the absence of better data.

C.8.8 General vs. Pitting Corrosion

At the reliability analysis stage two types of corrosion were considered. General corrosion was modeled by computing the remaining area of steel based on uniform loss of diameter. All 8 bars were assumed to be corroding at the same rate. It is unlikely that all 8 bars would be placed at the same depth, so this likely represents an extreme case. To consider pitting corrosion another random variable, R, was introduced. This variable represents the ratio of the depth of the deepest pits to the depth of general corrosion. Based on Stewart and Rosowsky (1998a), R was first modeled as a normal variable with a mean of 3 and COV of 0.33. As these values produced relatively high reliabilities, later a mean of 5 and COV of 0.22 were also considered following (Stewart, 2004); however Stewart used a Gumbel distribution for this set of parameters, while in this work a Normal distribution was used for both sets. Based on the random value of R, the depth of penetration in pits was calculated, and the

remaining area of steel in the section was computed using geometrical formulas from Stewart (2004). Pitting was not expected to be uniform from bar to bar. Therefore a unique value of R was generated for each of the 8 bars and the corresponding total loss of area was calculated.

C.8.9 Results of Sample Calibration with Corrosion

In many ways the results of this example were surprising. These results may be largely summarized by Figure C-18, which shows results for the representative case of composite Material 1 with ϕ equal to 0.9. Results for general corrosion and pitting corrosion with two different mean values for R (3 and 5) are shown for 10, 30, and 50-year designs. (The jump seen in the 50-year data is between designs with 2 layers and designs with 3 layers because the bond coefficient drops quickly with the additional layer.)
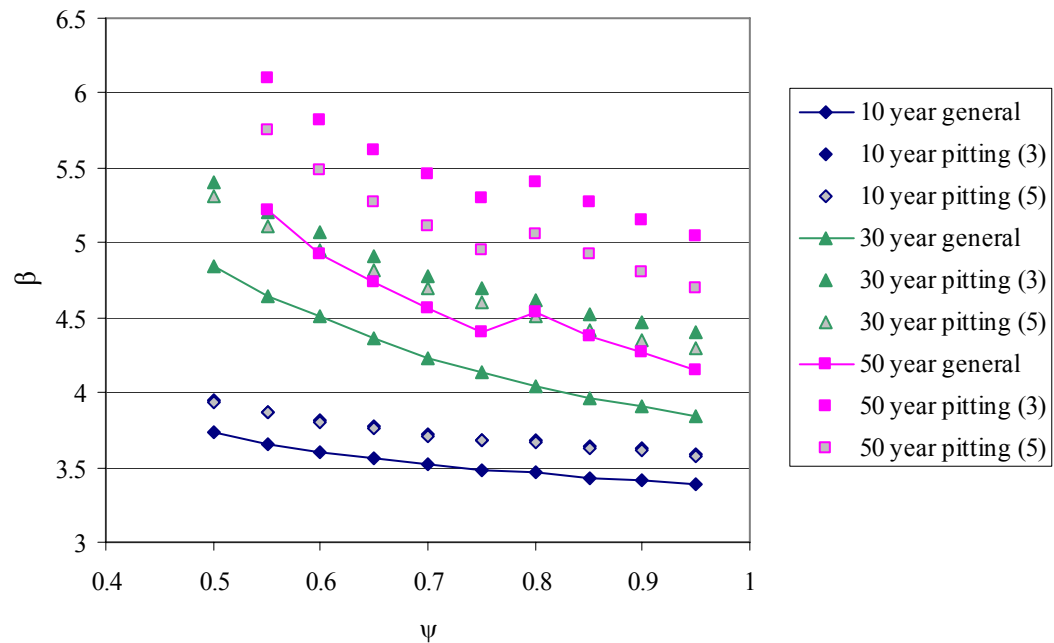
Figure C-18 Reliability Index vs. Composite Specific Resistance Factor for Material 1, $\phi = 0.90$, FRP Strength COV=0.15

In this figure it is clearly seen that for a given value of ψ the reliability of a design increases as the design life is extended. This result was unanticipated, as it was assumed that for designs of longer lifetimes there would be increased variability in the remaining area of steel and thus a reduction in reliability. In an attempt to explain these results, the variation in steel area for the different design lives was checked. Table C-16 shows the effect of increasing design life on the COV of steel area. The COV does increase by a significant amount as the design life increases; however the actual numerical values of the COV are so small that it is unlikely that the variation in the steel area is producing any real impact on the variation in the resistance. This small variation results because, compared to the overall diameter of the bar, the amount of steel lost to corrosion is quite small, and thus even though there is significant variation in the amount lost, the effect on the total area is not as significant.

Table C-16 COV of Remaining Steel Area for Different Design Lives

Design Life	COV of A_s
10	0.007602
30	0.023304
50	0.039072

Once the low level of steel variation was recognized, the increase in reliability for longer design lives could be explained in terms of a previously identified phenomenon. For a design life of ten years approximately 13% of the original steel is missing, compared to approximately 27% for a design life of 50 years. Thus the increased reliability is attributed to the increased reliability generally seen for designs with greater amounts of steel loss

It is also clear from Figure C-18 that general corrosion had a more negative effect on the reliability than pitting corrosion, at least for the cases of pitting corrosion considered herein. The more severe pitting (represented by the random variable R with a mean of 5) did

325

produce lower reliabilities than the less severe pitting, with the effect becoming more pronounced as the service life increased. Stewart (2004) found that general and pitting corrosion had nearly the same reliability up to a life of approximately 25 years, after which pitting corrosion became more critical. However, the current example cannot be directly compared to Stewart's study because pitting corrosion causes more severe results in reinforcing bars of smaller diameter. The present work assumed #9 bars with diameters of 28.6 mm (1.125 in.) compared to the bars used by Stewart with diameters of 8, 16, and 24 mm (0.315, 0.63, and 0.945 in.). Since the final calibration example will consider strengthening of girders, which are generally reinforced with large diameter bars, general corrosion will be assumed as a conservative approximation for the final calibration example. For future work with slabs or other failure modes that are reinforced with smaller diameter bars pitting corrosion may be a more critical consideration.

A final concern regarding the results of this example was the relatively high reliabilities despite the fact that the LRFR load factors were used to generate the strengthening designs. These high reliabilities made selection of design factors awkward for the likely target reliabilities. These high reliabilities were attributed to the incorrect calculations for cover.

C.9 Summary of Conclusions from Sample Calibrations

Based on the sample calibrations described above many decisions were made for use in the final calibration example. Some of the most important include:

- Load factors used by the LRFD Design Specifications produce very high reliabilities; therefore the LRFR load factors are used.

- The hybrid reliability method, which combines Monte Carlo Simulation of resistance statistics with FORM evaluation of the reliability index, appears to

produce reasonable predictions of reliability. Furthermore, it is much faster to implement and will allow the consideration of numerous cases in the final calibration.

- The amount or remaining steel is significant to the resulting reliability. Though this value cannot be accurately assessed in the field, a design procedure that does not at least consider this change in reliability will likely be highly conservative.

- The distributions of maximum live load taken from *NCHRP Report 368* (Nowak, 1999) appear to have some inconsistencies, thus a simplified description of live load as described in Section 2.6.2 of Chapter 2 will be used.

- Differences in composite materials appear to have relatively little effect on the reliability; however different materials will still be used in the final calibration.

- Changes in the composite modulus COV have limited impact on the final resistance factor for the bond model used in these examples.

- General corrosion appears to be more severe for the bar sizes commonly used in construction of girders.

Appendix D. Sectional Analysis

D.1 Introduction

Sectional analysis was used to compute the resistance of strengthened members for both design purposes and to analyze the reliability. This appendix provides a simplified discussion of this topic, covering only the practical aspects as employed in this report. For a more thorough discussion the reader is referred to books discussing concrete design, for example Hassoun (2002) and Collins and Mitchell (1991). Due to the awkward dimensions of the T-girders used in most of this report (very large flange widths) the following discussion will make use of a rectangular cross-section. In fact, at ultimate capacity, the neutral axis of the T-girders used herein was in the flange of the cross-section, and therefore they could be analyzed as rectangular sections.

D.2 RC Section without FRP

Figure D-1 shows the distributions of strain and stress in a concrete section reinforced with steel reinforcement at its ultimate flexural capacity. In this analysis shear deformations are neglected, and thus the strain distribution is linear. In the section shown below, the extreme compressive fiber in the concrete is at the ultimate compressive strain, $\varepsilon_c = 0.003$, as specified by ACI (1999). This cross-section is under-reinforced, and therefore, at ultimate, the steel is beyond its yield strain, ε_y. As a general rule, concrete sections are designed to be under-reinforced to provide ductility and ample warning of potential failure. Therefore, the failure mode is almost always steel yielding followed by concrete crushing.
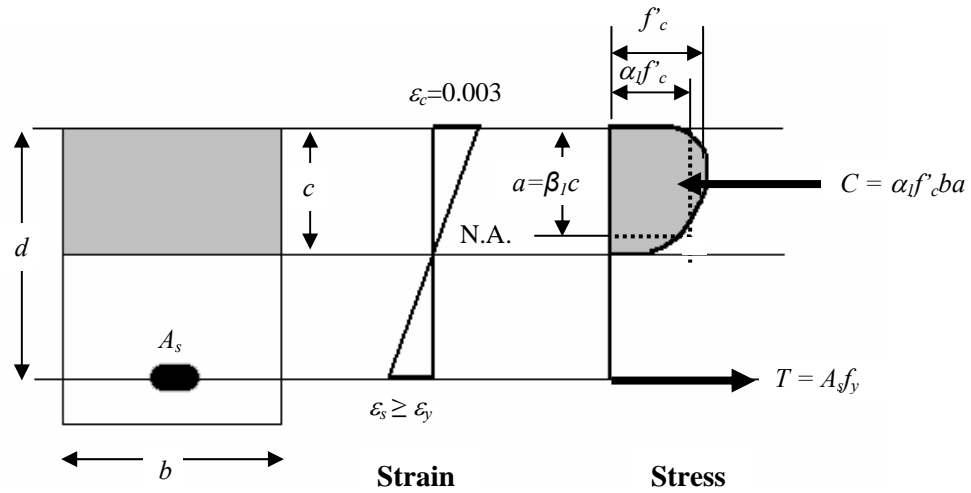
Figure D-1 Forces in a Rectangular Section at Ultimate (Only Steel Reinforcement)

The stress portion of the figure shows that all tensile forces are carried in the steel. The concrete is assumed to have no tensile capacity. Above the neutral axis (N.A.) the distribution of compressive stress in the concrete takes an irregular shape. Working with this irregular shape is difficult for design purposes; and thus a simplified shape is often assumed for use in design.

In Figure D-1, the dotted lines represent a common simplification, the rectangular stress block. The stress is approximated as being uniform, and equal to $\alpha_1 f'_c$, over a depth of a, equal to $\beta_1 c$. In ACI 318, the value of α_1 is taken as 0.85 when the concrete is at ultimate, and β_1 is equal to 0.85 for concrete strengths below 27.6 MPa (4 ksi). Above 27.6 MPa (4 ksi) the value of β_1 is decreased linearly by 0.05 for each 6.9 MPa (1 ksi). It has a minimum value of 0.65.

Assuming the rectangular stress block, the compressive stress resultant, C, is found equal to $\alpha_1 f'_c ba$, acting at the centroid of the rectangular block, $a/2$. The tensile stress resultant, T, is equal to $A_s f_y$. By enforcing equilibrium, the value of a can be found as shown in Eq. D-1.

$$\begin{aligned} T &= C \\ A_s f_y &= \alpha_1 f'_c ba \\ a &= \frac{A_s f_y}{\alpha_1 f'_c b} \end{aligned}$$

Eq. D-1

By taking moments about the location where the compressive resultant acts, the ultimate capacity of the section can be found as shown in Eq. D-2.

$$M = A_s f_y (d - a/2)$$

Eq. D-2

D.3 RC Section with Externally Bonded FRP

Sectional analysis of a RC section strengthened with FRP follows the same general principles described in Section D.2. However, with the addition of FRP, there are now several possibilities for the failure mode:

1. Rupture or debonding of the FRP assuming the steel has already yielded,

2. Crushing of the concrete after the steel has yielded,

3. Or if enough FRP is applied, the section could become over-reinforced and the concrete could fail before the steel has yielded.

The third possibility is highly undesirable, and should be avoided; therefore attention will be placed on the first two possibilities.

Figure D-2 shows the strains and stresses in a concrete section with externally bonded FRP. Again a linear strain distribution is assumed. It is apparent that there are now two tensile resultants: one from the steel and one from the FRP. The compressive resultant can still be modeled using the stress block approximation.
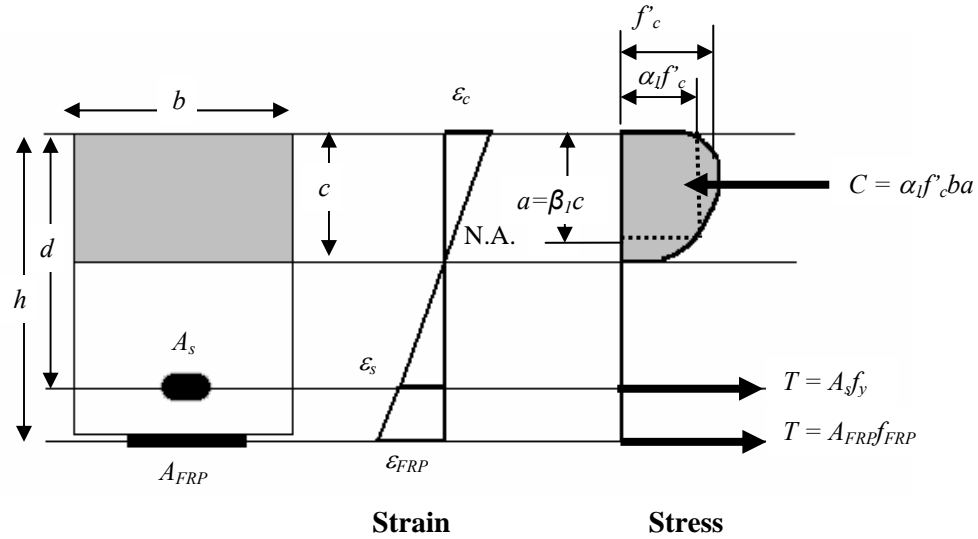
Figure D-2 Forces in a Rectangular Section (Steel and FRP Reinforcement)

The section will fail in one of the first two failure modes if either the FRP (rupture or debonding) or the concrete (crushing) reaches a critical strain. It is assumed that the steel will have already yielded when one of these critical strains is reached, however in order to find the full distribution of strain (and the capacity of the section) it is necessary to find the neutral axis. The neutral axis is found though iteration by enforcing equilibrium and compatibility on the section. The following steps briefly describe the iterative process. A numerical example of this procedure is provided in Section 5.2.5 of Chapter 5.

1. Calculate the limiting strain in the FRP, $\varepsilon_{FRP,lim}$. This value will be the minimum of the predicted debonding strain and the ultimate strain of the composite. The

model used to predict debonding in this work is described in Section 4.5.2.1 of Chapter 4.

2. Select a trial value for the depth to the neutral axis.

3. Based on the trial neutral axis depth check to see if the concrete or the FRP controls the design. An effective way to do this is to calculate the strain at the level of the FRP when the extreme compressive concrete is at the ACI limit for concrete strain, 0.003. This calculation is shown in Eq. D-3, where h is the total depth of the section, c is the estimated neutral axis depth, and ε_{soffit} is the initial strain at the bottom of the beam when the FRP is applied. If this value is less than the previously calculated FRP strain limit (due to debonding or rupture of the composite), the design is controlled by concrete crushing. Choose the minimum value of FRP strain to proceed.

$$\varepsilon_{FRPcrush} = 0.003\left(\frac{h-c}{c}\right) - \varepsilon_{soffit} \qquad \text{Eq. D-3}$$

4. Calculate the strain in the reinforcing steel, as shown in Eq. D-4, where d is the depth from the compression face to the steel, ε_{FRP} is the minimum value of FRP strain determined in step 3, and all other variables are as previously defined.

$$\varepsilon_s = (\varepsilon_{FRP} + \varepsilon_{soffit})\left(\frac{d-c}{h-c}\right) \qquad \text{Eq. D-4}$$

5. Calculate the stress in the steel, f_s, and FRP, f_{FRP}, using the strain profile and the modulus of elasticity for both materials (E_s and E_{FRP}, respectively), as shown in Eq. D-5 and Eq. D-6 . If the stress exceeds the yield strength of the steel, limit the stress to the yield stress, f_y.

$$f_s = E_s \varepsilon_s \le f_y \qquad\qquad \textbf{Eq. D-5}$$

$$f_{FRP} = E_{FRP} \varepsilon_{FRP} \qquad\qquad \textbf{Eq. D-6}$$

6. Estimate the stress block factors for the concrete. If concrete crushing controls the design, the values from ACI specified in Section D.2 can be used. However, the T-beams used in this work have a large area of concrete in the compressive zone, and therefore the FRP is typically the controlling material. Since the concrete is not at ultimate when debonding or composite rupture occurs it is not appropriate to use the ACI specified stress block factors; however equations for estimating stress block factors for other concrete conditions are provided by Collins and Mitchell (1990, pp 62-63, 176-177). Start by calculating the strain in the extreme compressive zone of the concrete using Eq. D-7. Use this value to calculate stress block factors, α_1 and β_1, as shown in Eq. D-8 through Eq. D-11. In this set of equations f'_c is the compressive strength of the concrete, E_c is the modulus of the concrete, and all other variables are as described previously or as derived in these equations.

$$\varepsilon_{ct} = c \left(\frac{\varepsilon_{soffit} + \varepsilon_{FRP}}{h - c} \right) \qquad\qquad \textbf{Eq. D-7}$$

$$\beta_1 = \frac{4 - \dfrac{\varepsilon_{ct}}{\varepsilon'_c}}{6 - 2\dfrac{\varepsilon_{ct}}{\varepsilon'_c}} \qquad\qquad \textbf{Eq. D-8}$$

$$\alpha_1 = \frac{1}{\beta_1} \left(\frac{\varepsilon_{tc}}{\varepsilon'_c} - \frac{1}{3} \left(\frac{\varepsilon_{tc}}{\varepsilon'_c} \right)^2 \right) \qquad\qquad \textbf{Eq. D-9}$$

$$\varepsilon_c' = \frac{f_c'}{E_c} \frac{n}{n-1} \qquad \text{Eq. D-10}$$

$$n = 0.8 + \frac{f_c'}{17} \ \text{MPa} \quad \text{or} \quad n = 0.8 + \frac{f_c'}{2500} \ \text{psi} \qquad \text{Eq. D-11}$$

7. Use equilibrium to calculate a new estimate of the neutral axis, as shown in Eq. D-12, where A_s is the area of steel, A_{FRP} is the area of composite, and b is the width of the concrete section. For most T-beam girders, the neutral axis at the ultimate capacity will be in the flange, and b can be taken as the effective width of the flange.

$$c = \frac{A_s f_s + A_{FRP} f_{FRP}}{\alpha_1 \beta_1 f_c' b} \qquad \text{Eq. D-12}$$

8. Iterate over values of the neutral axis (repeating steps 3-8) until the trial value and the value calculated in Eq. D-12 are equal (at least approximately).

9. Once the neutral axis is found, find the moment capacity of the section using Eq. D-13 , or the factored moment capacity using Eq. D-14.

$$M_n = A_s f_s \left(d - \frac{\beta_1 c}{2} \right) + A_{frp} f_{frp} \left(h - \frac{\beta_1 c}{2} \right) \qquad \text{Eq. D-13}$$

$$\phi M_n = \phi \left[A_s f_s \left(d - \frac{\beta_1 c}{2} \right) + \psi A_{frp} f_{frp} \left(h - \frac{\beta_1 c}{2} \right) \right] \qquad \text{Eq. D-14}$$

In order to use this procedure for design of strengthening an area of FRP must be assumed at the beginning, in terms of a width and number of layers. After calculating the capacity for a given area of FRP, the values describing the amount of FRP must be adjusted

until the capacity of the section meets the factored load demand. The width of the FRP should always be less than the width of the T-section. As many layers as necessary may be applied; however, unless the composite is constructed from very thin fabric, the allowable debonding strain will decrease quickly with the addition of layers and it is unlikely that viable designs will be created with more than three layers.

The iterative process can be easily implemented in Microsoft Excel, and the SOLVER routine can be used to find the neutral axis without manual iteration. If the iteration is conducted manually or is programmed, it is suggested that the average of the trial neutral axis (step 2) and the calculated estimate of neutral axis (step 7) should be used as the trial value for the next iteration. When the neutral axis iteration is automated, the amount of FRP needed can be calculated quite quickly.

This technique is an approximate method of analysis; however it is very convenient for design. This procedure was also used to calculate the resistance statistics because it is quick to implement, and this allowed the consideration of many different cases during the calibration stage.

Appendix E. Techniques Used in Reliability Assessment

This appendix describes many of the techniques used in this report to calculate the reliability. For those techniques implemented using computer programs, sample programs in Java are presented in Appendix F.

E.1 Monte Carlo Simulation

Monte Carlo Simulation (MCS) was used in two ways during this research. Initially it was most often used to directly assess the probability of failure. Later, a hybrid reliability approach was adopted wherein the mean and standard deviation of the resistance were estimated using simulation techniques, and then the overall reliability was calculated using FORM. The FORM technique is discussed in Section E.3 of this appendix.

Figure E-1 shows the basic procedure followed for the simulations run for this report. The first step is to input data detailing the specific dimensions of the structural element (i.e. the strengthened girder) for which the reliability is being assessed. Next all deterministic variables are initialized with their values. The simulation loop in the computer programs begins with the generation of random values for all random variables; this is discussed in Section E.2 of this appendix. Using these random values the limiting FRP strain is predicted based on the particular bond model in use, the neutral axis is found through sectional analysis (see Appendix D), and the ultimate capacity of the section is computed. For the hybrid reliability approach this is as far as the simulation needs to go. The program stores the resistance computed for a single trial, and then repeats the process until the desired number of trials have been run. At the end of all trials the mean and standard deviation of resistance are computed.

```
┌─────────────────────────────────────────┐
│   Accept input data detailing the design │
└─────────────────────────────────────────┘
                    │
                    ▼
┌─────────────────────────────────────────┐
│   Initialize any deterministic variables │
└─────────────────────────────────────────┘
                    │
                    ▼
┌─────────────────────────────────────────┐
│         Generate random values for all   │
│             random variables             │
│              See Section C.2             │
└─────────────────────────────────────────┘
                    │
                    ▼
┌─────────────────────────────────────────┐
│       Calculate the limiting FRP strain  │
│   See Section 4.5.2.1  or ACI 440 (2002) │
└─────────────────────────────────────────┘
                    │
                    ▼
┌─────────────────────────────────────────┐
│  Iterate to find the neutral axis by     │
│    enforcing compatibility and equilibrium│
└─────────────────────────────────────────┘
                    │
                    ▼
┌─────────────────────────────────────────┐
│  Calculate the moment capacity of the    │
│   section, R, using Eq. 4-6 with φ and ψ │
│              set equal to 1              │
└─────────────────────────────────────────┘
                    │
                    ▼
┌─────────────────────────────────────────┐
│  Generate random values for load         │
│  variables, and sum to calculate total   │
│           load demand, Q                 │
└─────────────────────────────────────────┘
                    │
                    ▼
                 ◇ R > Q ? ◇
              Yes           No
                       Count = count +1
```

Calculate the moment capacity of the section, R, using Eq. 4-6 with ϕ and ψ set equal to 1

Generate random values for load variables, and sum to calculate total load demand, Q

$R > Q$?

Yes

No
Count = count +1

n = desired number of simulations?

No

Yes
p_f = count / # of simulations

Calculate mean and standard deviation of resistance, R

Figure E-1 Flow Chart of Monte Carlo Simulation

337

The region shaded in grey is only used when the probability of failure is being directly estimated from the MCS. Calculation of the failure probability requires that random values also be generated for the load components. Then the random load demand is compared to the calculated resistance for a single trial. If the load demand is greater than the resistance, this is counted as a "failure", otherwise the count is unchanged. After the comparison, the program moves on to the next trial. At the end of all trials, the probability of failure is estimated as the number of "failures" divided by the total number of trials.

The accuracy of a MCS depends on the number of trials that are run. When the simulation is run to compute the probability of failure, the required number of samples can be estimated using confidence limits based on assuming the distribution of the estimated probability of failure will follow a Normal distribution (Thacker and Huyse, 2005). Eq. E-1 can be used to estimate the number of trials, N, needed to predict a probability of failure, p_f. In this equation k is used to express the two-sided confidence level in terms of the number of standard deviations; values of k for different confidence levels are given in Table E-1. The relative error is expressed in decimal form.

$$N = \left(\frac{1 - p_f}{p_f} \right) \left(\frac{k}{\text{Relative Error}} \right)^2$$

Eq. E-1

Table E-1 Values of k for Different Two-Sided Confidence Levels

k	Two-Sided Confidence Level
1.64	90%
1.96	95%
2.6	99%

For the purposes of this report, when the probability was being estimated, Eq. E-1 was used to get an idea of the minimum number of trials, but was generally rounded up to a round

number. For cases where only the resistance statistics were being estimated, a simple test of convergence was run (see Section 4.6.3.1.1 of Chapter 4).

E.2 Generating Random Numbers from a Statistical Distribution

Random number generation is an important part of Monte Carlo Simulation, and a simple Google search can illuminate the number of different algorithms available. However, this topic was not given extensive consideration for the purposes of this report. The Random class for the Java programming language is capable of providing both Uniformly and Normally distributed pseudorandom numbers (Java, 2005). The random numbers provided by this class were used as the basis for generating random numbers from all other distributions considered.

The vast majority of random variables considered for this work were modeled as Normal random variables. Generating random values from their respective distributions was quite simple given the Normally distributed random numbers provided by the Java class. The random numbers provided were from a standard Normal distribution, with a mean of 0 and a standard deviation of 1, and thus could be easily scaled to model any Normal distribution. Eq. E-2 shows this scaling, wherein x is the random value from the desired distribution, μ is the mean of the desired distribution, σ is the standard deviation of the desired distribution, and $nrand$ is the random number generated from the standard Normal distribution.

$$x = \mu + \sigma(nrand)$$

Eq. E-2

Random values from a Lognormal distribution were also generated from the random standard Normal values (Bury, 1999). Eq. E-3 shows how the Lognormal values were obtained. In this equation, x is once again the random number from the desired distribution, λ

and ζ are parameters of the Lognormal distribution as seen in Eq. 3-3 of Chapter 3, and *nrand* is the random number generated by the computer from the standard Normal distribution.

$$x = \exp\left(\lambda + \zeta(nrand)\right)$$

<div align="right">**Eq. E-3**</div>

Random values fitting a Weibull distribution were generated using the Uniformly distributed random numbers, through inversion of the CDF (Bury, 1999). This process is shown in Eq. E-4, where x is the random number from the desired Weibull Distribution, α and β are parameters of the two-parameter Weibull distribution as seen in Eq. 3-4 of Chapter 3, and *urand* is a uniformly distributed random number between 0 and 1.

$$x = \beta\left[\ln\left(\frac{1}{urand}\right)\right]^{\frac{1}{\alpha}}$$

<div align="right">**Eq. E-4**</div>

The final distribution needed for this work was the Beta distribution. This distribution required a slightly more complicated procedure as found in Bury (1999). The PDF of the Beta distribution is shown in Eq. E-5, wherein Γ is the Gamma function and λ_1 and λ_2 are parameters of the distribution.

$$f(x;\lambda_1,\lambda_2) = \frac{\Gamma(\lambda_1 + \lambda_2)}{\Gamma(\lambda_1)\Gamma(\lambda_2)}x^{\lambda_1-1}(1-x)^{\lambda_2-1}$$

<div align="right">**Eq. E-5**</div>

$$0 < x < 1 \; ; \; \lambda_1, \lambda_2 > 0$$

The technique for generating random values is a rejection technique. The first step is to calculate the mode, x_m, as shown in Eq. E-6, and the density value of the mode, M, from Eq. E-5.

$$x_m = \frac{\lambda_1 - 1}{\lambda_1 + \lambda_2 - 2}$$

<div align="right">**Eq. E-6**</div>

The second step is to generate two uniform random numbers, u_1 and u_2, between 0 and 1. Finally if $u_2 \leq f(u_1; \lambda_1, \lambda_2)/M$ then accept u_1 as a random value from the desired Beta distribution, if not reject u_1 and repeat the process.

All of these transformations were easily implemented in Java. However, many mathematical software packages, such as Matlab and Mathematica, are able to directly generate random numbers from a number of different distributions.

E.3 Implementation of FORM

In this work, the First-Order Reliability Method (FORM) is implemented almost exactly as described by Nowak in *NCHRP Report 368* (1999). This procedure is significantly simplified from the more general implementation of FORM by assuming that the load is a Normal variable and the resistance is a Lognormal variable. These assumptions mean that no transformation is necessary for the load portion of the problem. Further, the transformation of the resistance is not difficult due to the relationship between the Normal and Lognormal distributions. These simplifications almost reduce the NCHRP method to a second moment method since the only required pieces of information are the means and coefficients of variation for the resistance and the capacity. Given the required second moment information, the essential equations of this procedure are described below.

1. The limit state function is stated as:

$$Z = R - Q$$

Eq. E-7

R is the resistance and Q is the total load. The mean, standard deviation, and COV of resistance are denoted as μ_R, σ_R, and COV_R, respectively, and the mean, standard deviation, and COV of load are denoted as μ_Q, σ_Q, and COV_Q, respectively.

2. Assume that the resistance design point, $R*$, can be found using:

$$R* = \mu_R(1 - k \cdot COV_R)$$

Eq. E-8

In this formulation, k is an unknown. To start the iteration a trial value for k must be selected. *NCHRP Report 368* (Nowak, 1999) suggests 2 as a good starting point.

3. The standard deviation, σ'_R, and mean, μ'_R, of the Normal distribution used to approximate the non-Normal distribution for resistance at the design point $R*$ can be approximated following Rackwitz and Fiessler (1978) as:

$$\sigma'_R = \frac{\varphi\{\Phi^{-1}[F(R*)]\}}{f(R*)}$$

Eq. E-9

$$\mu'_R = R* - \sigma' \cdot \Phi^{-1}[F(R*)]$$

Eq. E-10

$F(\,)$ and $f(\,)$ are the cumulative distribution function and probability density function, respectively, of the non-normal distribution that is being approximated. $\Phi(\,)$ and $\varphi(\,)$ are the standard normal cumulative and density functions, respectively. (If the loading had not been assumed normal this same transformation would be required for Q.)

4. For the Lognormal distribution of resistance, $F(\,)$ and $f(\,)$ at the point $R*$ can be expressed as:

$$F(R*) = \Phi[\alpha]$$

Eq. E-11

$$f(R*) = \frac{\varphi[\alpha]}{COV_R \cdot R*}$$

Eq. E-12

$$\alpha = \frac{\ln R^* - \ln \mu_R}{COV_R}$$ **Eq. E-13**

5. Using $F(R^*)$ and $f(R^*)$, the transformation equations of step 3 simplify to:

$$\sigma'_R = COV_R \cdot R^*$$ **Eq. E-14**

$$\mu'_R = R^* - \alpha \cdot \sigma'_R$$ **Eq. E-15**

6. The reliability index is now calculated using the standard second-moment equation for β for this performance function:

$$\beta = \frac{\mu'_R - \mu_Q}{\sqrt{\sigma'^2_R + \sigma^2_Q}}$$ **Eq. E-16**

7. From here the new design point can be computed as:

$$R^* = \mu'_R - \frac{\beta \sigma'^2_R}{\sqrt{\sigma'^2_R + \sigma^2_Q}}$$ **Eq. E-17**

8. If this new R^* matches the R^* assumed in step 1 the computation is complete, and β is as calculated in step 5. If they do not match, return to step 4 with the new R^* and continue the iteration.

This procedure was implemented for the numerous design cases considered with the aid of a macro function programmed in Microsoft Excel with Visual Basic. Excel was used because it has built-in functions for the Normal distribution and its inverse. The only change from the above description is that rather than using the new value of R^* to continue the iteration, the Solver routine in Excel was used to directly find the value of k which minimized the difference between R^* and the updated value of R^*.

Appendix F. Java Programs

F.1   Program for Design of Strengthening

The following code is an example of the program that was used to create the numerous designs used in the final calibration described in Chapter 4. This program implements the design process described in Section 4.5.3 of Chapter 4. The dimensions of specific girders were hard coded into the program, and thus a different version was created for each of the 18 girders that could be strengthened.   The example code that follows is specific to Girder 6, as referred to in Table 4-4 of Chapter 4. All calculations are conducted in the U.S. customary system of units.

F.1.1   Variables

Table F-1 gives a brief description of all variables used in this program.

Table F-1 Variables in Design Program

Variable	Description
frpmodstore	Array holding stored values of composite modulus for all five sample materials (psi)
frpsstore	Array holding stored values of composite strength for all five sample materials (psi)
areasteelstore	Array holding stored values of steel area at the time of strengthening for all six corrosion conditions and all five design lives (in^2)
initstrainstore	Array holding the stored values of initial soffit strain corresponding to the steel areas in areasteelstore
b	Effective flange width (in)
d	Depth from compressive face to centroid of reinforcement (in)
h	Full depth of the T-section (in)
webw	Width of the web portion of the girder (in)
fc	Nominal compressive strength of concrete (psi)
Ec	Nominal modulus of elasticity of concrete (psi)
epsilonprime	Constant value used in calculation of stress block factors (see Appendix D)
fy	Nominal yield strength of steel (psi)
steelmod	Nominal modulus of elasticity of steel (psi)
loadtarget	The factored LRFR load for design (kip-ft) see Table 4-9
thickness	Thickness of a single layer of FRP (in)
corrcond	Variable referring to one of the 6 corrosion conditions described in Section 4.4.4 of Chapter 4
steeltime	Design life used for referencing the proper value from areasteelstore
areasteel	Specific value of steel area for a certain design (in^2)
initstrain	Specific value of initial soffit strain for a certain design
degstate	Variable used to reference different FRP degradation models as described in Section 4.4.1.2
frptime	Design life used for calculating degraded FRP properties (yr)
sdeg	The percent retention of FRP strength calculated from degradation models
matindex	Variable used to reference 5 different sample materials
frps	FRP strength for a specific design (psi)
frpmod	FRP modulus for a specific design (psi)
rupture	Ultimate strain of FRP
phi	General resistance factor
si	Composite specific resistance factor
phir	Rounded value of phi
sir	Rounded value of si
w	Width of FRP (in)
layers	Number of layers of FRP
mcalc	Calculated moment capacity (compared to targetload) (kip-ft)
frpthick	Total thickness of FRP (in)
af	Area of FRP (in^2)
fcmpa	Concrete compressive strength (MPa)
gf	Fracture energy for calculating debonding (N/mm)
maxstrain	Strain limit to prevent debonding
ruptlim	Strain limit to prevent FRP rupture
frplim	Controlling FRP strain

Table F-1 (Continued) Variables in Design Program

Variable	Description
c	Estimated neutral axis depth (in)
cnext	Estimated neutral axis depth used in iteration process (in)
steelstress	Stress in reinforcing steel (psi)
betaone, alphacon	Stress block factors (see Appendix D)
frpeff	Limiting strain in FRP including the possibility of concrete crushing
steeleff	Effective strain in reinforcing steel
crush	Strain in FRP at concrete crushing
epsilont	Strain in extreme compressive fiber of concrete
etep, etep2	Variables used to store intermediate value
oneoverbeta	Variable used to store intermediate value
apparentsteel	Stress in steel calculated from steel strain and modulus (psi)
factor, val, places, tmp	Variables used in function for rounding

F.1.2 Procedure

This code loops through the full range of calibration for the specific set of girder dimensions. The hierarchy of looping is:

1. Corrosion Conditions (6 different conditions)

2. Design lives (10, 20, 30, 40, and 50 years)

3. Degradation state (ND, AD, SD)

4. Material (5 sample materials)

5. Resistance Factors (ϕ and ψ)

For each specific set of conditions a design (consisting of a width and number of layers of FRP) is created. If no FRP is needed the condition is labeled as "nsn" for no strengthening needed. If it is not possible to bring the capacity up to the design load, the condition is labeled as "np" for not possible.

F.1.3 Code

```java
import java.io.*;
import java.lang.Math;
import java.util.Random;
import java.io.FileWriter;

public class designsix
{
      static double[] frpmodstore = new double[5];
      static double[] frpsstore = new double[5];
      static double[][] areasteelstore  = new double[6][5];
      static double[][] initstrainstore = new double[6][5];

public static void main(String[] args) throws IOException
{
    // This program determines the amount of composite needed to
    // strengthen a given beam for different materials, different
    // levels of corrosion, and different values of the resistance
    // factors.  The only input is the output file name, all
    // dimensions and material data are hard-coded into the program.

// ****************************************************************
// Read in name for output file
// ****************************************************************

    File outputFile = new File(args[0]);

    FileWriter out = new FileWriter(outputFile, true);

    instantiation();

// ****************************************************************
//  Define variables for girder
// ****************************************************************
    // Girder Dimensions

     double b = 88.0;  //in
     double d = 37.215;  //in
     double h = 42; //in
     double webw = 13; //in

    // Design values for properties of existing structure

     double fc = 3250; //psi
     double Ec = 3249500; //psi
     double epsilonprime = 0.001909;
     double fy = 40000; //psi
     double steelmod = 29000000; //psi

    // Target load for design

     double loadtarget = 1162.44; // kip/ft
```

```
        // FRP thickness per layer

          double thickness = 0.05; //in.

// ****************************************************************
// Define steel properties based on the corrosion condition
// ****************************************************************
        for (int corrcond = 1; corrcond <7; corrcond++)
        {
                out.write("Corrosion Condition: " +corrcond+ "\r\n");

        for (int steeltime=1;steeltime<6;steeltime++)
        {
                out.write("Steel Time: " + steeltime + "\r\n");

        double areasteel = areasteelstore[corrcond-1][steeltime-1];
        double initstrain = initstrainstore[corrcond-1][steeltime-1];

// ****************************************************************
// Loop over FRP Properties
// ****************************************************************
        for(int degstate = 1;degstate<4;degstate++)//loop for state of
        // FRP degradation
        {
        double frptime= 0;

        if(degstate == 1)
        {
                frptime = 0.0;
                out.write("No FRP deg" + "\r\n");
        }
        if(degstate == 2)
        {
                frptime = (double)steeltime*10.0;
                out.write("Araceli deg model"+"\r\n");
        }

        if(degstate == 3)
        {
                frptime = (double)steeltime*2;
                out.write("Slower deg model"+"\r\n");
        }

       // Degraded FRP properties aka strength

        double sdeg;
        if(frptime > 0)
                sdeg= (-3.366 * Math.log(frptime * 365.25)+106.07)/100.0;
        else
                sdeg = 1.0;

        for(int matindex = 1; matindex <6; matindex++)  //Loop  over  5
        // materials
        {
```

348

```
        double frpmod = frpmodstore[matindex-1];
        double frps =sdeg * frpsstore[matindex-1];

        out.write("Material: "+matindex+ "\r\n");

        double rupture = frps/frpmod;

// ****************************************************************
// Loop over design factors
// ****************************************************************
        double phi = 0.95;

        while(phi > 0.82)
        {
                double si = 0.95;

                while(si>0.47)
                {
                        double phir = round(phi,2);
                        double sir = round(si,2);
                        out.write(phir +"   " + sir);

// ****************************************************************
// Calculate needed width and number of layers of FRP
// ****************************************************************

        double w = -.25;
        double layers = 1;

        double mcalc = 0;

        while (mcalc<loadtarget)
        {

        w = w + 0.25;  //add to FRP width to add capacity

        if (w > webw)  // if width exceeds with of girder, add layer
        {
                w = 0.25;
                layers = layers + 1;
        }

        if (layers > 3)  // if number of layers exceeds 3, not possible
        {
                out.write(" np" + "\r\n");
                mcalc=loadtarget + 10;
        }

        else
        {

           double frpthick = layers * thickness;
           double af = frpthick * w;
```

349

```
// ****************************************************************
//  Calculate limiting FRP Strain
// ****************************************************************
      double fcmpa=fc/1000*6.894757;
      double gf= 3.54689* Math.pow(fcmpa,0.19);
      double maxstrain = 1.5* Math.sqrt(2.0*gf/frpmod/frpthick);

      //or

      double ruptlim = 0.9 * rupture;

      double frplim = Math.min(ruptlim, maxstrain);

// ****************************************************************
//  Calculate moment capacity for given w and layers
// ****************************************************************

    // guess neutral axis depth
        double c = 0.5;
        double cnext = 0.75;
        double steelstress = 0.0;
        double betaone = 0.0;
        double alphacon = 0.0;
        double frpeff = 0.0;
        double steeleff = 0.0;

        while (Math.abs(c - cnext) > 0.0001)
        {
           c = (cnext+c)/2;

            // effective strain in FRP
            double crush = 0.003 * (h-c)/c-initstrain;
            frpeff = Math.min(crush, frplim);

            // strain in extreme concrete fiber
           double epsilont = c*(frpeff+initstrain)/(h-c);
           double etep = epsilont/epsilonprime;
           double eteptwo = etep*etep;

           //Calculate stress block factors
           if (frpeff == crush)
           {
               betaone = .85;
               alphacon = .85;
            }
            else
           {
               betaone = (4.0-(epsilont/epsilonprime))/(6.0-
                         2.0*epsilont/epsilonprime);
               double oneoverbeta = 1.0/betaone;
               alphacon =(oneoverbeta)*((etep)-eteptwo/3.0);
           }

            // strain in reinforcing steel
```

```java
              steeleff = (frpeff+initstrain)*((d-c)/(h-c));

              // stress in reinforcing bar
              double apparentsteel = steelmod * steeleff;
              steelstress = Math.min(apparentsteel, fy);

              // use equilibrium to check estimate of c
               cnext = (areasteel * steelstress + af * frpmod *
                        frpeff)/ (alphacon* fc * betaone * b);

           }// End of while for neutral axis

         //  Calculate maximum moment kip-ft/ft
         mcalc = phi*(areasteel * steelstress * (d - betaone*c/2) +si *
                 af * frpeff * frpmod * (h-betaone*c/2))/(1000*12);

          if(mcalc>loadtarget)
          {
             if(w < 0.25)
                   out.write(" nsn"+ "\r\n");//no strengthening needed
             else
                   out.write("  " + matindex+ "  "+w +"   "+ layers +"
                    "+steeltime*10.0+ "   "+ frptime+"   "+corrcond+
                   "\r\n");
          }

             } // end of else controlling number of layers

             } // end of while to solve for design

             si = si-0.05;
             }//end of for loop for si

          phi = phi - 0.05;
             }//end of for loop for phi

        } // end of for loop for material properties
        } // end of for loop for degradation state
        } // end of steeltime loop
        } // end of loop for corrosion condition

     out.close();
      }

 static void instantiation() //this function initializes stored values
 // for material properties, remaining steel areas and initial strains
      {
        frpmodstore[0] = 7500000;
        frpmodstore[1] = 8900000;
        frpmodstore[2] = 8500000;
        frpmodstore[3] = 8600000;
        frpmodstore[4] = 10000000;

        frpsstore[0] = 90000;
```

```
frpsstore[1] = 100000;
frpsstore[2] = 110000;
frpsstore[3] = 120000;
frpsstore[4] = 130000;

areasteelstore[0][0] = 11.2424;
areasteelstore[0][1] = 11.2424;
areasteelstore[0][2] = 11.2424;
areasteelstore[0][3] = 11.2424;
areasteelstore[0][4] = 11.2424;
areasteelstore[1][0] = 9.9933;
areasteelstore[1][1] = 9.9933;
areasteelstore[1][2] = 9.9933;
areasteelstore[1][3] = 9.9933;
areasteelstore[1][4] = 9.9933;
areasteelstore[2][0] = 8.7441;
areasteelstore[2][1] = 8.7441;
areasteelstore[2][2] = 8.7441;
areasteelstore[2][3] = 8.7441;
areasteelstore[2][4] = 8.7441;
areasteelstore[3][0] = 10.9400;
areasteelstore[3][1] = 10.6416;
areasteelstore[3][2] = 10.3474;
areasteelstore[3][3] = 10.0573;
areasteelstore[3][4] = 9.7713;
areasteelstore[4][0] = 9.7082;
areasteelstore[4][1] = 9.4273;
areasteelstore[4][2] = 9.1505;
areasteelstore[4][3] = 8.8778;
areasteelstore[4][4] = 8.6092;
areasteelstore[5][0] = 8.4776;
areasteelstore[5][1] = 8.2151;
areasteelstore[5][2] = 7.9570;
areasteelstore[5][3] = 7.7028;
areasteelstore[5][4] = 7.4528;

initstrainstore[0][0] = 0.000285;
initstrainstore[0][1] = 0.000285;
initstrainstore[0][2] = 0.000285;
initstrainstore[0][3] = 0.000285;
initstrainstore[0][4] = 0.000285;
initstrainstore[1][0] = 0.000320;
initstrainstore[1][1] = 0.000320;
initstrainstore[1][2] = 0.000320;
initstrainstore[1][3] = 0.000320;
initstrainstore[1][4] = 0.000320;
initstrainstore[2][0] = 0.000363;
initstrainstore[2][1] = 0.000363;
initstrainstore[2][2] = 0.000363;
initstrainstore[2][3] = 0.000363;
initstrainstore[2][4] = 0.000363;
initstrainstore[3][0] = 0.000293;
initstrainstore[3][1] = 0.000301;
initstrainstore[3][2] = 0.000309;
```

```
        initstrainstore[3][3] = 0.000318;
        initstrainstore[3][4] = 0.000327;
        initstrainstore[4][0] = 0.000329;
        initstrainstore[4][1] = 0.000338;
        initstrainstore[4][2] = 0.000348;
        initstrainstore[4][3] = 0.000358;
        initstrainstore[4][4] = 0.000369;
        initstrainstore[5][0] = 0.000374;
        initstrainstore[5][1] = 0.000386;
        initstrainstore[5][2] = 0.000398;
        initstrainstore[5][3] = 0.000411;
        initstrainstore[5][4] = 0.000424;
        }

    //
public static double round(double val, int places)
// This function rounds the values of phi and si
        {
      long factor = (long)Math.pow(10,places);

      // Shift the decimal the correct number of places
      // to the right.
      val = val * factor;

      // Round to the nearest integer.
      long tmp = Math.round(val);

      // Shift the decimal the correct number of places
      // back to the left.
      return (double)tmp / factor;
        }
}
```

F.2   Program for Simulation and Evaluation of Resistance Statistics

The following code is an example of the program that was used to conduct the Monte

Carlo Simulation to obtain the mean and standard deviation of the resistance of different

designs for subsequent use in the FORM procedure to calculate the reliability index.   This

program implements the Monte Carlo Procedure described in Section E.1 of Appendix E and

generates random values for variables following Section E.2.   The dimensions of specific

girders were hard coded into the program, and thus a different version was created for each of

the 18 girders that could be strengthened.   The example code that follows is specific to Girder

9, as referred to in Table 4-4 of Chapter 4.   All calculations are conducted in the U.S.

customary system of units.

F.2.1 Variables

Table F-2 gives a brief description of all variables used in this program.

Table F-2 Variables in MCS Program

Variable	Description
alphastore, betastore	Arrays holding stored values of Weibull parameters for describing the variation in composite strength for all five materials (ksi)
modlambdastore, modsigmastore	Arrays holding stored values of Lognormal parameters for describing the variation in composite modulus for all five materials (ksi)
steelstore	Array holding stored values of steel area at the time of strengthening for all six corrosion conditions (in^2) and the initial bar diameter(mm)
n	Number of simulations to run
material	Variable to reference which of five sample materials
w	Width of FRP (in)
layers	Number of layers of FRP
steeltime	Design life used for referencing the proper value from areasteelstore
frptime	Design life used for calculating degraded FRP properties (yr)
steelstate	Variable referring to one of the 6 corrosion conditions described in Section 4.4.4
alphas, betas	Weibull parameters for composite strength
modsigma, modlambda	Lognormal parameters for composite modulus
sdeg	The percent retention of FRP strength calculated from degradation models
b, bt, berror	Variables describing effective flange width (in)
d, dt, derror	Variables describing depth from compressive face to centroid of reinforcement (in)
h, ht, herror	Variables describing full depth of the T-section (in)
slab, slabt, slaberror	Variables describing slab thickness (in)
web, webt, weberror	Variables describing width of the web portion of the girder (in)
cover, covert, cerror, covermm	Variables describing the concrete cover over the bottom reinforcing bars (in)
nbars	Number of reinforcing bars
areasteelinit	Area of reinforcing steel at time of strengthening (in^2)
initdiam	Diameter of reinforcement at time of strengthening (mm)
meand, stdevd	Normal distribution parameters for describing variation in dead load (used to calculate initial strain on the soffit.) (kip-ft)
z	Variable used to reference different values of strength COV
m	Array used to store capacity of section for each trial (kip-ft)
areaswitch, areaerror	Variables used to describe variation in initial steel area
areasteel	Area of steel at time when reliability is calculated (in^2)
fc	Random value of compressive strength of concrete (psi)
Ec	Random value of modulus of elasticity of concrete (psi)
nc, epsilonprime	Variables used in calculation of stress block factors (see Appendix D)
fy	Random value of yield strength of steel (psi)
steelmod	Random value of modulus of elasticity of steel (psi)
frps	Random value of FRP strength (psi)
frpmod	Random value of FRP modulus (psi)

Table F-2 (Continued) Variables in MCS Program

Variable	Description
thicksigma, thicklambda	Lognormal parameters for describing variation in FRP thickness (in)
frpthick	Random value of FRP thickness(in)
af	Area of FRP (in^2)
rupture	Ultimate strain of FRP
wcr	Random value of water-cement ratio
oneminwrc	Variable holding intermediate value
icorr , icmmyr	Corrosion rate ($\mu A/cm^2$) and penetration rate (mm/yr)
fdiam, diamin	Final reinforcing bar diameter (mm) and final diameter (in)
fcmpa	Concrete compressive strength (MPa)
meangf, stdevgf	Normal distribution parameters for describing variation in fracture energy (N/mm)
gf	Fracture energy for calculating debonding (N/mm)
deadm	Random value of dead load moment (kip-ft)
neutralaxis	Neutral axis for calculation of initial soffit strain (in)
icrack	Cracked moment of inertia for calculation of initial soffit strain (in^4)
initstrain	Initial soffit strain
toomany, kicked	Variables to prevent the program from getting stuck when iterating to find the neutral axis
maxstrain	Strain limit to prevent debonding
ruptlim	Strain limit to prevent FRP rupture
frplim	Controlling FRP strain
c	Estimated neutral axis depth (in)
cnext	Estimated neutral axis depth used in iteration process (in)
steelstress	Stress in reinforcing steel (psi)
betaone, alphacon	Stress block factors (see Appendix D)
frpeff	Limiting strain in FRP including the possibility of concrete crushing
steeleff	Effective strain in reinforcing steel
crush	Strain in FRP at concrete crushing
epsilont	Strain in extreme compressive fiber of concrete
etep, etep2	Variables used to store intermediate value
oneoverbeta	Variable used to store intermediate value
meanmoment, stdevmom	Mean and standard deviation of the girder capapcity, this is what the simulation is run to find!
apparentsteel	Stress in steel calculated from steel strain and modulus (psi)
sum, mean	Variables used in function to calculate mean resistance
sum, stdev, meanValue, diff	Variables used in function to calculate standard deviation of resistance
randvalue, check, uone, utwo, oneminusus, fuone, fuonem,	Variables used in function to generate random values from Beta distribution

F.2.2 Procedure

This code follows the MCS procedure outlined in Appendix E.

F.2.3 Code

```java
import java.io.*;
import java.lang.Math;
import java.util.Random;
import java.io.FileWriter;

public class girdereight
{
    static double[] alphastore = new double[6];
    static double[][] betastore  = new double[5][6];
    static double[] modlambdastore = new double[5];
    static double[] modsigmastore  = new double[5];
    static double[][] steelstore = new double[6][2];

public static void main(String[] args) throws IOException
{
    // This program runs a MCS to evaluate the mean and standard
    // deviation of resistance of a beam strengthened with FRP
    // composite materials.  The input variables are the number of
    // trials to run, the material number, the width and number of
    // layers of FRP applied, time parameters characterizing the
    // state of degradation in the FRP and steel, the number of the
    // corrosion case, and file names for the output file, and an
    // extra file used just in case the program gets stuck in the
    // loop calculating the neutral axis.
```

(It should be noted that getting stuck in this loop was an older problem, and this part of the code is just a remnant. This file was empty at the end of simulations for each girder)

```java
// ****************************************************************
// Read in data from command line, initialize output files
// ****************************************************************

    int n = Integer.parseInt(args[0]);
    int material = Integer.parseInt(args[1]);
    double w = Double.parseDouble(args[2]);
    double layers = Double.parseDouble(args[3]);
    double steeltime = Double.parseDouble(args[4]);
    double frptime = Double.parseDouble(args[5]);
    int steelstate = Integer.parseInt(args[6]);

    File outputFile = new File(args[7]);
    File kickedFile = new File(args[8]);

    FileWriter out = new FileWriter(outputFile, true);
    FileWriter kickedout = new FileWriter(kickedFile, true);

    instantiation();

// ****************************************************************
// Initialize variables for considering FRP degradation
// ****************************************************************
```

```java
    double alphas;
    double betas;

    double modsigma = modsigmastore[material-1];
    double modlambda = modlambdastore[material-1];

// Degraded FRP properties
    double sdeg;
    if(frptime > 0)
            sdeg=(-3.366 * Math.log(frptime * 365.25)+106.07)/100.0;
    else
            sdeg = 1.0;

// *****************************************************************
// Initialize random number generator
//  *****************************************************************

Random getrandoms = new Random();


// *****************************************************************
// Define geometric variables
// *****************************************************************

// Girder Dimensions

    double bt = 101.0;  //in
    double dt = 40.59;  //in
    double ht = 48; //in
    double slabt = 7.25; //in
    double webt = 14; //in
    double covert = 2; //in
    double nbars = 12.0;

    double areasteelinit = steelstore[steelstate-1][0];
    double initdiam = steelstore[steelstate-1][1]; //mm
    double initstrain; //= steelstore[steelstate-1][2];

    double b,d,h,cover, slab, web;

    //Parameters for dead load
    double meand = 344.37; //kip-ft
    double stdevd = 32.22; //kip ft

//Echo input

    out.write("Material " + material + " Width " + w + " layers " +
    layers + " frptime " + frptime+ " steeltime " + steeltime+"
    steelstate " + steelstate+"\r\n");

// *****************************************************************
// Loop over different COVs for strength
// *****************************************************************
```

357

```
for(int z=0;z<6;z++)
{
    alphas=alphastore[z];
    betas = betastore[material-1][z];

// ****************************************************************
// Begin simulation loop
// ****************************************************************
    double[] m = new double[n];
    for (int i=1;i<=n;i++)
    {

// *********************************************
// Define error in dimensions
// *********************************************

    double berror = (3.0/16.0)*getrandoms.nextGaussian()+(3.0/32.0);
    double derror = (1.0/4.0)*getrandoms.nextGaussian()-(1.0/8.0);
    double herror = (0.5)*getrandoms.nextGaussian()-(3.0/16.0);
    double cerror = (5.0/16.0)*getrandoms.nextGaussian()+(1.0/16.0);
    double slaberror = (15.0/32.0) * getrandoms.nextGaussian() +
        (1.0/32.0);

    b = bt + berror;
    d = dt + derror;
    h = ht + herror;
    web = webt + berror;
    slab = slabt + slaberror;
    cover = covert + cerror;
    double covermm = cover * 25.4;

    int areaswitch = 0;
    double areaerror = 0;

    while (areaswitch<1)
    {
        areaerror = 0.0232*getrandoms.nextGaussian()+0.97;
        if (0.96<areaerror)
           if(areaerror <1.06)
           areaswitch=1;
    }

    double areasteel=areasteelinit*areaerror;

// *********************************************
//  Define concrete properties in psi
// *********************************************
    //Model of concrete from McGregor
    double fc = 494.0625*getrandoms.nextGaussian()+3293.75;
    double Ec = 3466428+346642.8*getrandoms.nextGaussian();

    // parameters for determining stress block factors
    double nc = .8 + fc/2500.0;
```

```java
        double epsilonprime = fc/Ec*nc/(nc-1);

// *********************************************
//  Define steel properties in psi
// *********************************************

        double fy =(betarand()*(68.0-36.0)+36.0)*1000.0;
        double steelmod = 29200000+700800*getrandoms.nextGaussian();

// *********************************************
//  Define FRP properties in psi
// *********************************************

// Weibull Distribution for Strength

        double frps = betas * 1000 * Math.pow
            ((Math.log(1/getrandoms.nextDouble())) ,(1/alphas));

        // Lognormal Distribution for Modulus
        double frpmod = Math.exp(modsigma*getrandoms.nextGaussian()+
            modlambda)*1000;

        //  Lognormal Distribution for Thickness
        double thicksigma = 0.04997;
        double thicklambda = -2.99448;
        double frpthick = Math.exp(thicksigma*getrandoms.nextGaussian()
            + thicklambda) * layers;

        double af = frpthick * w;

        // Include degradation

        frps = frps * sdeg;

        //System.out.println(frps);
        double rupture = frps/frpmod;

// ****************************************************************
// Calculate remaining steel area
// ****************************************************************

        if(steelstate>3)
        {
            double wcr = 0.0225*getrandoms.nextGaussian()+0.45;
            double oneminwrc = 1.0 - wcr;

            double icorr = (37.8* Math.pow(oneminwrc,-1.64))/covermm;
            double icmmyr = 0.0116 * icorr * steeltime;

            double fdiam = initdiam - 2.0 * icmmyr;//mm
            double diamin = fdiam/25.4;
            areasteel =nbars* Math.PI * diamin * diamin /4.0;
        }
```

```java
// ****************************************************************
// Calculate limiting FRP Strain using debonding model
// ****************************************************************
    double fcmpa=fc/1000*6.894757;
    double meangf= 3.54689* Math.pow(fcmpa,0.19);
    double stdevgf = meangf*0.10;
    double gf = stdevgf*getrandoms.nextGaussian()+meangf;

    double maxstrain = 1.5* Math.sqrt(2.0*gf/frpmod/frpthick);

// ****************************************************************
// Caluclate initial strain on beam
// ****************************************************************
    //Random dead load

    double deadm = (stdevd*getrandoms.nextGaussian()+meand)*12*1000;

    if(b*slab*slab/2.0>steelmod/Ec*areasteel*(d-slab))
    {
        double neutralaxis = (-steelmod/Ec * areasteel +
            Math.sqrt((steelmod/Ec) * (steelmod/Ec) *areasteel*
            areasteel + 4.0*b / 2.0 * steelmod / Ec * areasteel *
            d))/b;
        double icrack = b * Math.pow(neutralaxis,3) / 3.0 + steelmod
            / Ec * areasteel * (d-neutralaxis)*(d-neutralaxis);
        initstrain = deadm * (h-neutralaxis)/icrack/Ec;

    }
    else
    {
        double neutralaxis = (-(b*slab-web * slab + steelmod / Ec *
            areasteel) +Math.sqrt(Math.pow(b*slab-web * slab +
            steelmod / Ec * areasteel,2)- 4.0* web / 2.0 * (-b * slab
            * slab / 2.0 + web * slab * slab / 2.0 – steelmod / Ec *
            areasteel * d))) / web;
        double icrack = b * Math.pow(slab,3) / 12.0 + b * slab *
            (neutralaxis - slab / 2.0) * (neutralaxis – slab / 2.0) +
            web * Math.pow(neutralaxis - slab,3) / 3.0 + steelmod / Ec
            * areasteel * (d-neutralaxis) * (d-neutralaxis);
        initstrain = deadm * (h-neutralaxis)/icrack/Ec;
    }


    if(0<initstrain & initstrain<0.0007)
    {

// ****************************************************************
// Determine neutral axis depth
// ****************************************************************

// guess neutral axis depth
    double c = 0.5;
    double cnext = 0.75;
    int toomany=0;
```

```
 int kicked=0;
 double steelstress = 0.0;
 double betaone = 0.0;
 double alphacon = 0.0;
 double frpeff = 0.0;
 double steeleff = 0.0;

while (Math.abs(c - cnext) > 0.0001)
{
  if(toomany < 75) //prevents getting stuck in the loop
  {
    c = (cnext+c)/2;

  // effective strain in FRP
    double crush = 0.003 * (h-c)/c-initstrain;
    double ruptlimit = rupture;
    double frplim =Math.min(ruptlimit, maxstrain);
    frpeff = Math.min(crush, frplim);


  // strain in extreme concrete fiber
    double epsilont = c*(frpeff+initstrain)/(h-c);
    double etep = epsilont/epsilonprime;
    double eteptwo = etep*etep;

    if (frpeff == crush)
    {
        betaone = .85;
        alphacon = .85;
    }
    else
    {
        betaone = (4.0 - (epsilont / epsilonprime)) / (6.0 -2.0 *
            epsilont / epsilonprime);
        double oneoverbeta = 1.0/betaone;
        alphacon =(oneoverbeta)*((etep)- eteptwo/3.0);
    }

  // strain in reinforcing steel
    steeleff = (frpeff + initstrain)*((d-c)/(h-c));

  // stress in reinforcing bar
    double apparentsteel = steelmod * steeleff;
    steelstress = Math.min(apparentsteel, fy);

  // use equilibrium to check estimate of c
    cnext = (areasteel * steelstress + af * frpmod * frpeff)/
            (alphacon* fc * betaone * b);

    toomany=toomany+1;
  }
  else
  {
     c=cnext;
```

```
        kicked=1;
       }// End of if
      }// End of while

    toomany=0;
    if(kicked==0)  //if kicked don't do
    {
// ****************************************************************
// Calculate maximum moment kip-ft/ft
// ****************************************************************'

   m[i-1] = (areasteel * steelstress * (d - betaone*c/2) + af *
        frpeff * frpmod * (h-betaone*c/2))/(1000*12);


    }
    else
    {
    kickedout.write(w + " " + frps + " " + frpmod + " " + frpthick
         + " " + fy + " " + fc);
    }// end of kicked loop
  }
  else
  {n=n-1;
  } //end of if to control initial strain
 }//end of giant loop

double meanmoment = mean(m);
double stdevmom = stdDev(m);

out.write(String.valueOf(meanmoment) + "   ");
out.write(String.valueOf(stdevmom)+ "\r\n");


}
out.close();
}
// Added functions for mean and standard deviation

static public double mean(double[] array)
{
    double mean = 0.0;
    if (array.length > 0)
    {
        double sum = 0.0;
        for (int i = 0; i < array.length; i++)
        {
            sum += array[i];
        }

        mean = sum/(array.length);
    }
    return mean;
}

static public double stdDev(double[] array)
```

362

```java
{
    double stdDev = 0.0;

    if (array.length > 1)
    {
        double meanValue = mean(array);
        double sum = 0.0;

        for (int i = 0; i < array.length; i++)
        {
            double diff = array[i] - meanValue;
            sum += diff*diff;
        }
        stdDev = Math.sqrt(sum/(array.length - 1));
    }
    return stdDev;
}


static public double betarand()
{
    Random myrandom = new Random();
    double randvalue = 0.00;

    boolean check = false;

    while(!check)
    {
    double uone = myrandom.nextDouble();
    double utwo = myrandom.nextDouble();

    double oneminusu = 1-uone;

    double fuone = 118.845 * Math.pow(uone,2.2105)*
      Math.pow(oneminusu,3.8157);
    double fuonem = fuone/2.264;

    if (utwo <= fuonem)
    {randvalue = uone;
      check = true;
    }
    }
    return randvalue;
}

static void instantiation()
    {
    alphastore[0] = 24.94978;
    alphastore[1] = 12.15343;
    alphastore[2] = 7.906927;
    alphastore[3] = 5.7974;
    alphastore[4] = 4.542213;
    alphastore[5] = 3.713773;
```

```
betastore[0][0] = 91.98713;
betastore[0][1] = 93.87339;
betastore[0][2] = 95.62201;
betastore[0][3] = 97.19778;
betastore[0][4] = 98.56877;
betastore[0][5] = 99.70775;

betastore[1][0] = 102.2079;
betastore[1][1] = 104.3038;
betastore[1][2] = 106.2467;
betastore[1][3] = 107.9975;
betastore[1][4] = 109.5209;
betastore[1][5] = 110.7864;

betastore[2][0] = 112.4287;
betastore[2][1] = 114.7341;
betastore[2][2] = 116.8713;
betastore[2][3] = 118.7973;
betastore[2][4] = 120.4729;
betastore[2][5] = 121.865;

betastore[3][0] = 122.6495;
betastore[3][1] = 125.1645;
betastore[3][2] = 127.496;
betastore[3][3] = 129.597;
betastore[3][4] = 131.425;
betastore[3][5] = 132.9437;

betastore[4][0] = 132.8703;
betastore[4][1] = 135.5949;
betastore[4][2] = 138.1207;
betastore[4][3] = 140.3968;
betastore[4][4] = 142.3771;
betastore[4][5] = 144.0223;

modsigmastore[0] = 0.173682;
modsigmastore[1] = 0.173682;
modsigmastore[2] = 0.173682;
modsigmastore[3] = 0.173682;
modsigmastore[4] = 0.173682;

modlambdastore[0] = 8.93774;
modlambdastore[1] = 9.108889;
modlambdastore[2] = 9.062904;
modlambdastore[3] = 9.074600;
modlambdastore[4] = 9.225423;

steelstore[0][0] = 16.8637;//in^2
steelstore[0][1] = 33.9761;//mm
steelstore[1][0] = 14.9899;
steelstore[1][1] = 32.0330;
steelstore[2][0] = 13.1162;
steelstore[2][1] = 29.9641;
steelstore[3][0] = 16.8637;
```

```
        steelstore[3][1] = 33.9761;
        steelstore[4][0] = 14.9899;
        steelstore[4][1] = 32.0330;
        steelstore[5][0] = 13.1162;
        steelstore[5][1] = 29.9641;
        }
}
```

Appendix G. Data from Bridge Survey

G.1 Summary of Dimensions Collected

This appendix provides all the dimensions gathered from the bridge survey conducted in order to determine representative girders for calibration, as described in Section 4.4.2. Table G-1 serves as a key to the tables containing the bridge data, it also repeats the assessment notes from Table 4-3 from Chapter 4. Please note that this data was only used to get a preliminary assessment of the whole data set and to aid in the selection of girders for analysis. Once specific girders had been chosen for use in calibration their individual plans were again studied in greater detail. Furthermore, all dimensions are in U.S. customary units.

Table G-1 Key to Bridge Dimensions in this Appendix

	Bridge Quantity	**Assessment Notes**
A	Bridge I.D. Number	Caltrans Reference Number
B	Span (ft)	Longest span on the bridge
C	Deck width (ft)	Assumes uniform width, includes sidewalks etc.
D	Roadway width (ft)	Assumes uniform width, does not include sidewalks, curbs, railings etc.
E	Number of girders	For expansion projects this was usually considered as the original number of uniform girders.
F	Girder spacing (ft)	Center-to-center distance between girders
G	Overhang (ft)	Amount of deck protruding past exterior girders
H	Slab thickness (in)	Designs didn't seem to specify any additional thickness for wearing
I	Depth of T-beam (in)	Depth including the thickness of the deck, when the depth varied the depth at the center of the span was taken
J	Width of T (in)	Taken as width away from diaphragms
K	Cover at bottom of girder (in)	
L	Cover at top of slab (in)	
M	Cover at bottom of slab (in)	
N	Concrete allowable stress (psi)	
O	Concrete ultimate strength (ksi)	
P	Steel allowable stress (psi)	
Q	Steel yield strength (ksi)	
R	Reinforcing steel, girder	At center of span in interior girder. Temperature and shrinkage steel along the side of the girders was not considered. # refers to bar size
S	Reinforcing steel, slab	Unless otherwise stated, the same reinforcement for top and bottom # refers to bar size, " refers to spacing in inches
T	Notes	See Table G-2 for details

Table G-2 Key to Notes Column

1	Widening project, data is usually for the original section, if available
2	Sidewalk on one side
3	Has some skew
4	Two parallel bridges
5	Project to raise bridge, data from original section
6	Hard to read pdf
7	Not enough detail in file
8	Sidewalks on both sides
9	Reinforcement/retrofit, no data collected
10	Bridge has curved elevation
11	Bridge did not have regular dimensions (4 different sized t-girders in original plans)
12	Overhang data is for the longer side
13	Expansion project, data is for the addition
14	Non-uniform cross-section
15	Bridge has acceleration lane
**	Variable dimension
Other bridge	This was a dual bridge, and dimensions were taken for both
Additional Span	Data was recorded for more than one span in a multi-span bridge

Table G-3 Data Collected in Bridge Survey

A	B	C	D	E	F	G	H	I	J	K	L	M	N	O	P	Q	R	S	T
11 0021																			1
11 0055	66.25	37.00	30.00	5	8.00	2.50	6.38	51	14		1.5	1	1200		20000		6 #11	#5 at 10"	2
11 0062	67	34.00	28.00	5	7.25	2.50	6.25	51	14		1.5	1	1200		20000		6 #11	#5 at 11"	3
11 0067	66.5	34.00	28.00	5	7.33	2.33	6.25	51	14	2	1.5	1					6# 11 & 2#8	#5 at 11"	
11 0068	66.5	34.00	28.00	5	7.33	2.33	6.25	51	14	2	1.5	1					6# 11 & 2#8	#5 at 11"	
11 0069	66.5	34.00	28.00	5	7.33	2.33	6.25	51	14	2	1.5	1					6# 11 & 2#8	#5 at 11"	
11 0070	66.5	34.00	28.00	5	7.33	2.33	6.25	51	14	2	1.5	1					6 #11 & 2 #8	#5 at 11"	
110071L	55	41.75	39.75	6	7.33	1.50	7.00	42	12		1.5	1					6 # 11	#5 at 11"	3, 4
110072L	50	34.00	28.00	5	7.25	2.50	6.25	42	12		1.5	1	1200	3.25	20000	60	6#11 & 2 #8	#5 at 11"	1
110073	67.75	34.00	28.00	5	7.33	2.33	6.25	51	14	2	1.5	1					6#11 & 2 #8	#5 at 11"	
110076	66.5	34.00	28.00	5	7.33	2.33	6.25	51	14	2	1.5	1					6#11 & 2 #8	#5 at 11"	
120046	22																		1
120049	30	24.00	21.00	4	5.92	2.96	8.00	71	14								8 #8		1

A	B	C	D	E	F	G	H	I	J	K	L	M	N	O	P	Q	R	S	T
120088	46.6	34.00	28.00	5	7.50	2.00	6.25	36	14		1.5	1		3.625		60	6 #10	#5 at 11"	4
120106	46.6	34.70	31.20	5	7.50	2.33	6.25	36	14		1.5	1	1200		20000		6 #10	#5 at 11"	
120107	48	40.33	32.00	5	8.67	2.83	6.63	36	14		1	1	1200		20000		6 #11	#5 at 10"	2, 3
120142	70	88.67	86.00	12	7.67	2.17	6.25	54	12		1.5	1	1200		20000		7#11	#5 at 10"	3
120146	56.5	88.67	86.00	12	7.67	2.17	6.25	44	12		1	1	1200		20000		6 #11	#5 at 10"	3
120147	49	88.67	86.00	12	7.75	1.71	6.25	36	14		1	1		3.25		60	6#11	#5 at 10", #4 at 18"	3
120149L	47	39.67	37.00	6	7.17	1.92	6.13	36	14		1.5	1	1200				6#11 & 2#9	#5 at 11"	4
120150L	47	39.67	37.00	6	7.17	1.92	6.13	36	14		1.5	1					6#11 & 2#9	#5 at 11"	4
120152L	52	44.75	40.42	7	6.83	1.88	6.00	36	14		1	1	1200		20000		6#11 & 2#9	#5 at 11"	2, 4
120154L	46	39.67	37.67	6	7.17	1.92	6.25	36	12		1.5	1					6#11	#5 at 11"	3, 4
120156L	46	34.00	28.00	5	7.50	2.00	6.25	33	12		1.5	1	1200		20000		6#11	#5 at 11"	3, 4
120157L	43	39.67	37.67	6	7.17	1.92	6.25	33	12		1.5	1					4#11	#5 at 11"	3, 4
540207L	56	41.00	39.00	6	7.00	3.00	6.13	51	11		1.5	1	1300		24000		7 #11	#5 at 11"	4

A	B	C	D	E	F	G	H	I	J	K	L	M	N	O	P	Q	R	S	T
540038		27.33	25.00	5	4.67	4.00	7.00		12	2	1.75	1.25					6 #?		1, 4, 6
540038 other bridge		19.17	16.83	4	4.00	3.67	7.00		12	2							6 #?		1, 4, 6
540281L		**		8	7.08	2.08	6.13	36	14		1.5	1	1200		20000		7 #11	#4 at 18", #5 at 5.5"	4
540281L other bridge		41.67	39.67	6	7.50	2.08	6.25	36	14		1.5	1	1200		20000		8 #11	#4 at 18", #5 at 5.5"	4
540292G																			7
540292L	61	42.00	34.00	5	8.5 or 7.17	4.92	7.25		16 or 18		1.75	1.25						#5 at 18"	1, 8
540360	56	33.50	30.00	3	12.75	3.75	9.00	60	21		2	1.5	750		18000		15 #10	#5 at 12"	
540438L	48.25	42.67	37.00	6	7.17	3.42	6.00	42	18		1	1	1000		20000		8 #10	#4 at 10"	1, 4
540454L	64.33	68.00	66.00	9	7.83	**	6.25	60	13		1.5	1	1200		20000		5 #11	#5 at 10"	1, 4
540454S	63.11	33.67	28.00	5	**	**	6.00	60	14		1	1	1000		20000		6 #10	#4 at 10"	4, 8

A	B	C	D	E	F	G	H	I	J	K	L	M	N	O	P	Q	R	S	T
540471F	76.73	38.33	34.00	5	8.25	2.67	6.50	45	13		1.5	1	1200		20000		6 #11	#5 at 10"	2
540471L	62		40.00	**	8.83	4.46	6.75	45			1	1					6 #10	#5 at 14"	
540471L other bridge	62	57.33	52.00	7	8.83	1.63	6.75	45	13-21**		1	1					6 #10	#5 at 14"	8
540471R																			9
540474	50	45.33	40.00	7	6.67	2.67	6.13	39	10	2	1	1					8 #10	#4 at 9.5"	1, 4
540483	75	33.33	28.00	4	8.50	3.92	6.63	60	16		1	1	1250		20000		9 #11	#5 at 13"	1, 4, 8
540485	40	45.33	40.00	7	6.67	2.67	6.13	36	10		1	1	1200		20000		6 #8	#4 at 9.5"	1, 4
540485 other bridge	40	51.33	46.00	8	6.67	2.33	6.13	36	10		1	1	1200		20000		6 #8	#4 at 9.5"	1, 4
540486M	52	45.33	40.00	7	6.67	2.67	6.13	39	10	2	1	1	1250		20000		6 #10	#4 at 9.5"	4
540486M other bridge	52	51.33	46.00	8	6.67	2.33	6.13	39	10	2	1	1	1250		20000		6 #10	#4 at 9.5"	4
540489	45	59.67	53.00	8	7.67	2.58	6.25	39										#4 at 9"	1, 2, 4
540492R	48	54.33	49.00	8	7.00	2.25	6.25	39						5		44	6 #9	#4 at 9"	3, 8

A	B	C	D	E	F	G	H	I	J	K	L	M	N	O	P	Q	R	S	T
540496	77	64.17	52.00	8	8.00	4.08	6.50	54	13		1	1	1200		20000		8 #11, 2 #9	#5 at 15"	8, 10
540498	77	64.17	52.00	8	8.00	4.08	6.50	54	13		1	1	1200		20000		8 #11, 2 #9 bars	#5 at 15"	8,10
540499L	50	33.33	28.00	4	9.00	3.17	7.00	39	18		1.25	1	1200		20000		8 #11	#5 at 13.5"	3, 4
540500L	44	33.33	28.00	4	9.00	3.17	7.00	39	14	2	1.25	1	1200		20000		6 #11	#5 at 13.5"	3, 4, 8
540500R	44	**	**	4	8.50	3.00	7.13	39	12			1	1200		24000		2 #11, 2 #10	#5 at 5"	1
540511	40	33.33	28.00	4	9.00	3.17	7.00	36	14		1.25	1	1200		20000		6 #11	#5 at 13.5"	4
260007	65	34.00	28.00	4	9.33	3.00	7.25	48	14		1.25	1.25	1200		20000		12 #11	#6 at 13"	3, 8
260035	48	36.50	26.00	4	9.17	4.50	7.75	60	18		1.5	1.5	1000		18000		10 #10	#6 at 14"	1
290002	54	19.33		3	7.75	2.17	7.50	48	14		2	1.5							13
290002 other bridge	54	18.58		3	6.83	2.25	7.38	55	16		2.5	1							13
290003	34	33.75	27.54	5	7.27	2.42	6.75	3	15		1.38	1.38						#5 at 11.5"	1
260007	65	34.00	28.00	4	9.33	3.00	7.25	48	14		1.25	1.25	1200		20000		12 #11	#6 at 13"	3, 8

A	B	C	D	E	F	G	H	I	J	K	L	M	N	O	P	Q	R	S	T
290003	34	29.25		4	8.00	2.13	6.25	38	15		1.5	1						#5 at 10"	13
29006	27	28.25		4	8.00	2.13	6.25	35	15	2	1.5	1	1200		20000		4 #10	#5 at 10"	13
290008L																			1
290032G	44	41.00	39.00	6	7.25	2.38	6.25	36	11		1.5	1	1200		20000			#5 at 11"	
290037																			11
290064	70	32.33	28.00	4	9.00	2.75	6.75	66	14	2	1	1	1000		20000		9 #10	#5 at 13"	1
290074L		41.00	39.00	6	7.25	2.54	9.50	48	12				1200		20000			#8 at 7.5"	4
290081L	62	42.17	39.67	6	7.50	2.00	6.25	48	11	2	1.5	1	1200		20000		6 #11	#5 at 10" right #6 at 10" left	4
290120G	67	32.83	27.00	5	6.75	2.92	6.50	60	10	2			1000		18000		8 #9	#5	8, 10
290149	68.25	53.92	40.00	7	8.00	2.96	6.50	51	13		1	1	1200		20000		6 #11	#5 at 14.5"	8
290150	68.26	77.25	64.00	10	8.00	2.96	6.50	51	13		1	1					8 #11	#5 at 14.5"	8
290152	71.92	48.31	40.00	6	9.00	1.66	6.75	51	13		1	1					10 #11	#5 at 13.5"	2

A	B	C	D	E	F	G	H	I	J	K	L	M	N	O	P	Q	R	S	T
290162	67.25	34.67	32.67	5	7.25	2.83	6.25	48	13		1.5	1	1200	3	20000		7 #11	#5 at 11"	
290173R	57	74.00	72.00	10	7.58	2.88	6.25	42	13		1.5	1	1200		20000		10 #11	#5 at 11"	4, 10
290173R additional span	57	68.00	66.00	9	7.58	3.67	6.25	42	13		1.5	1	1200		20000		10 #11	#5 at 11"	4
290174L	53	59.67	57.67	8	7.83	3.33	6.25	42	13		1.5	1	1200		20000		8 #11	#5 at 10"	4
290177L	40	54.50	50.50	6	9.00	5.00	8.00	33	11		2	1	1700		24000		**	#5 at 10" right #6 at 10" left	4
290200L	40	54.50	51.00	6	9.00	5.00	8.00	33	11		2	1	1700		2400		**	#5 at 10" right #6 at 10" left	4
290207																			6
290247R	40	42.50	38.50	5	9.00	4.50	8.00	33	11	2	2	1	1300		2400		8 #11	#6 at 13"	4, 12
300007		32.83	26.00	4	6.75	3.79	7.25	31	20		1.75	1.25	1000		18000			#5 at 12"	8

A	B	C	D	E	F	G	H	I	J	K	L	M	N	O	P	Q	R	S	T
570006R	48	68.00	66.00	9	7.83	2.67	6.25	36	13		1.5	1	1200		20000		8 #11	#5 at 10"	
570056	52	29.83	26.00	3	11.00	4.04	7.25		18	1	1.13	1.13	1000		18000		10 #10	#6 at 15.5"	
57062L	80	**	**	8	7.83	2.00	6.38	57			1.5	1	1200		20000		8 #11	#5 at 10"	4
57062L other bridge	80	**	**	7	7.83	2.00	6.38	57			1.5	1	1200		20000		8 #11	#5 at 10"	4
570094																			13
570096	48	28.67	26.00	3	10.50		7.00	39	20.5	3	1.5	1.5	1000		18000			#6 at 16"	3
570107L	45	**	48.00	10	8.83	1.67	6.75	54	14	2	1	1					6 #11	#5 at 13"	8
570113		27.00	24.00	5	5.25	3.00			15								12 bars		7
570115	75	33.67	28.00	4	9.00	3.00	6.75	72	14	2	1	1	1000		20000		8 #10	#5 at 13.5"	
570124	64	33.67	28.00	4	6.83	3.58	6.50	60	20		1	1	1000		20000		8 #10	#5 at 14.5"	1, 4, 6
570124	44.88	**	**	6	7.50	2.67	6.25	60	14		1.5	1	1300		24000		6 #11	#5 at 10"	13
570006R	48	68.00	66.00	9	7.83	2.67	6.25	36	13		1.5	1	1200		20000		8 #11	#5 at 10"	

A	B	C	D	E	F	G	H	I	J	K	L	M	N	O	P	Q	R	S	T
570125	55	33.67	28.00	4	6.83	3.58	6.50	60	20		1	1	1000		20000		8 #9	#5 at 14.5"	1, 4
570125 expansion	55	29.17		5	7.29		6.25	60	13				1200		20000		4 #11	#5 at 11"	13
570125 expansion	55	**	**	6	6.83	3.29	6.50	60	13		1.5	1.5	1200		20000		4 #11	#6 at 14.5"	13
570126	50	35.96	28.00	5	7.00	3.81	6.63	30	18	3	1.38	1.38	1000		18000		12 #10	#5 at 18"	2, 14
570126H																			6
570216K	87	36.33	26.00	5	8.25	0.00	7.00	***	20				1000		18000			#5 at 16.5"	3, 8, 14
570218																				
570219	52	34.33	26.00	5	8.17	0.00	7.00		20		1.38	1.38	1000		18000		7 #10	#5 at 11"	8, 14
570220																				6
570241	48	31.83	26.00	5	6.50	2.92	6.50	**	18	3	1.38	1.38	1000		18000		6 #10	#5 at 12"	10, 14
570323K	42.38	27.67	22.00	4	7.00	3.33	6.50	42	10				1250		18000		4 #10, 2 #7	#5 at 15"	10
570330	63.5	69.33	60.00	9	7.67	4.00	6.38	54	14	2	1	1	1250		20000		8 #9	#5 at 15"	1

A	B	C	D	E	F	G	H	I	J	K	L	M	N	O	P	Q	R	S	T
570355	58	71.83	69.00	8	9.00	4.00	6.75	48	14		1		1200		20000		8 #11	#5 at 13.5"	1, 4, 10
570355 other bridge	58	59.83	57.00	7	9.00	4.00	6.75	48	14		1		1200		20000		8 #11	#5 at 13.5"	4
570355G	58	27.67	22.00	3	9.00	4.75	6.75	48			1		1200		20000		8 #11	#5 at 13.5"	10
570356	58	59.83	57.00	7	9.00	**	6.75	48			1		1200		20000		8 #11	#5 at 13.5"	1, 4
570356 other bridge	58	**	**	9	9.00	3.42	6.75	48			1		1200		20000		8 #11	#5 at 13.5"	4
570368	64	33.67	28.00	6	5.83			36											6, 14
570371R	60	72.33	48.00	11	6.92	1.00	6.25	45			1	1	1200		20000		7 #11	#5 at 15"	1, 3, 15
570427L	43.5	39.67	24.00	6	7.00	2.33	6.13	33	14		1.5	1					6 #11	#5 at 11"	4